

# Accuracy of Calculation Procedures for Offshore Wind Turbine Support Structures

Pauline de Valk

August 21, 2013



# Accuracy of Calculation Procedures for Offshore Wind Turbine Support Structures

Master of Science Thesis

**Author:** Pauline de Valk

**Committee:** Prof. dr. ir. Fred van Keulen TU Delft - Chairman  
Dr. ir. Paolo Tiso TU Delft  
Ir. Paul van der Valk Siemens Wind Power, TU Delft  
Dr. ir. Sven Voormeeren Siemens Wind Power  
Ir. Pim van der Male TU Delft

August 21, 2013

---



# Summary

The demand for energy will continue to increase in the coming years and offshore wind energy shows great potential to become a key player in Europe's renewable energy future. The wind flow offshore is more stable and the average wind velocity is higher than onshore. Moreover, no size restriction exists for offshore wind turbines. However, the levelized cost of electricity for offshore wind energy should be decreased in order to ensure that the transition to offshore wind energy is economically feasible. One way to realize this cost reduction is by optimizing the structural design of the offshore wind turbine. As the support structure is one of the main cost items of the offshore wind turbine, structural optimization of this structure should be investigated.

In the current support structure design procedure, the turbine designer (TD) is responsible for the design of the tower, whereas the foundation designer (FD) is responsible for the design of the foundation and the transition piece. These designs are driven by the dynamic loads acting on these structures during the lifetime of the offshore wind turbine. Hence, accurate load predictions are a prerequisite to enable design optimization of the support structure. Therefore the TD runs a large number of aero-elastic simulations with the complete offshore wind turbine model to determine the global loads on the offshore wind turbine. From these simulations, loads or displacements at the tower/foundation interface are extracted and provided to the FD. Subsequently, the FD uses these interface responses in a post-processing analysis in order to obtain loads in the foundation structure.

However, inaccuracies can arise at two points in the support structure calculation procedure:

- In the aero-elastic model if a reduced or simplified foundation model is integrated in order to keep the aero-elastic model compact and to minimize computation costs.
- In the post-processing analysis applied by the FD. To retrieve the response of the foundation model the FD can use either interface loads or displacements, applied either in a dynamic or a quasi-static analysis.

By combining different model reduction and post-processing methods, various calculation procedures can be defined. In this thesis the accuracy of these different calculation procedures, that eventually determine the design of the offshore support structure, are analyzed. To this end, both a qualitative and a quantitative study are performed.

In the first part of this thesis the different calculation procedures are analyzed from a theoretical perspective. Model reduction methods are explained and the impact of the reduction on the accuracy of the results is investigated. Furthermore, the accuracy of the post-processing methods is investigated and the differences between a quasi-static and a dynamic analysis and between a force and a displacement controlled approach will be outlined. The second part of this thesis concerns a case study in which the various calculation procedures will be applied to a representative offshore wind turbine model on both a monopile and jacket type of foundation. Finally, as fatigue is often

the main design driver of the support structure, this case study is used to analyze the impact of an error in the response on the fatigue damage result.

This study shows that the use of reduced foundation models in the aero-elastic model can decrease the accuracy of the results, as the reduced model is an approximation of the full model. Therefore, in order to obtain accurate results, the offshore wind turbine model with the reduced components should be spectrally and spatially converged within the frequency range of the external load spectrum.

With respect to the post-processing methods, it will be shown that a quasi-static analysis provides accurate results only if the first free or fixed interface eigenfrequency of the foundation structure is higher than the highest excitation frequency in the external load for respectively the force or the displacement controlled approach. Moreover, as the first fixed interface eigenfrequency of a structure is higher than its first free interface eigenfrequency, a quasi-static displacement controlled approach will remain accurate up to higher excitation frequencies than a quasi-static force controlled approach.

Furthermore, since both a monopile and a jacket based support structure are modeled, it is found that the accuracy of the different calculation procedures strongly depends on the type of foundation structure. This is reflected by the results from the fatigue calculations; as the monopile behaves in a quasi-static manner within the excitation bandwidth the fatigue damage results are relatively accurate for all calculation procedures. However, the jacket shows much more dynamic behavior and subsequently the fatigue damage results of the quasi-static force controlled approach are highly underestimated. Finally, it is shown that when expanding the response of reduced models, the fatigue damage results can be greatly improved through a quasi-static residual load correction.

In conclusion, this work gives an overview of the accuracy of different calculation procedures to determine the design of an offshore wind turbine support structure. As the accuracy depends on several aspects (i.e. characteristics of the structure, use of reduced models, post-processing method and external load spectrum), several requirements are formulated for specific calculation procedures in order to make sure the obtained results are accurate. As a result, one can have more confidence in the optimized design of the support structure and over-dimensioning or the application of additional safety factors is unnecessary. In the end, this will lead to a reduction of costs for the support structure which thereby reduces the levelized cost of electricity for offshore wind energy.

# Acknowledgements

With the completion of this Master Thesis at the Faculty of Mechanical Engineering, a wonderful period of my life as a student in Delft has come to an end. It has been a period in which I have learned a lot about science and about mechanics in particular, but also about myself and about others.

The last nine months at Siemens Wind Power have also been a tremendous experience in which I learned a lot, especially about Siemens Wind Power and the offshore wind energy industry. I would hereby like to express my gratitude to David-Pieter Molenaar for giving me the opportunity to graduate within this division. My interest in renewable energy and wind energy in particular has increased and I hope that my thesis will contribute to make offshore wind energy a key player in the future of the renewable energy.

At first I would like to thank all my colleagues within the department for their willingness to help and for the nice atmosphere. A special thanks goes to Michiel van der Meulen for helping me with modeling the wave loads.

In particular, I would like to thank Sven Voormeeren and Paul van der Valk. I sincerely appreciate all the time and effort you spend to help me during this project. The input you provided during the weekly meetings kept me on track and helped me to distinguish the important matters from the issues which were of less importance. Next to this, I appreciate the way you helped me during the period in which I was writing my thesis. Your endless devotion in providing feedback helped me to bring this thesis to a higher level.

Furthermore, I would like to thank my supervisors Fred van Keulen and Paolo Tiso at the Technical University of Delft for their support, guidance and detailed comments and discussions.

Last but not least, I would like to thank Wouter, my family and friends for supporting me during this project. You provided the required assistance, and sometimes the necessary distraction, which helped me to gain new energy during my internship. I greatly appreciate this.

Amsterdam, July 2013

Pauline de Valk





# Contents

<b>Summary</b>	<b>i</b>
<b>Acknowledgements</b>	<b>iii</b>
<b>Nomenclature</b>	<b>ix</b>
<b>1 Introduction</b>	<b>1</b>
1.1 Research context . . . . .	1
1.1.1 Wind energy . . . . .	2
1.1.2 Offshore wind turbine . . . . .	3
1.2 Cost reduction through integrated support structure design . . . . .	5
1.3 Design cycle for offshore wind turbine support structure . . . . .	7
1.4 Sources of errors in the design cycle . . . . .	8
1.5 Thesis objective . . . . .	9
1.6 Thesis outline . . . . .	9
<b>2 Loads and design considerations</b>	<b>11</b>
2.1 Introduction . . . . .	11
2.2 Operational and wind loads . . . . .	11
2.2.1 Operational loads . . . . .	11
2.2.2 Wind loads . . . . .	12
2.3 Wave and current loads . . . . .	13
2.4 Design considerations . . . . .	14
2.4.1 First eigenfrequency . . . . .	14
2.4.2 Ultimate Limit State (ULS) . . . . .	15
2.4.3 Fatigue Limit State (FLS) . . . . .	15
<b>3 Theory of dynamics, substructuring and reduction methods</b>	<b>19</b>
3.1 Introduction . . . . .	19
3.2 Basic dynamics . . . . .	19
3.2.1 Response of a structure . . . . .	20
3.2.2 Frequency response function . . . . .	20
3.3 Substructuring . . . . .	21
3.3.1 Assembly of substructures . . . . .	22
3.3.2 Assembly in the time domain . . . . .	23
3.3.3 Assembly in the frequency domain . . . . .	24
3.4 Reduction methods . . . . .	24
3.4.1 Reduction basis . . . . .	24
3.4.2 Guyan reduction . . . . .	27

3.4.3	Craig-Bampton method . . . . .	27
3.4.4	Augmented Craig-Bampton method . . . . .	28
<b>4</b>	<b>Calculation procedures</b>	<b>31</b>
4.1	Introduction . . . . .	31
4.2	Detailed foundation used in complete OWT analysis . . . . .	32
4.2.1	Analysis of complete OWT model . . . . .	33
4.2.2	Post-processing on detailed foundation . . . . .	35
4.3	Reduced foundation used in complete OWT analysis . . . . .	38
4.3.1	Analysis of complete OWT model . . . . .	39
4.3.2	Post-processing on detailed foundation model . . . . .	41
4.4	Simplified foundation used in complete OWT analysis . . . . .	43
4.5	Separated models . . . . .	44
4.6	Summary . . . . .	45
<b>5</b>	<b>Modeling</b>	<b>47</b>
5.1	Introduction . . . . .	47
5.2	Finite element model . . . . .	47
5.2.1	Element damping matrix . . . . .	48
5.3	Strains and stresses . . . . .	49
5.3.1	Strains . . . . .	49
5.3.2	Stresses . . . . .	51
5.4	OWT model . . . . .	51
5.4.1	Model I - OWT with a monopile . . . . .	53
5.4.2	Model II - OWT with a jacket . . . . .	55
5.5	Loads . . . . .	57
5.5.1	Wind and operational loads . . . . .	58
5.5.2	Wave loads . . . . .	59
<b>6</b>	<b>Results of calculation procedures - Monopile</b>	<b>63</b>
6.1	Introduction . . . . .	63
6.2	Analyses of complete OWT . . . . .	64
6.2.1	Energy distribution in the structure . . . . .	65
6.2.2	Interface loads . . . . .	66
6.2.3	Expansion of the response of the reduced foundation models . . . . .	67
6.3	Post-processing . . . . .	70
6.3.1	OWT with a detailed foundation . . . . .	70
6.3.2	OWT with a Guyan reduced foundation . . . . .	73
6.3.3	OWT with a Craig-Bampton reduced foundation . . . . .	75
6.4	Fatigue damage calculation . . . . .	76
6.5	Summary . . . . .	79
<b>7</b>	<b>Results of calculation procedures - Jacket</b>	<b>81</b>
7.1	Introduction . . . . .	81
7.2	Analysis of complete OWT . . . . .	82
7.2.1	Energy distribution in the structure . . . . .	83
7.2.2	Interface loads . . . . .	84
7.2.3	Expansion of the response of the reduced foundation models . . . . .	86
7.3	Post-processing . . . . .	89

7.3.1	OWT with a detailed foundation . . . . .	89
7.3.2	OWT with a Guyan reduced foundation . . . . .	91
7.3.3	OWT with a Craig-Bampton reduced foundation . . . . .	93
7.3.4	OWT with an Augmented Craig-Bampton reduced foundation . . . . .	95
7.4	Fatigue damage calculation . . . . .	97
7.5	Summary . . . . .	103
<b>8</b>	<b>Conclusions and recommendations</b>	<b>105</b>
8.1	Conclusions . . . . .	105
8.2	Recommendations . . . . .	107
8.2.1	Recommendations for calculation procedure of support structure . . . . .	107
8.2.2	Recommendations for future research . . . . .	108
<b>A</b>	<b>Proper Orthogonal Decomposition Method</b>	<b>111</b>
<b>B</b>	<b>Newmark time integration method</b>	<b>113</b>
B.1	Implicit Newmark scheme . . . . .	114
B.2	Explicit Newmark scheme . . . . .	114
<b>C</b>	<b>3D Euler beam element</b>	<b>115</b>
C.1	Shape functions . . . . .	115
C.2	Element stiffness and mass matrices . . . . .	116
<b>D</b>	<b>Verification in Ansys for stress computations 3D structures</b>	<b>118</b>
D.1	Transformation from global to local axes . . . . .	118
D.2	Ansys verification stress computations . . . . .	119
D.2.1	Monopile structure . . . . .	119
D.2.2	More complex 3D structure . . . . .	121
<b>E</b>	<b>OWT models - eigenfrequencies and eigenmodes</b>	<b>122</b>
E.1	OWT model with a monopile . . . . .	122
E.1.1	Eigenmodes monopile . . . . .	123
E.1.2	Eigenmodes OWT with a monopile . . . . .	124
E.2	OWT model with a jacket . . . . .	125
E.2.1	Eigenmodes jacket . . . . .	126
E.2.2	Eigenmodes OWT with a jacket . . . . .	127
<b>F</b>	<b>Response of one DoF - Monopile and Jacket</b>	<b>129</b>
F.1	Monopile . . . . .	129
F.2	Jacket . . . . .	132
	<b>Bibliography</b>	<b>135</b>



# Nomenclature

## Latin symbols

$B$	Signed boolean matrix	
$C$	Damping matrix	
$F$	Matrix of external force vectors	
$f$	External force vector	
$G$	Flexibility matrix	
$g$	Interface force vector	
$K$	Stiffness matrix	
$L$	Boolean matrix	
$M$	Mass matrix	
$P$	Projection matrix	
$q$	Generalized DoF vector	
$R$	Reduction matrix	
$r$	Residual force vector	
$T$	Transformation matrix	
$u$	Displacement DoF vector	
$Y$	Receptance matrix	
$Z$	Dynamic stiffness matrix	
$D$	Diameter	$[m]$
$E$	Young's modulus	$[Pa]$
$f$	Frequency	$[Hz]$
$H_s$	Significant wave height	$[m]$
$I$	Moment of inertia	$[m^4]$
$t$	Time	$[s]$
$T_p$	Peak period	$[s]$

## Greek symbols

$\eta$	Intensity parameters
$\Phi_f$	Free interface vibration modes
$\Phi_i$	Fixed interface vibration modes
$\Phi_r$	Rigid body modes
$\Phi_{MTA}$	MTA vectors

$\Psi_C$	Static constraint modes	
$\omega$	Circular frequency	[rad/s]
$\omega_{ext}$	Excitation eigenfrequency of external load	[rad/s]
$\omega_{fixed}^{\{1\}}$	1st fixed interface eigenfrequency	[rad/s]
$\omega_{free}^{\{1\}}$	1st free interface eigenfrequency	[rad/s]
$\epsilon$	Strain	
$\sigma_*$	Stress	[Pa]

### Subscripts

$b$	Boundary degree(s) of freedom
$dyn$	Dynamic part
$i$	Internal degree(s) of freedom
$stat$	Static part
$x$	x-Direction
$y$	y-Direction

### Superscripts

$(f)$	Belonging to substructure foundation
$(s)$	Belonging to substructure $s$
$(w)$	Belonging to substructure tower+RNA
$\sim$	Reduced
$\wedge$	An error is introduced in the result
$T$	Transpose

### Abbreviations

1P	First excitation frequency
3P	Second excitation (blade passing) frequency
CAPEX	Capital expenditures
CB	Craig-Bampton
CB10	Craig-Bampton reduction basis with 10 fixed interface modes
CB10MTA	Augmented Craig-Bampton reduction basis with 10 fixed interface modes and 10 MTA vectors
CB20	Craig-Bampton reduction basis with 20 fixed interface modes
D	Dynamic
DC	Displacement controlled approach
DoF	Degree(s) of freedom
DS	Dynamic substructuring
FC	Force controlled approach
FD	Foundation designer
FE	Finite element
FLS	Fatigue limit state

FRF	Frequency response function
GDP	Global domestic product
LCOE	Levelized cost of electricity
MA	Mode acceleration
MTA	Modal truncation augmentation
OC4	Offshore Code Comparison Collaboration Continuation
OPEX	Operational expenditures
OWT	Offshore wind turbine
POD	Proper orthogonal decomposition
POM	Proper orthogonal mode
POV	Proper orthogonal value
Qs	Quasi-static
RNA	Rotor nacelle assembly
SVD	Singular value decomposition
SWP	Siemens Wind Power
TD	Turbine designer
ULS	Ultimate limit state





# Chapter 1

## Introduction

### 1.1 Research context

The demand for energy is increasing, this is mainly due to population growth and economic growth. Over the last 20 years the global population has increased by 1.6 billion people. Although the growth rate is trending down, the population is assumed to grow 1.4 billion over the next 20 years. Next to this, the global gross domestic product (GDP) growth is likely to accelerate, driven by low and medium income economies.

The energy efficiency, which is defined as energy over GDP, will continue to improve globally. Despite these improvements in energy efficiency, a total increase of global energy demand of 80% is forecasted by 2035, see Figure 1.1. Furthermore, the fuel mix changes slowly as gas and non-fossil fuels gain share at the expense of coal and oil [8]. The fastest growing fuels are renewables as can be seen in Figure 1.1.

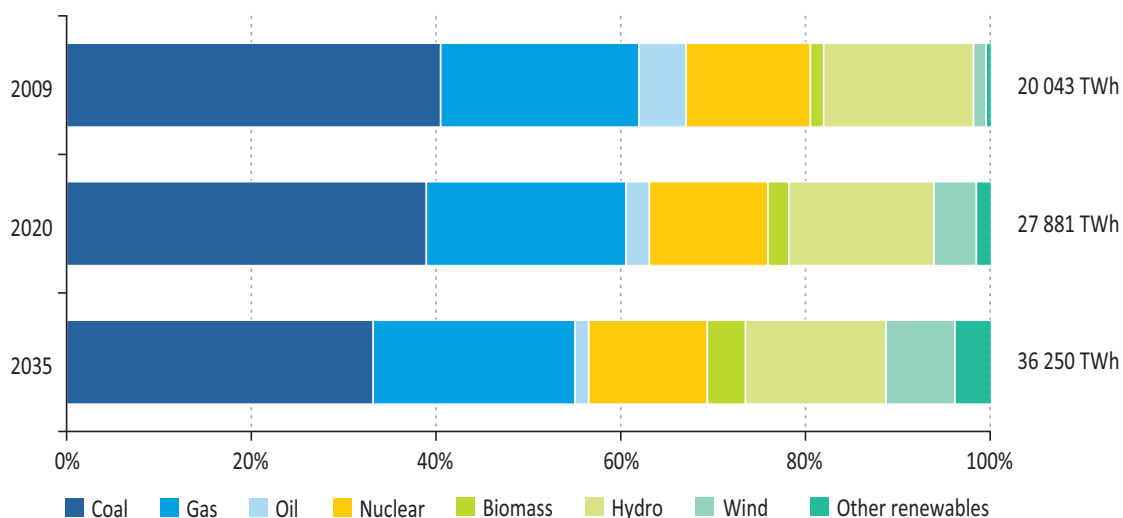
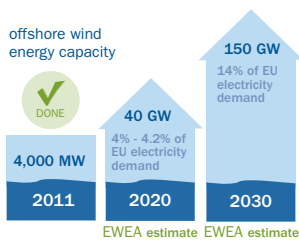


Figure 1.1: Share of world electricity generation [18].

### 1.1.1 Wind energy

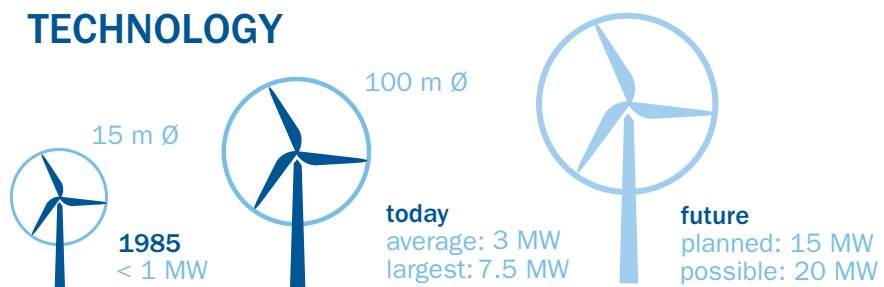
Wind has been used as a source of energy since the early Middle Ages. Initially, windmills were used for mechanical purposes such as the milling of grain and the pumping of water. The modern wind turbine however converts the energy extracted from the wind to electrical power which can be used elsewhere. Over the past decades, the modern wind turbines have shown strong technical improvements in terms of power output and size, see Figure 1.2b. Likewise, the wind power industry has grown significantly. Figure 1.2c shows that the European Wind Energy Association (EWEA) targets a total of installed wind capacity of 230 GW in Europe by 2020, of which 40 GW is installed offshore [12, 13]. The installed wind capacity offshore is expecting to grow significantly, see Figure 1.2a.

#### OFFSHORE



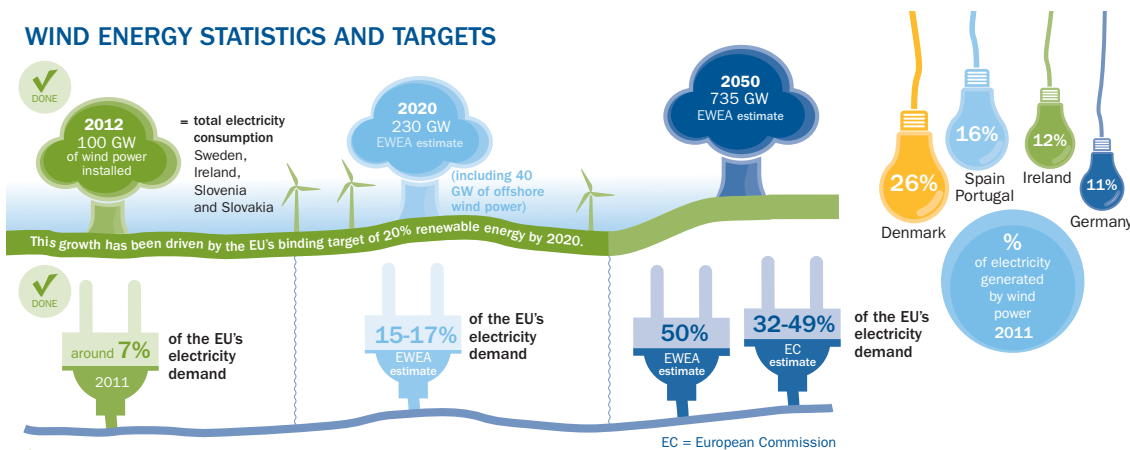
(a) Forecast of offshore wind energy

#### TECHNOLOGY



(b) Size growth of wind turbines over time

#### WIND ENERGY STATISTICS AND TARGETS



(c) Wind energy statistics and targets

Figure 1.2: Development offshore wind energy [13].

The wind conditions offshore are more optimal than onshore as the wind flow is more stable and the average wind velocity is higher. Moreover, onshore wind turbines are bound to size restrictions to reduce visual and noise pollution. As this is not an issue offshore, large turbines can be installed in offshore wind fields to convert as much wind energy into electrical energy as possible. As a result, offshore wind energy shows great potential to become a key player in Europe's renewable energy future.

In order to ensure that the transition to offshore wind energy is economically feasible, the levelized cost of electricity (LCOE) for offshore wind should be decreased. The LCOE for offshore wind

is still above that of onshore wind. Since an offshore wind turbine contains an extra component, the foundation structure, to install the wind turbine at sea, extra costs are generated. Furthermore, extra costs are caused by increased installation, operation and maintenance costs.

One way to realize this necessary cost reduction is by optimizing the structural design of the offshore wind turbines. This leads to a reduction in the fabrication, installation and maintenance costs which can make offshore wind energy one of the main energy suppliers.

### 1.1.2 Offshore wind turbine

In order to determine which components of an offshore wind turbine can be optimized, the different components will first be introduced. Afterwards, a breakdown of the costs of an offshore wind turbine will be presented.

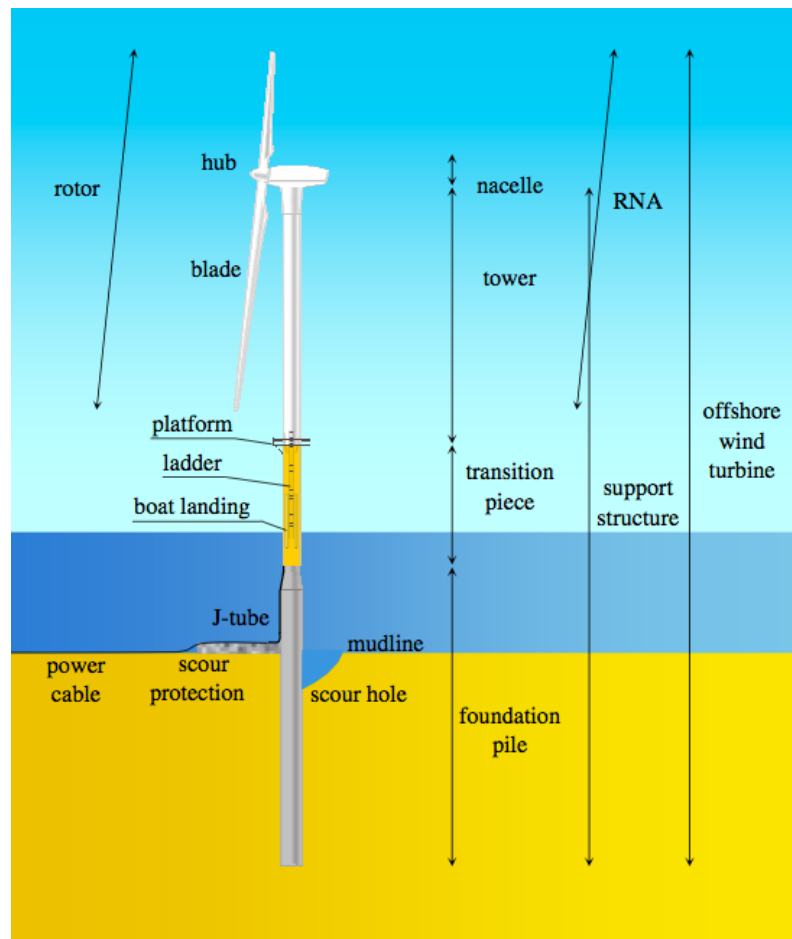


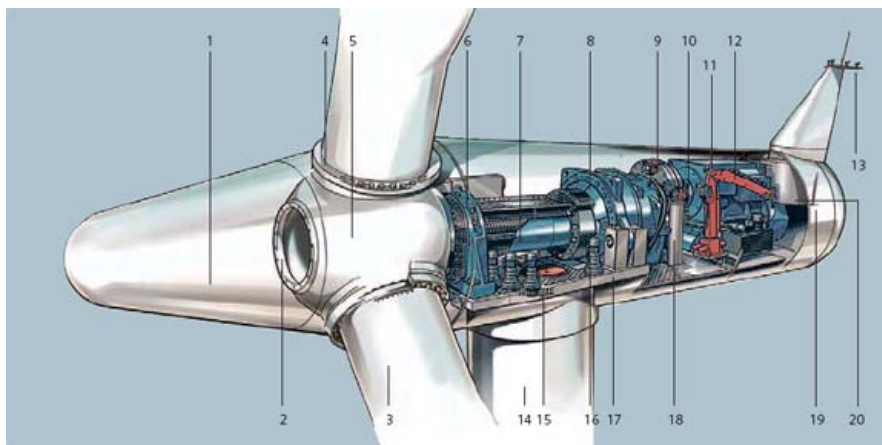
Figure 1.3: Schematic overview of a wind turbine [35].

An offshore wind turbine (OWT) consists of several components, see Figure 1.3. The most important components are listed below:

- The **nacelle** houses the generator, the gearbox and all other components to convert wind energy into electrical energy as efficiently as possible. Figure 1.4 shows the different components which are located in the nacelle.

- The **rotor** consists of the hub and the blades. The blades are connected to the hub, which transmits the rotational energy to the gearbox via the main shaft. The blades can span 75 meters in length.
- The **tower** provides support to the rotor-nacelle-assembly (RNA). The tower is a tubular structure and is constructed out of several sections. Typical tower heights range from 80-130 meters.
- The **transition piece** connects the tower to the foundation pile. Next to this, a boat landing, an access deck and ladder can be installed on the transition piece which allows one to enter the tower. Note that this component is not always present.
- The **foundation** provides support to the wind turbine in offshore environments. Different types of foundation structures exist and will be discussed in this section. The type of foundation structure used depends mainly on the water depth.

The tower, transition piece and foundation together are defined as the support structure and the rotor-nacelle-assembly (RNA) consists of the rotor and the nacelle.



1	Spinner	11	Generator
2	Spinner Bracket	12	Service crane
3	Blade	13	Meteorological sensors
4	Pitch bearing	14	Tower
5	Rotor hub	15	Yaw ring
6	Main bearing	16	Yaw gear
7	Main shaft	17	Nacelle bedplate
8	Gearbox	18	Oil filter
9	Brake disc	19	Canopy
10	Coupling	20	Generator fan

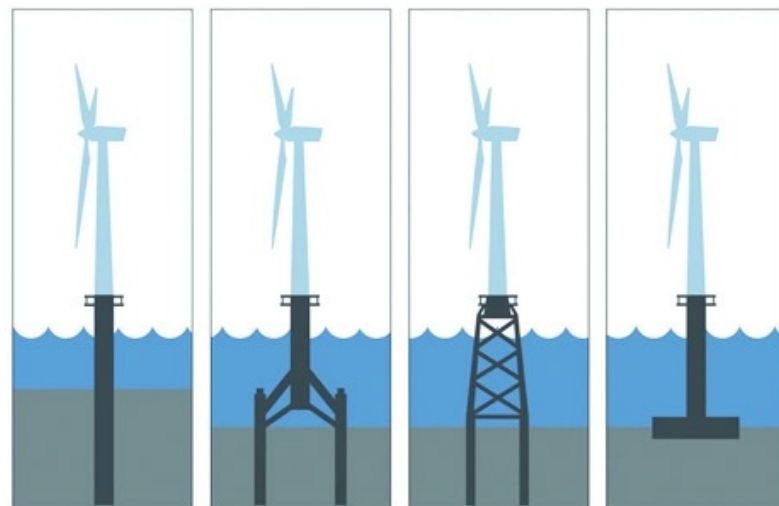
**Figure 1.4:** SWT-2.3-93 Nacelle

Various foundation types exist to install a wind turbine offshore, see Figure 1.5. The type of foundation structure used at sea depends mainly on the water depth.

- A **monopile** is a large diameter, thick walled, steel tubular structure which is hammered into the seabed. Monopiles are the most commonly used foundation structures for offshore wind turbines in relatively shallow waters, up to depths of 30-40 meters.

- A **tripod** consists of a central vertical pile connected to three cylindrical steel tubes which are driven into the seabed. Tripods are more suitable for deeper waters with depths ranging from 20-80 meters.
- A **jacket** is built up of three or four main legs, connected to each other by bracings. The main legs are supported by soil piles that are driven into the seabed. The members of the jacket are made from circular tubes and are manually welded to each other. Due to the high labor costs associated to the construction of the jacket, a jacket structure can be expensive. Jackets can be used in deeper waters, up to 80 meters.
- A **gravity based** foundation uses its own weight to hold the wind turbine in place on the seabed. The extra weight at the bottom can be in the form of sand, rocks or iron. The gravity based foundation is only economically feasible in very shallow waters.

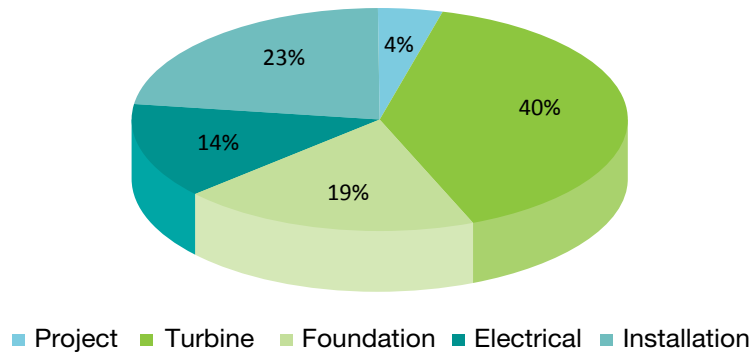
The monopile is most often used to install wind turbines offshore. However, for large water depths, the dimensions of the monopile rapidly increase in order to withstand the high loading and to maintain the right natural frequency. As a result, due to high material costs this type of foundation structure is economically infeasible. Therefore the jacket structure is often used in deeper waters.



**Figure 1.5:** Different foundation types to install wind turbines offshore [1].  
From left to right: monopile, tripod, jacket and gravity based foundation.

## 1.2 Cost reduction through integrated support structure design

Installing and operating an offshore wind turbine requires capital expenditures (CAPEX) and operational expenditures (OPEX). CAPEX consists of the costs of the components of an offshore wind turbine as well as the installation costs, while OPEX is defined as the costs needed for the operation and maintenance of the OWT during its lifetime. A breakdown of the CAPEX for offshore wind turbines is shown in Figure 1.6. The ‘turbine’ costs, consisting of the costs for the tower and the RNA, is the largest expenditure of the total CAPEX of around 40%. Another main cost item is the foundation which can be around 20% of the total CAPEX. Note that this breakdown of CAPEX is site dependent.



**Figure 1.6:** Breakdown of CAPEX into key elements of an offshore wind turbine [41].

Given its large share in the total CAPEX and the relatively simple nature of the structure, the support structure shows great potential for cost savings. The offshore wind industry is well aware of this potential and therefore several parties are spending great efforts to achieve these cost savings. Specifically, within Siemens Wind Power (SWP) research and development work is concentrated on the following topics:

- The dynamic behavior of the OWT in response to external loading, is determining the load levels and hence the design of its support structure. Insight in this behavior is crucial and requires accurate and efficient modeling techniques. However, in the wind industry simple models and crude assumptions are often applied when computing the loads from simulations. Therefore, within SWP methods have been developed for the detailed analysis of the structural dynamic behavior of wind turbines, with applications focused on support structure modeling [24, 34, 37].
- An important bottleneck for cost reduction of offshore support structures is the lack of knowledge about soil-structure interaction. This is handled by making conservative assumptions to ensure that the modeled behavior of the soil is always less favorable than in real life. To eliminate unnecessary conservatism, research has been performed within SWP to gain fundamental understanding of soil-structure interaction and to translate this understanding to improved engineering models that can be used in practice [36, 40].
- Another source of conservatism is the design split between the foundation designer (FD) and the turbine designer (TD) as both parties are responsible for the design of the support structure. Due to the fact that only a limited number of design iterations are performed and both parties use their own design methods and safety factors, an overly conservative foundation design is obtained. Therefore, an important research topic within SWP is the concept of *integrated support structure design*. Initial studies showed that this approach, combined with structural optimization, can lead to considerable savings of up to 15% in steel mass [17, 32]. In order to enable implementation of this design methodology, several research projects have been carried out over the past years. For instance, the effect of different modeling methods for wave loading has been investigated [23], grouted connections were analyzed [21], and finally the use of high fidelity support structure models in the load calculation process was investigated [11].

This thesis also focuses on the topic of integrated support structure design. The perspective taken here however is that the support structure design is still performed by two parties. In this thesis,

the process before the actual design and optimization of the support structure is analyzed, namely the calculation procedures to determine the loads on these structures. Indeed, in order to have confidence in the optimized results, one needs to make sure that the calculation procedures for designing the support structure provide accurate results. Before formulating the thesis objective in section 1.5, the next section therefore first outlines this design process.

### 1.3 Design cycle for offshore wind turbine support structure

In order to verify the accuracy of the different calculation procedures used to design a support structure, the design cycle for offshore wind turbine support structures should be discussed first to gain more insight in the design process. The support structure of an offshore wind turbine is custom engineered for every wind park due to site specific conditions as wind climate, wave conditions, water depth and soil properties. Generally, the three most important design criteria for the OWT are withstanding ultimate loading, having sufficient fatigue lifetime and having the first eigenfrequency of the OWT between the rotating frequency of the rotor (1P) and the blade passing frequency (3P). These design criteria will be explained in more detail in Section 2.4.

Siemens Wind Power is a TD and is responsible for the design of the RNA and the tower and the FD is responsible for the design of the transition piece and the foundation structure. In order to ensure that the design of the support structure meets the design criteria, SWP simulates thousands of load-case scenarios with the complete offshore wind turbine model using an aero-elastic code. The global dynamic behavior can be determined with the aero-elastic model. SWP uses its in-house developed Bonus Horizontal axis wind turbine Code (BHawC), which is a non-linear code which includes all relevant phenomena as listed below [37]:

- Aero-elasticity, this means coupling of structural deformation and aerodynamic loads
- Hydrodynamic loads
- Soil-structure interaction
- The wind turbine's controller dynamics
- Rotational effects caused by the spinning rotor

The design of the support structure can be seen as a calculation cycle and several iterations are usually necessary before a satisfactory design is reached, see Figure 1.7. In order to design the support structure, the wind climate, the wave conditions, the water depth and the soil properties for the specific wind park area are required input parameters. If these input parameters are known, the design cycle can begin and consists of 6 steps:

1. The FD creates an initial design of the foundation structure based on the wave conditions, the soil properties, the water depth and generic load values provided by the turbine designer. The FD communicates this initial design and the computed wave loads to the turbine designer.
2. The TD integrates this foundation structure in the aero-elastic model, as a result the aero-elastic model contains all the components of the OWT.
3. The aero-elastic simulations are run under wind and wave loading and the different design considerations are checked. The TD adjusts the design of the tower to ensure it meets the design criteria.

4. The loads or the displacements at the interface between the tower and the foundation structure are extracted and communicated to the FD.
5. The FD applies the interface loads or displacements and the wave loads on the detailed foundation model.
6. A simulation is run to compute the loads on the foundation, from which the fatigue lifetime and the ultimate loads are determined.

The FD adjusts the design of the foundation to ensure it meets the design criteria and the FD communicates the new design of the foundation structure to SWP. After this, the design cycle continues. Several iterations will be necessary until a satisfactory design of the offshore wind turbine support structure is reached. In general, 2-3 iterations are performed as the available engineering time for a given project is limited.

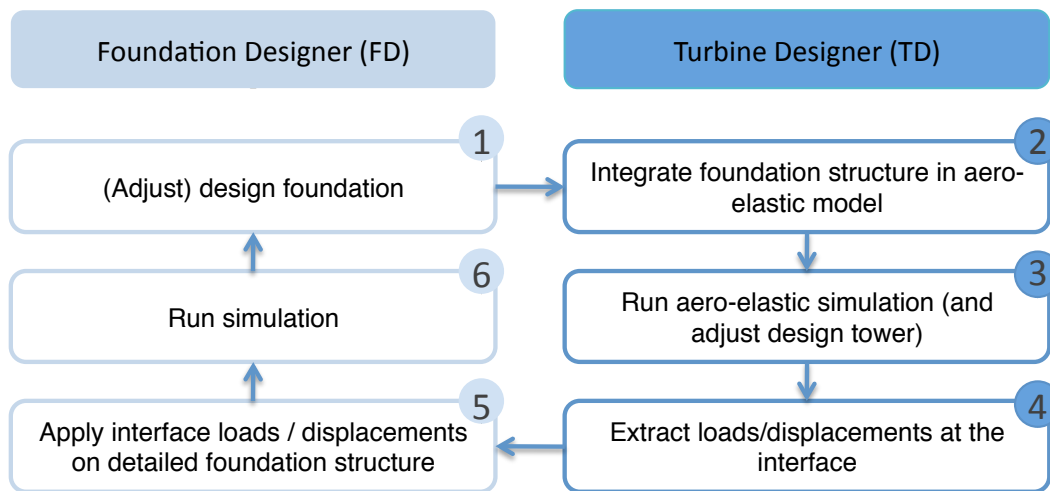


Figure 1.7: Design cycle of offshore wind turbine support structures.

## 1.4 Sources of errors in the design cycle

In order to counteract large computation costs for the large number of aero-elastic simulations, the aero-elastic model is kept compact. Therefore, the detailed models of the tower and the foundation are simplified or reduced. Reduction techniques are explained in Section 3.4. If the models are simplified/reduced, the interface loads/displacements can contain errors due to the simplification/reduction. These interface loads/displacements are used by the FD to retrieve the response of the detailed foundation model. Therefore, if the interface loads/displacements contain an error, the results after analyzing the detailed foundation model are expected not to be accurate either. This is especially true for a jacket structure, as this structure experiences local dynamics which might be neglected or overly simplified by the reduced model. This will be explained in more detail in Chapter 5 and 7.

Furthermore, the FD can perform a quasi-static analysis, in which the damping and inertia forces are neglected, to compute the response of the detailed foundation model. The accuracy of this calculation procedure is questionable from a structural dynamics perspective. If one neglects damping and inertia forces for the foundation, one assumes that the foundation structure behaves in a quasi-static



manner in the global dynamic behavior. Hence, this could lead to errors in the predictions of the fatigue loads. Currently, no clear guidelines are available which describe under what conditions a quasi-static analysis is valid. Furthermore, it is often claimed that the design approach where the detailed foundation structure is quasi-static analyzed is conservative, meaning that the results obtained overestimate reality, leading to a safe over-designed support structure. However, this statement is not proven.

This thesis has focused on the accuracy of the calculation procedures to design the foundation structure of the OWT. However, the design of the tower is based on the design of the foundation (and vice versa), as both components are integrated in the aero-elastic model and the results from these simulations are used to optimize the design of both components. If the design of one component is based on inaccurate calculation procedures, an optimal accurate design of the support structure will never be reached. Therefore, if one knows that the design of the foundation structure is based on accurate results, the design of the tower can be optimized accurately as well and eventually an accurate design of the support structure is reached.

Summarizing, some inaccuracies arise in the design cycle of the support structure and the impact of these inaccuracies on the accuracy of the results will be investigated in this thesis. If one has confidence in the accuracy of the calculation procedures, a less conservative design for the foundation structure can be developed which will eventually reduce the LCOE of offshore wind energy.

## 1.5 Thesis objective

In the previous sections it was explained that in order to ensure that offshore wind energy will have a leading role in the future energy supply, the LCOE must be further reduced. This cost reduction can be achieved by structural design optimization of the OWT components. The support structure is one of the main cost items, hence, it is worthwhile to optimize the structural design of this component. In order to optimize the structural design, one needs to be sure the underlying calculation procedures provide accurate results. Therefore, it is valuable to gain more insight in the accuracy of the current calculation procedures in the design cycle of the support structure.

The aim of this thesis is twofold. Firstly, it is important to examine and quantify the validity and conservatism of the current calculation procedures. Secondly, it should be shown how these findings can be combined to come to more optimal design procedures. From the above, the goal of the assignment can be formulated as:

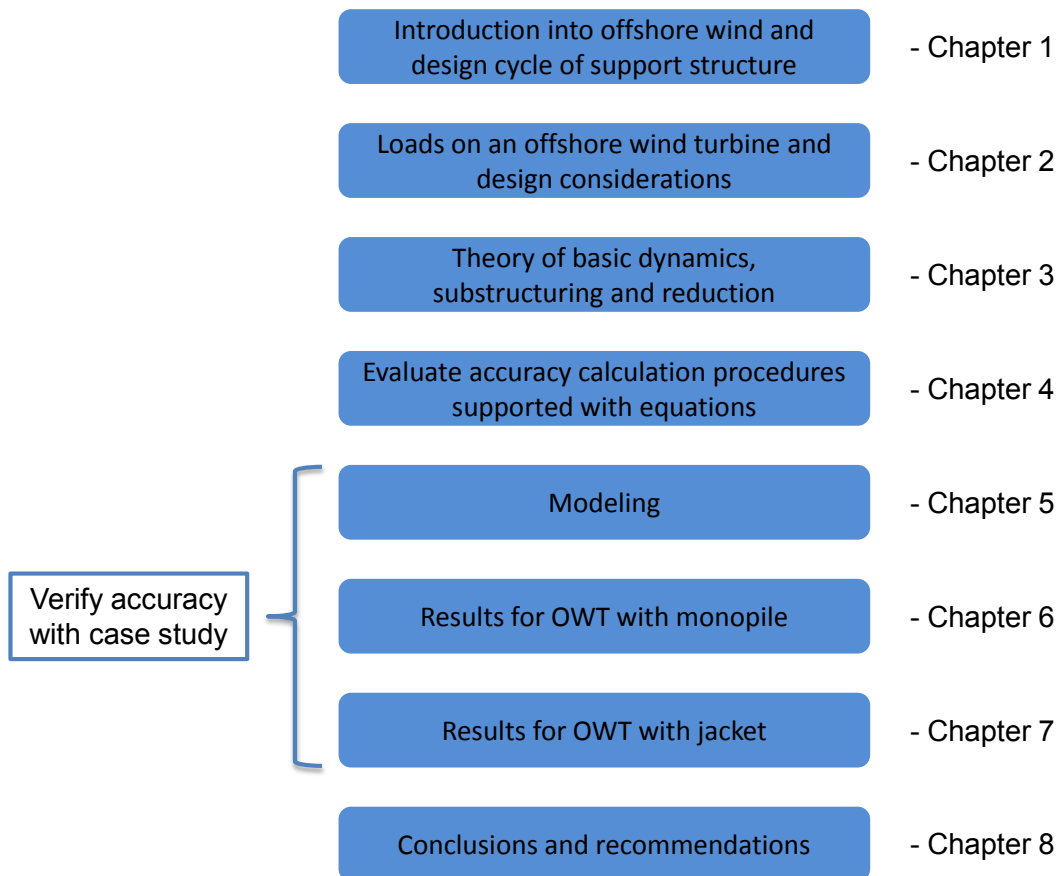
*“Investigate the validity and conservatism of the current calculation procedures for offshore wind turbine support structures and propose improved procedures based on these findings.”*

The focus is on the accuracy of the calculation procedures for foundation structures. The calculation procedures to determine the design of a monopile and a jacket will be investigated.

## 1.6 Thesis outline

According to the thesis objective, the content of this thesis is divided into several chapters. As the loads on the offshore wind turbine mainly determine the design of the support structure, the loads and their modeling will be discussed in Chapter 2. Furthermore, the main design criteria are

discussed in more detail. Chapter 3 presents the general theory about structural dynamics, substructuring and model reduction. Firstly, the difference between dynamic and quasi-static behavior will be determined. Secondly, the theory of substructuring will be presented and the chapter concludes with a section where different reduction techniques are discussed. Chapter 4 will give an overview of the current calculation procedures to design a support structure. These calculation procedures will be supported with the associated equations to get more insight in the accuracy of the procedures. In order to investigate if the potential inaccuracies observed in Chapter 4 are experienced in the design procedure, a case study is performed. This case study will give more insight in the quantitative errors of the different calculation procedures. To this end two different OWT models will be built, one with a monopile foundation structure and one with a jacket foundation structure. The construction of the models is described in Chapter 5. Chapters 6 and 7 will present the results of the different calculation procedures for the OWT with a monopile and with a jacket foundation, respectively. Finally, in Chapter 8 the conclusions and recommendations are presented.



**Figure 1.8:** Thesis outline

# Chapter 2

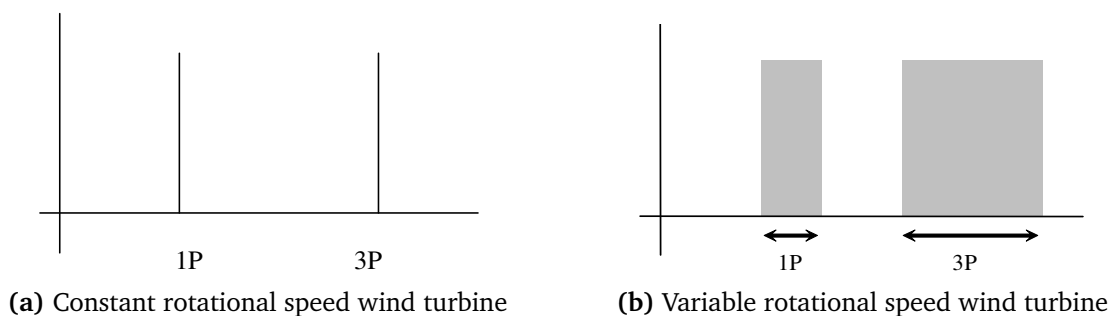
## Loads and design considerations

### 2.1 Introduction

The design cycle of an offshore wind turbine support structure is presented in Subsection 1.3. In order to determine the design of the support structure an input is necessary. Next to the initial design of the different components, the loads on the OWT are essential as well. An OWT is exposed to three types of loads during operation, loads due to waves and wind and operational loads. The general concept to model these loads will be presented in this chapter as these loads will be modeled to perform the case study, discussed in Chapter 5. Section 2.4 will discuss the three most important design criteria for the design of the support structure; withstand ultimate loading, a sufficient fatigue lifetime and the first eigenfrequency of the OWT should be between the rotating frequency (1P) and the blade passing frequency (3P).

### 2.2 Operational and wind loads

#### 2.2.1 Operational loads



**Figure 2.1:** Operational loads on a wind turbine depend on the rotational frequency [35].

An important source of excitation in a wind turbine system is the rotor. The rotational speed is the first excitation frequency, usually referred to as 1P. The structure can experience an excitation at this frequency due to any unbalance in the rotor. The second excitation frequency is the rotor blade passing frequency:  $N_b P$  in which  $N_b$  is the number of rotor blades, i.e. for a turbine with two rotor blades the second excitation frequency is 2P and for a three bladed rotor it is 3P. The loads on the blade are temporarily changed as it is in passing the tower and therefore excite the structure. As harmonic rotor loads at multiples of the rotor speed can also excite the system's natural vibration

modes, the higher harmonics, 6P, 9P and so on, should be incorporated in the operational loads as well.

Most of the wind turbines can operate at variable speed, regularly ranging from 12 to 18 RPM, as a result the two excitations cover frequency bands instead of just two values, see Figure 2.1b.

### 2.2.2 Wind loads

Wind loads on a wind turbine depend on different aspects:

- Wind speed
- Wind shear coefficient
- Turbulence intensity
- Structure that is excited by the wind

SWP receives all the wind data for the area where the wind farm is installed for a certain time period. In general, the wind speed offshore is higher than the wind speed onshore. Furthermore, the wind speed is height dependent. How much the wind speed is changing in height depends on the wind shear coefficient which is based on the surface roughness of the area. The wind speed will vary in height a lot if the area has a high surface roughness, for example in cities as there is a lot of friction imposed by the surface that slows down the wind flow. However, the surface roughness at sea is very low, as a result the wind speed is less height dependent.

Wind fields in nature are time dependent and are never laminar and uniform. The mean wind speed is superimposed by temporal and spatial fluctuations of the wind speed at a specific location. These temporal and spatial fluctuations are defined as turbulence. The amount of turbulence is specified by the so-called turbulence intensity which is defined as the turbulence velocity fluctuation of the time varying wind speed divided by the mean wind speed. This turbulence intensity is generally larger for onshore sites than offshore sites, as a result the wind flow offshore is more stable.

If the wind climate is known, the loads on the offshore wind turbine can be determined. The largest wind loads are caught by the blades of the turbine, these loads consists of lift and drag forces. These forces are determined by the relative speed (difference between the wind speed and the speed of the blades) and the drag and lift coefficient. As the drag and lift coefficient are structure dependent, the wind loads on the OWT differ per OWT.

For more specific details how wind loads can be modeled, the reader is referred to [7, 14, 35].

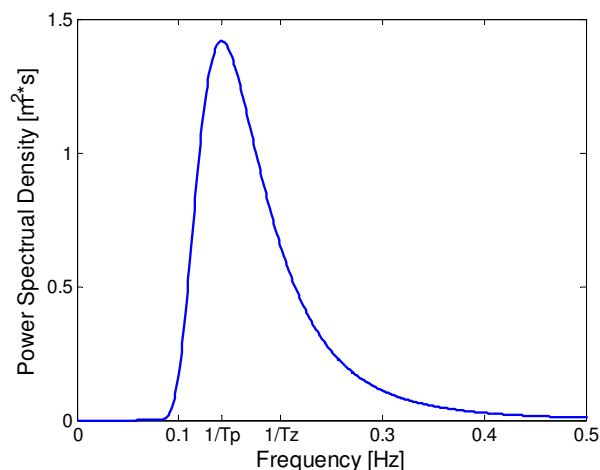
## 2.3 Wave and current loads

The main driver behind sea waves is wind. When examining the sea surface, multiple waves can be distinguished, traveling in every possible direction. The sea surface appears to be composed of random waves of various lengths and periods.

Wave loads depend on several aspects:

- Wave energy spectrum
- Wave kinematics
- Structure that is excited by the waves

The wave spectrum contains mainly high energy for low frequencies. The shape of the power spectral density spectrum is shown in Figure 2.2. Several methods have been defined to model this spectrum for a certain location in the sea. The maximum amplitude in the spectrum depends on the significant wave height  $H_s$ , which is defined as the mean of the 1/3 highest waves in the time series. The frequency where the peak occurs is defined as  $f_p$  or with its associated peak period  $T_p$ .



**Figure 2.2:** Wave spectrum for  $H_s=1.5$  m and  $f_p=0.14$  Hz [35].

The wave energy spectrum is used to determine the wave kinematics, using a linear or non-linear wave theory [4, 15]. The flow velocity of the wave at the surface is determined with this wave theory. In the end, the wave loads on the structure are computed based on these flow velocities of the wave. These wave loads depend, next to the flow velocity, on the geometry of the structure. For example, one can imagine that the wave loads for a monopile are larger than for a jacket, due to the larger frontal area of a monopile with respect to the more transparent jacket structure.

In addition to the wave induced loads, one can also distinguish current induced loads. Sea currents are mostly driven by the tides and ocean circulations. These current loads vary over the water depth. This variation over the water depth is based on the variation of the current flow velocity over water depth. Generally, three basic current profiles over depth are distinguished, see Figure 2.3. The flow velocity at a certain water depth is based on the flow velocity at the sea surface  $U_{c0}$ .

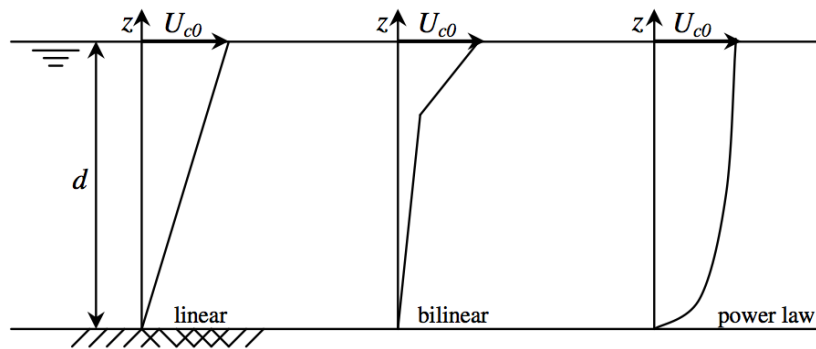


Figure 2.3: Current profiles over water depth [35].

For more extensive information about waves and current modeling the reader is referred to [23, 29].

## 2.4 Design considerations

The design of the OWT, and thus the support structure, should meet different design requirements. To avoid resonance, the first eigenfrequency of the structure should not be in the load spectrum of the external load. Next to this, the structure should withstand the maximum loads and furthermore, the fatigue lifetime of the structure should be between 20-25 years. All these requirements will be discussed in more detail in this section.

### 2.4.1 First eigenfrequency

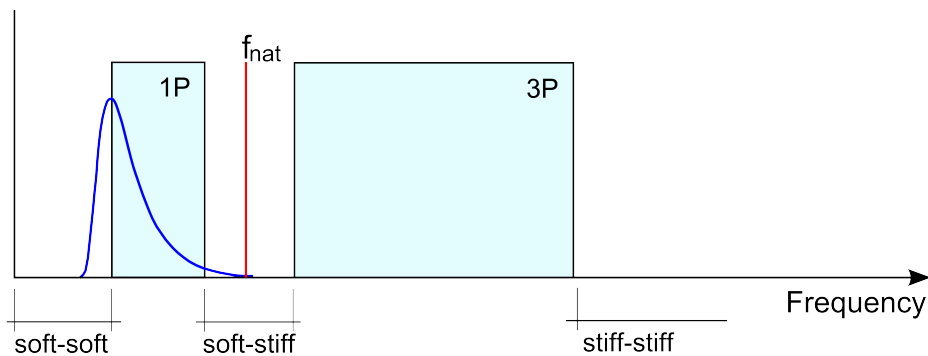


Figure 2.4: Frequency intervals for a variable speed wind turbine [17].

1st eigenfrequency OWT (red line) in soft-stiff region as resonance due to waves is avoided (blue line) and no excessive material is used.

In order to make sure that the structure is not excited in its eigenfrequency, the structure should be designed such that its first eigenfrequency does not coincide with either 1P or 3P. In case of a variable speed wind turbine, the operational excitations cover frequency bands instead of just two values, see Figure 2.4. This leaves three possible intervals. A very stiff structure, with a natural frequency greater than 3P (stiff-stiff), a natural frequency between 1P and 3P (soft-stiff) and a very soft structure with a natural frequency less than 1P (soft-soft).

When the OWT has its first eigenfrequency in the stiff-stiff region, the structure is very stiff and presumably needlessly expensive due to excessive material usage. When the structure is designed with the first eigenfrequency in the soft-soft region, resonance may occur due to excitation of waves, see blue line in Figure 2.4. Hence, the first eigenfrequency of an offshore wind turbine is designed such that it is in the soft-stiff region. This way resonance due to waves is avoided and the structure is not unnecessarily stiff and expensive.

### 2.4.2 Ultimate Limit State (ULS)

To satisfy the ultimate limit state, the structure must not collapse when subjected to the peak design load for which it was designed. A structure is deemed to satisfy the ultimate limit state criterion if all bending, shear and tensile or compressive stresses are below the yield stress [17], see Figure 2.5. This way the structure is only deforming elastically and not plastically. The maximum stress should be extracted from the simulation data to check whether this stress is below the yield stress.

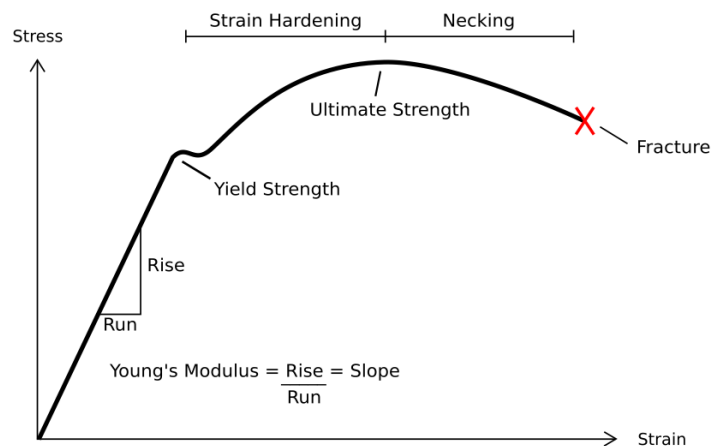


Figure 2.5: Stress strain graph [2].

### 2.4.3 Fatigue Limit State (FLS)

In material science, fatigue is the damage that occurs when a structure is subjected to repeated loading and unloading. The maximum stresses in the structure are below the ultimate stress limit, and may be below the yield stress of the material. If a structure is subjected to cyclic loading, the stresses in the material continuously change. Microscopic cracks appear in the material due to these stress changes and the material could break eventually [35].

As an offshore wind turbine is subjected to cyclic loading, because wave and wind loads vary in time, fatigue is an important design criteria. The fatigue lifetime of an OWT should be between 20-25 years. This subsection gives an overview how the fatigue design criteria can be checked.

The fatigue damage and lifetime can be estimated by different methods. One of the methods to compute the fatigue lifetime is using S-N curves, which are also known as *Wohler's curves* [17]. In these curves the stress amplitude is plotted versus the logarithm number of cycles which provides information about the maximum number of cycles per stress amplitude. In order to use the S-N curve it is thus necessary to rearrange a random stress signal into the number of cycles for each

stress amplitude. Different methods are developed to do this rearrangement, for instance *Rainflow* counting. In the end, using the stress amplitudes with its associated number of cycles and the S-N curve, the fatigue damage of the structure can be computed with the *Palmgren-Miner* rule. The Palmgren-Miner rule can be formulated as follows

$$D = \sum \frac{n_i}{N_i} \quad (2.1)$$

where  $D$  is the damage due to fatigue,  $n_i$  is number of cycles for a specific stress amplitude and  $N_i$  is the allowed number of cycles for that specific stress amplitude based on the S-N curve. The total damage is the summation of all the damages for all stress levels. To prevent failure this summation should be smaller than one.

### Rainflow counting method

In order to use the S-N curve it is necessary to know the number of cycles per stress amplitude. An offshore wind turbine is subjected to wave and wind loads with different excitation frequencies, therefore the stress signal will be random. This signal should be rearranged to obtain the number of cycles per stress amplitude. This can be done with the rainflow counting algorithm. The rainflow counting algorithm was developed by Tatsuo Endo and M. Matsuishi in 1968 [22]. Although there are a number of different cycle-counting algorithms for such applications, the rainflow method is the most popular. The method will be explained based on an example.

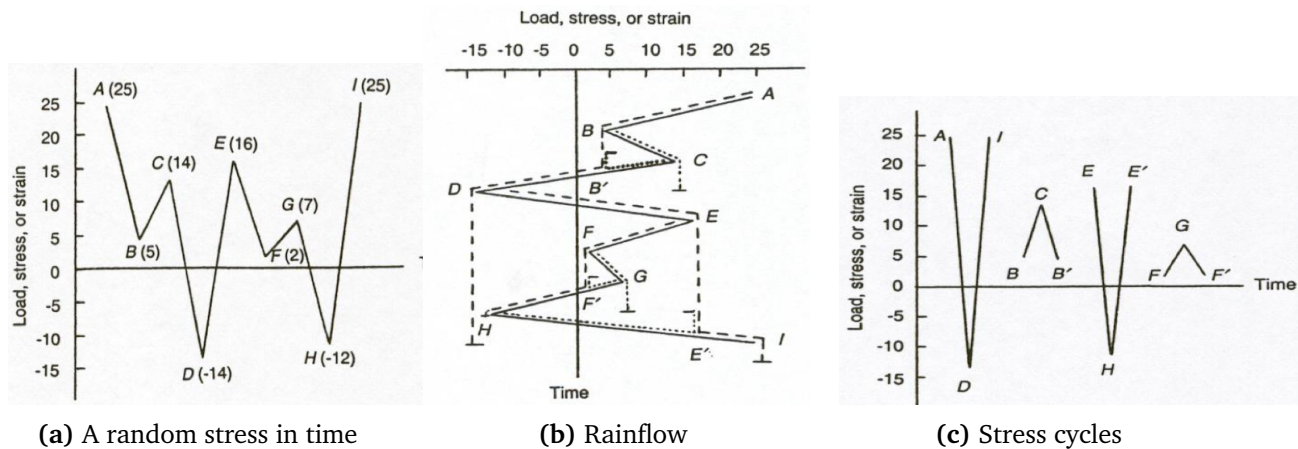


Figure 2.6: Rainflow counting method [22].

The peaks and troughs of the random stress signal should be labeled with a letter, see Figure 2.6a. Then the sheet can be turned clockwise  $90^\circ$ , as a result the peaks and troughs may now be considered as rooftops, Figure 2.6b. The random stress signal can be rearranged into a number of cycles per stress amplitude by imagining a raindrop flows down the roof starting at every peak or trough. The number of half-cycles should be counted by looking for terminations in the flow. The magnitude of each half-cycle is equal to the stress difference between its start and termination. Finally, the half-cycles with similar magnitudes should be combined to count the number of complete cycles, Figure 2.6c. Typically, there remain some half-cycles [5].



### Fatigue life computation

If the number of cycles are known at a certain stress level, the fatigue life can be computed with the S-N curve and the Palmgren-Miner rule.

$$\sigma_a = \frac{\sigma_{max} - \sigma_{min}}{2} \quad (2.2)$$

$$\sigma_m = \frac{\sigma_{max} + \sigma_{min}}{2} \quad (2.3)$$

The mean stress  $\sigma_m$  is the average level of a constant amplitude cyclic loading and the stress amplitude  $\sigma_a$  is the variation about this mean. The wind load has a certain mean value and to take this resulting mean stress into account when computing the fatigue damage there are several methods [10].

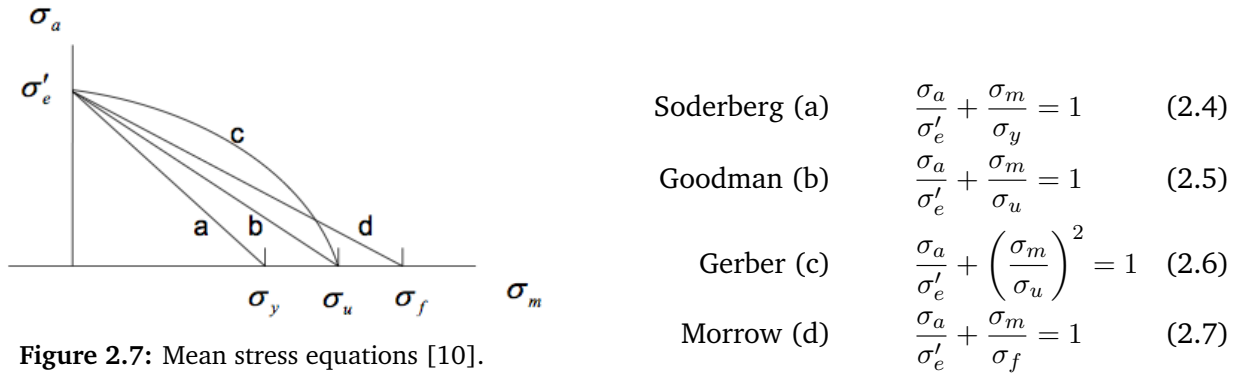


Figure 2.7: Mean stress equations [10].

$\sigma_y$  is the yield stress,  $\sigma_u$  is the ultimate stress,  $\sigma_f$  is the true fracture stress and  $\sigma'_e$  is the effective alternating stress at failure for a life time of  $N_f$  cycles. In order to take the mean stress into account when computing the fatigue damage,  $\sigma'_e$  should be determined.

The Goodman method and the Morrow method are the most widely used methods to take the mean stress into account. However, the Morrow method is a good method to take the mean stress into account for steel structures [10].

The rainflow counting method computes the mean stress  $\sigma_m$ , the stress amplitude  $\sigma_a$  and the number of cycles for every stress amplitude  $n_i$ .  $\sigma'_e$  can be computed with equation (2.7). When  $\sigma'_e$  is known, the fatigue life can be computed with help of the S-N curve.

The S-N curve is material specific and consists of several lines, Figure 2.8. The correct line for a particular structure depends on the type of connections or the way the structure is fabricated. Line 71 can be used for the wind turbine, as this line can be used for 'Butt-welded end-to-end connections between circular structural hollow sections' and 'Tube socket joint with 80% full penetration butt welds' [3]. The first one is the connection between the different tubes welded to each other and the second one is the way the transition piece is fabricated. In order to compute the maximum number of cycles per stress level, the following formula is used [3]:

$$(\sigma'_e)^m N = (\sigma_c)^m 2 \cdot 10^6 \quad \text{with } m=3 \text{ for } N \leq 5 \cdot 10^6 \quad (2.8)$$

$$N = 2 \cdot 10^6 \left(\frac{\sigma_c}{\sigma'_e}\right)^m \quad (2.9)$$

The slope  $m$  is three and  $\sigma_c$  is the endurance limit and is equal to  $71 \cdot 10^6$  Pa. The fatigue damage of

the structure is computed for a certain time period  $T_0$ , using the Palmgren-Miner rule

$$D = \sum \frac{n_i}{N_i} = \sum \frac{n_i}{2 \cdot 10^6} \left( \frac{\sigma'_e}{\sigma_c} \right)^m \tag{2.10}$$

Finally, the fatigue lifetime can be computed based on the fatigue damage and the time period  $T_0$ . The structure should be designed such that the fatigue life is between 20-25 years for offshore wind turbines.

$$T = \frac{T_0}{D} \tag{2.11}$$

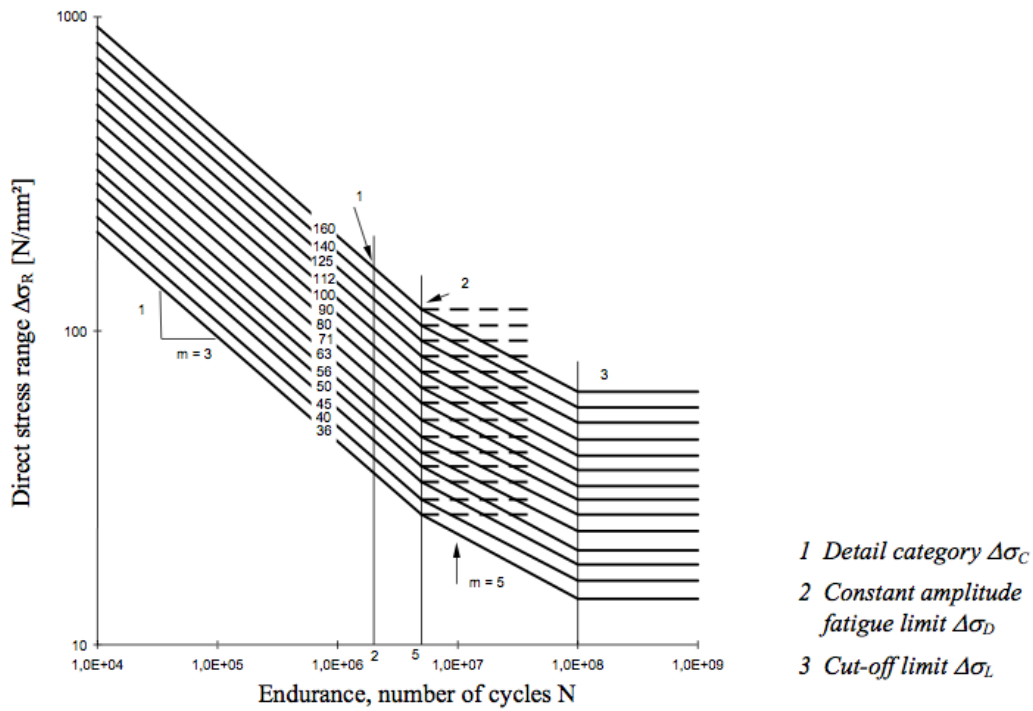


Figure 2.8: S-N curve steel [3].

## Chapter 3

# Theory of dynamics, substructuring and reduction methods

### 3.1 Introduction

In order to gain more insight in the accuracy of the different calculation procedures to design the support structure, the theory behind the different aspects that occur in the procedures will be presented in this chapter. First the basics of dynamics will be discussed and the difference between a quasi-static and a dynamic analysis will be explained. Section 3.3 will present the theory of substructuring. An offshore wind turbine consists of several components, substructures, and the response of a substructure can be obtained by analyzing either the complete model or just the substructure. The important aspects to perform an accurate analysis on the substructure will be discussed in this section. The chapter concludes with the explanation of different reduction techniques in Section 3.4. The foundation structure is often reduced when it is integrated in the aero-elastic model. The different reduction techniques will be discussed and this will give insight in the accuracy of the response of a reduced foundation structure.

### 3.2 Basic dynamics

The importance of proper modeling of the structural dynamics can be demonstrated with a single degree of freedom (DoF) mass-spring-damper system, see Figure 3.1. The complete offshore wind turbine system can be considered as a structure consisting of a number of coupled mass-spring-damper systems.

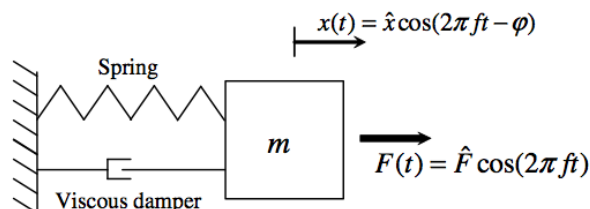
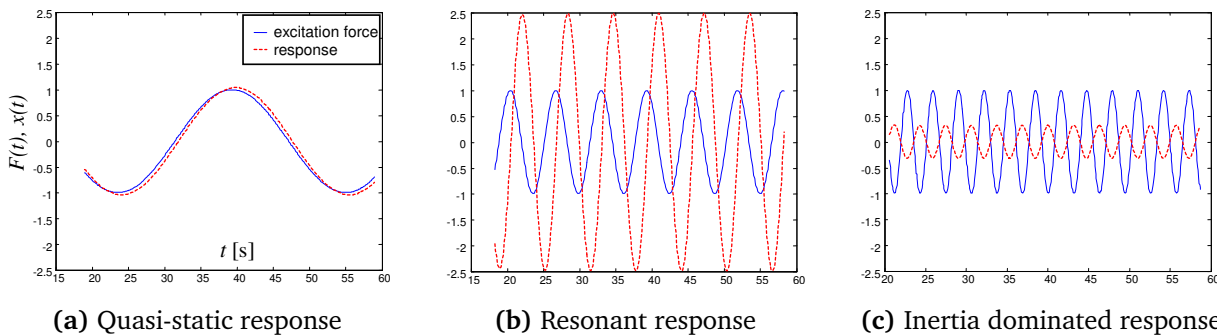


Figure 3.1: Single degree of freedom mass-spring-damper system [35].

### 3.2.1 Response of a structure

If a harmonic excitation force  $F(t)$ , i.e. a sinusoid, is applied to the mass, the magnitude and phase of the resulting displacement  $x$  strongly depends on the frequency of excitation  $f$ . Three response regions can be distinguished [35]:

- **Quasi-static** - the response is quasi-static if a structure is excited with a frequency well below the eigenfrequency of the system. The structure will displace as it is excited by a static force. In other words, the structure follows the time varying force almost instantaneously, presumably with a small phase lag, see Figure 3.2a.
- **Resonance** - The response is resonating if the structure is excited in its eigenfrequency, the elastic forces are cancelled by the inertia forces. As a result, the amplitude of the response will be a number of times larger than for the quasi-static response, see Figure 3.2b.
- **Inertia dominated** - the response is inertia dominated, if the structure is excited with a frequency well above the eigenfrequency, the mass cannot “follow” the movement any longer. The amplitude of an inertia dominated response is much smaller than for the quasi-static response. The inertia of the system dominates the response, see Figure 3.2c.

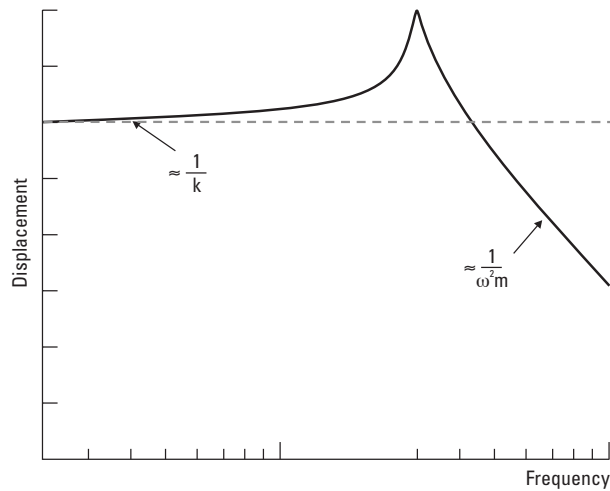


**Figure 3.2:** Different types of responses for different excitation frequencies [35]. Note that the stiffness is equal to one.

### 3.2.2 Frequency response function

Figure 3.2 shows that sinusoidal inputs applied to a linear system generate sinusoidal outputs of the same frequency, but differ in magnitude and phase. The magnitude of the response can be summarized in one plot: the frequency response function (FRF), see Figure 3.3. The FRF shows the amplitude ratio of the sinusoidal output to the input as a function of the excitation frequency.

For low excitation frequencies the FRF is horizontal and this horizontal part of the FRF is called the stiffness line. Hence, the amplitude of the response mainly depends on the stiffness of the structure in this frequency range and the response is quasi-static. The peak in the FRF plot corresponds to the eigenfrequency of the system. The height of the peak is determined by damping. Therefore, the response of the structure can be controlled with adequate damping if it is excited near its eigenfrequency. At higher frequencies the amplitude of the response is dominated by the inertia of the structure, this is the diagonal part of the line in the graph, also defined as the mass line.



**Figure 3.3:** Frequency Response Function [25].

The excitation frequency of the force is at least as important as its magnitude in dynamics. If dynamics is expected to be a problem for a structure, detailed knowledge of the expected excitation frequencies of the forces and the eigenfrequencies of the structure, or substructure, is important.

If a quasi-static analysis is performed, the static response is computed for the time varying force. The amplitude of the response depends on the stiffness of the structure, the damping and inertia forces are neglected. As the elastic forces do not depend on the excitation frequency, the amplitude of the FRF is constant for all frequencies. The dashed line in Figure 3.3 shows the FRF for a quasi-static computation. It shows that a quasi-static analysis will under- and overestimate the exact response for some excitation frequencies. Hence, the accuracy of a quasi-static analysis depends on the excitation frequency of the external force. If the structure is excited at frequency well below the eigenfrequency, the response will be quasi-static and a quasi-static analysis will provide an accurate result. On the other hand, if the structure is excited near its eigenfrequency, the structure will resonate in reality, but the quasi-static analysis neglects the damping and inertia forces and as a result it underestimates the exact response. Furthermore, if the structure is excited at a frequency well above the eigenfrequency, the exact response is inertia dominated and as the inertia forces are neglected in the quasi-static analysis, the response overestimates the exact response.

### 3.3 Substructuring

Dynamic substructuring (DS) is an important and well known method in the field of structural dynamics. DS consists of three steps:

1. Divide complete structure into various components, defined as *substructures*.
2. Define a reduction matrix  $\mathbf{R}^{(s)}$  for every substructure that retains the interface(s) DoF.
3. Assemble the substructures to construct the complete reduced model by assembling the interface(s) DoF of the different substructures.

It allows the evaluation of structures that would otherwise be too large and/or complex to be simulated or measured as a whole. For example the computation costs for analyzing a complete offshore

wind turbine as a whole would be very high. After analyzing the reduced complete OWT model, the detailed substructures can be analyzed per component to retrieve the detailed response. Additional advantages of DS are that local dynamic behavior and its influence on the global behavior can be determined more easily and substructuring allows sharing and combining of substructures from different project groups [34].

Dynamic substructuring is used in the design cycle of the support structure. The complex complete OWT model is analyzed in a reduced form to gain insight in the global dynamic behavior. Furthermore, applying interface loads or displacements to the top of the foundation structure is like decoupling the complete structure and analyzing the substructure. This section will explain how substructures should be assembled to obtain the response of the complete structure and what the important aspects are in order to analyze the substructures per component.

### 3.3.1 Assembly of substructures

Two conditions must be satisfied when substructures are assembled:

1. **Compatibility condition** - Interface displacements of the substructures must be compatible, so the displacements of both sets of interface DoF must be the same.
2. **Equilibrium condition** - The forces connecting the substructures' interface DoF must be in equilibrium, so opposite in direction and equal in magnitude.

The equation of motion for substructure  $s$  in the total structure is given as

$$\mathbf{M}^{(s)}\ddot{\mathbf{u}}^{(s)} + \mathbf{C}^{(s)}\dot{\mathbf{u}}^{(s)} + \mathbf{K}^{(s)}\mathbf{u}^{(s)} = \mathbf{f}^{(s)} + \mathbf{g}^{(s)} \quad (3.1)$$

where  $\mathbf{M}^{(s)}$  is the mass matrix of the substructure,  $\mathbf{C}^{(s)}$  the damping matrix and  $\mathbf{K}^{(s)}$  the stiffness matrix,  $\mathbf{f}^{(s)}$  is the force vector containing the external forces acting on the substructure and  $\mathbf{g}^{(s)}$  is the force vector containing the interface forces resulting from the neighboring substructures. The time dependence of the response, the external and interface forces are omitted for compactness.

The equation of motion of  $n$  substructures, that have to be coupled, can be rewritten in a block-diagonal format as

$$\mathbf{M}\ddot{\mathbf{u}} + \mathbf{C}\dot{\mathbf{u}} + \mathbf{K}\mathbf{u} = \mathbf{f} + \mathbf{g} \quad (3.2)$$

with

$$\begin{aligned} \mathbf{M} &\triangleq \text{diag}(\mathbf{M}^{(1)}, \dots, \mathbf{M}^{(n)}) = \begin{bmatrix} \mathbf{M}^{(1)} & & \\ & \ddots & \\ & & \mathbf{M}^{(n)} \end{bmatrix} \\ \mathbf{C} &\triangleq \text{diag}(\mathbf{C}^{(1)}, \dots, \mathbf{C}^{(n)}) \\ \mathbf{K} &\triangleq \text{diag}(\mathbf{K}^{(1)}, \dots, \mathbf{K}^{(n)}) \\ \mathbf{u} &\triangleq \begin{bmatrix} \mathbf{u}^{(1)} \\ \vdots \\ \mathbf{u}^{(n)} \end{bmatrix}, \quad \mathbf{f} \triangleq \begin{bmatrix} \mathbf{f}^{(1)} \\ \vdots \\ \mathbf{f}^{(n)} \end{bmatrix}, \quad \mathbf{g} \triangleq \begin{bmatrix} \mathbf{g}^{(1)} \\ \vdots \\ \mathbf{g}^{(n)} \end{bmatrix} \end{aligned}$$

The compatibility condition is expressed by

$$\mathbf{B}\mathbf{u} = \mathbf{0} \quad (3.3)$$

Every compatibility condition corresponds to a line in the Boolean matrix  $\mathbf{B}$ .  $\mathbf{B}$  operates on the interface DoF and if the interface DoF are matching,  $\mathbf{B}$  is a signed Boolean matrix. If  $\mathbf{B}$  is a signed Boolean matrix, the compatibility condition states that any pair of matching interface DoF must have the same displacement [19].

The equilibrium condition is expressed by

$$\mathbf{L}^T \mathbf{g} = \mathbf{0} \quad (3.4)$$

where the matrix  $\mathbf{L}$  is a Boolean matrix localizing the interface DoF of the substructures in the global dual set of DoF. The expression states that when the dual connection forces are summed, their resultant must be zero. It can be shown that  $\mathbf{B}$  and  $\mathbf{L}$  are in the null space of each other [19].

### 3.3.2 Assembly in the time domain

Two assembly methods can be distinguished to assemble the different substructures, the primal and the dual assembly method. The primal assembly method will be used in the further research of this thesis and, therefore, will be presented in this subsection. For information about the dual assembly method, the reader is referred to [37].

In a primal assembly a unique set of interface DoF is defined. Each substructure in equation (3.2) has its separated equation of motion and its own degrees of freedom. As each substructure has a number of boundary DoF, some DoF have multiple entries in vector  $\mathbf{u}$ . From vector  $\mathbf{u}$  a set of unique DoF  $\mathbf{q}$  can be determined [34].

$$\mathbf{u} = \mathbf{L}\mathbf{q} \quad (3.5)$$

Substituting this equation in the compatibility condition, equation (3.3) becomes

$$\mathbf{B}\mathbf{u} = \mathbf{B}\mathbf{L}\mathbf{q} = \mathbf{0} \quad (3.6)$$

As  $\mathbf{B}$  and  $\mathbf{L}$  are in each others null space, the compatibility condition is satisfied for any set of  $\mathbf{q}$ . The system can now be described as

$$\begin{cases} \mathbf{M}\mathbf{L}\ddot{\mathbf{q}} + \mathbf{C}\mathbf{L}\dot{\mathbf{q}} + \mathbf{K}\mathbf{L}\mathbf{q} = \mathbf{f} + \mathbf{g} \\ \mathbf{L}^T \mathbf{g} = \mathbf{0} \end{cases} \quad (3.7)$$

Premultiplication of the equation by  $\mathbf{L}^T$  and noting that according to the equilibrium condition  $\mathbf{L}^T \mathbf{g}$  is equal to zero, the primal assembled system reduces to

$$\check{\mathbf{M}}\ddot{\mathbf{q}} + \check{\mathbf{C}}\dot{\mathbf{q}} + \check{\mathbf{K}}\mathbf{q} = \check{\mathbf{f}} \quad (3.8)$$

where

$$\begin{cases} \check{\mathbf{M}} = \mathbf{L}^T \mathbf{M} \mathbf{L} \\ \check{\mathbf{C}} = \mathbf{L}^T \mathbf{C} \mathbf{L} \\ \check{\mathbf{K}} = \mathbf{L}^T \mathbf{K} \mathbf{L} \\ \check{\mathbf{f}} = \mathbf{L}^T \mathbf{f} \end{cases} \quad (3.9)$$

The matrices  $\mathbf{M}$ ,  $\mathbf{C}$  and  $\mathbf{K}$  are the uncoupled block diagonal mass, damping and stiffness matrices.  $\check{\mathbf{M}}$ ,  $\check{\mathbf{C}}$  and  $\check{\mathbf{K}}$  are the assembled block diagonal mass, damping and stiffness matrices and thus form the equation of motion of the assembled structure.

### 3.3.3 Assembly in the frequency domain

The equation of motion written in the frequency domain can be obtained by the Fourier transform of the equation of motion in the time domain.

$$(-\omega^2 \mathbf{M} + j\omega \mathbf{C} + \mathbf{K})\mathbf{u}(\omega) = \mathbf{f}(\omega) + \mathbf{g}(\omega) \quad (3.10)$$

$$\mathbf{Z}(\omega) = -\omega^2 \mathbf{M} + j\omega \mathbf{C} + \mathbf{K} \quad (3.11)$$

where  $\mathbf{Z}(\omega)$  is the (uncoupled block diagonal) dynamic stiffness matrix.

Similar to the primal assembly method in the time domain a set of unique DoF  $\mathbf{q}$  is chosen

$$\mathbf{u}(\omega) = \mathbf{L}\mathbf{q}(\omega) \quad (3.12)$$

As a result, the compatibility condition is automatically satisfied,  $\mathbf{B}\mathbf{L}\mathbf{u}(\omega) = \mathbf{0}$ . By premultiplying the set of equations by  $\mathbf{L}^T$ , the primal assembled system is obtained

$$\check{\mathbf{Z}}(\omega)\mathbf{q}(\omega) = \check{\mathbf{f}}(\omega) \quad (3.13)$$

where

$$\begin{cases} \check{\mathbf{Z}}(\omega) = \mathbf{L}^T \mathbf{Z}(\omega) \mathbf{L} \\ \check{\mathbf{f}}(\omega) = \mathbf{L}^T \mathbf{f}(\omega) \end{cases} \quad (3.14)$$

## 3.4 Reduction methods

Detailed Finite Element (FE) models are often used to compute stress concentrations in the offshore wind turbine. These models can have more than thousands of degrees of freedom. Solving dynamic problems with these detailed models will result in very large computation costs. However, the dynamic behavior can be well approximated using a coarser mesh. As creating a new, coarser mesh, model is time-consuming, a more efficient solution is to reduce the detailed mathematical model by model reduction techniques [28, 37].

Model reduction consists of replacing the large number of DoF of the detailed FE model into a much smaller set of generalized DoF. The dynamic response of the reduced model is expressed in terms of a limited number of deformation shapes and associated amplitudes.

To capture the global dynamic behavior of the OWT model, several components are reduced to limit computation costs. Different reduction techniques will be discussed in this section in order to get more insight which reduction methods will suit best for the OWT model to retrieve the correct dynamic behavior.

### 3.4.1 Reduction basis

Equation (3.1) presented the equation of motion for a substructure  $s$  and is here repeated.

$$\mathbf{M}^{(s)}\ddot{\mathbf{u}}^{(s)} + \mathbf{C}^{(s)}\dot{\mathbf{u}}^{(s)} + \mathbf{K}^{(s)}\mathbf{u}^{(s)} = \mathbf{f}^{(s)} + \mathbf{g}^{(s)} \quad (3.15)$$

If the substructure is reduced, a set of generalized DoF  $\mathbf{q}^{(s)}$  is determined

$$\mathbf{u}^{(s)} = \mathbf{R}^{(s)}\mathbf{q}^{(s)} \quad (3.16)$$



where  $\mathbf{R}^{(s)}$  represents the reduction basis. Using equation (3.16), the equation of motion becomes

$$\mathbf{M}^{(s)}\mathbf{R}^{(s)}\ddot{\mathbf{q}}^{(s)} + \mathbf{C}^{(s)}\mathbf{R}^{(s)}\dot{\mathbf{q}}^{(s)} + \mathbf{K}^{(s)}\mathbf{R}^{(s)}\mathbf{q}^{(s)} = \mathbf{f}^{(s)} + \mathbf{g}^{(s)} + \mathbf{r}^{(s)} \quad (3.17)$$

An error  $\mathbf{r}^{(s)}$  is introduced, since the new set of DoF does not span the full solution space. It is an approximation of the exact solution. Furthermore, it is stated that the error only exists in the space outside the reduction basis. This means that the residual force does not produce any work on the modes contained in matrix  $\mathbf{R}^{(s)}$ . This orthogonalization is realized by premultiplying by  $\mathbf{R}^{(s)T}$  [28, 34].

$$\mathbf{R}^{(s)T}\mathbf{r}^{(s)} = \mathbf{0} \quad (3.18)$$

$$\tilde{\mathbf{M}}^{(s)}\ddot{\mathbf{q}}^{(s)} + \tilde{\mathbf{C}}^{(s)}\dot{\mathbf{q}}^{(s)} + \tilde{\mathbf{K}}^{(s)}\mathbf{q}^{(s)} = \tilde{\mathbf{f}}^{(s)} + \tilde{\mathbf{g}}^{(s)} \quad (3.19)$$

where

$$\begin{cases} \tilde{\mathbf{M}}^{(s)} = \mathbf{R}^{(s)T}\mathbf{M}^{(s)}\mathbf{R}^{(s)} \\ \tilde{\mathbf{C}}^{(s)} = \mathbf{R}^{(s)T}\mathbf{C}^{(s)}\mathbf{R}^{(s)} \\ \tilde{\mathbf{K}}^{(s)} = \mathbf{R}^{(s)T}\mathbf{K}^{(s)}\mathbf{R}^{(s)} \\ \tilde{\mathbf{f}}^{(s)} = \mathbf{R}^{(s)T}\mathbf{f}^{(s)} \\ \tilde{\mathbf{g}}^{(s)} = \mathbf{R}^{(s)T}\mathbf{g}^{(s)} \end{cases} \quad (3.20)$$

All kinds of ‘modes’ can be used to create a reduction basis, such as exact eigenmodes, approximated modes, static modes, interface modes, etcetera. In general, a basis is built from a set of vibration modes, which contain information of the dynamic behavior of the structure, and a set of static modes, representing the static behavior. The different modes will be derived for a substructure without damping, the superscript  $^{(s)}$  is dropped for compactness.

$$\mathbf{M}\ddot{\mathbf{u}} + \mathbf{K}\mathbf{u} = \mathbf{f} + \mathbf{g} \quad (3.21)$$

### Free vibration modes

Free vibration modes are the natural vibration shapes of the substructure if the interface DoF are unconstrained. These modes are the fundamental properties of the substructure and are obtained by solving the free vibration eigenvalue problem [24, 34]:

$$(\mathbf{K} - \omega_n^2\mathbf{M})\phi_{f,n} = \mathbf{0} \quad (3.22)$$

$\phi_{f,n}$  is the  $n^{\text{th}}$  free vibration mode with its associated nonzero eigenfrequency  $\omega_n^2$ . A free vibration mode can be seen as an elastic deformation shape where the elastic forces are in equilibrium with the inertia forces,  $\Phi_f$  denotes a (reduced) set of these modes.

### Rigid body modes

If the substructure is not fully constrained by boundary conditions, a number of rigid body modes exists. Rigid body modes represent displacements of a structure without deformations, with a zero eigenfrequency, it displaces as a rigid body.

$$\mathbf{K}\Phi_r = \mathbf{0} \quad (3.23)$$

where  $\Phi_r$  represents a matrix having the rigid body modes as its columns. For a free floating structure these modes represent its global translations and rotations, or a linear combination of both. The number of rigid body modes is equal to the rank of the null space of the stiffness matrix [24, 34].

### Static constraint modes

Static constraint modes represent the static response of the internal DoF to a unit displacement at one of the interface DoF, the other interface DoF remain restrained, and no forces are applied to the internal DoF.

The set of constraint modes thus contains the static response to applied interface displacements. The computation of the constraint modes starts with splitting the DoF into boundary DoF  $\mathbf{u}_b$  and internal DoF  $\mathbf{u}_i$ , the equation of motion becomes

$$\begin{bmatrix} \mathbf{M}_{bb} & \mathbf{M}_{bi} \\ \mathbf{M}_{ib} & \mathbf{M}_{ii} \end{bmatrix} \begin{bmatrix} \ddot{\mathbf{u}}_b \\ \ddot{\mathbf{u}}_i \end{bmatrix} + \begin{bmatrix} \mathbf{K}_{bb} & \mathbf{K}_{bi} \\ \mathbf{K}_{ib} & \mathbf{K}_{ii} \end{bmatrix} \begin{bmatrix} \mathbf{u}_b \\ \mathbf{u}_i \end{bmatrix} = \begin{bmatrix} \mathbf{f}_b \\ \mathbf{f}_i \end{bmatrix} + \begin{bmatrix} \mathbf{g}_b \\ \mathbf{0} \end{bmatrix} \quad (3.24)$$

If one now assumes no external excitation acting on the internal DoF ( $\mathbf{f}_i = \mathbf{0}$ ). The bottom line of equation (3.25) reduces to

$$\mathbf{M}_{ib}\ddot{\mathbf{u}}_b + \mathbf{M}_{ii}\ddot{\mathbf{u}}_i + \mathbf{K}_{ib}\mathbf{u}_b + \mathbf{K}_{ii}\mathbf{u}_i = \mathbf{0} \quad (3.25)$$

The response of the internal DoF can be split up into a static and a dynamic part

$$\mathbf{u}_i = \mathbf{u}_{i,stat} + \mathbf{u}_{i,dyn} \quad (3.26)$$

When the inertia forces are neglected, the static part of the response can be obtained

$$\mathbf{u}_{i,stat} = -\mathbf{K}_{ii}^{-1}\mathbf{K}_{ib}\mathbf{u}_b \quad (3.27)$$

where  $-\mathbf{K}_{ii}^{-1}\mathbf{K}_{ib}$  is the static condensation matrix which columns contain the so-called *static constraint modes* which represent the static response of  $\mathbf{u}_i$  for unit displacements at  $\mathbf{u}_b$ . By neglecting the dynamic response of the internal DoF  $\mathbf{u}_{i,dyn}$  the DoF of the system can be replaced by

$$\begin{bmatrix} \mathbf{u}_b \\ \mathbf{u}_i \end{bmatrix} = \begin{bmatrix} \mathbf{I} \\ -\mathbf{K}_{ii}^{-1}\mathbf{K}_{ib} \end{bmatrix} \mathbf{u}_b = \mathbf{\Psi}_C \mathbf{u}_b \quad (3.28)$$

where the static constraint modes are added in  $\mathbf{\Psi}_C$ . The static response of the substructure to an excitation at the interface DoF is merely a combination or superposition of the static constraint modes and can therefore be computed exactly [24].

### Fixed interface vibration modes

The static constraint modes only describe the static response of the internal DoF. To capture the dynamic response of the internal DoF the fixed interface vibration modes can be used. These modes represent the natural vibration shapes of the structure when the interfaces are fixed and no forces are applied to the internal DoF.

If it is assumed that  $\mathbf{f}_i = \mathbf{0}$  and the interface DoF are constrained,  $\mathbf{u}_b = \mathbf{0}$ , equation (3.25) reduces to

$$\mathbf{M}_{ii}\ddot{\mathbf{u}}_i + \mathbf{K}_{ii}\mathbf{u}_i = \mathbf{0} \quad (3.29)$$

The solution for the internal DoF can be obtained from the eigenvalue problem.

$$(\mathbf{K}_{ii} - \omega_{i,n}^2 \mathbf{M}_{ii})\phi_{i,n} = \mathbf{0} \quad (3.30)$$

The result is a set of eigenmodes and eigenfrequencies of the substructure constrained at its boundary DoF. A fixed interface vibration mode will be denoted by  $\phi_i$  and a set of fixed interface vibration modes by  $\mathbf{\Phi}_i$  [24, 34].

### 3.4.2 Guyan reduction

The Guyan reduction method uses a reduction basis containing only the static constraint modes [16, 24], which were discussed in Section 3.4.1. The system's response can be constructed using

$$\begin{bmatrix} \mathbf{u}_b \\ \mathbf{u}_i \end{bmatrix} = \begin{bmatrix} \mathbf{I} \\ -\mathbf{K}_{ii}^{-1}\mathbf{K}_{ib} \end{bmatrix} \mathbf{u}_b = \mathbf{R}_G \mathbf{u}_b \quad (3.31)$$

Where  $\mathbf{R}_G$  is the reduction basis for the Guyan reduction method, note that  $\mathbf{R}_G = \mathbf{\Psi}_C$ . The reduced system becomes

$$\tilde{\mathbf{M}}\ddot{\mathbf{u}}_b + \tilde{\mathbf{K}}\mathbf{u}_b = \tilde{\mathbf{f}} \quad (3.32)$$

where

$$\begin{cases} \tilde{\mathbf{K}} = \mathbf{R}_G^T \mathbf{K} \mathbf{R}_G = \mathbf{K}_{bb} - \mathbf{K}_{bi} \mathbf{K}_{ii}^{-1} \mathbf{K}_{ib} \\ \tilde{\mathbf{M}} = \mathbf{R}_G^T \mathbf{M} \mathbf{R}_G = \mathbf{M}_{bb} - \mathbf{M}_{bi} \mathbf{K}_{ii}^{-1} \mathbf{K}_{ib} - \mathbf{K}_{bi} \mathbf{K}_{ii}^{-1} \mathbf{M}_{ib} + \mathbf{K}_{bi} \mathbf{K}_{ii}^{-1} \mathbf{M}_{ii} \mathbf{K}_{ii}^{-1} \mathbf{K}_{ib} \\ \tilde{\mathbf{f}} = \mathbf{R}_G^T \mathbf{f} \end{cases} \quad (3.33)$$

If the static condensation algorithm is applied to static problems, the exact solution is obtained if a force is only applied on the interface DoF  $\mathbf{u}_b$ . If the static condensation algorithm is applied to dynamic problems, an approximate solution is found. The dynamic response of the internal DoF of the substructure is neglected and it is assumed that all internal DoF respond quasi-statically to the interface displacements. The validity of the condensation algorithm thus depends on the extent to which correction  $\mathbf{u}_{i,dyn}$  is negligible. The static condensation technique is valid if

$$\omega^2 \ll \mu_1^2 \quad (3.34)$$

where  $\omega$  is the highest eigenfrequency that one wants to compute for the complete structure and  $\mu_1$  is the first eigenfrequency of the structure when  $\mathbf{u}_b$  are constrained [28].

### 3.4.3 Craig-Bampton method

The Craig-Bampton method can be seen as an enrichment of the Guyan reduction. Instead of reducing with only static constraint modes, the Craig-Bampton method also includes internal vibrational information using fixed interface modes and thereby creates a more complete basis for the reduction. The Craig-Bampton method is one of the most well known and popular reduction methods [9, 24, 34].

In order to obtain the response of the internal DoF  $\mathbf{u}_i$ , the response is split up in a static and a dynamic part.

$$\mathbf{u}_i = \mathbf{u}_{i,stat} + \mathbf{u}_{i,dyn} \quad (3.35)$$

Where  $\mathbf{u}_{i,stat}$  is the static response to the interface displacements  $\mathbf{u}_b$  via the static constraint modes  $\mathbf{\Psi}_C$ . The dynamic response  $\mathbf{u}_{i,dyn}$  is now approximated using the fixed interface vibration modes  $\mathbf{\Phi}_i$ , where only a limited number of these modes are included in the reduction basis. As a result, the size of the Craig-Bampton reduced system matrices will be larger than the size of the Guyan reduced system matrices, the increase of the size of the reduced system matrices depends on the amount of fixed interface modes included.

The fixed interface modes are orthonormalized with respect to  $\mathbf{M}_{ii}$  and thus matrix  $\mathbf{\Phi}_i$  has the following properties:

$$\begin{aligned} \mathbf{\Phi}_i^T \mathbf{M}_{ii} \mathbf{\Phi}_i &= \mathbf{I} \\ \mathbf{\Phi}_i^T \mathbf{K}_{ii} \mathbf{\Phi}_i &= \text{diag}(\omega_1^2, \dots, \omega_k^2) = \mathbf{\Omega}_i^2 \end{aligned} \quad (3.36)$$

The response of the internal DoF  $\mathbf{u}_i$  is now given by

$$\mathbf{u}_i \approx \Psi_C \mathbf{u}_b + \Phi_i \boldsymbol{\eta}_i \quad (3.37)$$

The Craig-Bampton reduction matrix  $\mathbf{R}_{CB}$  can be built and the response of the system can be constructed using

$$\begin{bmatrix} \mathbf{u}_b \\ \mathbf{u}_i \end{bmatrix} \approx \begin{bmatrix} \mathbf{I} & \mathbf{0} \\ \Psi_{C,i} & \Phi_i \end{bmatrix} \begin{bmatrix} \mathbf{u}_b \\ \boldsymbol{\eta}_i \end{bmatrix} = \mathbf{R}_{CB} \begin{bmatrix} \mathbf{u}_b \\ \boldsymbol{\eta}_i \end{bmatrix} \quad (3.38)$$

Where the DoF of the reduced system are the interface DoF  $\mathbf{u}_b$  and the intensity parameters of the substructure fixed interface vibration modes  $\boldsymbol{\eta}_i$ . The reduced system becomes

$$\tilde{\mathbf{M}} \begin{bmatrix} \ddot{\mathbf{u}}_b \\ \ddot{\boldsymbol{\eta}}_i \end{bmatrix} + \tilde{\mathbf{K}} \begin{bmatrix} \mathbf{u}_b \\ \boldsymbol{\eta}_i \end{bmatrix} = \tilde{\mathbf{f}} \quad (3.39)$$

where

$$\begin{aligned} \tilde{\mathbf{K}} &= \mathbf{R}_{CB}^T \mathbf{K} \mathbf{R}_{CB} = \begin{bmatrix} \tilde{\mathbf{K}}_{bb} & \mathbf{0} \\ \mathbf{0} & \Omega_i^2 \end{bmatrix} \\ \tilde{\mathbf{K}}_{bb} &= \mathbf{K}_{bb} - \mathbf{K}_{bi} \mathbf{K}_{ii}^{-1} \mathbf{K}_{ib} \\ \tilde{\mathbf{M}} &= \mathbf{R}_{CB}^T \mathbf{M} \mathbf{R}_{CB} = \begin{bmatrix} \tilde{\mathbf{M}}_{bb} & \tilde{\mathbf{M}}_{b\eta} \\ \tilde{\mathbf{M}}_{\eta b} & \mathbf{I} \end{bmatrix} \\ \tilde{\mathbf{M}}_{bb} &= \mathbf{M}_{bb} - \mathbf{M}_{bi} \mathbf{K}_{ii}^{-1} \mathbf{K}_{ib} - \mathbf{K}_{bi} \mathbf{K}_{ii}^{-1} \mathbf{M}_{ib} + \mathbf{K}_{bi} \mathbf{K}_{ii}^{-1} \mathbf{M}_{ii} \mathbf{K}_{ii}^{-1} \mathbf{K}_{ib} \\ \tilde{\mathbf{M}}_{\eta b} &= \Phi_i^T (\mathbf{M}_{ib} - \mathbf{M}_{ii} \mathbf{K}_{ii}^{-1} \mathbf{K}_{ib}) = \tilde{\mathbf{M}}_{b\eta}^T \end{aligned} \quad (3.40)$$

#### 3.4.4 Augmented Craig-Bampton method

The approximated response made by the component reduction basis is accurate as long as the modes discarded in the reduction basis are not excited by the external loading. In general, it can be stated that the convergence of the approximation depends on:

- **Spectral convergence:** The frequency content of the excitation should not exceed that of the eigenfrequencies of the modes included in the reduction basis. This way, the excitation frequency is in the range of the frequencies of the included modes and the discarded modes will not be excited.
- **Spatial convergence:** The included modes should adequately represent the spatial distribution of the external loading. This is equivalent to stating that the discarded modes should be orthogonal to the external load.

This last aspect is often unnoted. One way to improve the spatial convergence is by including more modes in the reduction basis. The convergence rate depends on the correlation between the mode shapes and the spatial load vectors.

Several methods have been developed to improve the accuracy of the forced response of reduced models. A well known method, the mode acceleration (MA) method, can be used to improve this approximation of the response by adding the quasi-static response of the discarded modes. If the reduced model is spectrally converged, which means that the highest excitation frequency is lower than the discarded modes, it can be assumed that the response of the discarded modes will be static-like [24, 37].

An extension of the MA method is known to as the modal truncation augmentation (MTA) method. This method can be used to compute load dependent vectors (or pseudo-modes) which capture the spatial part of the forced response not captured by the modes that are included in the reduction basis. These load dependent vectors will account for an enrichment of the reduction basis.

A Craig-Bampton reduced model is able to accurately represent the response of the full model, as long as the loading is applied at the retained interface DoF. However, this is often not the case and large parts of structures can be subjected to external forces. For example, the foundation structure is excited by wave and current loads on a large part of the structure. One way to overcome this limitation of the Craig-Bampton reduction, is to use the MTA vectors to augment the Craig-Bampton reduction basis.

In order to efficiently compute a set of basis vectors that improve the spatial convergence, a representative set of force vectors is needed. Therefore it is assumed that the external loading  $\mathbf{f}$  can be represented by a spatial and temporal part.

$$\sum_{p=1}^g \mathbf{f}_p \alpha_p(t) = \mathbf{F} \boldsymbol{\alpha}(t) \quad (3.41)$$

Where  $\mathbf{f}_p$  is the  $p^{th}$  spatial force vector which is modulated by its corresponding time function  $\alpha_p(t)$ . The spatial force vectors can represent any type of loading and can be collected in the matrix  $\mathbf{F}$ . Since the aim is to improve the spatial convergence, only the force distribution in  $\mathbf{F}$  are taken into account and the time dependent part is discarded. One way to obtain the spatial force distributions is using *Proper Orthogonal Decomposition* (POD), this way one can calculate the principle components in a large set of data, further explanation is given in Appendix A.

The static response of the structure to these spatial force shapes are computed and the Craig-Bampton reduction basis is augmented with these pseudo modes, also defined as MTA vectors. Since the MTA vectors have to be orthogonalized with respect to the fixed interface vibration modes the projection matrix is defined as  $\mathbf{P} = \mathbf{I} - \Phi_i \Phi_i^T \mathbf{M}_{ii}$ . The MTA vectors can be computed using:

$$\tilde{\Phi}_{MTA} = \mathbf{P} \mathbf{K}_{ii}^{-1} \mathbf{F} \quad (3.42)$$

The MTA vectors can be orthonormalized with respect to each other by solving the following reduced eigenvalue problem, also known as the *interaction problem*:

$$(\tilde{\Phi}_{MTA}^T \mathbf{K}_{ii} \tilde{\Phi}_{MTA}) \mathbf{y} = \boldsymbol{\sigma}^2 (\tilde{\Phi}_{MTA}^T \mathbf{M}_{ii} \tilde{\Phi}_{MTA}) \mathbf{y} \quad (3.43)$$

Where  $\boldsymbol{\sigma}^2$  is a diagonal matrix containing the pseudo-frequencies of the MTA vectors and  $\mathbf{y}$  are the eigenvectors. The orthonormalized MTA vectors  $\Phi_{MTA}$  are subsequently calculated using:

$$\Phi_{MTA} = \tilde{\Phi}_{MTA} \mathbf{y} \quad (3.44)$$

Mass normalization can be enforced by requiring:

$$\Phi_{MTA}^T \mathbf{M}_{ii} \Phi_{MTA} = \mathbf{I} \quad (3.45)$$

Finally, after solving the interaction problem in equation (3.43) and mass normalize the MTA vectors (3.45), the internal DoF can now be approximated by

$$\mathbf{u}_i = \Psi_C \mathbf{u}_b + \Phi_i \boldsymbol{\eta}_i + \Phi_{MTA} \boldsymbol{\zeta} \quad (3.46)$$

The Augmented Craig-Bampton reduction matrix  $\mathbf{R}_{ACB}$  can be built and the response of the system can be constructed using

$$\begin{bmatrix} \mathbf{u}_b \\ \mathbf{u}_i \end{bmatrix} = \begin{bmatrix} \mathbf{I} & \mathbf{0} & \mathbf{0} \\ \Psi_C & \Phi_i & \Phi_{MTA} \end{bmatrix} \begin{bmatrix} \mathbf{u}_b \\ \boldsymbol{\eta}_i \\ \boldsymbol{\zeta} \end{bmatrix} = \mathbf{R}_{ACB} \begin{bmatrix} \mathbf{u}_b \\ \boldsymbol{\eta}_i \\ \boldsymbol{\zeta} \end{bmatrix} \quad (3.47)$$

The size of the reduction basis  $\mathbf{R}_{ACB}$  depends on the included static constraint modes, the number of fixed interface modes and the number of MTA vectors. The reduced system becomes

$$\tilde{\mathbf{M}} \begin{bmatrix} \mathbf{u}_b \\ \boldsymbol{\eta}_i \\ \boldsymbol{\zeta} \end{bmatrix} + \tilde{\mathbf{K}} \begin{bmatrix} \mathbf{u}_b \\ \boldsymbol{\eta}_i \\ \boldsymbol{\zeta} \end{bmatrix} = \tilde{\mathbf{f}} \quad (3.48)$$

where

$$\begin{aligned} \tilde{\mathbf{K}} &= \mathbf{R}_{ACB}^T \mathbf{K} \mathbf{R}_{ACB} = \begin{bmatrix} \tilde{\mathbf{K}}_{bb} & \mathbf{0} & \mathbf{0} \\ \mathbf{0} & \Omega_i^2 & \mathbf{0} \\ \mathbf{0} & \mathbf{0} & \sigma^2 \end{bmatrix} \\ \tilde{\mathbf{K}}_{bb} &= \mathbf{K}_{bb} - \mathbf{K}_{bi} \mathbf{K}_{ii}^{-1} \mathbf{K}_{ib} \\ \tilde{\mathbf{M}} &= \mathbf{R}_{ACB}^T \mathbf{M} \mathbf{R}_{ACB} = \begin{bmatrix} \tilde{\mathbf{M}}_{bb} & \tilde{\mathbf{M}}_{b\eta} & \tilde{\mathbf{M}}_{b\zeta} \\ \tilde{\mathbf{M}}_{\eta b} & \mathbf{I} & \mathbf{0} \\ \tilde{\mathbf{M}}_{\zeta b} & \mathbf{0} & \mathbf{I} \end{bmatrix} \\ \tilde{\mathbf{M}}_{bb} &= \mathbf{M}_{bb} - \mathbf{M}_{bi} \mathbf{K}_{ii}^{-1} \mathbf{K}_{ib} - \mathbf{K}_{bi} \mathbf{K}_{ii}^{-1} \mathbf{M}_{ib} + \mathbf{K}_{bi} \mathbf{K}_{ii}^{-1} \mathbf{M}_{ii} \mathbf{K}_{ii}^{-1} \mathbf{K}_{ib} \\ \tilde{\mathbf{M}}_{\eta b} &= \Phi_i^T (\mathbf{M}_{ib} - \mathbf{M}_{ii} \mathbf{K}_{ii}^{-1} \mathbf{K}_{ib}) = \tilde{\mathbf{M}}_{b\eta}^T \\ \tilde{\mathbf{M}}_{\zeta b} &= \Phi_{MTA}^T (\mathbf{M}_{ib} - \mathbf{M}_{ii} \mathbf{K}_{ii}^{-1} \mathbf{K}_{ib}) = \tilde{\mathbf{M}}_{b\zeta}^T \end{aligned} \quad (3.49)$$

# Chapter 4

## Calculation procedures

### 4.1 Introduction

Offshore wind turbines are highly dynamically responding structures. Therefore, consideration of the dynamic interaction of different structural components is essential in the design process of offshore wind turbine support structures. Subsection 1.3 presented the design cycle of the support structure which showed that two parties are responsible for the design of the support structure. The turbine manufacturer is responsible for the tower design and the foundation designer for the foundation and the transition piece. Different calculation procedures have been developed to determine the design of a support structure, where this design split is taken into account.

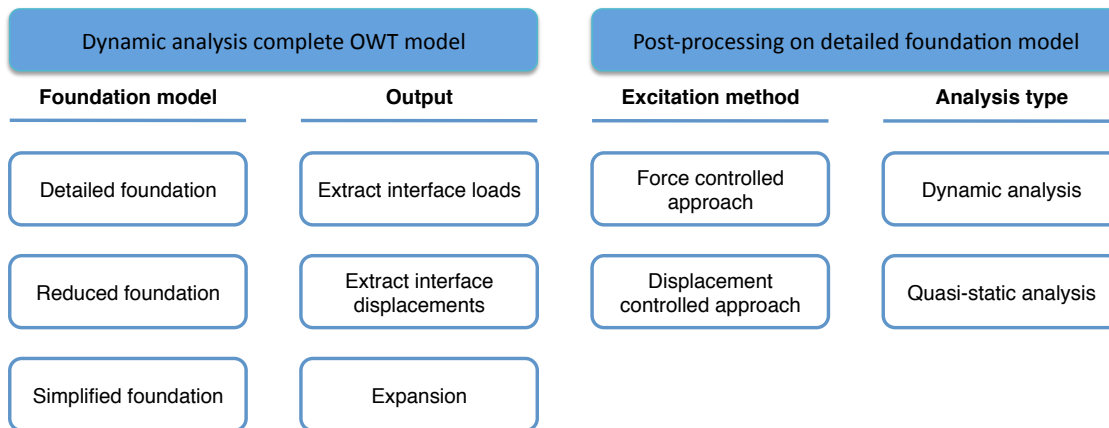
The methods and approaches differ in terms of accuracy and computation costs. In general, the more accurate an approach is, the more expensive it is computationally. The approaches and methods discussed in this chapter are, in descending order of complexity: the fully integrated method, the fully coupled method, the sequential approach, the semi-integrated approach and the superposition method. These calculation procedures differ in various aspects, the difference is mainly in the use of different foundation models in the complete OWT model analysis and the way of post-processing.

Figure 4.1 shows the different aspects for the different calculation procedures. The first column shows the different foundation models that can be integrated in the complete OWT model to perform a dynamic analysis. The second column shows different outputs from the dynamic analysis of the complete OWT model. If a reduced foundation model is used in the complete OWT analysis, the response of the reduced foundation can be expanded to obtain the response of the detailed foundation. An other way to retrieve the detailed response of the foundation is by post-processing on the detailed foundation model. The interface loads or displacements are needed as an input, which can be extracted from the dynamic analysis of the complete OWT model. The first two columns of Figure 4.1 show the calculation steps that are performed by the turbine designer. The last two columns represent the calculation steps performed by the foundation designer. As the turbine designer determines the global dynamic behavior of the complete OWT model, the analyses to retrieve the response of the detailed foundation model are defined as ‘post-processing’. In order to retrieve the response of the detailed foundation structure, the foundation designer can apply either the interface loads, defined as *force controlled approach*, or the interface displacement, *displacement controlled approach*. Within these approaches a dynamic or a quasi-static analysis can be performed.

The different calculation procedures to obtain the response of the detailed foundation structure will be discussed and supported with equations to examine the accuracy of these methods. As dis-

cussed in Chapter 2, fatigue is often the main design driver of the support structure and therefore it is important that fatigue is computed accurately. In order to compute the fatigue damage of a structure, the stresses in the structure are needed as an input. These stresses are related to the strains and thus to the displacements of the structure, the computation of stresses will be discussed in more detail in Section 5.3. If the fatigue damage needs to be computed accurately, the response of the foundation model should be accurate as well. Therefore, the accuracy of the response of the foundation structure is examined first. The impact of an introduced error in the response on the fatigue damage will be examined in the case study.

In order to determine the qualitative error in the different calculation procedures, the inaccuracies that arise in the dynamic analysis of the complete OWT model will be examined first and secondly the inaccuracies in the post-processing on the detailed foundation model. The equations will be written in the frequency domain, because the differences between the various calculation procedures will be more clear then. The frequency dependence of the response and the applied loads will be omitted in the equations for compactness.



**Figure 4.1:** Overview of different aspects involved in computing the response of the detailed foundation model as explained in the text above.

## 4.2 Detailed foundation used in complete OWT analysis

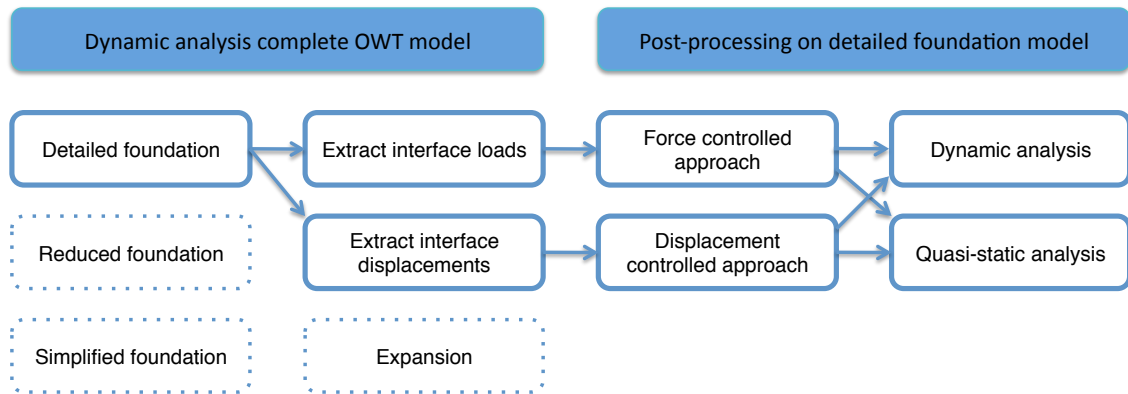
Figure 4.2 shows a flowchart of the calculation procedures if the detailed foundation model is integrated in the complete OWT model. This method is defined as the *fully integrated method*. The turbine designer performs a dynamic analysis on the complete OWT model with the detailed foundation and the response of the complete OWT can directly be used to check the ULS and the FLS for the complete structure. These results are then communicated to the foundation designer, and the foundation designer can optimize the design of the foundation. Hence, the fully integrated method needs only one software package. This approach is not preferable as all the risks and responsibilities are carried by the turbine designer and next to this, the foundation designer wants to check the results by himself. Furthermore, if the detailed foundation model is integrated in the complete OWT model, the complete model is very complex and has a lot of degrees of freedom which will result in large computation costs.

Another approach is to extract the interface loads or displacement from the dynamic analysis of the complete OWT model and communicate these interface loads/displacements to the foundation



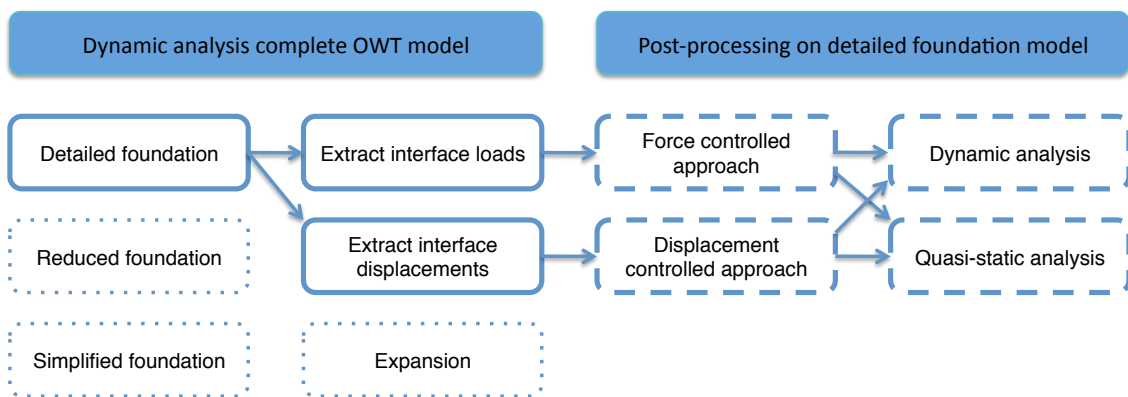
designer. The foundation designer applies the interface loads or displacements on the detailed foundation structure and performs a dynamic or a quasi-static analysis. This approach gives the foundation designer the opportunity to check the results by himself. Next to this, it splits the risks and responsibilities between the two parties, the turbine designer does not carry the risk of loads on the foundation model with this approach.

If the detailed foundation model is integrated in the complete OWT model and a dynamic analysis is performed, the exact response is obtained. Due to high computation costs this method is not often used. Still, the equations for this method will be written down as this response for the foundation will serve as a reference solution.



**Figure 4.2:** Calculation procedures in case of a detailed foundation model is integrated in the complete OWT model. Note that the response of the foundation extracted from the dynamic analysis of the complete OWT model will serve as **reference solution**.

### 4.2.1 Analysis of complete OWT model



**Figure 4.3:** Different calculation procedures in the analysis of the complete OWT model with a detailed foundation model.

Figure 4.3 shows the different calculation steps in the dynamic analysis of the complete OWT model with a detailed foundation model. If the detailed foundation model is integrated in the complete OWT model, the response of the detailed foundation structure will be directly obtained with a

dynamic analysis of the complete OWT model. The interface loads and displacement should be extracted for any other party that wants to reconstruct the response of only the foundation model. The equations to obtain the response of the complete OWT model and to extract the interface loads and displacements will be presented in this section.

The equation of motion of the complete OWT model in the frequency domain is

$$(-\omega^2 \mathbf{M} + j\omega \mathbf{C} + \mathbf{K})\mathbf{u} = \mathbf{Z}\mathbf{u} = \mathbf{f} \quad (4.1)$$

where  $\mathbf{M}$  is the mass matrix of the complete OWT model,  $\mathbf{C}$  the damping matrix and  $\mathbf{K}$  the stiffness matrix. The external load  $\mathbf{f}$  consists of wind and wave loads and  $\mathbf{u}$  is the response of the complete OWT model. Matrix  $\mathbf{Z}$  is defined as the dynamic stiffness matrix. In order to find the response  $\mathbf{u}$ , the inverse of the dynamic stiffness matrix should be multiplied with the external force.

$$\mathbf{u} = \mathbf{Z}^{-1}\mathbf{f} = \mathbf{Y}\mathbf{f} \quad (4.2)$$

The inverse of the dynamic stiffness matrix is defined as the receptance matrix  $\mathbf{Y}$ .

In order to determine the differences between the various calculation procedures to obtain the response of the foundation structure, the equation of motion of the complete OWT model is rewritten for two substructures, following the theory discussed in Section 3.3. The foundation model is one substructure, denoted by  $^{(f)}$ , and the other substructure consists of the remaining components, the tower and the RNA, and is denoted by  $^{(w)}$ . The equation of motion becomes

$$\begin{bmatrix} -\omega^2 \mathbf{M}^{(f)} + j\omega \mathbf{C}^{(f)} + \mathbf{K}^{(f)} & \mathbf{0} \\ \mathbf{0} & -\omega^2 \mathbf{M}^{(w)} + j\omega \mathbf{C}^{(w)} + \mathbf{K}^{(w)} \end{bmatrix} \begin{bmatrix} \mathbf{u}^{(f)} \\ \mathbf{u}^{(w)} \end{bmatrix} = \begin{bmatrix} \mathbf{f}^{(f)} \\ \mathbf{f}^{(w)} \end{bmatrix} + \begin{bmatrix} \mathbf{g}^{(f)} \\ \mathbf{g}^{(w)} \end{bmatrix} \quad (4.3)$$

$$\mathbf{B} \begin{bmatrix} \mathbf{u}^{(f)} \\ \mathbf{u}^{(w)} \end{bmatrix} = \mathbf{0} \quad \mathbf{L}^T \begin{bmatrix} \mathbf{g}^{(f)} \\ \mathbf{g}^{(w)} \end{bmatrix} = \mathbf{0} \quad (4.4)$$

Due to splitting the complete OWT model into two substructures, the internal loads,  $\mathbf{g}^{(f)}$  and  $\mathbf{g}^{(w)}$ , appear in the equation of motion, these forces are equal of amplitude and opposite in direction following the equilibrium condition described in Section 3.3. Next to this, the displacements for the interface DoF for both substructures should be the same, following the compatibility condition described in Section 3.3. Both, the compatibility and the equilibrium condition are presented in equation (4.4).

The interface loads are used as an input for the force controlled approach. To extract the interface loads  $\mathbf{g}^{(f)}$ , the response  $\mathbf{u}^{(f)}$  is used.

$$\begin{aligned} \mathbf{g}^{(f)} &= (-\omega \mathbf{M}^{(f)} + j\omega \mathbf{C}^{(f)} + \mathbf{K}^{(f)})\mathbf{u}^{(f)} - \mathbf{f}^{(f)} \\ &= \mathbf{Z}^{(f)}\mathbf{u}^{(f)} - \mathbf{f}^{(f)} \end{aligned} \quad (4.5)$$

For the displacement controlled approach the response at the boundary of the foundation  $\mathbf{u}_b$  is used as an input, this response can be extracted from the response  $\mathbf{u}$  in equation (4.2).

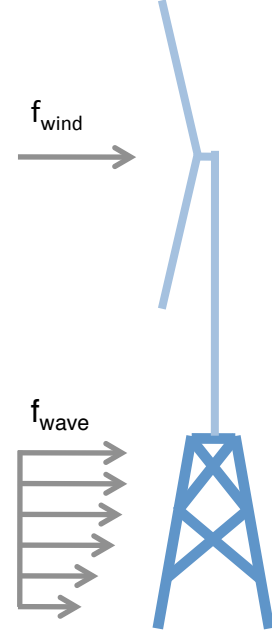


Figure 4.4: Representation of detailed OWT model.

### 4.2.2 Post-processing on detailed foundation

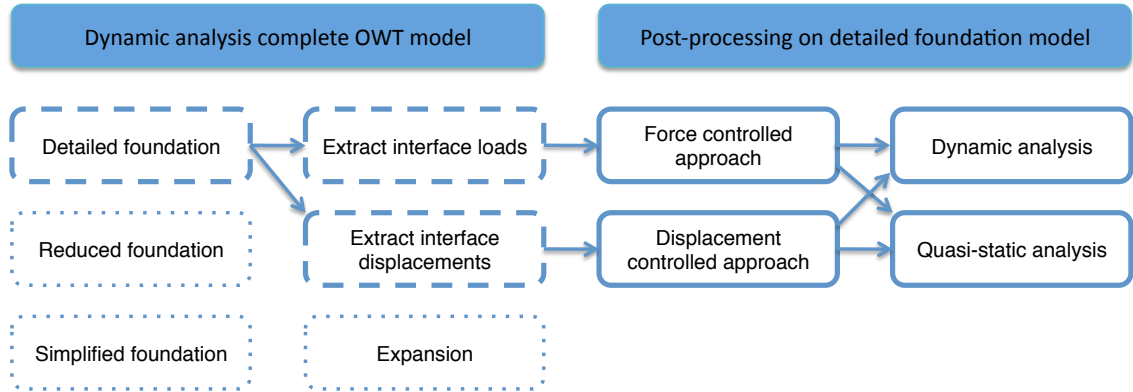


Figure 4.5: Different calculation procedures in the post-processing on the detailed foundation model.

Figure 4.5 shows the different calculation steps in the post-processing phase. The foundation designer can obtain the response of the foundation with a force or a displacement controlled approach, within these approaches a dynamic or a quasi-static analysis can be performed. The FLS and ULS of the foundation structure are checked with the response obtained from these simulations.

#### Force controlled approach

The foundation designer applies the interface loads and the wave loads on the detailed foundation model and runs a simulation. When a dynamic analysis is executed, the response will be exact to the reference response. However, a quasi-static analysis will provide a different response and this will be shown below.

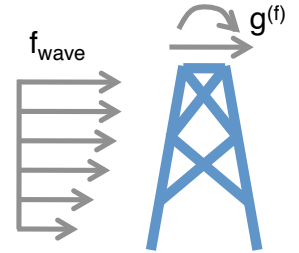


Figure 4.6: Representation of FC approach.

**Dynamic analysis** The equation to solve the response of the detailed foundation structure with a dynamic force controlled approach (*DFC*) is

$$(-\omega^2 \mathbf{M} + j\omega \mathbf{C} + \mathbf{K}) \mathbf{u} = \mathbf{f} + \mathbf{g} \quad (4.6)$$

$$\begin{aligned} \mathbf{u}_{DFC} &= (-\omega^2 \mathbf{M}^{(f)} + j\omega \mathbf{C}^{(f)} + \mathbf{K}^{(f)})^{-1} (\mathbf{f}^{(f)} + \mathbf{g}^{(f)}) \\ &= \mathbf{Z}^{(f)-1} (\mathbf{f}^{(f)} + \mathbf{g}^{(f)}) \\ &= \mathbf{Y}^{(f)} (\mathbf{f}^{(f)} + \mathbf{g}^{(f)}) \end{aligned} \quad (4.7)$$

The response  $\mathbf{u}_{DFC}$  is exactly the same as  $\mathbf{u}^{(f)}$ , see the upper row of equation (4.3).

**Quasi-static analysis** A quasi-static force controlled approach (*QsFC*) neglects the inertia and the damping forces. The response of the foundation  $\mathbf{u}_{QsFC}$  can be obtained with the following equation

$$\begin{aligned} \mathbf{u}_{QsFC} &= \mathbf{K}^{(f)-1} (\mathbf{f}^{(f)} + \mathbf{g}^{(f)}) \\ &= \mathbf{G}^{(f)} (\mathbf{f}^{(f)} + \mathbf{g}^{(f)}) \end{aligned} \quad (4.8)$$

The inverse of the stiffness matrix is defined as the flexibility matrix  $\mathbf{G}$ . In order to determine the accuracy of response  $\mathbf{u}_{QsFC}$ , this response can be compared to the exact response of the foundation

$\mathbf{u}^{(f)}$ . Differences between the responses will appear around the first free interface eigenfrequency of the foundation, defined as  $\omega_{free}^{\{1\}}$ . Note that the structure is still properly constrained, but the interface DoF between the tower and the foundation are free. The dynamic stiffness matrix  $\mathbf{Z}^{(f)}$  is around zero for this eigenfrequency and thus the receptance matrix goes to infinity and a resonance peak appears in the FRF. However, in a quasi-static analysis, the inertia and damping forces are neglected and the response of the structure depends only on the stiffness of the foundation model. The elastic forces are not frequency dependent, as a result the amplitude is constant for all frequencies. Figure 3.3 shows the FRF of a single mass-spring-damper system, it shows that a quasi-static analysis will first underestimate the response and at higher frequencies overestimate the response due to neglecting the inertia forces.

A quasi-static analysis provides an accurate result if  $\omega_{free}^{\{1\}}$  is higher than the highest excitation frequency of the external loads, the structure behaves still quasi-statically in this frequency range. The highest excitation frequency of the external loads is defined as  $\max(\omega_{ext})$ .

### Displacement controlled approach

The displacement controlled approach uses the response at the boundary of the foundation  $\mathbf{u}_b$  as an input. The output is the response for the internal DoF  $\mathbf{u}_i$ . Therefore, the response of the foundation can be split up into internal and boundary DoF, and the mass, damping and stiffness matrix can be reorganized according to this.

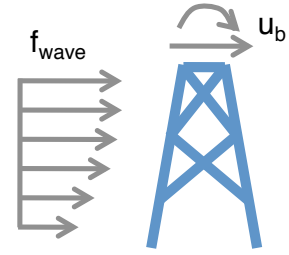


Figure 4.7: Representation of DC approach.

$$\mathbf{u}^{(f)} = \begin{bmatrix} \mathbf{u}_i \\ \mathbf{u}_b \end{bmatrix} \quad \mathbf{M}^{(f)} = \begin{bmatrix} \mathbf{M}_{ii} & \mathbf{M}_{ib} \\ \mathbf{M}_{bi} & \mathbf{M}_{bb} \end{bmatrix} \quad \mathbf{C}^{(f)} = \begin{bmatrix} \mathbf{C}_{ii} & \mathbf{C}_{ib} \\ \mathbf{C}_{bi} & \mathbf{C}_{bb} \end{bmatrix} \quad \mathbf{K}^{(f)} = \begin{bmatrix} \mathbf{K}_{ii} & \mathbf{K}_{ib} \\ \mathbf{K}_{bi} & \mathbf{K}_{bb} \end{bmatrix} \quad (4.9)$$

If the detailed foundation model is integrated in the complete OWT model, the displacements, velocities and accelerations at the interface between the tower and the foundation will be exact. Often, only the interface displacements are communicated to the foundation designer and the interface velocities and accelerations are set to zero. The effect of neglecting these boundary velocities and accelerations will be investigated as well.

**Dynamic analysis** The equation of motion for the foundation can be written as

$$\left( -\omega^2 \begin{bmatrix} \mathbf{M}_{ii} & \mathbf{M}_{ib} \\ \mathbf{M}_{bi} & \mathbf{M}_{bb} \end{bmatrix} + j\omega \begin{bmatrix} \mathbf{C}_{ii} & \mathbf{C}_{ib} \\ \mathbf{C}_{bi} & \mathbf{C}_{bb} \end{bmatrix} + \begin{bmatrix} \mathbf{K}_{ii} & \mathbf{K}_{ib} \\ \mathbf{K}_{bi} & \mathbf{K}_{bb} \end{bmatrix} \right) \begin{bmatrix} \mathbf{u}_i \\ \mathbf{u}_b \end{bmatrix} = \begin{bmatrix} \mathbf{f}_i \\ \mathbf{f}_b \end{bmatrix} + \begin{bmatrix} \mathbf{g}_i \\ \mathbf{g}_b \end{bmatrix} \quad (4.10)$$

where  $\mathbf{g}_i$  is equal to zero as the interface load vector  $\mathbf{g}^{(f)}$  contains only terms at the interface node(s) of the foundation. The displacement controlled approach uses the response at the boundary as an input. Therefore, to determine the response for the internal DoF  $\mathbf{u}_i$  the upper row of equation (4.10) is solved. The response of the detailed foundation with a dynamic displacement controlled approach (DDC) becomes

$$(-\omega^2 \mathbf{M}_{ii} + j\omega \mathbf{C}_{ii} + \mathbf{K}_{ii}) \mathbf{u}_i + (-\omega^2 \mathbf{M}_{ib} + j\omega \mathbf{C}_{ib} + \mathbf{K}_{ib}) \mathbf{u}_b = \mathbf{f}_i \quad (4.11)$$

$$(-\omega^2 \mathbf{M}_{ii} + j\omega \mathbf{C}_{ii} + \mathbf{K}_{ii}) \mathbf{u}_i = \mathbf{f}_i - (-\omega^2 \mathbf{M}_{ib} + j\omega \mathbf{C}_{ib} + \mathbf{K}_{ib}) \mathbf{u}_b \quad (4.12)$$

$$\begin{aligned} \mathbf{Z}_{ii} \mathbf{u}_i &= \mathbf{f}_i - \mathbf{Z}_{ib} \mathbf{u}_b \\ \mathbf{u}_i &= \mathbf{Y}_{ii} (\mathbf{f}_i - \mathbf{Z}_{ib} \mathbf{u}_b) \end{aligned} \quad (4.13)$$

$$\mathbf{u}_{DDC} = \begin{bmatrix} \mathbf{u}_i \\ \mathbf{u}_b \end{bmatrix} = \mathbf{u}^{(f)} \quad (4.14)$$

The response of the detailed foundation  $\mathbf{u}_{DDC}$  is identical to the response  $\mathbf{u}^{(f)}$ , as  $\mathbf{u}_b$  is exact, because it is extracted from the dynamic analysis of the complete OWT model with a detailed foundation structure, and  $\mathbf{u}_i$  is solved dynamically.

**Quasi-static analysis** A quasi-static displacement controlled approach (QsDC) neglects the inertia and damping forces. The response of the internal DoF of the foundation can be obtained in two ways, one that neglects the inertia and damping forces only for the internal DoF defined as  $\mathbf{u}_{QsaDC}$  and one that neglects the damping and inertia coupling forces as well  $\mathbf{u}_{QsDC}$ .

$$\begin{aligned} \mathbf{u}_{i,Qsa} &= \mathbf{K}_{ii}^{-1} (\mathbf{f}_i - (-\omega^2 \mathbf{M}_{ib} + j\omega \mathbf{C}_{ib} + \mathbf{K}_{ib}) \mathbf{u}_b) \\ &= \mathbf{G}_{ii} (\mathbf{f}_i - \mathbf{Z}_{ib} \mathbf{u}_b) \end{aligned} \quad (4.15)$$

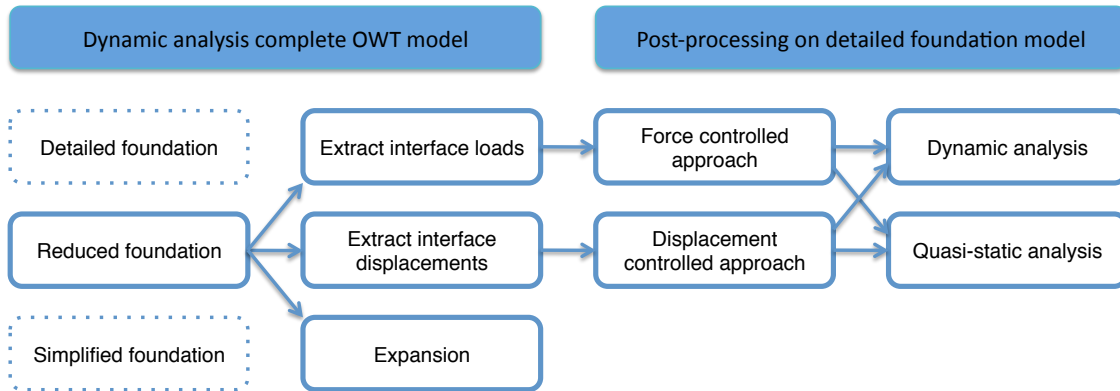
$$\begin{aligned} \mathbf{u}_{i,Qs} &= \mathbf{K}_{ii}^{-1} (\mathbf{f}_i - \mathbf{K}_{ib} \mathbf{u}_b) \\ &= \mathbf{G}_{ii} (\mathbf{f}_i - \mathbf{K}_{ib} \mathbf{u}_b) \end{aligned} \quad (4.16)$$

$$\mathbf{u}_{QsaDC} = \begin{bmatrix} \mathbf{u}_{i,Qsa} \\ \mathbf{u}_b \end{bmatrix} \quad \mathbf{u}_{QsDC} = \begin{bmatrix} \mathbf{u}_{i,Qs} \\ \mathbf{u}_b \end{bmatrix} \quad (4.17)$$

The response  $\mathbf{u}_{i,Qsa}$  takes the elastic, inertia and damping coupling forces resulting from the boundary response  $\mathbf{u}_b$  into account. The elastic, damping and inertia coupling forces are, respectively,  $\mathbf{K}_{ib} \mathbf{u}_b$ ,  $j\omega \mathbf{C}_{ib} \mathbf{u}_b$  and  $-\omega^2 \mathbf{M}_{ib} \mathbf{u}_b$ . The response  $\mathbf{u}_{i,Qs}$  neglects the inertia and damping coupling forces and takes only the elastic coupling forces into account. The effect of neglecting these damping and inertia coupling forces can be examined by comparing  $\mathbf{u}_{QsDC}$  with  $\mathbf{u}_{QsaDC}$ . Whether the effect of neglecting these coupling terms is small depends on the structure. The different coupling load terms  $\mathbf{K}_{ib} \mathbf{u}_b$ ,  $j\omega \mathbf{C}_{ib} \mathbf{u}_b$  and  $-\omega^2 \mathbf{M}_{ib} \mathbf{u}_b$  should be determined to define if the elastic coupling forces are dominant and thus the inertia and damping coupling forces can be neglected. Note that this only concerns the coupling terms between the internal and the boundary DoF. The influence of neglecting the damping and the inertia forces for the internal DoF is discussed next.

The response  $\mathbf{u}_{QsDC}$  should be compared to the exact response of the foundation  $\mathbf{u}^{(f)}$  to gain insight in the accuracy of a quasi-static analysis. A difference between the response from a quasi-static and a dynamic analysis will appear around the first fixed interface eigenfrequency of the foundation,  $\omega_{fixed}^{\{1\}}$ , i.e. where  $\mathbf{Z}_{ii}$  is around zero. The quasi-static analysis neglects the inertia and damping forces and no resonance peaks will appear at this eigenfrequency. Whether a quasi-static displacement controlled approach is accurate depends on  $\max(\omega_{ext})$  and  $\omega_{fixed}^{\{1\}}$ . If  $\omega_{fixed}^{\{1\}}$  is higher than  $\max(\omega_{ext})$ , the quasi-static displacement controlled approach will provide an accurate result. As  $\omega_{fixed}^{\{1\}}$  is higher than  $\omega_{free}^{\{1\}}$  of the foundation, differences between a quasi-static and a dynamic analysis will appear at higher excitation frequencies for a quasi-static displacement controlled approach than for a quasi-static force controlled approach.

### 4.3 Reduced foundation used in complete OWT analysis

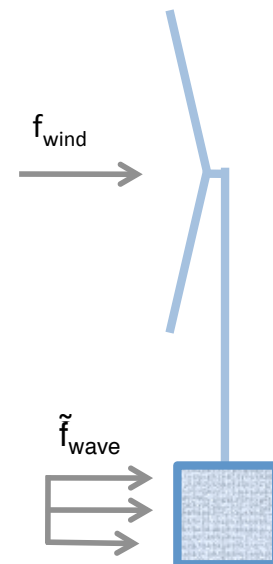


**Figure 4.8:** Calculation procedures in case of a reduced foundation model is integrated in the complete OWT model.

Figure 4.8 is a flowchart of the calculation procedures in case a reduced foundation model is integrated in the complete OWT model analysis. The method is defined as *fully coupled method* if the response of the reduced foundation model, obtained from the dynamic analysis of the complete OWT model, is expanded and the ULS and FLS are checked with this expanded response. The fully coupled method requires only one software package which leads to the same problems as for the fully integrated method. As two parties are responsible for the design of the support structure, both parties have to check the results themselves. Moreover, if a reduced foundation structure is integrated in the complete OWT model analysis, the reduction basis will influence the accuracy of the results of the foundation. However, the computation costs will be less compared to the fully integrated method due to the reduction.

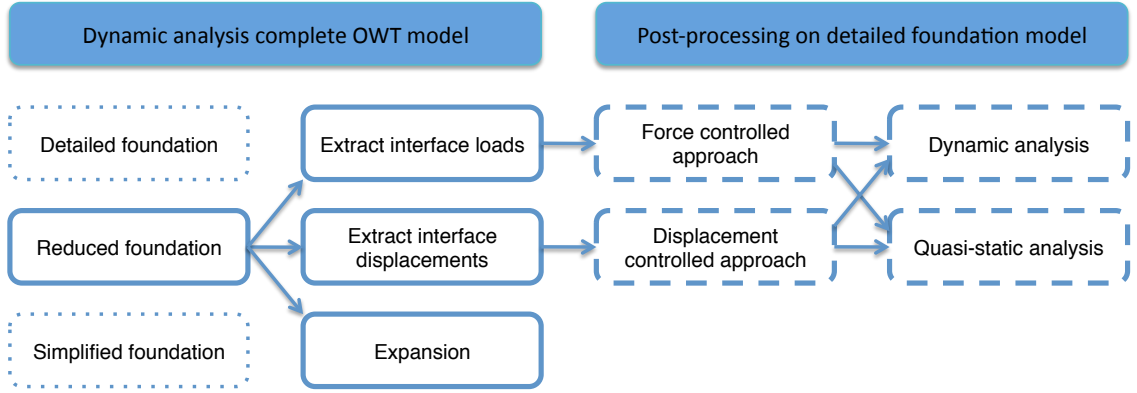
An other method is the *sequential approach* where a dynamic simulation is run with a reduced foundation structure in the complete OWT model and the foundation designer uses the interface loads/displacements to retrieve the response of the detailed foundation structure with a dynamic or a quasi-static analysis.

The accuracy of the different calculation procedures if a reduced foundation model is integrated in the complete OWT model will be investigated and discussed.



**Figure 4.9:** Representation of OWT model with reduced foundation.

## 4.3.1 Analysis of complete OWT model



**Figure 4.10:** Different calculation procedures in the analysis of the complete OWT model with a reduced foundation model.

Figure 4.10 shows the different calculation steps in the dynamic analysis of the complete OWT model with a reduced foundation model.

Equation (4.3) showed the equation of motion in the frequency domain when the detailed foundation model is integrated into the OWT model. If a reduced foundation model is used, equation (4.3) becomes

$$\begin{bmatrix} -\omega^2 \tilde{\mathbf{M}}^{(f)} + j\omega \tilde{\mathbf{C}}^{(f)} + \tilde{\mathbf{K}}^{(f)} & \mathbf{0} \\ \mathbf{0} & -\omega^2 \mathbf{M}^{(w)} + j\omega \mathbf{C}^{(w)} + \mathbf{K}^{(w)} \end{bmatrix} \begin{bmatrix} \tilde{\mathbf{u}}^{(f)} \\ \hat{\mathbf{u}}^{(w)} \end{bmatrix} = \begin{bmatrix} \tilde{\mathbf{f}}^{(f)} \\ \mathbf{f}^{(w)} \end{bmatrix} + \begin{bmatrix} \tilde{\mathbf{g}}^{(f)} \\ \hat{\mathbf{g}}^{(w)} \end{bmatrix} \quad (4.18)$$

$$\mathbf{B} \begin{bmatrix} \tilde{\mathbf{u}}^{(f)} \\ \hat{\mathbf{u}}^{(w)} \end{bmatrix} = \mathbf{0} \quad \mathbf{L}^T \begin{bmatrix} \tilde{\mathbf{g}}^{(f)} \\ \hat{\mathbf{g}}^{(w)} \end{bmatrix} = \mathbf{0} \quad (4.19)$$

where  $\tilde{\mathbf{M}}^{(f)}$ ,  $\tilde{\mathbf{C}}^{(f)}$  and  $\tilde{\mathbf{K}}^{(f)}$  are the reduced mass, damping and stiffness matrices of the foundation. The response  $\tilde{\mathbf{u}}^{(f)}$  is the reduced response of the foundation and  $\tilde{\mathbf{f}}^{(f)}$  and  $\tilde{\mathbf{g}}^{(f)}$  are the reduced external load and the reduced interface load. Since the foundation structure is reduced an error is introduced in the (expanded) response of the foundation as the reduced foundation structure does not span the full solution space. The response of the reduced foundation structure is an approximation of the exact solution. Therefore, due to the use of a reduced foundation model in the complete OWT model, the response of the tower and RNA substructure  $\hat{\mathbf{u}}^{(w)}$  will differ from the reference solution  $\mathbf{u}^{(w)}$ . The superscript  $\wedge$  is used for the response of a substructure or an interface load where an (extra) error is introduced due to the use of a reduced models.

As an error is introduced in the response  $\tilde{\mathbf{u}}^{(f)}$  due to reduction, the interface load  $\tilde{\mathbf{g}}^{(f)}$  will contain an error as well, because this load is computed with the response  $\tilde{\mathbf{u}}^{(f)}$ . In order to use the interface load during post-processing on the detailed foundation model, the interface load should be expanded, see equation (4.21).

$$\tilde{\mathbf{g}}^{(f)} = (-\omega^2 \tilde{\mathbf{M}}^{(f)} + j\omega \tilde{\mathbf{C}}^{(f)} + \tilde{\mathbf{K}}^{(f)}) \tilde{\mathbf{u}}^{(f)} - \tilde{\mathbf{f}}^{(f)} \quad (4.20)$$

$$\begin{aligned} &= \tilde{\mathbf{Z}}^{(f)} \tilde{\mathbf{u}}^{(f)} - \tilde{\mathbf{f}}^{(f)} \\ \hat{\mathbf{g}}^{(f)} &= \mathbf{R} \tilde{\mathbf{g}}^{(f)} \end{aligned} \quad (4.21)$$

The interface load contains information about the behavior of the complete OWT model, large amplitudes will appear at the eigenfrequencies of the complete OWT model that are excited by the external load. Integrating reduced components in the complete OWT model can result in deviated eigenfrequencies for the complete OWT model. In order to achieve accurate results the OWT model with the reduced foundation model should be spectrally and spatially converged in the frequency range of the external load spectrum. The frequency range of the external load spectrum is abbreviated to ‘excitation bandwidth’. It is necessary to know which eigenfrequencies of the OWT model are excited within the excitation bandwidth. Furthermore, the reduction basis should be complete enough to accurately describe the response of the substructure due to the external force. If the OWT model with the reduced foundation model is not spectrally and spatially converged within the excitation bandwidth, an error is introduced in the (expanded) response of the foundation and as a result, the interface loads/displacements will not be accurate. As the interface loads are used as an input for the force controlled approach, the response of the detailed foundation structure after post-processing will not be accurate either. Moreover, if the frequency spectrum of the interface load contains large amplitudes at the wrong frequencies, the response of the detailed foundation structure after post-processing can be such that the eigenfrequencies of the foundation structure are excited. As a result extra forced response peaks appear, these peaks are defined as *pseudo resonances*.

The displacement controlled approach uses the response at the boundary of the foundation  $\tilde{\mathbf{u}}_b$  as an input, this response can be extracted from  $\tilde{\mathbf{u}}^{(f)}$ . The accuracy of the interface displacements depends on the same aspects as the accuracy of the interface load.

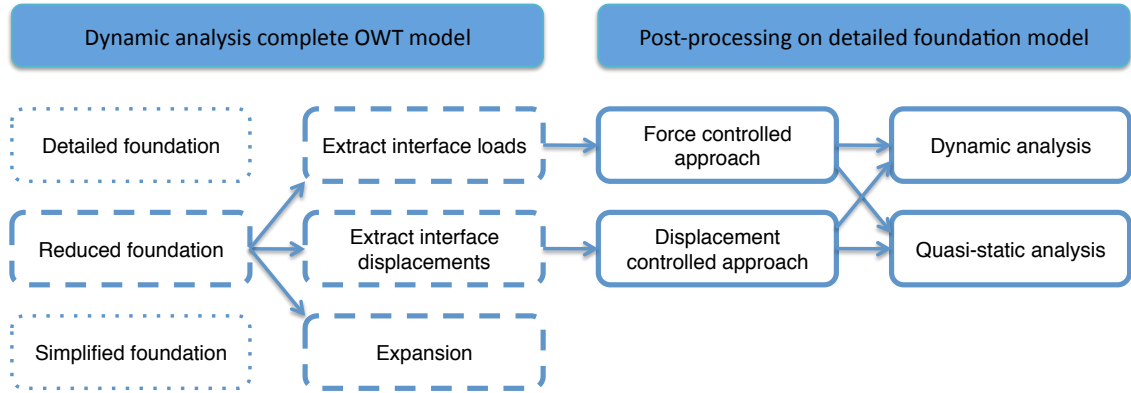
The response of the detailed foundation structure can be obtained also without post-processing on the detailed foundation structure, by simply expanding the response of the reduced foundation structure, (the fully coupled method).

$$\mathbf{u}_{exp}^{(f)} = \mathbf{R}\tilde{\mathbf{u}}^{(f)} \quad (4.22)$$

The accuracy of this method depends on the reduction method used for the foundation structure. In Section 3.4 several reduction methods are discussed: Guyan reduction, Craig-Bampton reduction and Augmented Craig-Bampton reduction. In order to retrieve an accurate expanded response for the foundation structure depends on the same aspects as to compute accurate interface loads/displacements. In other words, the OWT model with a reduced foundation structure should be spectrally and spatially converged within the excitation bandwidth to retrieve an accurate response of the foundation after expansion.



### 4.3.2 Post-processing on detailed foundation model



**Figure 4.11:** Different calculation procedures in the post-processing on the detailed foundation model.

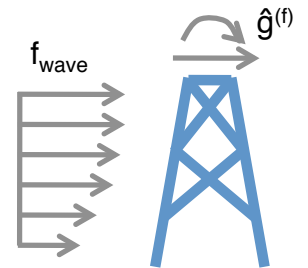
Figure 4.11 shows the calculation steps that can be performed in the post-processing phase. The interface loads and displacements are obtained from the dynamic analysis of the complete OWT model with a reduced foundation model. In this case, a dynamic analysis on the detailed foundation model will not provide the exact same response as the reference solution due to an error in the interface loads/displacements, resulting from the foundation model reduction. Pseudo resonances could appear in the response of the foundation after dynamic post-processing. A quasi-static analysis will provide a different response as well, where the error in the response is caused by two error sources. Firstly, the interface loads/displacements contain an error, resulting from the foundation model reduction, and secondly, the quasi-static analysis neglects the inertia and damping forces.

#### Force controlled approach

**Dynamic analysis** The equation for a dynamic force controlled approach to obtain the response  $\hat{\mathbf{u}}_{DFC}$  is

$$\begin{aligned}\hat{\mathbf{u}}_{DFC} &= (-\omega^2 \mathbf{M}^{(f)} + j\omega \mathbf{C}^{(f)} + \mathbf{K}^{(f)})^{-1} (\mathbf{f}^{(f)} + \hat{\mathbf{g}}^{(f)}) \quad (4.23) \\ &= \mathbf{Z}^{(f)-1} (\mathbf{f}^{(f)} + \hat{\mathbf{g}}^{(f)}) \\ &= \mathbf{Y}^{(f)} (\mathbf{f}^{(f)} + \hat{\mathbf{g}}^{(f)})\end{aligned}$$

The response  $\hat{\mathbf{u}}_{DFC}$  will not be exactly the same as  $\mathbf{u}^{(f)}$ , due to an error in the interface load  $\hat{\mathbf{g}}^{(f)}$ . How accurate the response  $\hat{\mathbf{u}}_{DFC}$  is depends on the accuracy of the interface load and thus the reduction method used for the foundation structure.



**Figure 4.12:** Representation of FC approach.

**Quasi-static analysis** A quasi-static force controlled approach neglects the inertia and damping forces, the response of the foundation  $\hat{\mathbf{u}}_{QsFC}$  becomes

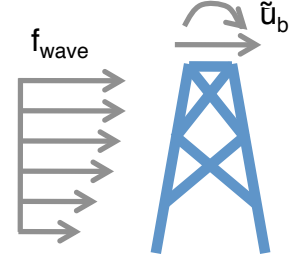
$$\begin{aligned}\hat{\mathbf{u}}_{QsFC} &= \mathbf{K}^{(f)-1} (\mathbf{f}^{(f)} + \hat{\mathbf{g}}^{(f)}) \quad (4.24) \\ &= \mathbf{G}^{(f)} (\mathbf{f}^{(f)} + \hat{\mathbf{g}}^{(f)})\end{aligned}$$

The response  $\hat{\mathbf{u}}_{QsFC}$  can be compared to the exact response of the foundation  $\mathbf{u}^{(f)}$ . Difference between  $\hat{\mathbf{u}}_{QsFC}$  and  $\mathbf{u}^{(f)}$  will appear around  $\omega_{free}^{\{1\}}$  of the foundation, resulting from neglecting the

inertia and damping forces. Next to this, extra differences can appear in  $\hat{\mathbf{u}}_{Q_sFC}$  due to an error in the interface loads, resulting from the foundation model reduction.

### Displacement controlled approach

If a reduced foundation is used in the complete OWT model, the displacements extracted at the interface  $\tilde{\mathbf{u}}_b$  are not exact. As the interface displacements are used as an input for the displacement controlled approach, the introduced error in the interface displacements will introduce an error in the output of the post-processing calculation procedures as well. Therefore, the response from a dynamic displacement controlled approach will not be similar to the reference solution.



**Figure 4.13:** Representation of DC approach.

**Dynamic analysis** In the frequency domain the response  $\hat{\mathbf{u}}_{DDC}$  can be obtained

$$(-\omega^2 \mathbf{M}_{ii} + j\omega \mathbf{C}_{ii} + \mathbf{K}_{ii}) \hat{\mathbf{u}}_i = \mathbf{f}_i - (-\omega^2 \mathbf{M}_{ib} + j\omega \mathbf{C}_{ib} + \mathbf{K}_{ib}) \tilde{\mathbf{u}}_b \quad (4.25)$$

$$\mathbf{Z}_{ii} \hat{\mathbf{u}}_i = \mathbf{f}_i - \mathbf{Z}_{ib} \tilde{\mathbf{u}}_b \quad (4.26)$$

$$\hat{\mathbf{u}}_i = \mathbf{Z}_{ii}^{-1} (\mathbf{f}_i - \mathbf{Z}_{ib} \tilde{\mathbf{u}}_b) \quad (4.26)$$

$$\hat{\mathbf{u}}_{DDC} = \begin{bmatrix} \hat{\mathbf{u}}_i \\ \tilde{\mathbf{u}}_b \end{bmatrix} \quad (4.27)$$

The response  $\hat{\mathbf{u}}_{DDC}$  is not exactly the same as  $\mathbf{u}^{(f)}$ , due to the error in the input  $\tilde{\mathbf{u}}_b$ . The amplitude of the error depends on how well the reduced foundation structure can approximate the exact solution.

**Quasi-static analysis** As already showed in equation (4.15) and (4.16), the quasi-static analysis can be performed in two ways. Firstly, the inertia and damping forces are only neglected for the internal DoF. Secondly, the damping and inertia coupling forces,  $\mathbf{C}_{ib} \tilde{\mathbf{u}}_b$  and  $-\omega^2 \mathbf{M}_{ib} \tilde{\mathbf{u}}_b$ , are also neglected and only the elastic coupling forces,  $\mathbf{K}_{ib} \tilde{\mathbf{u}}_b$ , are taken into account. The response  $\hat{\mathbf{u}}_{i,Qsa}$  takes the elastic, inertia and damping coupling forces resulting from the boundary response  $\tilde{\mathbf{u}}_b$  into account. The response  $\hat{\mathbf{u}}_{i,Qs}$  neglects the inertia and damping coupling forces and takes only the elastic coupling forces into account. The equations to obtain the response of the foundation structure with a quasi-static displacement controlled approach are

$$\begin{aligned} \hat{\mathbf{u}}_{i,Qsa} &= \mathbf{K}_{ii}^{-1} (\mathbf{f}_i - (-\omega^2 \mathbf{M}_{ib} + j\omega \mathbf{C}_{ib} + \mathbf{K}_{ib}) \tilde{\mathbf{u}}_b) \\ &= \mathbf{G}_{ii} (\mathbf{f}_i - \mathbf{Z}_{ib} \tilde{\mathbf{u}}_b) \end{aligned} \quad (4.28)$$

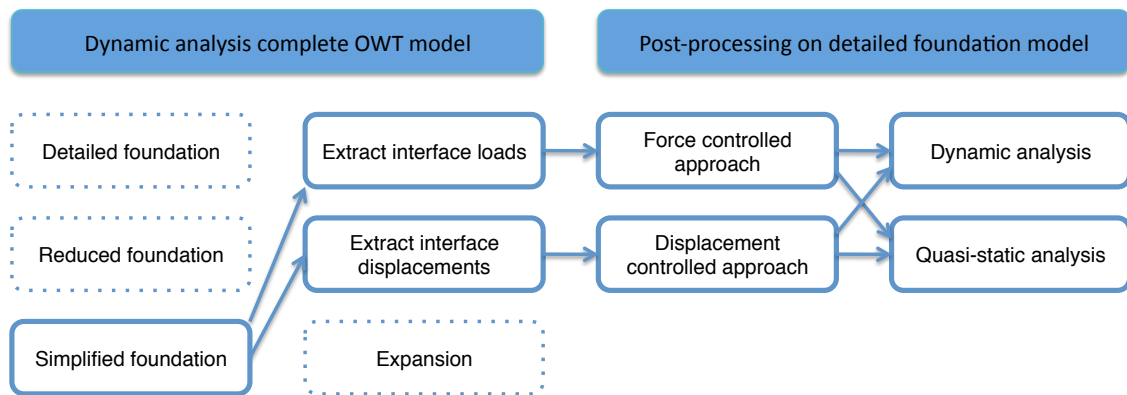
$$\begin{aligned} \hat{\mathbf{u}}_{i,Qs} &= \mathbf{K}_{ii}^{-1} (\mathbf{f}_i - \mathbf{K}_{ib} \tilde{\mathbf{u}}_b) \\ &= \mathbf{G}_{ii} (\mathbf{f}_i - \mathbf{K}_{ib} \tilde{\mathbf{u}}_b) \end{aligned} \quad (4.29)$$

$$\hat{\mathbf{u}}_{QsaDC} = \begin{bmatrix} \hat{\mathbf{u}}_{i,Qsa} \\ \tilde{\mathbf{u}}_b \end{bmatrix} \quad \hat{\mathbf{u}}_{QsDC} = \begin{bmatrix} \hat{\mathbf{u}}_{i,Qs} \\ \tilde{\mathbf{u}}_b \end{bmatrix} \quad (4.30)$$

What the effects of neglecting the inertia and damping coupling forces,  $\mathbf{C}_{ib} \tilde{\mathbf{u}}_b$  and  $-\omega^2 \mathbf{M}_{ib} \tilde{\mathbf{u}}_b$ , can be examined by comparing  $\hat{\mathbf{u}}_{QsDC}$  with  $\hat{\mathbf{u}}_{QsaDC}$ .

The accuracy of the quasi-static displacement controlled approach can be determined by comparing  $\hat{\mathbf{u}}_{QsDC}$  with  $\mathbf{u}^{(f)}$ . The response  $\hat{\mathbf{u}}_{QsDC}$  will differ compared to  $\mathbf{u}^{(f)}$  due to neglecting the inertia and damping forces (both internal and in the coupling terms) and the error in the boundary response  $\tilde{\mathbf{u}}_b$ . Difference between the response  $\hat{\mathbf{u}}_{QsDC}$  and  $\mathbf{u}^{(f)}$  will appear around  $\omega_{fixed}^{\{1\}}$ , furthermore, extra differences can appear due to an error in the boundary response.

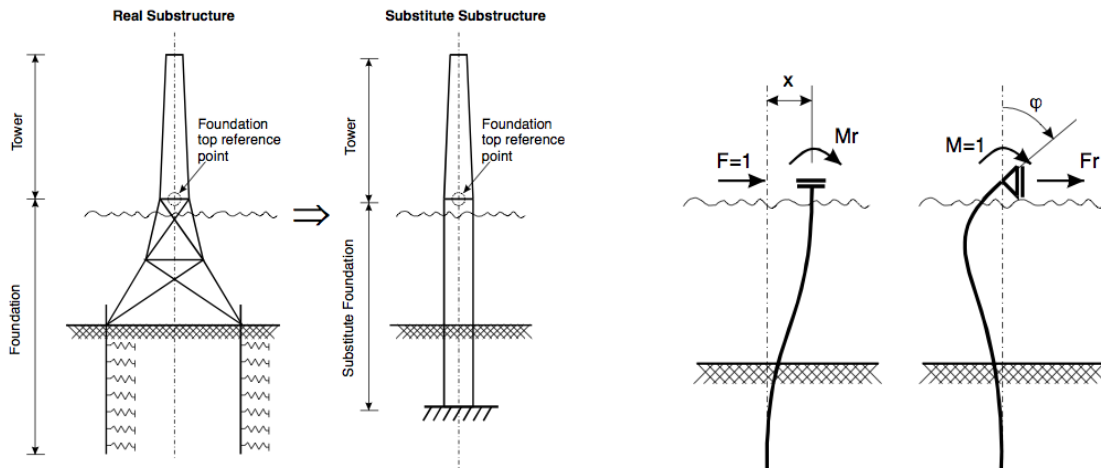
## 4.4 Simplified foundation used in complete OWT analysis



**Figure 4.14:** Different calculation procedures in case of a simplified foundation model is integrated in the complete OWT model.

Figure 4.14 shows a flowchart of the calculation procedures if a simplified foundation model is integrated in the complete OWT model, this method is defined as the *semi-integrated approach*. The semi-integrated approach is described by Seidel [30, 31]. The idea is to generate an equivalent monopile for the complex foundation structure, see Figure 4.15a. This equivalent monopile is integrated in the complete OWT model and a dynamic analysis is performed. As a result, the complete model is not too complex, which limits the computation costs.

This method can be described with the same equations as shown in Section 4.3 when a reduced foundation model is integrated in the complete OWT model. However, the response of the simplified foundation model can not be expanded to get the response of the detailed foundation model. Hence, post-processing on the detailed foundation model is necessary. The accuracy of the method depends on the accuracy of the interface loads/displacements. It is thus important to achieve identical kinematics at the foundation top for ‘real’ and ‘substitute model’, which is impossible as the substitute model differs a lot from the real model. The monopile has to be equivalent in terms of stiffness, mass and hydrodynamics. Seidel derives equivalent stiffness properties of the monopile by applying unit deformations and unit rotation, see Figure 4.15b [31]. Next to this, the eigenfrequencies of both models should match. Matching the eigenfrequencies alone is not sufficient; these depend both on stiffness and mass and errors in both may cancel out for the eigenfrequencies. Moreover, only mode shapes that are similar to those of a monopile can be modeled accurately [7]. As a result, the semi-integrated method can not describe the behavior of the complex foundation structure well. The method is inaccurate and therefore this method will not be further investigated in the case study.



(a) Replace complex foundation structure by equivalent monopile (b) Determination of foundation top stiffness matrix

Figure 4.15: Visualization of semi-integrated approach [31].

## 4.5 Separated models

The *superposition method* treats an offshore wind turbine basically like an onshore wind turbine plus offshore support structure. The foundation structure and the wind turbine are modeled separately. A dynamic analysis is performed on the wind turbine model under only wind loading and the response of the foundation model is analyzed under only wave loading [7, 20].

In order to compute the response in a certain point in the foundation structure, the loads at the bottom of the tower are extracted and applied to the foundation model to compute the response. This response is added to the response obtained from the analysis under only wave loading. Figure 4.16 is a visualization of the superposition method.

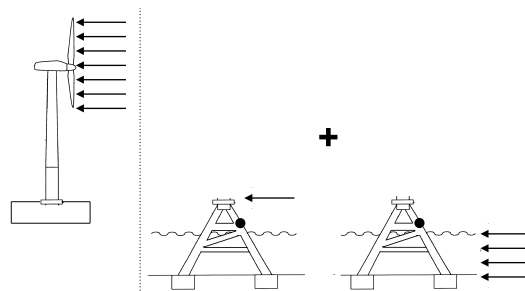


Figure 4.16: Visualization of the superposition method [26].

To determine the accuracy of this method, support of equations is not essential. The method is not accurate as there is no dynamic interrelation between the wind turbine and the support structure at all. Particularly the aerodynamic damping that occurs during operation remains unconsidered. The aerodynamic damping has a large influence on the structural loads. Kühn gives approximate constant aerodynamic damping values that can be taken into account in the structural simulations for the support structures [20]. However, this can only be a very rough estimate as aerodynamic

damping depends on the specific configuration and the operating conditions. It is clear that the superposition method is not accurate [7, 26], therefore no further investigation of its accuracy is done in the case study.

## 4.6 Summary

Different calculation procedures exist to compute the response of the foundation structure. The two most simple methods, the superposition method and the semi-integrated method, are not accurate and will not be further investigated to determine the quantitative error in the case study. The accuracy of the other methods depends on the characteristics of the foundation structure and the applied reduction method. Table 4.1 and 4.2 give an overview of the in- and output and the accuracy of the different calculation procedures with a detailed or reduced foundation model in the complete OWT model. The upper row describes the foundation model used in the dynamic analysis of the complete OWT model and the left column describes the different analyses. A green checkmark means that the calculation procedures provides accurate results and an orange question mark means that the accuracy of the calculation procedure depends on different aspects.

		Detailed foundation in complete OWT model
<b>Dynamic analysis on complete OWT model</b>		Input: $\mathbf{f} = \begin{bmatrix} \mathbf{f}^{(f)} \\ \mathbf{f}^{(w)} \end{bmatrix}$ Output: $\mathbf{g}^{(f)}, \mathbf{u}^{(f)}, \mathbf{u}_b$ Accuracy: Numerically exact, $\mathbf{g}^{(f)}, \mathbf{u}^{(f)}$ and $\mathbf{u}_b$ are used as reference solution to determine the accuracy of the other results
<b>Post-processing Force controlled</b>		Input: $\mathbf{f}^{(f)}, \mathbf{g}^{(f)}$
Dynamic		Output: $\mathbf{u}_{DFC} = \mathbf{u}^{(f)}$ Accuracy: Response equal to reference solution
Quasi-static		Output: $\mathbf{u}_{QsFC}$ Accuracy: Accurate if $\omega_{free}^{\{1\}} \gg \max(\omega_{ext})$
<b>Post-processing Displacement controlled</b>		Input: $\mathbf{f}_i, \mathbf{u}_b$
Dynamic		Output: $\mathbf{u}_i, \mathbf{u}_{DDC} = \begin{bmatrix} \mathbf{u}_i \\ \mathbf{u}_b \end{bmatrix} = \mathbf{u}^{(f)}$ Accuracy: Response equal to reference solution
Quasi-static		Output: $\mathbf{u}_{i,Qs}, \mathbf{u}_{QsDC} = \begin{bmatrix} \mathbf{u}_{i,Qs} \\ \mathbf{u}_b \end{bmatrix}$ Accuracy: Accurate if $\omega_{fixed}^{\{1\}} \gg \max(\omega_{ext})$

**Table 4.1:** Input, output and accuracy of different calculation procedures in case of the detailed foundation structure is integrated in the complete OWT model.

		Reduced foundation in complete OWT model
<b>Dynamic analysis on complete OWT model</b>		<p>Input: <math>\tilde{\mathbf{f}} = \begin{bmatrix} \tilde{\mathbf{f}}^{(f)} \\ \tilde{\mathbf{f}}^{(w)} \end{bmatrix}</math></p> <p>? Output: <math>\tilde{\mathbf{g}}^{(f)}, \tilde{\mathbf{u}}^{(f)}, \tilde{\mathbf{u}}_b</math> and <math>\mathbf{u}_{exp}^{(f)}</math></p> <p>Accuracy: Accurate if OWT model is spectrally and spatially converged</p>
<b>Post-processing</b>		
Force controlled		<p>Input: <math>\mathbf{f}^{(f)}, \hat{\mathbf{g}}^{(f)}</math></p>
Dynamic	?	<p>Output: <math>\hat{\mathbf{u}}_{DFC}</math></p> <p>Accuracy: Accurate if OWT model is spectrally and spatially converged, as a result the interface loads are accurate</p>
Quasi-static	?	<p>Output: <math>\hat{\mathbf{u}}_{QsFC}</math></p> <p>Accuracy: Accurate if OWT model is spectrally and spatially converged (accurate interface loads) and if <math>\omega_{free}^{\{1\}} \gg \max(\omega_{ext})</math></p>
<b>Post-processing</b>		
Displacement controlled		<p>Input: <math>\mathbf{f}_i, \tilde{\mathbf{u}}_b</math></p>
Dynamic	?	<p>Output: <math>\hat{\mathbf{u}}_i, \hat{\mathbf{u}}_{DDC} = \begin{bmatrix} \hat{\mathbf{u}}_i \\ \tilde{\mathbf{u}}_b \end{bmatrix}</math></p> <p>Accuracy: Accurate if OWT is spectrally and spatially converged, as a result the boundary response is accurate</p>
Quasi-static	?	<p>Output: <math>\hat{\mathbf{u}}_{i,Qs}, \hat{\mathbf{u}}_{QsDC} = \begin{bmatrix} \hat{\mathbf{u}}_{i,Qs} \\ \tilde{\mathbf{u}}_b \end{bmatrix}</math></p> <p>Accuracy: Accurate if OWT is spectrally and spatially converged (accurate interface displacements) and if <math>\omega_{fixed}^{\{1\}} \gg \max(\omega_{ext})</math></p>

**Table 4.2:** Input, output and accuracy of different calculation procedures in case of a reduced foundation model is integrated in the complete OWT model.

# Chapter 5

## Modeling

### 5.1 Introduction

A case study will be performed to determine the quantitative error for the various calculation procedures, the response of the different calculation procedures will be compared to a reference solution. The reference solution is the response of the foundation obtained from the dynamic analysis of the complete OWT model with the detailed foundation model.

As the accuracy of the different calculation procedures is structure dependent, two different OWT models are constructed. Both models consist of identical component models, except for the foundation structure. One OWT model is installed with a monopile foundation structure and the other with a jacket. These two foundation structures are most used in practice. The monopile is often used in shallow waters and the jacket structure in deeper waters. Next to this, the jacket structure experiences local dynamics due to its construction, this does not apply to the monopile. Therefore, the hypothesis is that a quasi-static analysis of a jacket structure will provide less accurate results than for the monopile. Furthermore, reducing a jacket structure will have more impact on the accuracy of the interface loads/displacements than reducing a monopile.

To create the OWT models, a FE model is constructed. An Euler Bernoulli beam element will be used to describe the behavior of the element of the FE model. The formulation of an Euler beam element will be reminded, with a special emphasis to the displacement-strain-stress conversion. Computing stresses is important to determine the fatigue damage of the structure, which is often the main design driver for the support structure.

Section 5.4 will present the properties and characteristics of the different components of the OWT model. This will give insight in the spectral and spatial convergence of the OWT models when a reduced foundation model is integrated. The last section will present how the external loads on the OWT structures are modeled for this specific case study.

### 5.2 Finite element model

The wind turbine will be modeled as a FE model. The FE method is a numerical analysis technique to obtain approximated solutions for a wide variety of problems. In the FE method a structure is divided into subdomains, which are discretized using shape functions [28].

The first step in constructing a finite element model of a structure is dividing the structure into

smaller sections where each section is represented by an element. The length of these elements are essential variables for the finite element model. A more precise and accurate result will be achieved by using a large number of elements. However, it implies higher computation time and costs [17].

The second step in constructing a FE model is defining the shape function for the elements. After defining the shape function, the displacement field for each element can be described based on that. In general, this description is formulated as [28]:

$$u_i(x_1, x_2, x_3, t) = \sum_{j=1}^n f_{ij}(x_1, x_2, x_3) q_j(t) \quad i = 1, 2, 3 \quad (5.1)$$

where  $u_i$  is the displacement field,  $f_{ij}(x_1, x_2, x_3)$  is the shape function, and  $q_j(t)$  is a time dependent amplitude. Equation (5.1) can be stated in matrix form as

$$\mathbf{u}(x_1, x_2, x_3, t) = \mathbf{F}(x_1, x_2, x_3) \mathbf{q}(t) \quad (5.2)$$

The FE model of the offshore wind turbine is described by beam elements. Several shape functions for beam elements exist, the *Euler-Bernoulli* beam will be used in this model.

The Euler-Bernoulli beam is the classical formulation of a beam and estimates vertical and lateral deflection of the element, shear deformation is neglected. The shape functions for a 3D Euler beam element and the associated element stiffness and mass matrix are presented in Appendix C. After defining the element stiffness and mass matrix, the element damping matrix can be determined.

### 5.2.1 Element damping matrix

In order to determine the damping matrix  $\mathbf{C}$  there are several methods. If light damping is assumed and if the modal damping ratios  $\epsilon_s$  are known two different strategies can be used. In the first approach one can build the damping matrix by *modal expansion* [27].

$$\mathbf{C} = \sum_{s=1}^n \mathbf{M} \mathbf{x}_{(s)} \frac{2\epsilon_s \omega_s}{\mu_s} \mathbf{x}_{(s)}^T \mathbf{M} \quad (5.3)$$

Where  $\mathbf{x}_{(s)}$  are eigenmodes,  $\omega_s$  eigenfrequencies and  $\mu_s$  is the modal mass coefficient.

Another method is to build the damping matrix  $\mathbf{C}$  as a combination of the mass and the damping matrix, namely

$$\mathbf{C} = a\mathbf{K} + b\mathbf{M} \quad (5.4)$$

This construction is called *Rayleigh damping* and this method assumes that the damping forces in the system are distributed partly like the elastic forces and partly like the inertia forces. As a result, the modal damping ratios are defined as

$$\epsilon_s = \frac{\beta_{ss}}{2\mu_s \omega_s} = \frac{1}{2} \left( a\omega_s + b\frac{1}{\omega_s} \right) \quad (5.5)$$

One can choose the coefficients  $a$  and  $b$  such that the modal damping ratios of 2 modes fit the measured data. In that case all other modal damping ratios are determined but do in general over- or underestimate the real modal damping.



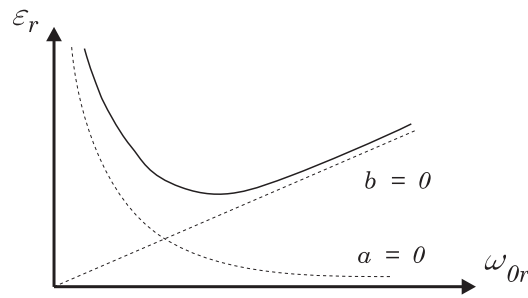


Figure 5.1: Modal damping matrix: weighted sum of mass and stiffness matrices [27].

The damping matrices are constructed per each substructure of the OWT model, so not per element. The global damping matrix is obtained by assembling the substructure damping matrices. The damping matrix is a full matrix and by constructing the damping matrices per substructure substructuring is still possible. In other words, the foundation structure and the tower do not have any coupling terms in the damping matrix, this way the substructures can be analyzed componentwise. The damping per substructure is modeled such that the global model damping ratios for both OWT models are about 1%.

The damping matrices of the substructures of the OWT model with a monopile are modeled with Rayleigh damping and the damping matrices of the substructures of the OWT model with the jacket are modeled by modal expansion.

## 5.3 Strains and stresses

Fatigue damage is often the main design driver of the support structure and can be computed based on stresses in the structure. In order to compute the stresses in an element, the strains are needed as an input. These strains are computed with the shape functions of an Euler beam element and the displacements in the elements. Eventually the fatigue damage is determined as explained in Subsection 2.4.3.

### 5.3.1 Strains

To determine the strains in an Euler-Bernoulli beam element, some kinematic assumptions are made [28]:

- The beam cross section is not deformable
- The axial displacement component results from the rotation of the cross section. The rotation is such that the cross sections remain orthogonal to the neutral axis  $u(x, z) = -z \frac{\partial w}{\partial x} - y \frac{\partial v}{\partial x}$ . Figure 5.2 shows this assumption visually.

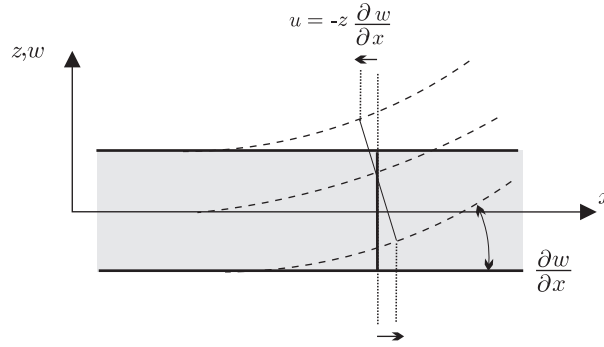


Figure 5.2: Bernoulli kinematic assumptions [28].

The displacement in the local x-direction is  $u$ , in the local y-direction is  $v$  and in the local z-direction is  $w$ . With the assumption of geometric linearity, the strain expressions can be written based on the shape functions of an Euler beam, presented in Appendix C.

$$\epsilon_{xx} = \frac{\partial u}{\partial x} = -z \frac{\partial^2 w}{\partial x^2} - y \frac{\partial^2 v}{\partial x^2} \quad (5.6)$$

$$\epsilon_{yy} = \frac{\partial v}{\partial y} = 0 \quad (5.7)$$

$$\epsilon_{zz} = \frac{\partial w}{\partial z} = 0 \quad (5.8)$$

$$\epsilon_{xy} = \frac{1}{2} \left( \frac{\partial v}{\partial x} + \frac{\partial u}{\partial y} \right) = 0 \quad (5.9)$$

$$\epsilon_{yz} = \frac{1}{2} \left( \frac{\partial v}{\partial z} + \frac{\partial w}{\partial y} \right) = 0 \quad (5.10)$$

$$\epsilon_{zx} = \frac{1}{2} \left( \frac{\partial w}{\partial x} + \frac{\partial u}{\partial z} \right) = 0 \quad (5.11)$$

The last equations (5.9), (5.10) and (5.11) show that the last assumption is equivalent to neglecting the shear deformation of the material [33]. This assumption is called the *Bernoulli* assumption. From the shape functions of the Euler beam follows

$$\epsilon_{xx} = -z \frac{\partial^2 w}{\partial x^2} - y \frac{\partial^2 v}{\partial x^2} = -z \begin{bmatrix} \frac{-6}{\ell^2} + \frac{12x}{\ell^3} & \frac{4}{\ell} - \frac{6x}{\ell^2} & \frac{6}{\ell^2} - \frac{12x}{\ell^3} & -\frac{6x}{\ell^2} + \frac{2}{\ell} \end{bmatrix} \begin{bmatrix} w_1 \\ \psi_{y1} \\ w_2 \\ \psi_{y2} \end{bmatrix} \quad (5.12)$$

$$-y \begin{bmatrix} \frac{-6}{\ell^2} + \frac{12x}{\ell^3} & \frac{-4}{\ell} + \frac{6x}{\ell^2} & \frac{6}{\ell^2} - \frac{12x}{\ell^3} & \frac{6x}{\ell^2} - \frac{2}{\ell} \end{bmatrix} \begin{bmatrix} v_1 \\ \psi_{z1} \\ v_2 \\ \psi_{z2} \end{bmatrix}$$

### 5.3.2 Stresses

To obtain the stress in a structure Hooke's law is used. In a Euler beam there is only a strain in the axial direction, so there will be only a stress in this direction [33].

$$\sigma_x(x, y, z) = E\epsilon_x(x, y, z) = E \left( -z \frac{\partial^2 w}{\partial x^2} - y \frac{\partial^2 v}{\partial x^2} \right) \quad (5.13)$$

$$= -zE \left( [B_1 \ B_2 \ B_3 \ B_4] \begin{bmatrix} w_1 \\ \psi_{y1} \\ w_2 \\ \psi_{y2} \end{bmatrix} \right) - yE \left( [B_1 \ -B_2 \ B_3 \ -B_4] \begin{bmatrix} v_1 \\ \psi_{z1} \\ v_2 \\ \psi_{z2} \end{bmatrix} \right) \quad (5.14)$$

$$B_1 = \frac{-6}{\ell^2} + \frac{12x}{\ell^3} \quad (5.15)$$

$$B_2 = \frac{4}{\ell} - \frac{6x}{\ell^2} \quad (5.16)$$

$$B_3 = \frac{6}{\ell^2} - \frac{12x}{\ell^3} \quad (5.17)$$

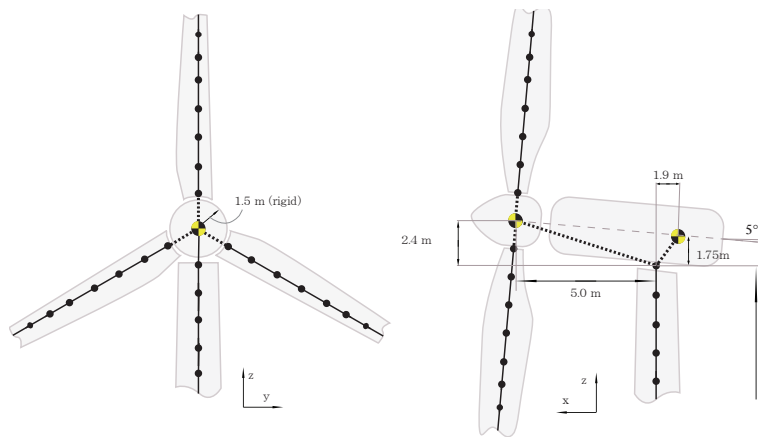
$$B_4 = \frac{-6x}{\ell^2} + \frac{2}{\ell} \quad (5.18)$$

where  $E$  is the Young's modulus and the subscripts 1 and 2 of the local displacements and rotations represent node 1 and node 2 of an element. Finally, a stress signal is obtained for every node. These stress signals are rearranged with the rainflow counting method and with the S-N curve the fatigue damage is determined.

In the case study a model of the OWT is built and an external load is applied on this model. The global displacements are computed which should be converted to local displacements in order to compute the stresses in the elements. This can be achieved using a transformation matrix. To verify if the transformation from global to local frame is correct and the stresses computed in Matlab are accurate, a verification in ANSYS is done. The theory of converting displacements from the global frame to the local frame and the verification in ANSYS is presented in Appendix D.

## 5.4 OWT model

In order to verify the quantitative error of the different calculation procedures two offshore wind turbine model are constructed, one with a monopile and one with a jacket. The tower and the RNA models are similar in both models. The dimensions and other properties of the different components are summarized and the characteristics per OWT model will be presented.



**Figure 5.3:** RNA of the NREL 5MW baseline turbine [24].

The **Rotor-Nacelle-Assembly** (RNA) consists of the nacelle, the hub and three blades which are 61.5 meters long, see Figure 5.3. The nacelle is modeled as a point mass and is connected to the tower top with one rigid and massless element. The point mass represents the mass, 240,000 kg, and inertia of the nacelle. The hub is modeled in the same way as the nacelle, a point mass represents the mass and inertia of the hub and a massless and rigid element is used to connect the hub to the tower top. The rotor, consisting of the hub and the blades, weighs 110,000 kg. The RNA model is obtained by assembling the different components, and has 276 DoF. The RNA model is reduced with the Craig-Bampton method with 30 fixed interface modes included, accordingly, the reduced RNA model has 36 DoF. The reduced RNA model is used in both OWT models.

The **tower** is made of steel and has a conical shape with a base diameter of 6.0 meter and top diameter of 3.87 meter. It has a length of 87.6 meters and a constant wall thickness of 0.05 meter. The tower is subdivided into 19 elements and has thus 120 DoF. The tower has two interfaces, one at the bottom, which will be connected to the foundation structure and one at the top, which will be connected to the RNA.

The **monopile** is made of steel and has a cylindrical shape with a diameter of 6.0 meter and a constant wall thickness of 0.08 meter. The monopile has a length of 30 meters and is subdivided into 10 elements. The bottom of the monopile is constrained in all directions and, consequently, it has 60 DoF. The monopile has one interface, at the top, which will be connected to the tower bottom.

The **jacket** is originally designed the Upwind project and used in the OC4 project [39]. The jacket consists of four main legs which are interconnected via four levels of X-braces, see Figure 5.4. The jacket is made of steel and is constructed with circular tubes with various dimensions, see Table 5.1. The total height of the jacket is 68 meters and the four main legs are constrained in all directions at the bottom. The jacket model contains a concrete transition piece, weighing 666,000 kg. This transition piece rigidly connects the top elements of the jacket. The jacket has 1014 DoF and one interface at the top of the jacket, which will be connected to the tower bottom. As the water counteracts the movements of the jacket, additional point masses are added to the nodes of the structure to take this effect into account.

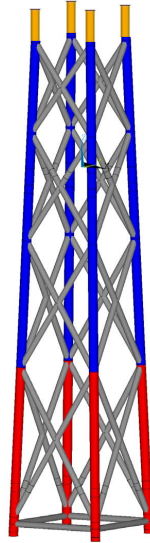


Figure 5.4: OC4 jacket model [39].

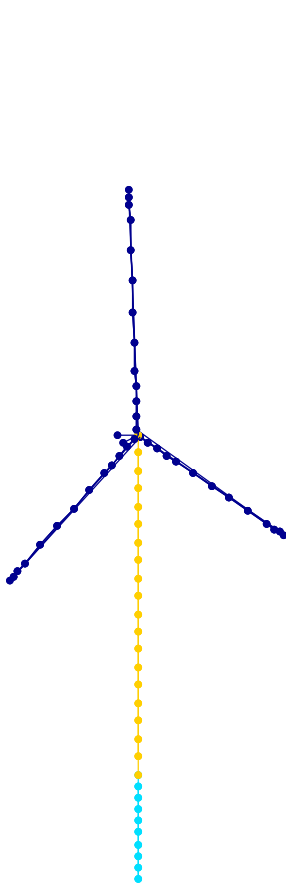
Property set	Component	Color in Figure 5.4	Outer diameter [m]	Wall thickness [m]
1	x- and mud braces	grey	0.8	0.02
2	leg at lowest level	red	1.2	0.05
3	leg 2nd to 4th level	red	1.2	0.035
4	leg crossing TP	orange	1.2	0.04
5	pile	not shown	2.082	0.06

Table 5.1: Dimensions of the components of the OC4 jacket model [39].


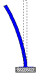
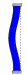
#### 5.4.1 Model I - OWT with a monopile

A schematic representation of the OWT model with a monopile is shown in Figure 5.5. The dots represent nodes, which all have 6 DoF, and the bottom of the monopile is constrained in all directions. Different characteristics of the OWT will be presented, which will be important for analyzing the accuracy of different calculation procedures.

The first twenty eigenfrequencies of the complete OWT model, the foundation with a free interface and the foundation with a fixed interface are shown in Table 5.2. Differences between a quasi-static and a dynamic analysis will appear around  $\omega_{free}^{\{1\}}$  for the force controlled approach and around  $\omega_{fixed}^{\{1\}}$  for the displacement controlled approach. The external force spectrum should be known in order to get insight in the excitation bandwidth and if a quasi-static analysis will provide an accurate result. In general, frequencies are excited up to 7 Hz and from Table 5.2 it is expected that a quasi-static displacement controlled approach will provide an accurate result as  $\omega_{fixed}^{\{1\}}$  is 42.8 Hz. The difference between a quasi-static analysis and a dynamic analysis for the force controlled approach will appear around 6.7 Hz, so within the excitation bandwidth. The hypothesis is that a quasi-static force controlled approach will not provide an accurate result for the OWT model with a monopile.



**Figure 5.5:** OWT model with monopile.

Eigenfrequency	 [Hz]	Foundation  $\omega_{free}$ [Hz]	Foundation  $\omega_{fixed}$ [Hz]
1st	0.30	6.73	42.84
2nd	0.30	6.73	42.84
3rd	0.76	26.76	53.68
4th	0.78	42.19	86.56
5th	0.80	42.19	108.69
6th	1.17	43.15	118.11
7th	1.26	80.94	118.11
8th	1.27	118.15	166.36
9th	1.91	118.15	175.25
10th	2.05	130.50	228.03
11th	2.16	137.11	231.71
12th	2.38	196.62	231.71
13th	2.43	221.08	268.25
14th	3.73	231.69	294.75
15th	4.43	231.69	366.75
16th	4.67	260.71	367.68
17th	4.80	317.04	383.65
18th	5.07	330.14	383.65
19th	5.44	383.61	441.99
20th	5.69	383.61	475.26

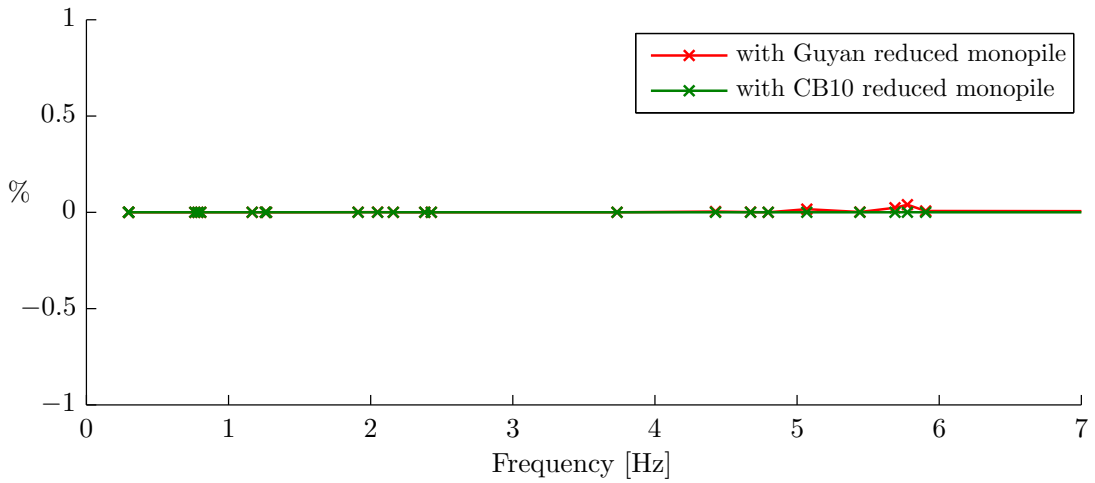
**Table 5.2:** Eigenfrequencies of OWT model, free interface foundation and fixed interface foundation.

The reduction of the foundation could influence the accuracy of the interface loads and displacement. Two different reduction methods will be examined for the monopile model to verify the quantitative error in the response of the foundation structure, the Guyan reduction and the Craig-Bampton reduction with 10 fixed interface modes included (CB10). The different reduction methods are respectively described in Section 3.4.2 and 3.4.3.

Figure 5.6 shows the relative error between the exact eigenfrequencies and the eigenfrequencies of the complete OWT model with the Guyan and the CB10 reduced monopile model. The markers represent the exact eigenfrequencies, thus the eigenfrequencies of the OWT model with a detailed foundation model. The relative error in the eigenfrequencies provides information about the spectral convergence of the OWT models with a reduced foundation model. The eigenfrequencies of the different OWT models are given in Appendix E, Table E.1. The Guyan reduction method uses a reduction basis containing only the static constraint modes. This reduction method artificially ‘stiffens’ the structure and the eigenfrequencies will be higher. The relative difference is increasing for higher frequencies. Still, the relative difference remains small in this frequency range, this is because a monopile does not experience a lot of local dynamics. Therefore, the OWT model with a Guyan reduced monopile is spectrally converged.

The Craig-Bampton method can be seen as an enrichment of the Guyan reduction. Instead of reducing with only static constraint modes, the Craig-Bampton method also includes fixed interface

modes and thereby creates a more complete basis for the reduction. In this case 10 modes are included. The first fixed interface eigenfrequency is at 42.8 Hz and the tenth is at 228.0 Hz. As the foundation is a substructure, the modes that are included do not provide any insight in the global spectral convergence. However, Figure 5.6 shows that the relative difference in eigenfrequencies for an OWT model with a CB10 reduced foundation model is very small, and it can be concluded that the OWT model is spectrally converged up to 7 Hz. As the OWT model with the Guyan reduced foundation is spectrally converged as well, the ten fixed interface modes that are included in the Craig-Bampton reduction basis will therefore especially improve the spatial convergence.



**Figure 5.6:** Relative error eigenfrequencies of OWT model with a reduced monopile with respect to detailed OWT model. The markers represent the exact eigenfrequencies.

The spatial convergence provides information about how well the reduction basis can capture the effect of the external loads on the structure. An error  $\mathbf{r}^{(f)}$  is introduced in the equation of motion, see equation (5.19), since the new set of DoF does not span the full solution. This error is defined as the residual and the response of the foundation is an approximation of the exact solution. If the model is spectrally and spatially converged, the residual load will be small. The residual load provides information about the spatial convergence only if the model is spectrally converged, otherwise, the residual will provide information about both the spectral and spatial convergence. The spatial convergence of the OWT models will be determined in Subsection 6.2.3.

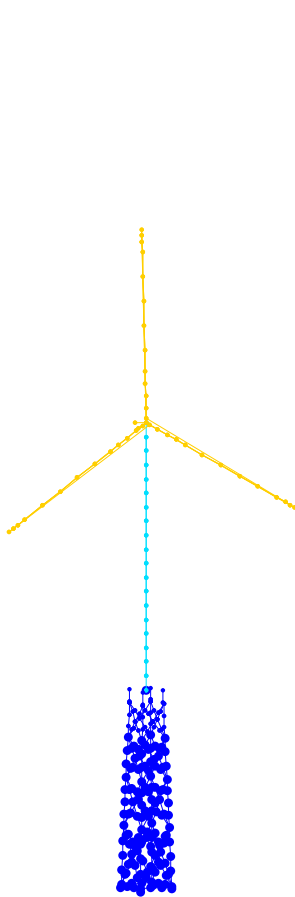
$$(-\omega^2 \mathbf{M}^{(f)} + j\omega \mathbf{C}^{(f)} + \mathbf{K}^{(f)}) \mathbf{R} \tilde{\mathbf{u}}^{(f)} = \mathbf{f}^{(f)} + \mathbf{g}^{(f)} + \mathbf{r}^{(f)} \quad (5.19)$$

The first ten mode shapes of the monopile and the complete OWT with a monopile foundation are presented in Appendix E.

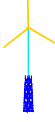


#### 5.4.2 Model II - OWT with a jacket

A schematic representation of the OWT model with a jacket is shown in Figure 5.7. The jacket is constrained at the bottom in all directions. Table 5.3 shows the first twenty eigenfrequencies of the complete OWT model, the jacket with a free interface and the jacket with a fixed interface. It is clear that the eigenfrequencies of the jacket are significantly lower than for the monopile. In

general, the external load excites frequencies up to 7 Hz, as a result lots of eigenfrequencies of the jacket are excited whereas for the monopile eigenfrequencies are hardly excited. The hypothesis is that a quasi-static analysis of a jacket foundation structure will not provide accurate results, as the eigenfrequencies of this foundation structure are within the excitation bandwidth.



**Figure 5.7:** OWT model with jacket.

Eigenfrequency	 [Hz]	Foundation  $\omega_{free}$ [Hz]	Foundation  $\omega_{fixed}$ [Hz]
1st	0.27	1.06	4.09
2nd	0.28	1.06	4.09
3rd	0.75	2.96	4.44
4rd	0.78	3.73	4.70
5th	0.80	3.73	4.74
6th	1.01	4.44	4.86
7th	1.08	4.68	4.86
8th	1.25	4.74	5.21
9th	1.26	4.76	5.60
10th	1.30	4.76	6.28
11th	2.00	5.60	6.70
12th	2.31	6.07	6.70
13th	2.40	6.59	6.88
14th	2.79	6.59	6.88
15th	2.86	6.66	6.95
16th	2.87	6.71	7.25
17th	4.06	6.88	7.28
18th	4.12	6.88	7.41
19th	4.20	7.25	7.80
20th	4.44	7.28	7.80

**Table 5.3:** Eigenfrequencies of OWT model, free interface foundation and fixed interface foundation.

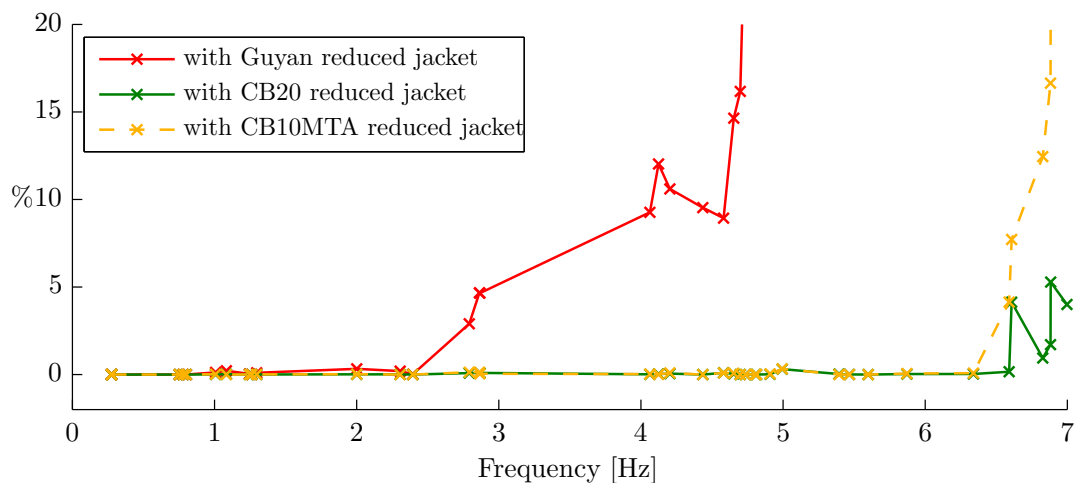
The jacket structure experiences more local dynamics than the monopile, the hypothesis is that the reduction of a jacket structure will have large impact on the accuracy of the interface loads and displacements. Three different reduction methods will be examined for the jacket model, the Guyan reduction, the Craig-Bampton reduction with 20 fixed interface modes (CB20) and the Augmented Craig-Bampton model with 10 fixed interface modes and 10 MTA vectors (CB10MTA).

Figure 5.8 shows the relative error between the exact eigenfrequencies and the eigenfrequencies of the complete OWT models with the different reduced foundation models. The eigenfrequencies of the different OWT models are presented in Appendix E, Table E.4. It is clear that reduction of a jacket model influences the eigenfrequencies of the complete OWT model more than for a reduced monopile. Differences between the eigenfrequencies of the detailed OWT model and the OWT model with a Guyan reduced foundation are getting large from 3 Hz. The difference is increasing for higher frequencies. This difference in eigenfrequencies will result in inaccurate interface loads/displacements. The interface loads/displacements will contain high amplitudes at wrong frequencies. Moreover, the eigenfrequencies of the foundation could be excited due to inaccuracies



in the interface loads/displacements, extra peaks appear in the FRF of the foundation, *pseudo resonances*. The OWT model with a Guyan reduced jacket is not spectrally converged in this case.

The OWT model with a CB20 reduced foundation and the OWT model with a CB10MTA reduced foundation have more accurate eigenfrequencies. The fixed interface modes, that are included in the reduction basis, improve especially the spectral convergence and the MTA vectors the spatial convergence. Comparing the eigenfrequencies of the different OWT models provides information about the spectral convergence. The OWT model with a CB20 reduced foundation model is spectrally converged, as difference appears from 6.5 Hz and it is less likely that these higher frequencies are excited. Differences appear from 6.2 Hz for the OWT model with a CB10MTA reduced foundation model. As it is less likely that these higher frequencies are excited, it can be assumed that the OWT model with a CB10MTA reduced foundation model is spectrally converged as well. Information about the spatial convergence can not be obtained by comparing the eigenfrequencies of the complete OWT model. The spatial convergence of the different jacket models will be checked in Subsection 7.2.3 based on the residual load that is introduced in the equation of motion after expansion of the reduced response, see equation (5.19).



**Figure 5.8: Relative error eigenfrequencies** of OWT model with a reduced jacket with respect to the detailed OWT model. The markers represent the exact eigenfrequencies. Note that reduction of the jacket has more impact on the accuracy of results as the relative error is larger than for the OWT with a reduced monopile (Figure 5.6).

The first ten mode shapes of the jacket and the complete OWT with a jacket foundation structure are given in Appendix E.

## 5.5 Loads

In order to gain more insight in the differences between the calculation procedures a load spectrum is created for the wind and the wave load. Some simplifications in modeling the load spectrum are made, as accurate modeling of loads is complex and not within the scope of the research.

Section 2.2 presented that modeling wind loads is complex and depends on different parameters as the wind speed, the wind shear coefficient, the turbulence intensity and the wind turbine itself.

As the OWT models are not constructed for a specific area, data about wind velocity is not available. Therefore, the wind load spectrum will be modeled based on an already known wind load spectrum in a certain area. Although the amplitude of the wind load is dependent on the structure, it is assumed that the shape of the wind load spectrum will be similar. The modeled wind load will be such that it will excite the OWT model in the right frequency range. The operational loads will be integrated in this wind load spectrum as well. As the drag forces due to rotation of the blades are large, it is assumed that the wind loads exciting the tower can be neglected. The wind load is not applied on certain nodes of the RNA model, but at the tower top, because the deformation of support structure is of interest in this research and the deformation of the blades will not be analyzed. Although the modeled load is simplified, the results from the analyses will provide insight in the accuracy of different calculation procedures which is the aim of the research.

Section 2.3 presented the different steps in modeling wave loads. As this modeling process has some complex aspects as well, the wave loads are modeled using existing tools. The wave loads for the monopile are modeled with a tool developed by Michiel van der Meulen [23]. In general, the wave loads on a monopile are higher than on a jacket, because of the geometry of the monopile. The wave loads on the jacket structure were already present, as the model was used for the OC4 project. These wave loads were generated in the commercially available ANSYS ASAS software suite.

The case study is performed in the frequency domain to verify the inaccuracies defined in Chapter 4 for the different calculation procedures. However, in order to evaluate what the impact is of the inaccuracies in the response on the fatigue damage of the structure for the different calculation procedures, the loads are converted to the time domain.

### 5.5.1 Wind and operational loads

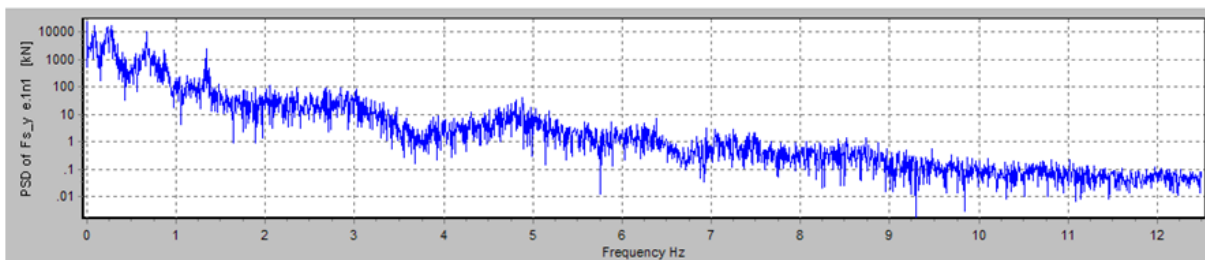
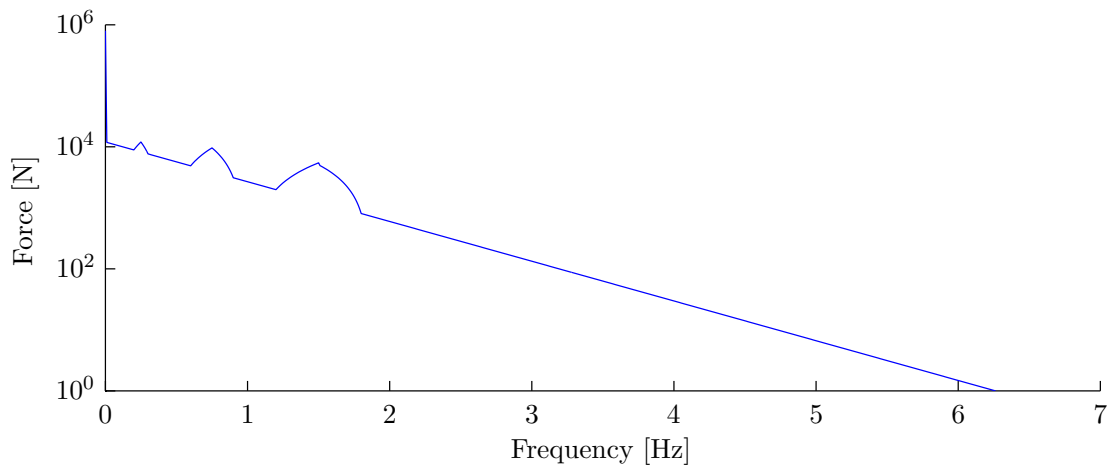


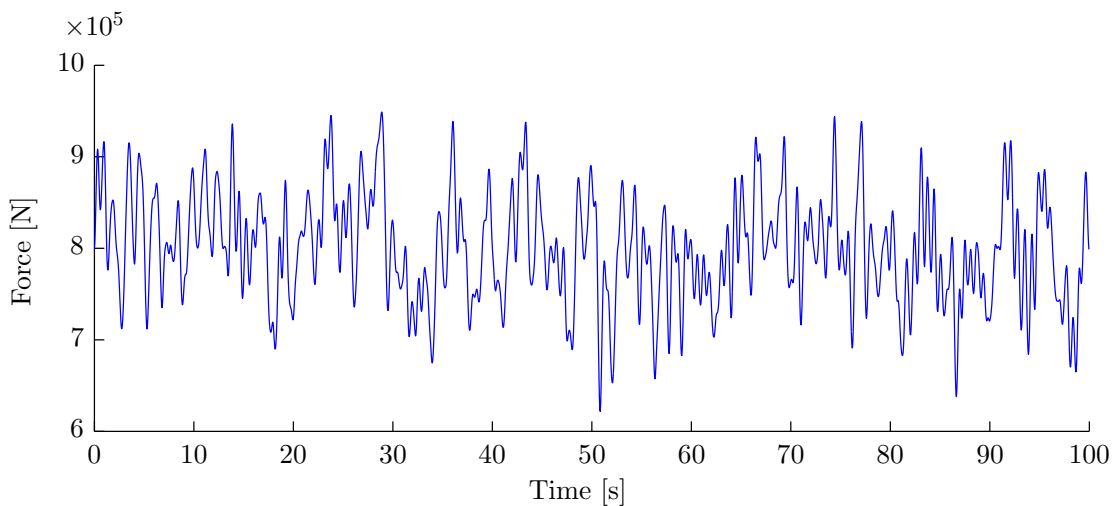
Figure 5.9: Real wind load spectrum,

A real wind load spectrum was used to model the wind load spectrum for this load case, see Figure 5.9. The real wind load spectrum contains lots of fluctuations and is dependent on the turbine. In order to simplify this spectrum a linear decreasing line is drawn in the real spectrum and this line is modeled. Next to this, the operational loads for 1P, 3P and 6P are included. A variable speed between 12-18 RPM is assumed. To get a more realistic response of the OWT model an offset of 800 kN at 0 Hz is applied. The modeled wind load spectrum is shown in Figure 5.10a.

In order to verify the accuracy of the fatigue damage results for the different calculation procedures, the wind load spectrum is converted to the time domain. A sinus function is created for every excitation frequency with the associated amplitude and a random phase. The excitation frequencies ranging from 0-7 Hz with steps of 0.01 Hz, in total 700 sinus functions are created. All these sinus functions are added together to create the wind load in the time domain, see Figure 5.10b.



(a) Operational and wind load spectrum



(b) Operational and wind load in the time

**Figure 5.10:** Modeled operational and wind load in the frequency and time domain.

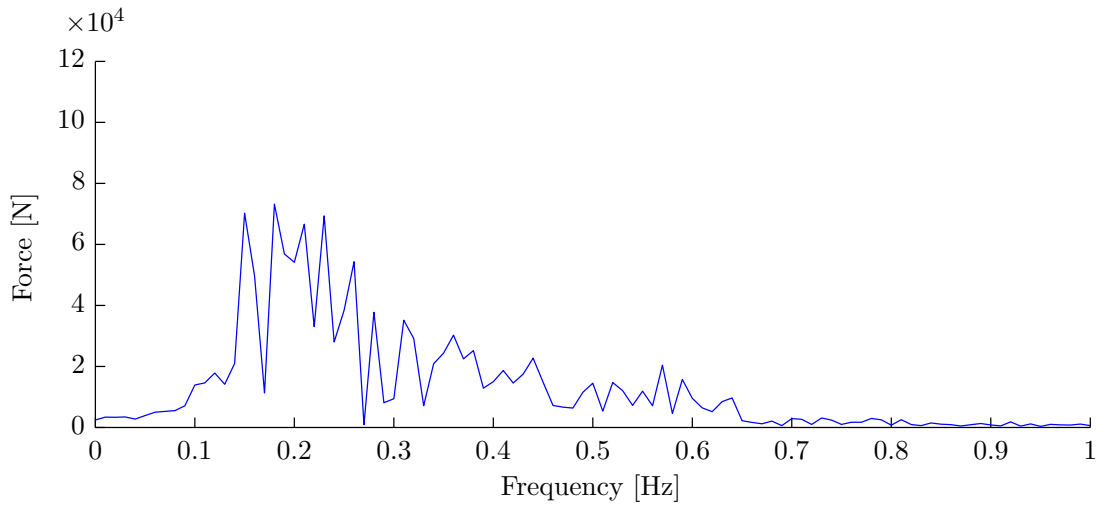
## 5.5.2 Wave loads

### Monopile

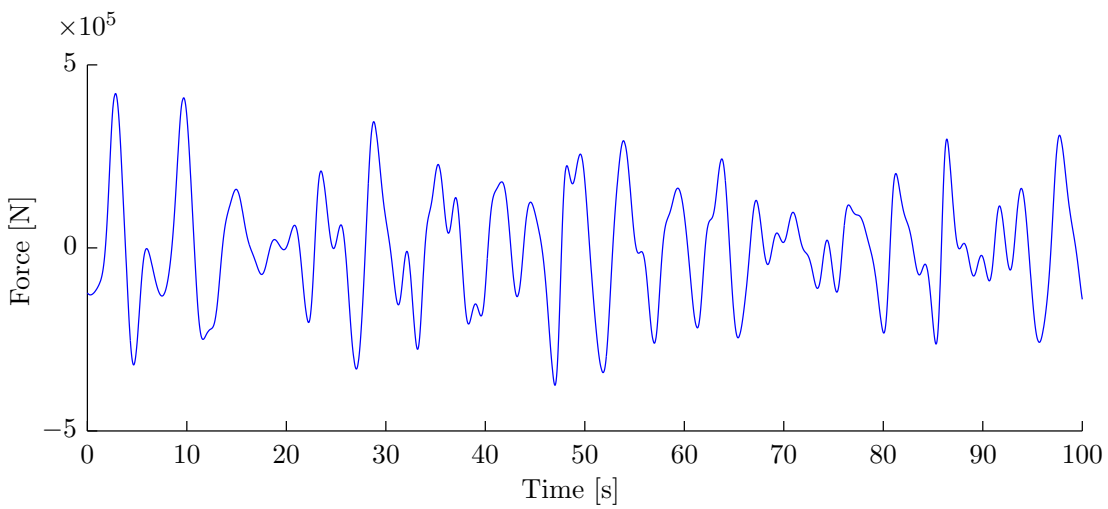
The wave loads on a monopile are modeled with a tool developed by Michiel van der Meulen [23]. As described in Section 5.4 the jacket model was used for the OC4 project and the associated wave loads in the time domain were modeled in ANSYS ASAS software package [38]. The sea state to develop the wave loads for the jacket model is used to create the wave loads for the monopile as well. First the wave load spectrum is determined based on the same significant wave height and the peak period used for the jacket wave loads. Then the wave kinematics are defined based on non-linear wave theory and finally the wave loads are computed with the Morison equation [23]. The difference between the tool of Michiel van der Meulen and ASAS is that the wave kinematics in the ASAS are based on the linear wave theory.

The resultant wave load on the monopile will be higher due to the larger frontal area of the monopile

with respect to the jacket . The wave loads are created in the time domain and converted to the frequency domain to perform the different calculation procedures in the frequency domain. The wave load spectrum for the monopile is given in Figure 5.11a and the resultant wave load on the monopile in the time domain is shown in Figure 5.11b.



(a) Wave load spectrum for the monopile

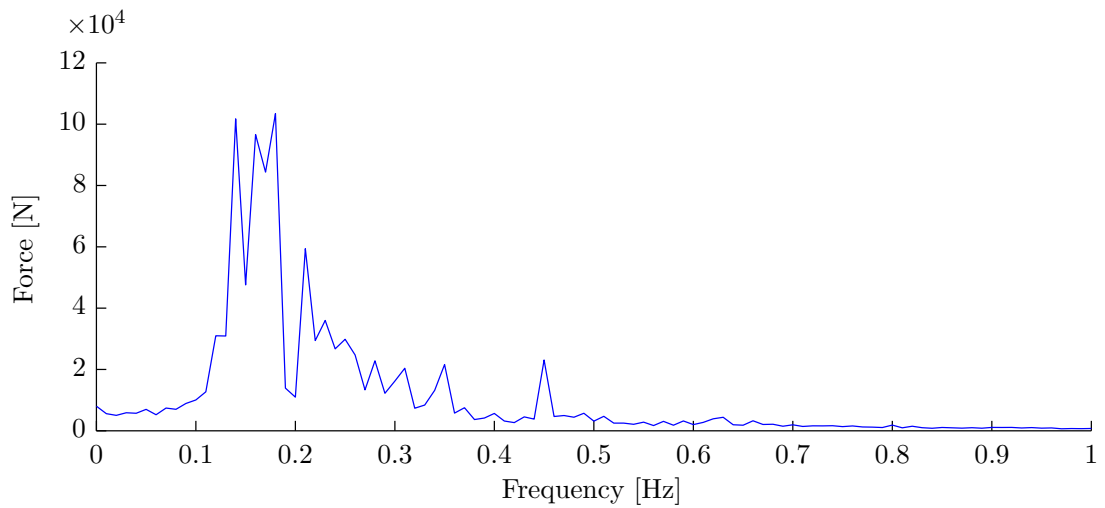


(b) Resultant wave load on monopile in the time

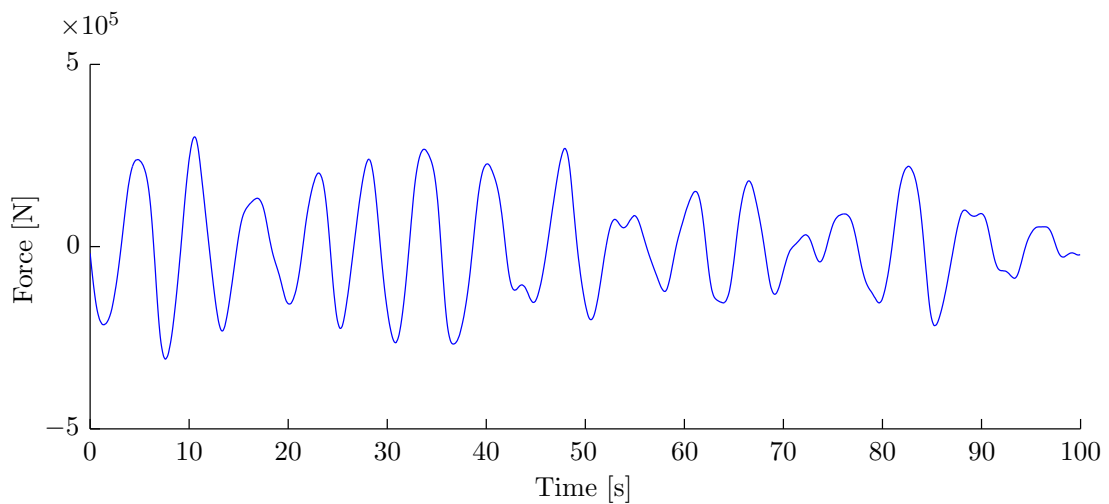
**Figure 5.11:** Modeled wave load for the monopile in the frequency and time domain.

### Jacket

Wave loads for the jacket model were already present in the time domain and are created in ASAS. ASAS determines the wave kinematics based on linear wave theory. In order to create the wave load spectrum for the jacket, the wave loads in the time domain are converted to the frequency domain, Figure 5.12a. Figure 5.12b shows that the resultant wave load on the jacket model and as expected, this wave load is lower than the wave load on a monopile.



(a) Wave load spectrum jacket



(b) Resultant wave load on jacket in the time

**Figure 5.12:** Modeled wave load for the jacket in the frequency and time domain.



## Chapter 6

# Results of calculation procedures - Monopile

### 6.1 Introduction

To determine the quantitative error that can arise in the different calculation procedures presented in Chapter 4, two models of an offshore wind turbine are constructed, described in Section 5.4. This chapter will present the results of the different calculation procedures performed on the OWT model with a monopile. To identify their accuracy a reference solution is necessary. Therefore, the fully integrated method will be executed. In other words, the detailed monopile model will be integrated in the complete OWT model and a dynamic analysis will be performed under wind and wave loading. The response for the detailed monopile will be used as a reference solution.

All the different calculation procedures described in Chapter 4 will be simulated. Firstly, the inaccuracies that arise in the dynamic analysis of the complete OWT model with reduced components will be examined and secondly the inaccuracies in the post-processing analyses on the detailed foundation model. The difference between a quasi-static and a dynamic analysis will be investigated for a force and a displacement controlled approach. Furthermore, the impact of the error due to the use of a reduced foundation model in the complete OWT model analysis on the post-processing analyses will be defined. As presented in Subsection 5.4.1 two different reduction methods will be examined for the monopile model: the Guyan reduction and the Craig-Bampton reduction with 10 fixed interface modes included (CB10).

Finally, with the response obtained from the various calculation procedures the fatigue damage is computed and it will be investigated what the impact is of the error in the response on the fatigue damage results.

Table 6.1 gives an overview of the different analyses performed in the different sections of this chapter.

	Complete model analysis			Post-processing			
	Detailed monopile	CB reduced monopile	Guyan reduced monopile	Force controlled		Displ controlled	
				Dyn	Qs	Dyn	Qs
Section 6.2	✓	✓	✓				
Section 6.3.1	✓				✓		✓
Section 6.3.2		✓		✓	✓	✓	✓
Section 6.3.3			✓	✓	✓	✓	✓

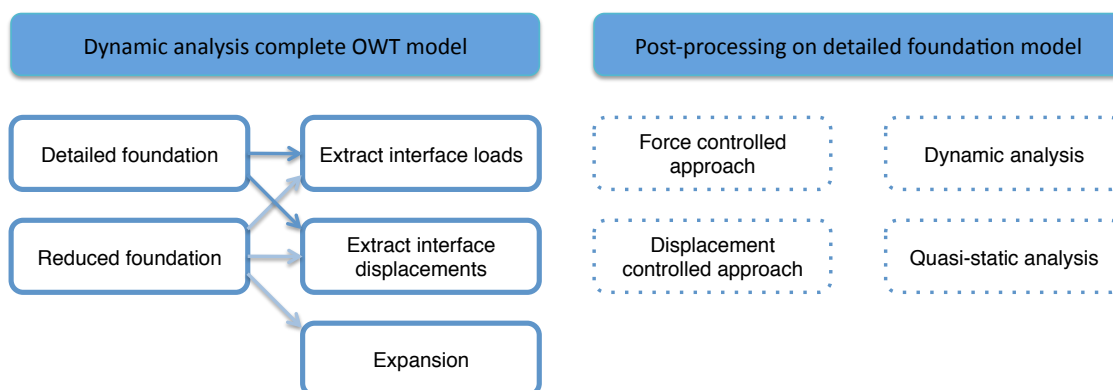
**Table 6.1:** Overview of different analyses considered in the different sections of this chapter.

## 6.2 Analyses of complete OWT

If the detailed monopile model is integrated in the complete OWT model, the exact response of the foundation will be obtained, the reference solution, and the exact interface loads and displacements will be extracted between the tower and the foundation.

Equation (4.2) shows how the response of the offshore wind turbine model can be computed and equation (4.5) shows the computation of the interface loads. If a reduced monopile model is integrated in the complete OWT model, an error arises in the interface loads/displacements, equation (4.18). The magnitude of this error depends on the reduction method used for the foundation. Next to the accuracy of the interface loads/displacements, the accuracy of the responses after expansion is investigated. In other words, the reduced response of the monopile is expanded and is compared to the reference solution. An overview of the different computations in this section is given in Figure 6.1.

In order to gain more insight in the dynamic behavior of the structure, the kinetic and the elastic energy is computed and compared to each other. If a structure contains mainly elastic energy, it behaves in a quasi-static manner. With the knowledge that a structure/component behaves in a quasi-static manner, one can conclude that a quasi-static analysis of this structure/component presumably provides accurate results. The frequency dependence of the response and of the kinetic and elastic energy will be omitted in the equations for compactness.



**Figure 6.1:** Schematic overview of complete OWT model analyses for different foundation models.



### 6.2.1 Energy distribution in the structure

The complete OWT model has been solved under wind and wave loading, as described in Section 5.5. Figure 6.2a shows the ratio between the kinetic and the elastic energy of the complete OWT model for the different excitation frequencies. Equation (6.1) shows how the kinetic and the elastic energy are computed. To determine the distribution between elastic and kinetic energy per excitation frequency, equation (6.2) is used.

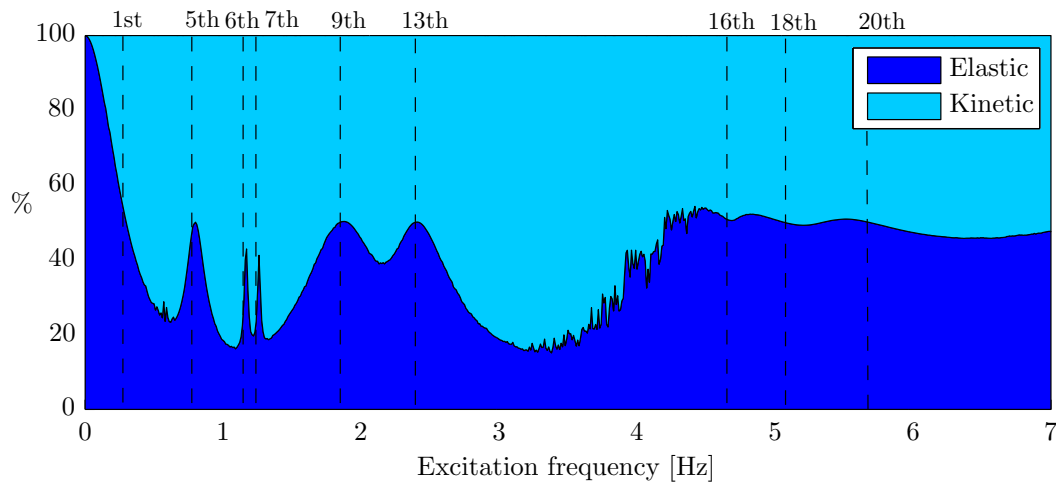
$$\mathbf{E}_k = \frac{1}{2}(j\omega\mathbf{u})^T\mathbf{M}(j\omega\mathbf{u}) \quad \mathbf{E}_e = \frac{1}{2}\mathbf{u}^T\mathbf{K}\mathbf{u} \quad (6.1)$$

$$\% \text{ of kinetic energy} = \frac{\mathbf{E}_k}{\mathbf{E}_e + \mathbf{E}_k} \quad \% \text{ of elastic energy} = \frac{\mathbf{E}_e}{\mathbf{E}_e + \mathbf{E}_k} \quad (6.2)$$

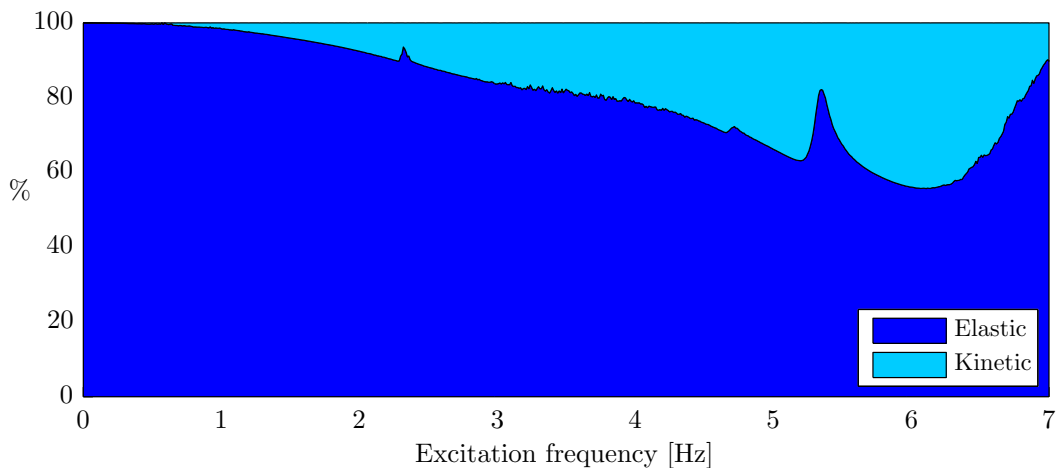
If the structure is in resonance the elastic energy is equal to the kinetic energy. The eigenfrequencies of the complete OWT model that are excited due to the external load are shown in Figure 6.2a with vertical dashed lines and the associated mode numbers. The loads are applied in the x-direction, as a result only modes in the x-direction are excited. At lower excitation frequencies the structure contains mainly elastic energy up to the first eigenfrequency, after this frequency, the inertia forces get more dominant and the kinetic energy is larger than the elastic energy until the next excited eigenfrequency, and so on.

As the dynamic behavior of the monopile is of interest in order to verify whether a quasi-static analysis of the monopile will provide accurate results, the energy distribution graph is also created for the monopile substructure, Figure 6.2b. The response of the foundation  $\mathbf{u}^{(f)}$ , extracted from the response of the complete OWT, is used to compute the elastic and kinetic energy of the foundation. The different energies are computed with equation (6.3). Figure 6.2b provides information about the behavior of the monopile compared to the complete OWT. If the foundation contains mainly elastic energy, it behaves in a quasi-static manner in the global dynamic behavior. Above 3 Hz the kinetic energy of the monopile becomes significant, but on the other hand it is less likely that these higher frequencies are excited by the wave and wind loads. Hence, the dynamic behavior of the foundation due to these higher excitation frequencies occurs with really small amplitudes.

$$\mathbf{E}_k^{(f)} = \frac{1}{2}(j\omega\mathbf{u}^{(f)})^T\mathbf{M}^{(f)}(j\omega\mathbf{u}^{(f)}) \quad \mathbf{E}_e^{(f)} = \frac{1}{2}\mathbf{u}^{(f)T}\mathbf{K}^{(f)}\mathbf{u}^{(f)} \quad (6.3)$$



(a) Distribution of energy in the complete OWT. The vertical dashed lines represent the excited eigenfrequencies as a result of the externally applied loads.

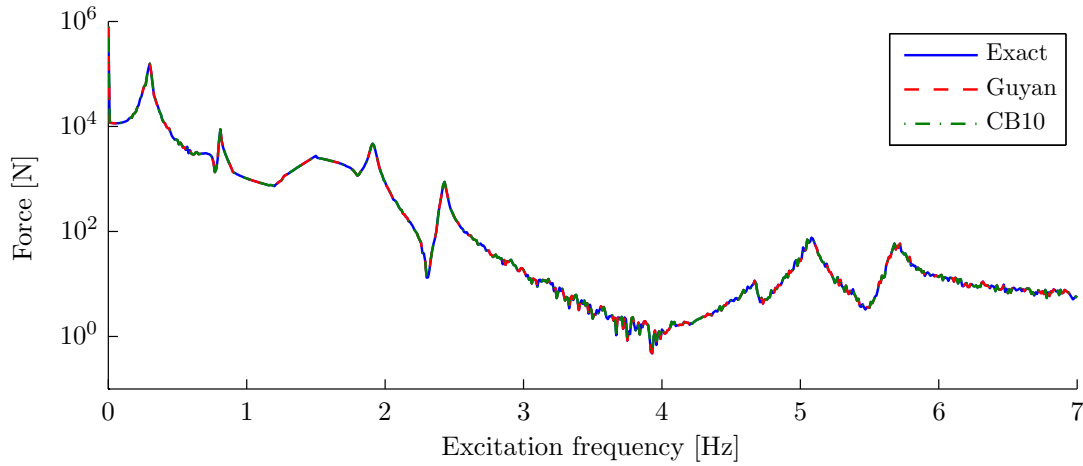


(b) Distribution of energy in the isolated monopile. Note that the monopile model contains mainly elastic energy which suggests that the monopile behaves in a quasi-static manner in this frequency range.

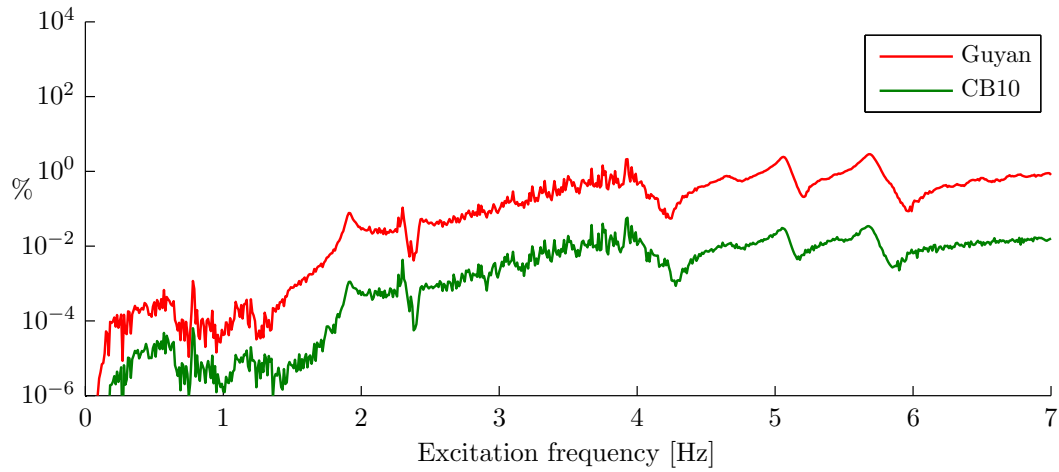
Figure 6.2: Distribution of energy in the complete OWT and the isolated monopile.

### 6.2.2 Interface loads

As the interface load contains information about the complete OWT model, high amplitudes appear in the interface load for the eigenfrequencies of the complete OWT model that are excited by the external load. Figure 5.6 showed that the OWT model with a Guyan reduced monopile and a CB10 reduced monopile are both spectrally converged. Hence, Figure 6.3a and 6.3b show that for excitation frequencies up to 7 Hz the interface force in the x-direction is almost equal to the exact interface force; the relative difference of the interface load computed with a reduced monopile model with respect to the exact interface load is very small for both reduction methods. Figure 6.3b shows a clear offset between the relative difference for the Guyan reduction and for the CB10 reduction, this is due to difference in spatial convergence. As both models are spectrally converged up to 7 Hz and the CB10 reduction basis is an enrichment of the Guyan reduction basis, the 10 included fixed interface modes in the CB10 reduction basis improve especially the spatial convergence.



(a) Interface load in the x-direction obtained with different monopile models.



(b) Relative difference of the interface loads for the reduced monopiles with respect to the exact interface load. Note that an offset between the two lines is present as a result of difference in spatial convergence.

Figure 6.3: Interface load for different monopile models.

### 6.2.3 Expansion of the response of the reduced foundation models

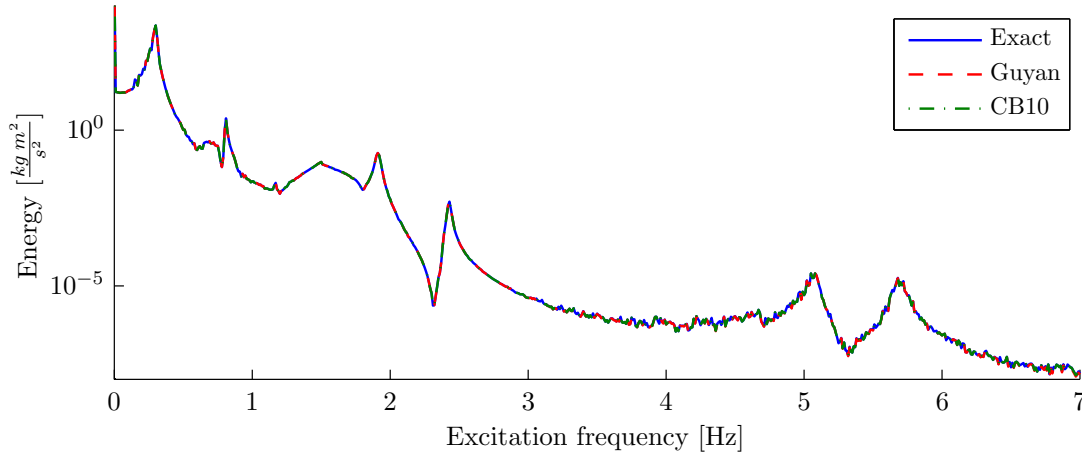
If a reduced monopile model is used in the complete OWT analysis, the response of the detailed structure can be obtained by simply expanding the response of the reduced structure using the reduction basis. In order to determine the accuracy of the expanded monopile response, the elastic energy of the monopile is computed for the different responses. The elastic energy takes the complete response of the foundation into account and is computed with equation (6.3), (6.4) and (6.5) for the different monopile models.

$$\mathbf{E}_{e,Guyan} = \frac{1}{2}(\mathbf{R}_{Guyan}\mathbf{u}_{Guyan}^{(f)})^T\mathbf{K}^{(f)}(\mathbf{R}_{Guyan}\mathbf{u}_{Guyan}^{(f)}) \quad (6.4)$$

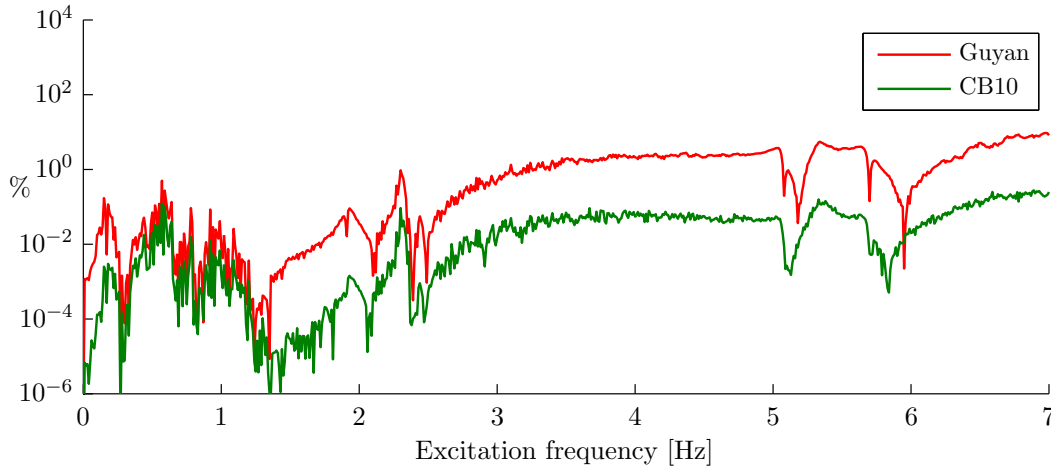
$$\mathbf{E}_{e,CB10} = \frac{1}{2}(\mathbf{R}_{CB10}\mathbf{u}_{CB10}^{(f)})^T\mathbf{K}^{(f)}(\mathbf{R}_{CB10}\mathbf{u}_{CB10}^{(f)}) \quad (6.5)$$

Figure 6.4a shows the elastic energies computed with the responses of the reduced monopile models after expansion. Expansion of the CB10 reduced response provides an accurate result as the relative difference with respect to the reference solution remains small, see Figure 6.4b. Expansion of a

Guyan reduced response is less accurate, but the relative difference still remains small. Again, Figure 6.4b shows the Guyan reduction has an offset to the CB10 reduction due to a lack of spatial convergence.



(a) Elastic energy of foundation, computed with the response after expansion of the reduced monopile.



(b) Relative difference of the elastic energy computed with the response after expansion of the reduced monopile with respect to the exact elastic energy. The same observation concerning spatial convergence is detected as in Figure 6.3b.

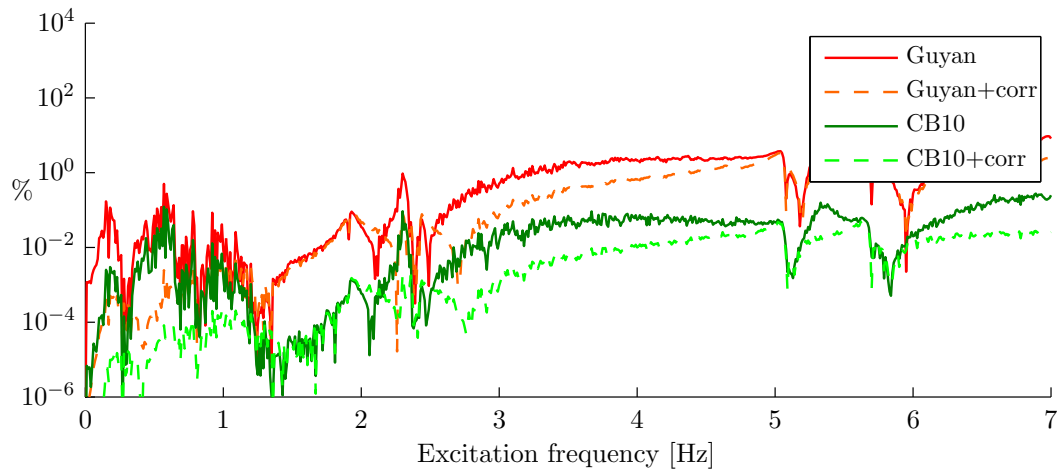
**Figure 6.4:** Elastic energy of the foundation after expansion.

If a foundation model is reduced, the obtained solution is an approximation of the exact solution. A residual load is introduced in the equation of motion, see equation (5.19). If the model is spectrally and spatially converged the residual remains small. If the residual is significant, the response after expansion can be improved by subtracting the quasi-static response due to the residual force from the expanded response. This method is comparable to the MA method, where the static contribution of the discarded modes is added to computed response [28].

$$\mathbf{u}_{exp\ augm}^{(f)} = \mathbf{R}\tilde{\mathbf{u}}^{(f)} - \mathbf{K}^{(f)-1}\mathbf{r}^{(f)} \quad (6.6)$$

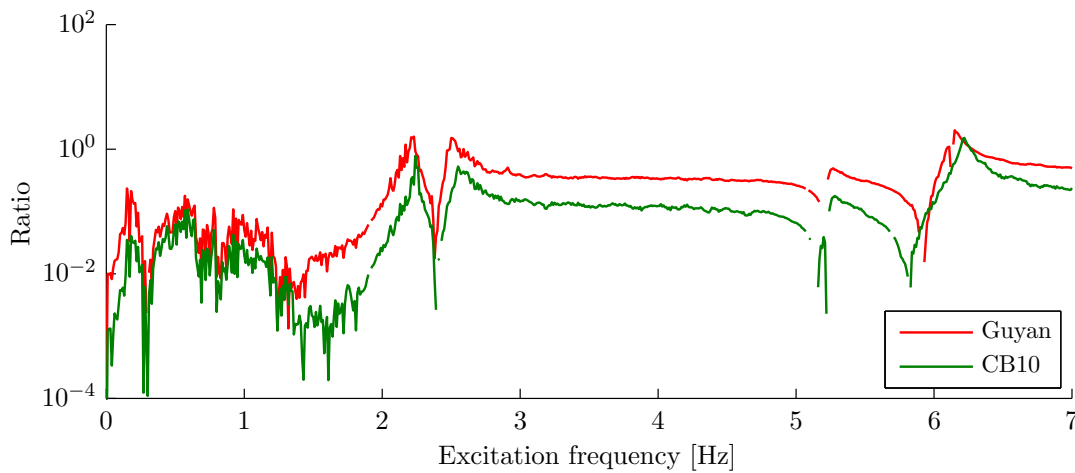
Figure 6.5 shows the relative difference between the exact elastic energy and the elastic energy after expansion, with and without taking the quasi-static residual correction into account. The

relative difference in the complete excitation bandwidth becomes smaller if the quasi-static response due to the residual is subtracted from the response after expansion. This result is expected as the monopile will behave mostly in a quasi-static manner in this frequency range and a quasi-static residual correction will thus have impact on the complete excitation bandwidth.



**Figure 6.5:** Relative difference of the elastic energy computed with the response after expansion of the reduced monopile (with a quasi-static correction due to residual) with respect to the exact elastic energy. Note that the quasi-static correction improves the results for the whole frequency range as the monopile behaves in a quasi-static manner in this frequency range.

As both OWT models with reduced monopile models are spectrally converged, the spatial convergence can be checked by comparing the norm of the residual with the norm of the elastic forces, see Figure 6.6. Although the ratio between the residual and the elastic forces is quite large for some excitation frequencies, the results do not have to be necessarily inaccurate. If the residual is small, the results will be accurate. However, if the residual is large, the accuracy of the results is undetermined. Projection of the external load on the reduction basis will discard some terms within the load. These terms will appear in the residual load, but these load terms can be such that the structure is not responding to this excitation.

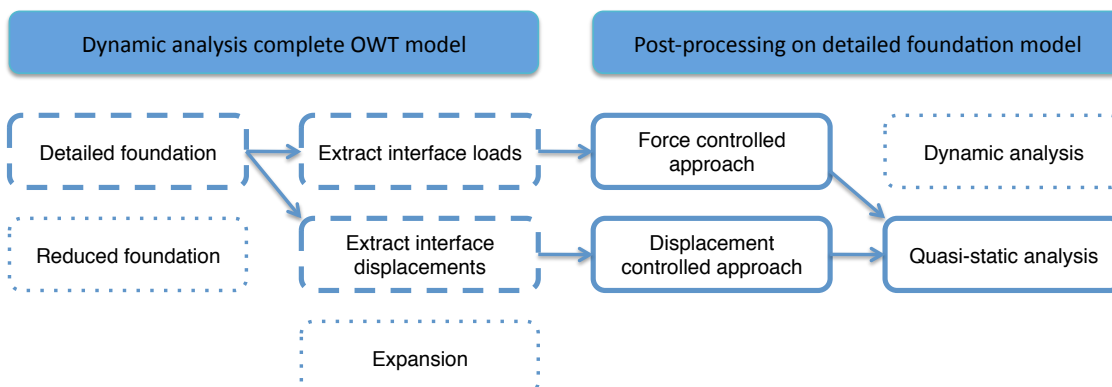


**Figure 6.6:** Ratio between the residual and the elastic forces. Note that the ratio is large for some excitation frequencies. However, the results do not have to be necessarily inaccurate for these excitation frequencies.

### 6.3 Post-processing

In this section, the different calculation procedures in the post-processing phase will be evaluated. The analyses in the post-processing phase are all performed on the detailed monopile model. Differences between the calculation procedures are therefore due to differences in post-processing analyses and due to differences in the input, i.e. differences in interface loads or displacements. When a reduced monopile model is used in the complete OWT model analysis, a small error appears in the interface loads/displacements. The impact of the error in the interface loads/displacements on the response obtained after post-processing will also be investigated.

#### 6.3.1 OWT with a detailed foundation



**Figure 6.7:** Schematic overview of post-processing analyses in case of a detailed foundation is integrated in the complete OWT model.

If the detailed monopile is used in the complete OWT analysis, the interface loads and displacements are exact and a dynamic analysis of the detailed monopile structure will provide the same response as the reference solution. Therefore, only the accuracy of the quasi-static analyses during post-processing will be investigated. The different calculation procedures discussed in this subsection are shown in Figure 6.7. In order to compare the results from different calculation procedures, the elastic energy is computed using equation (6.7) and (6.8).

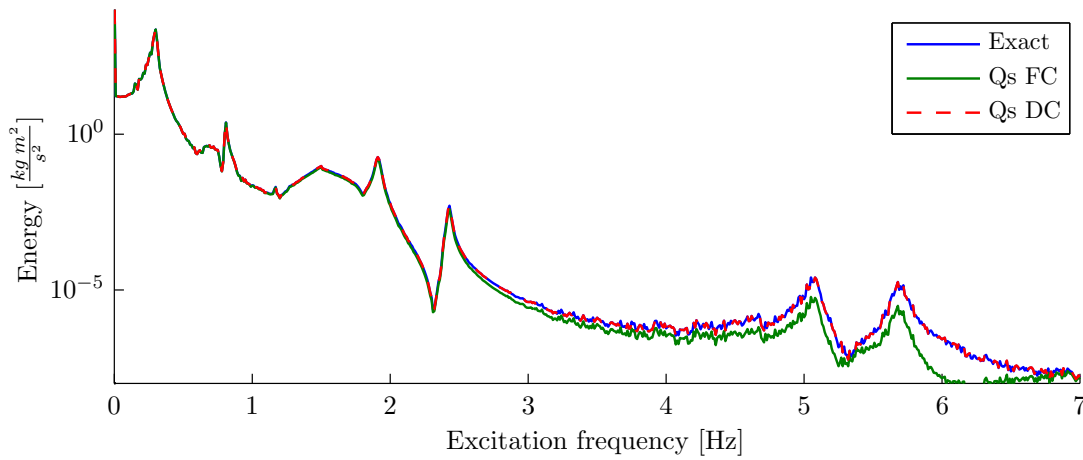
$$\mathbf{E}_{e,QsFC} = \frac{1}{2} \mathbf{u}_{QsFC}^T \mathbf{K}^{(f)} \mathbf{u}_{QsFC} \quad (6.7)$$

$$\mathbf{E}_{e,QsDC} = \frac{1}{2} \mathbf{u}_{QsDC}^T \mathbf{K}^{(f)} \mathbf{u}_{QsDC} \quad (6.8)$$

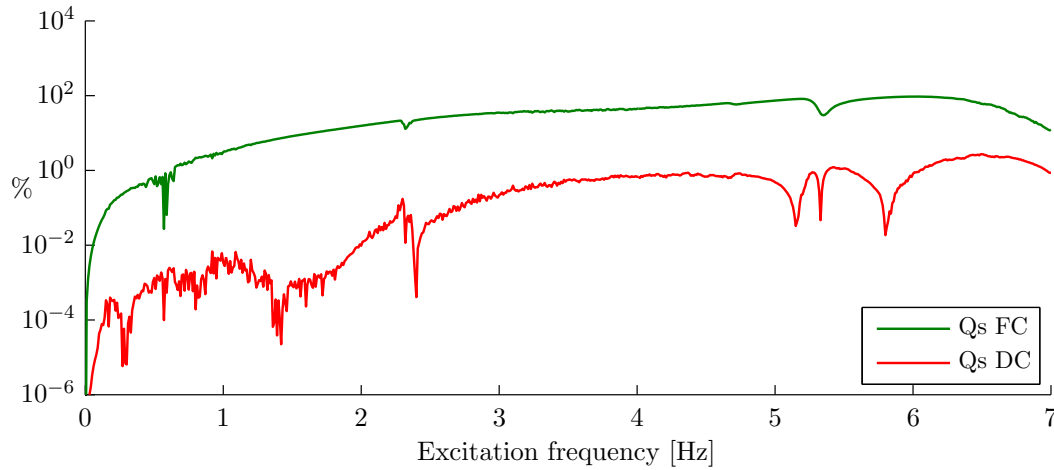
Figure 6.8a shows the elastic energy obtained with a quasi-static displacement controlled approach follows the exact solution well. However, the quasi-static force controlled approach begins to deviate from the exact solution from around 3 Hz, it underestimates the exact solution. If the response is underestimated, the stresses in the structure will be smaller and as a result the fatigue lifetime can be overestimated. This effect will be investigated in Section 6.4.

Subsection 4.2.2 presented the equations of the force controlled approach, a difference between a quasi-static and a dynamic force controlled approach starts to appear around  $\omega_{free}^{\{1\}}$ , in this case at 6.7 Hz. Appendix F provides information about the response of one DoF of the monopile model. It shows that the flexibility component starts to deviate from the receptance component from around 3 Hz, see Figure F.1.

The difference between a quasi-static and a dynamic analysis for the displacement controlled approach starts around  $\omega_{fixed}^{\{1\}}$ , in this case at 42.8 Hz. As this eigenfrequency lies far outside the excitation bandwidth, there is no significant difference between a quasi-static and a dynamic displacement controlled analysis; the internal DoF behave in a quasi-static manner up to 7 Hz. The relative difference for the quasi-static displacement controlled approach compared to the exact solution remains small, see Figure 6.8b. The relative difference for the quasi-static force controlled approach is much larger. However, the amplitude of the elastic energy between 3-7 Hz is very small and consequently the large relative difference for the quasi-static force controlled approach will probably not have a large impact on the fatigue damage of the structure.



(a) **Elastic energy of foundation.** The response is computed with a quasi-static analysis with interface loads/displacements extracted from OWT model with detailed monopile.

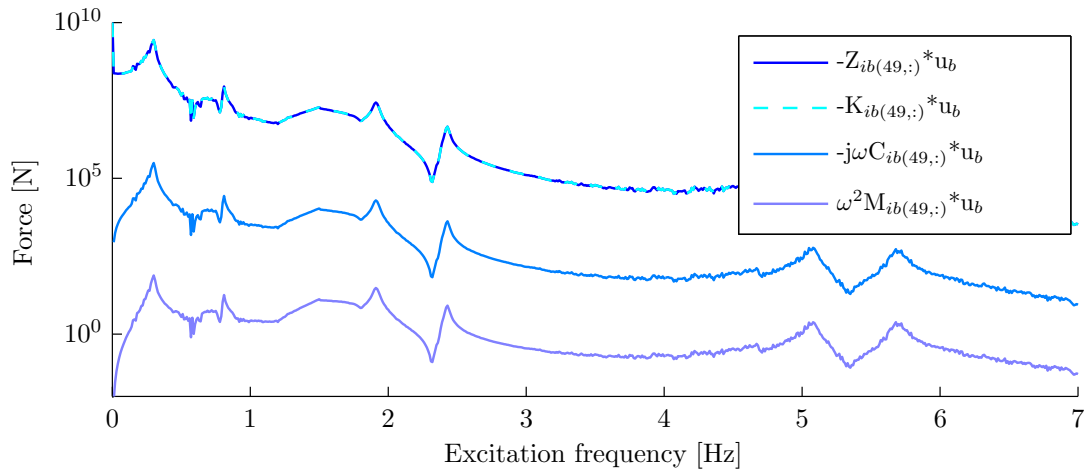


(b) **Relative difference** of the elastic energy computed with the quasi-static post-processing analyses with respect to the exact elastic energy. The Qs FC approach is inaccurate as  $\omega_{free}^{\{1\}}$  lies within the excitation bandwidth and Qs DC approach is accurate as  $\omega_{fixed}^{\{1\}}$  lies outside the excitation bandwidth.

**Figure 6.8:** Elastic energy of quasi-static post-processing analyses, using the interface loads/displacements extracted from OWT model with detailed monopile as an input.

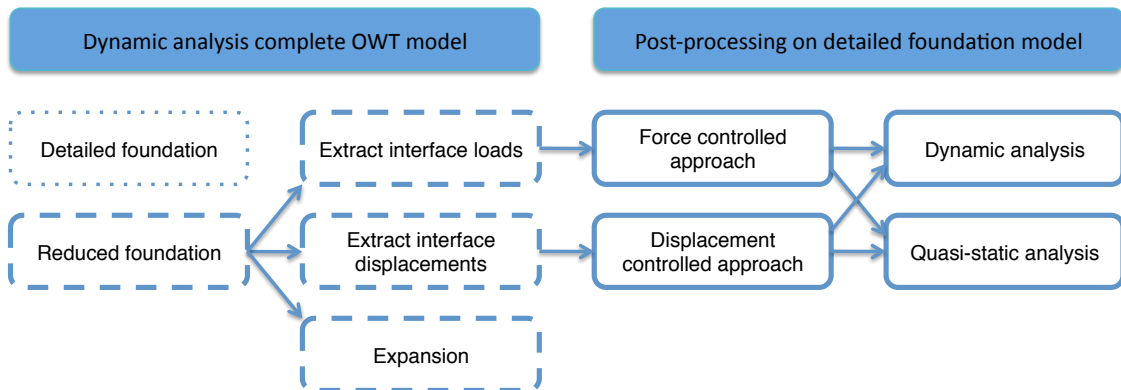
Equations (4.16) showed that the quasi-static displacement controlled approach can be performed by using only the boundary displacements as an input and neglecting the boundary velocities and accelerations. In order to determine the difference in the response for a quasi-static displacement controlled approach where the boundary velocities and accelerations are included or neglected, the different coupling load terms are plotted in Figure 6.9. The elastic coupling forces  $\mathbf{K}_{ib}\mathbf{u}_b$  are dominant and the damping and inertia coupling forces,  $j\omega\mathbf{C}_{ib}\mathbf{u}_b$  and  $-\omega^2\mathbf{M}_{ib}\mathbf{u}_b$ , are much smaller. Hence, the boundary velocities and accelerations can be safely neglected in this case as no difference will appear in the response if these terms are included.





**Figure 6.9:** Amplitude of coupling load terms in the x-direction,  $-\mathbf{Z}_{ib(49,:)}\mathbf{u}_b = \omega^2\mathbf{M}_{ib(49,:)}\mathbf{u}_b - j\omega\mathbf{C}_{ib(49,:)}\mathbf{u}_b - \mathbf{K}_{ib(49,:)}\mathbf{u}_b$ . Note that the elastic coupling forces are dominant.

### 6.3.2 OWT with a Guyan reduced foundation



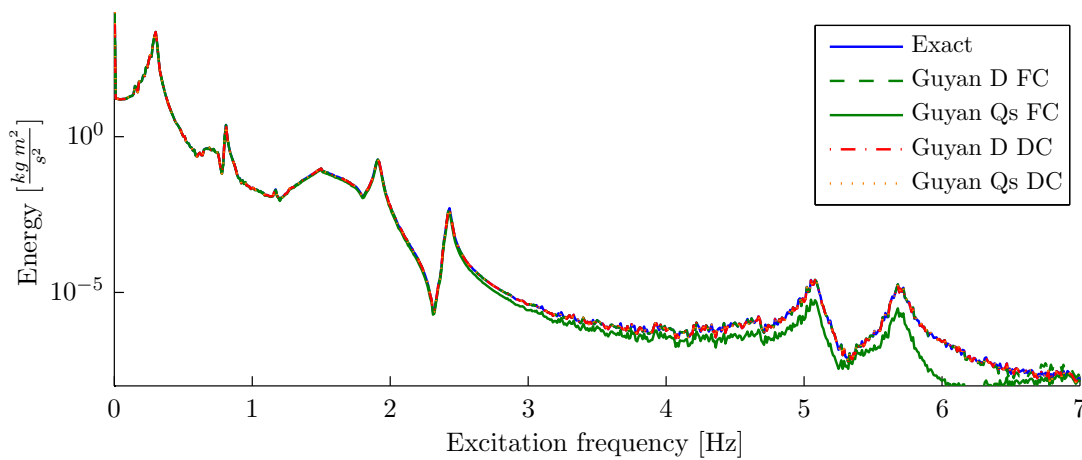
**Figure 6.10:** Schematic overview of post-processing analyses in case of a Guyan reduced foundation is integrated in complete OWT model.

Using a Guyan reduced monopile model in the complete OWT model, differences in the eigenfrequencies compared to the detailed OWT model can appear. As Figure 5.6 showed, these differences remain small and the OWT model with a Guyan reduced monopile is spectrally converged in the excitation bandwidth. The interface loads/displacements are quite accurate as shown in Figure 6.3. Hence, the hypothesis is that the accuracy of the post-processing methods is not influenced by the use of a Guyan reduced monopile in the complete OWT model. Figure 6.10 gives an overview of the different calculation procedures that will be performed in this subsection.

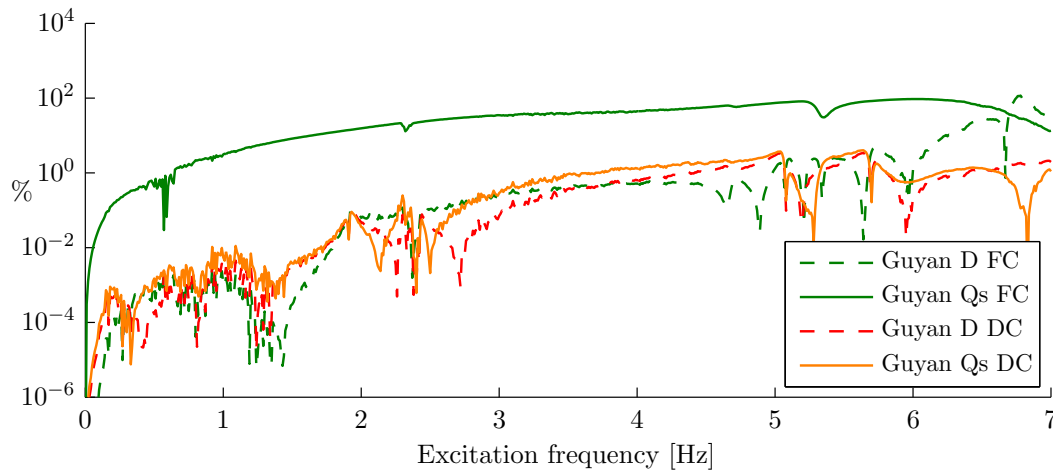
Figure 6.11a shows that the elastic energies obtained with the quasi-static and the dynamic displacement controlled approach follow the exact solution well. As  $\omega_{fixed}^{\{1\}}$  of the monopile is at 42.8 Hz, the monopile with a fixed interface behaves in a quasi-static manner in the frequency range 0-7 Hz. Therefore, a quasi-static displacement controlled approach provides accurate results. The rel-

ative difference remains small for both displacement controlled approaches and is more or less the same, see Figure 6.11b. As the monopile is reduced with a Guyan reduction, the internal dynamics of the foundation are neglected. The interface loads/displacements only contain information about the static behavior of the monopile. As a result, no differences appear between a quasi-static and a dynamic displacement controlled approach.

As  $\omega_{free}^{\{1\}}$  of the monopile is at 6.7 Hz and thus within the excitation bandwidth, there is a difference between a dynamic and a quasi-static force controlled approach. The dynamic force controlled approach provides an accurate result and the relative difference is significantly smaller than for the quasi-static force controlled approach.



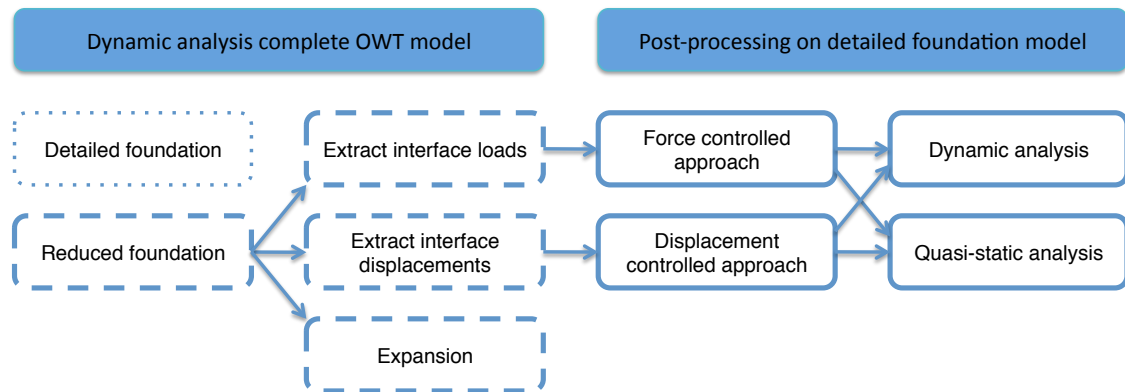
(a) **Elastic energy of foundation.** The response is computed with a dynamic/quasi-static analysis with interface loads/displacements extracted from OWT model with Guyan reduced monopile.



(b) **Relative difference** of the elastic energy resulting from the different post-processing analyses with respect to the exact elastic energy. Note that the relative difference is more or less the same for the quasi-static and the dynamic displacement controlled approach as the interface displacements neglect the internal dynamics due to the Guyan reduction.

**Figure 6.11:** Elastic energy of different post-processing analyses, using the interface loads/displacements extracted from OWT model with **Guyan reduced monopile** as an input.

### 6.3.3 OWT with a Craig-Bampton reduced foundation

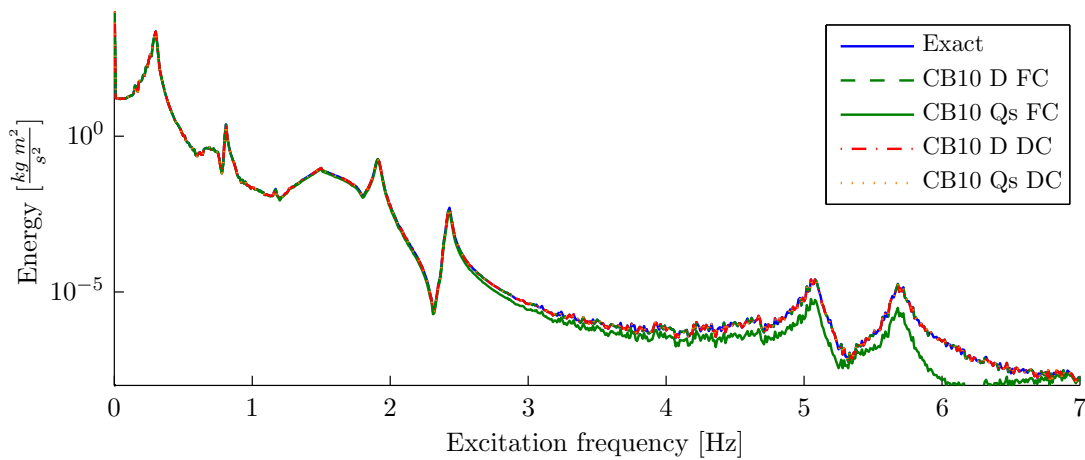


**Figure 6.12:** Schematic overview of post-processing analyses in case of a Craig-Bampton reduced monopile is integrated in complete OWT model.

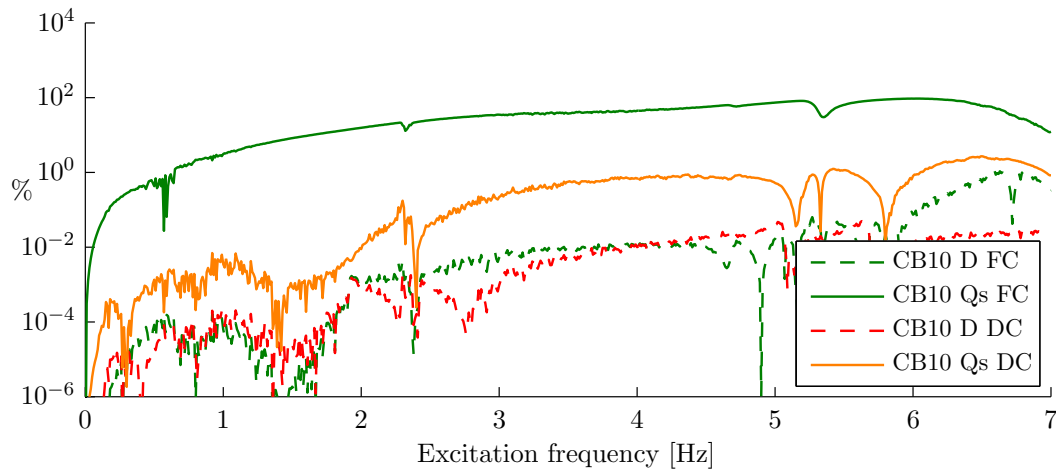
Using a reduced CB10 monopile in the complete OWT model, the error in the interface loads and displacements remains very small and thus the hypothesis is that the results after post-processing are accurate as well, except for the quasi-static force controlled approach. This approach is not accurate due to neglecting the inertia and damping forces and not due to the use of a reduced model in the complete OWT analysis. Figure 6.12 gives an overview of the different calculation procedures that will be performed in this subsection.

Figure 6.13a shows the elastic energies obtained with the different post-processing analyses. More or less the same observations as for the Guyan reduced monopile can be identified. The dynamic post-processing analyses provide accurate results. Figure 6.13b shows that the relative difference for the dynamic calculation procedures is even smaller than for the dynamic calculation procedures where the interface loads/displacements were extracted from an OWT model with a Guyan reduced monopile. As the CB10 reduction basis is an enrichment of the Guyan reduction basis, the CB10 reduced monopile is better spatially converged. Therefore, the CB10 reduced monopile is better able to capture the effect of the wave loads on the structure and the relative difference for the dynamic calculation procedures is even smaller.

The monopile model with a fixed interface behaves in a quasi-static manner in the excitation bandwidth, therefore the relative difference for the quasi-static displacement controlled approach remains small. However, the relative difference for the quasi-static displacement controlled approach is larger than the relative difference for the dynamic displacement controlled approach, see Figure 6.13b. The reduction basis of the Craig-Bampton reduction contains information about the internal dynamics of the foundation, whereas the Guyan reduction basis only includes the static constraint modes. Hence, the interface loads/displacements obtained from an OWT model with a CB10 reduced monopile will contain extra information about the dynamic behavior of the foundation. This dynamic behavior is neglected in the quasi-static post-processing analysis and included in the dynamic post-processing analysis, therefore, a difference in the accuracy appears between the quasi-static and the dynamic displacement controlled approach, as can be seen in Figure 6.13b.



(a) **Elastic energy of foundation.** The response is computed with a dynamic/quasi-static analysis with interface loads/displacements extracted from OWT model with CB10 reduced monopile.



(b) **Relative difference** of the elastic energy resulting from the different post-processing analyses with respect to the exact elastic energy. Note that due to including internal dynamics in the reduction basis the relative difference is smaller for the dynamic than for the quasi-static displacement controlled approach.

**Figure 6.13:** Elastic energy of different post-processing analyses, using the interface loads/displacements extracted from OWT model with **CB10 reduced monopile** as an input.

## 6.4 Fatigue damage calculation



**Figure 6.14:** Schematic overview of computing damage of a structure.

Fatigue is often the main design driver for the support structure, so it is interesting to investigate the impact of the errors in the responses, due to different calculation procedures, on the fatigue damage and thus the fatigue life. These simulations are performed in the time domain and the responses

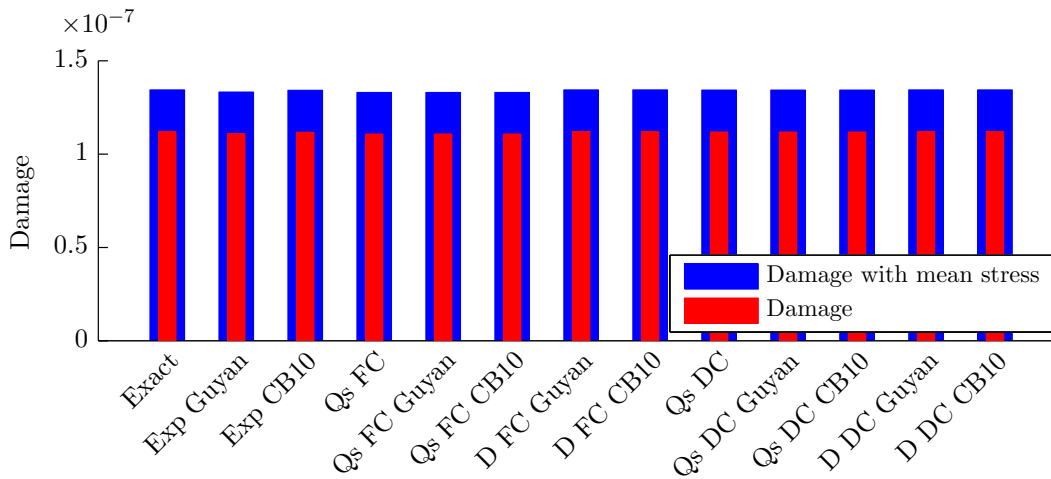
of the OWT model for the different calculation procedures are computed with a Newmark time integration, the theory of this method is explained in Appendix B. Afterwards, these responses are converted into stresses, following Subsection 5.3.2. These random stress signals are rearranged with the rainflow counting method and finally, the fatigue damage can be computed with the S-N curve and the Palmgren-Miner rule. A schematic overview of these computation steps is given in Figure 6.14. Section 2.4.3 describes the basics of the rainflow counting method and how the mean stress in the structure can be integrated in the fatigue computation. The fatigue damage of the monopile structure will be computed with and without taking the mean stress into account.

Figure 6.15a shows the fatigue damage for the different calculation procedures at the bottom of the monopile. As the monopile is clamped at the bottom, the stress will be maximum here as the geometry of the monopile is constant. It is clear that the mean stress has a significant effect on the damage. However, the difference in damage results for the various calculation procedures is not clear from this figure. Therefore the relative difference to the reference solution is computed to determine the accuracy of the different calculation procedures, see Figure 6.15b. The fatigue damage obtained with expansion of the reduced Guyan response is less accurate than the fatigue damage obtained with expansion of the reduced CB10 response. This result is expected, as the CB10 reduction is an enrichment of the Guyan reduction, hence, the CB10 reduction basis is more able to capture the effect of the wave loads on the structure. A response after expansion is only accurate if the model is spectrally and spatially converged.

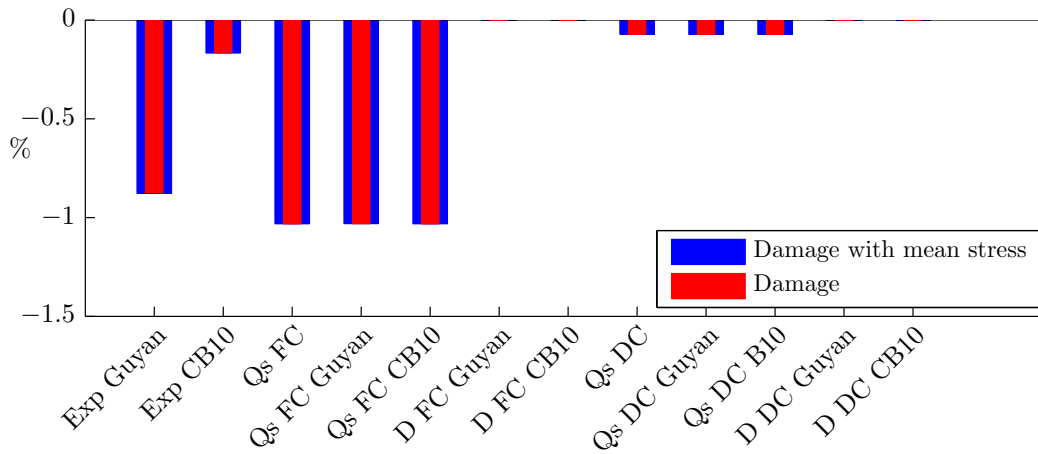
If post-processing on the detailed monopile model is applied, the fatigue damage obtained with the quasi-static force controlled approach is the least accurate. The quasi-static force controlled approach provides less accurate results than the quasi-static displacement controlled approach, this was to be expected from the previous results. However, the large relative differences that appeared for the elastic energy obtained with a quasi-static force controlled approach do not appear in the fatigue damage results, the relative difference is about 1%. This is probably because large differences appear between 3-7 Hz for the quasi-static force controlled approach and it is less likely that these higher frequencies are excited by the wave and wind loads. The response of the quasi-static force controlled approach underestimates the response of the exact solution, as a result the damage is underestimated, the quasi-static force controlled approach is a not conservative calculation procedure for this structure with this specific load case. Moreover, the fatigue damage results obtained with expansion of the reduced responses are not conservative either. However, the relative differences remain small.

Dynamic post-processing on the detailed monopile model provides the most accurate damage results. Expansion of a reduced response provides less accurate damage results, because the reduction basis is not fully able to capture the effect of the wave loads on the structure. As the dynamic post-processing analyses are performed on the detailed model, the effect of the wave loads on the structure is captured and a small error in the interface loads/displacements seems to have less effect on the accuracy of the results.

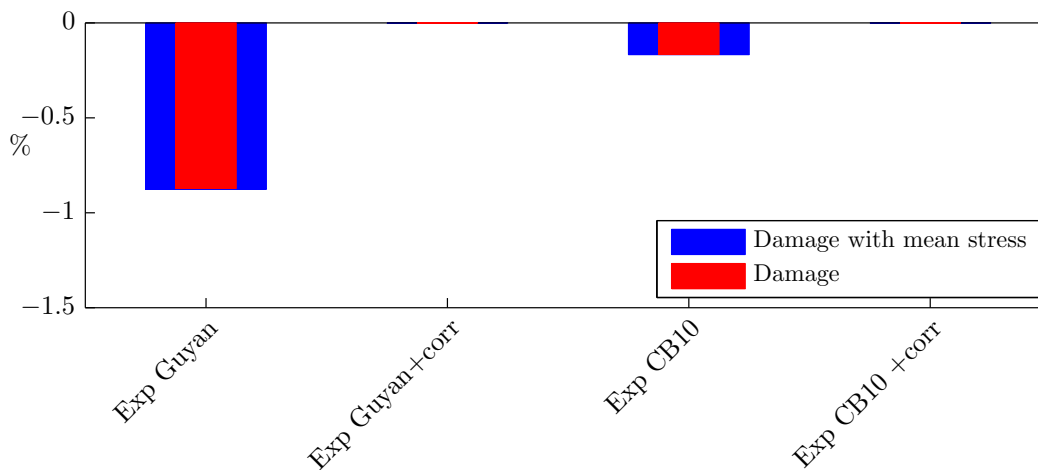
A reduction basis discards a number of modes, dependent on the reduction method used, and is therefore an approximation of the reference solution. As Figure 6.5 showed, the response after expansion can be improved by subtracting the quasi-static response due to the residual from the response after expansion. Figure 6.15c shows that the residual correction significantly improves the accuracy of the fatigue damage.



(a) Fatigue damage



(b) Relative difference between the exact damage and the damage for different calculation procedures



(c) Relative difference between the exact damage and the damage for different calculation procedures

Figure 6.15: Fatigue damage of the monopile for different calculation procedures

## 6.5 Summary

In Table 6.2 the accuracy of the different calculation procedures is summarized. The upper row describes which monopile model is used in the analysis of the complete OWT model and the left column describes the different calculation procedures.

As fatigue is often the main design driver for the support structure, the accuracy of the different calculation procedures is determined based on the relative difference of the fatigue damage results with respect to the reference solution:

- ✓ - **Accurate** - the relative difference is <1%
- ~ - **Reasonably accurate** - the relative damage difference is between 1-2%
- ✗ - **Inaccurate** - the relative damage difference is >2%

	Detailed monopile in complete model	Guyan reduced monopile in complete model	CB10 reduced monopile in complete model
<b>Expansion</b>	n/a	~ <b>Error:</b> Not fully spatially converged	✓
with residual correction	n/a	✓	✓
<b>Force controlled</b>			
Dynamic	✓	✓	✓
Quasi-static	~ <b>Error:</b> Neglecting inertia and damping forces; $\omega_{free}^{\{1\}}$ within excitation bandwidth	~ <b>Error:</b> Neglecting inertia and damping forces; $\omega_{free}^{\{1\}}$ within excitation bandwidth	~ <b>Error:</b> Neglecting inertia and damping forces; $\omega_{free}^{\{1\}}$ within excitation bandwidth
<b>Displacement controlled</b>			
Dynamic	✓	✓	✓
Quasi-static	✓ $\omega_{fixed}^{\{1\}} > \max(\omega_{ext})$	✓ $\omega_{fixed}^{\{1\}} > \max(\omega_{ext})$	✓ $\omega_{fixed}^{\{1\}} > \max(\omega_{ext})$

**Table 6.2:** Accuracy of the different calculation procedures for an OWT with a monopile





## Chapter 7

# Results of calculation procedures - Jacket

### 7.1 Introduction

In the previous chapter, the quantitative error was determined for the different calculation procedures for the OWT model with a monopile. The monopile does not experience a lot of local dynamics, as a result the reduction method did not influence the accuracy of the results too much. Next to this, the behavior of the monopile is mostly quasi-static within the excitation bandwidth, hence the quasi-static post-processing analyses provided quite accurate results. To determine the quantitative error for a structure that experiences more local dynamics, the OWT model is constructed with a jacket as foundation structure. The results of the different calculation procedures performed on this model will be presented in this chapter. Section 5.4 described the characteristics of the jacket structure,  $\omega_{free}^{\{1\}}$  and  $\omega_{fixed}^{\{1\}}$  of the jacket are both within the excitation bandwidth. The hypothesis is that a quasi-static force or displacement controlled approach will provide less accurate results than for the monopile. Furthermore, the reduction of the jacket can only provide accurate results if the reduction basis can capture the local dynamics of the structure well. If so, accurate interface loads and displacements will be extracted and an accurate response of the foundation will be obtained after expanding the reduced response.

The responses obtained from the different calculation procedures will be compared to a reference response. The reference response is obtained by a dynamic analysis of the complete OWT model with the detailed jacket model under wind and wave loading. All the different calculation procedures described in Chapter 4 will be simulated. Similar to Chapter 6, the inaccuracies that arise in the dynamic analysis of the complete OWT model with a reduced jacket will be examined first. Thereafter, the inaccuracies in the post-processing on the detailed jacket model will be determined. The accuracy of a quasi-static force and displacement controlled approach will be evaluated and the impact due to the use of a reduced jacket in the complete OWT model analysis on the post-processing results.

As presented in Subsection 5.4.2 three different reduction methods will be examined for the jacket model: the Guyan reduction, the Craig-Bampton reduction with 20 fixed interface modes (CB20) and the Augmented Craig-Bampton method with 10 fixed interface modes and 10 MTA vectors (CB10MTA). Figure 5.8 showed that the OWT model with a Guyan reduced jacket model is not spectrally converged, whereas the OWT model with a CB20 reduced jacket model is spectrally converged. The OWT model with a CB10MTA reduced jacket model is spectrally converged for frequencies up

to 6.6 Hz. However, it is less likely that these higher frequencies are excited by the external load and therefore, it can be assumed that the OWT model with a CB10MTA reduced jacket is spectrally converged as well.

The spatial convergence is still unknown, but will be investigated by comparing the residual to the elastic forces. The hypothesis is that the residual for the CB10MTA reduced jacket model is very small as the OWT model with the CB10MTA reduced jacket is spectrally converged and the reduction basis includes 10 MTA vectors to improve the spatial convergence. Expansion of the reduced CB10MTA response will probably provide accurate results.

Finally, with the response obtained from the various calculation procedures the fatigue damage is computed and it will be investigated what the impact is of the error in the response on the accuracy of the damage results. Since larger differences are expected in the responses of the jacket obtained with the different calculation procedures compared to the OWT model with a monopile, larger differences between fatigue damage results are also expected.

Table 7.1 gives an overview of the different analyses performed in the different sections of this chapter.

	Complete model analysis Type of jacket	Post-processing			
		Force controlled		Displ controlled	
		Dyn	Qs	Dyn	Qs
Section 7.2	Comparison all jacket models				
Section 7.3.1	Detailed		✓		✓
Section 7.3.2	Guyan reduced	✓	✓	✓	✓
Section 7.3.3	CB20 reduced	✓	✓	✓	✓
Section 7.3.4	CB10MTA reduced	✓	✓	✓	✓

**Table 7.1:** Overview of different analyses considered in the different sections of this chapter.

## 7.2 Analysis of complete OWT

If the detailed jacket model is integrated in the complete model, the exact response of the jacket structure will be obtained and the exact interface loads/displacements will be extracted between the tower and the jacket.

Equation (4.2) shows how the response of the OWT model can be computed and equation (4.5) shows the computation of the interface loads. If a reduced model of the jacket is integrated in the complete model, an error in the interface loads/displacements will arise, see equation (4.20). The amplitude of the error depends on the reduction method used for the foundation. Next to the accuracy of the interface loads/displacements, the accuracy of the response after expansion is investigated. In other words, the reduced response of the jacket is expanded and is compared to the reference solution. An overview of the different computations in this section is given in Figure 7.1.

Likewise for the monopile, the energy distribution is determined for the OWT model with a jacket and for the jacket as a substructure.

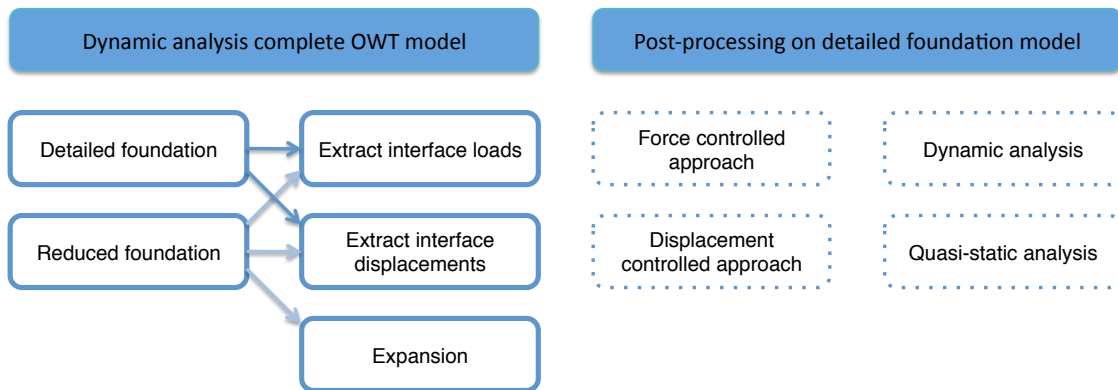


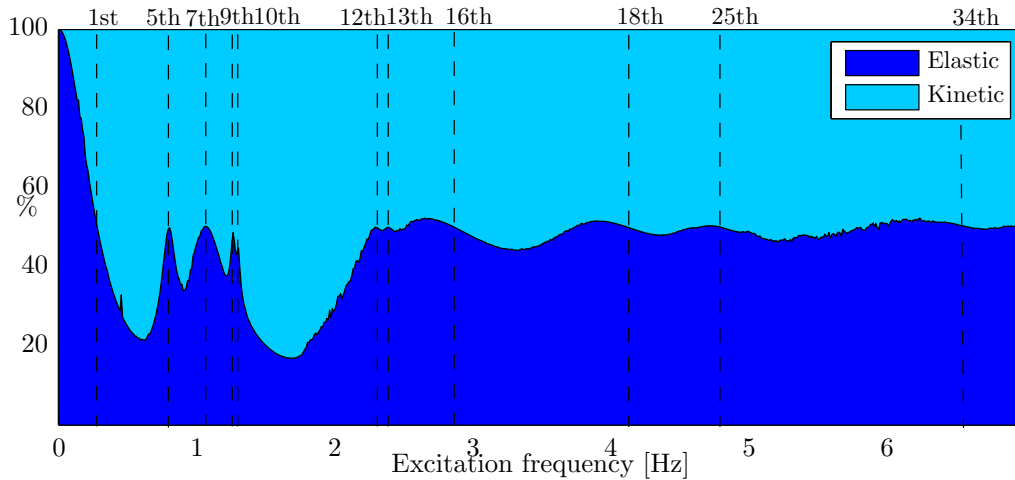
Figure 7.1: Schematic overview of complete OWT model analyses for different foundation models.

### 7.2.1 Energy distribution in the structure

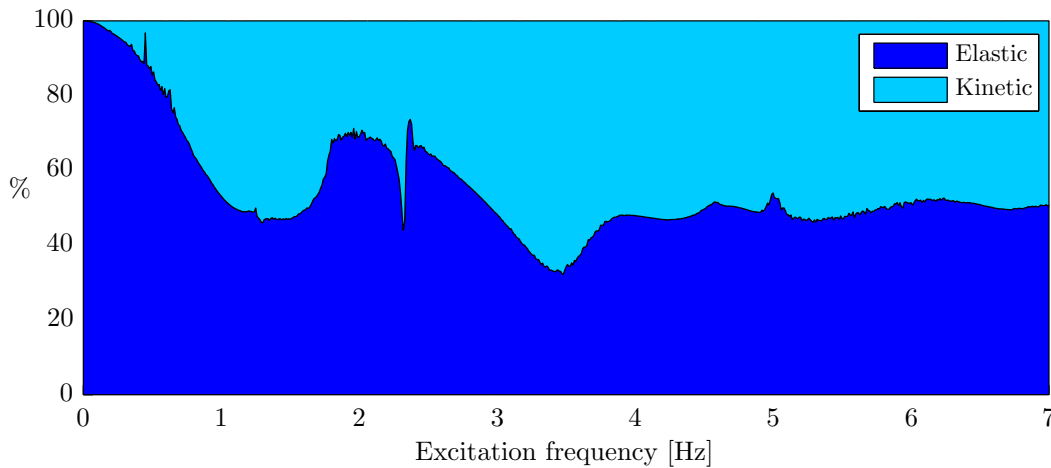
The energy distribution of the complete OWT model for the different excitation frequencies is shown in Figure 7.2a. This graph shows for every frequency what the ratio is between the kinetic and the elastic energy for the complete OWT model. Equation (6.1) shows how the kinetic and the elastic energy is computed. In order to find the distribution between the elastic and the kinetic energy per excitation frequency, equation (6.2) is used.

Figure 7.2a shows the eigenfrequencies that are excited due to the external load with the vertical dashed lines. The kinetic energy is equal to the elastic energy at these eigenfrequencies. At very low excitation frequencies the structure contains mainly elastic energy up to the first eigenfrequency. After this eigenfrequency, the inertia forces get more dominant and the kinetic energy is larger than the elastic energy until the next eigenfrequency that is excited, and so on. For higher excitation frequencies, above 4 Hz, the energy distribution is about 50/50, which implies that the structure responds dynamically.

To verify if a quasi-static analysis of the jacket substructure provides accurate results, the dynamic behavior of the jacket must be determined. Therefore, the energy distribution graph is also created for the jacket itself, Figure 7.2b. The response of the foundation  $\mathbf{u}^{(f)}$ , extracted from the response for the complete OWT, is used to compute the elastic and the kinetic energy of the foundation with equation (6.3). Figure 7.2b contains information about the behavior of the jacket compared to the complete OWT. It is clear that the jacket contains relatively more kinetic energy compared to the monopile, the jacket will behave in a more dynamic manner in the excitation bandwidth than the monopile. Therefore, a quasi-static analysis will probably not be able to capture the behavior of the structure well.



(a) Distribution of energy in the complete OWT. The vertical dashed lines represent the excited eigenfrequencies as a result of the externally applied loads.



(b) Distribution of energy in the isolated jacket. Note that the jacket structure contains relatively more kinetic energy than the monopile (Figure 6.2b) which suggests that the jacket shows more dynamic behavior in this frequency range.

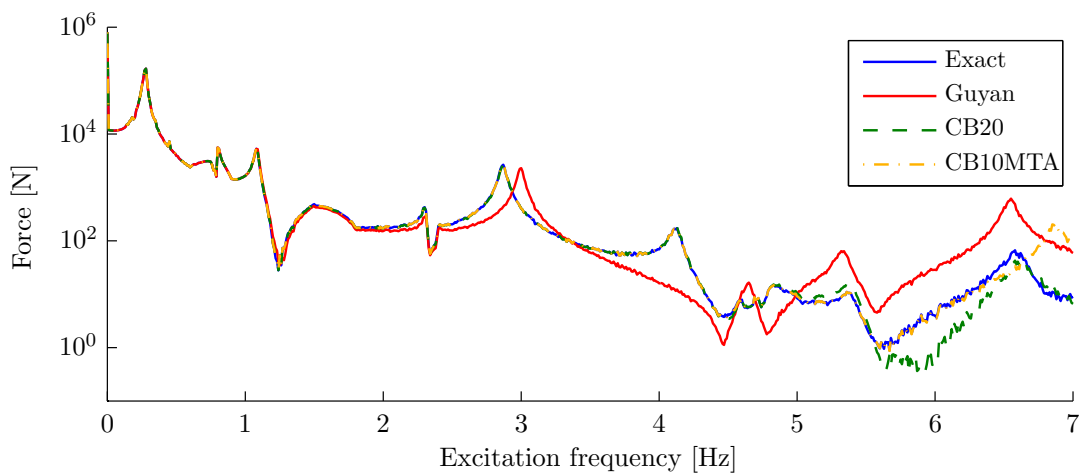
Figure 7.2: Distribution of energy in the complete OWT and the isolated jacket.

### 7.2.2 Interface loads

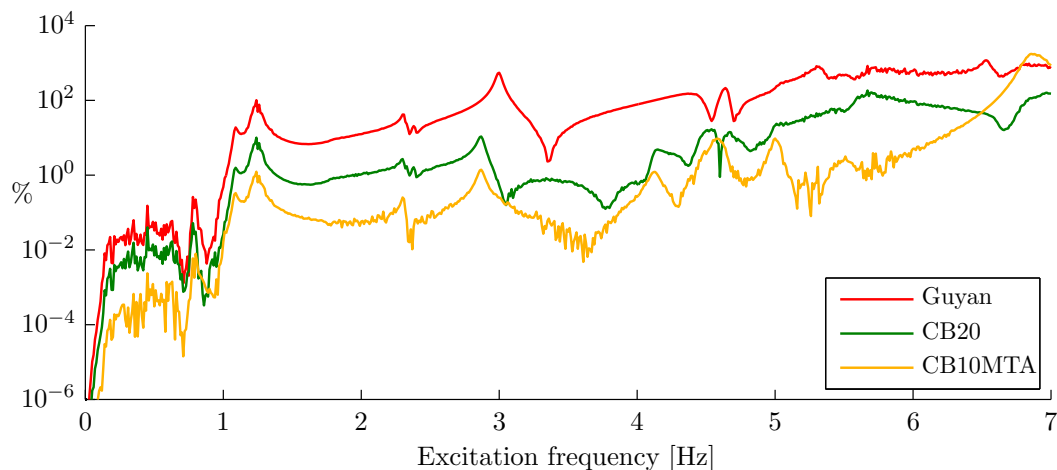
As the interface load contains information about the dynamic behavior of the complete OWT model, large amplitudes will appear in the interface load at the eigenfrequencies of the complete OWT model excited by the external load. Figure 7.3a shows the interface force in the x-direction. As the OWT model with the Guyan reduced jacket is not spectrally converged within the excitation bandwidth, the interface force is inaccurate. The differences in eigenfrequencies between the detailed OWT model and the OWT model with a Guyan reduced jacket appear in the interface load as well. The 16th eigenfrequency of the detailed OWT model is at 2.87 Hz and for the OWT model with a Guyan reduced jacket at 3.00 Hz, this difference can be clearly seen in the interface load. The interface load obtained from the OWT model with a CB20 reduced jacket and a CB10MTA reduced jacket, follow the exact interface load well, except for the higher excitation frequencies between 6-7 Hz. The OWT with a CB20 reduced jacket is not fully spatially converged and the OWT with a

CB10MTA reduced jacket is not fully spectrally converged in this frequency range.

Figure 7.3b shows the relative difference of the interface load obtained from the OWT models with different reduced jacket models with respect to the exact interface load. A clear offset between the different jacket models for the lower excitation frequencies up to 2 Hz can be seen, all OWT models are spectrally converged in this frequency range, but the spatial convergence differs. The OWT with a CB10MTA reduced jacket contains MTA vectors in the reduction basis, as a result this model can best capture the effect on the structure due to the wave loads and thus is best spatially converged. At higher frequencies the relative difference increases for the OWT model with a CB10MTA reduced jacket as the model is no longer spectrally converged. The relative difference becomes more or less the same as for the OWT model with a CB20 reduced jacket.



(a) Interface load in the x-direction obtained with different jacket models.



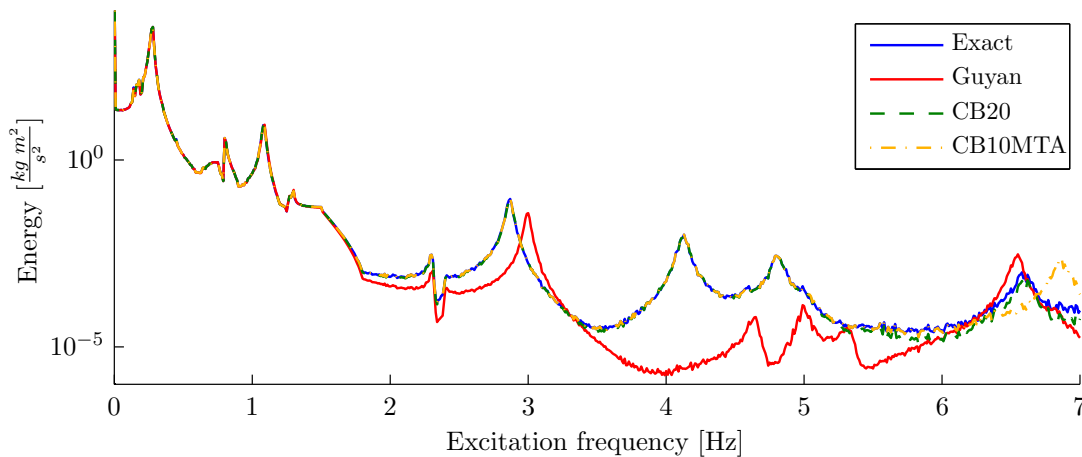
(b) Relative difference of the interface loads obtained with the reduced jackets with respect to the exact interface load. Note that the relative difference with respect to the exact interface load is a result of the lack of spatial and spectral convergence.

Figure 7.3: Interface load for different jacket models.

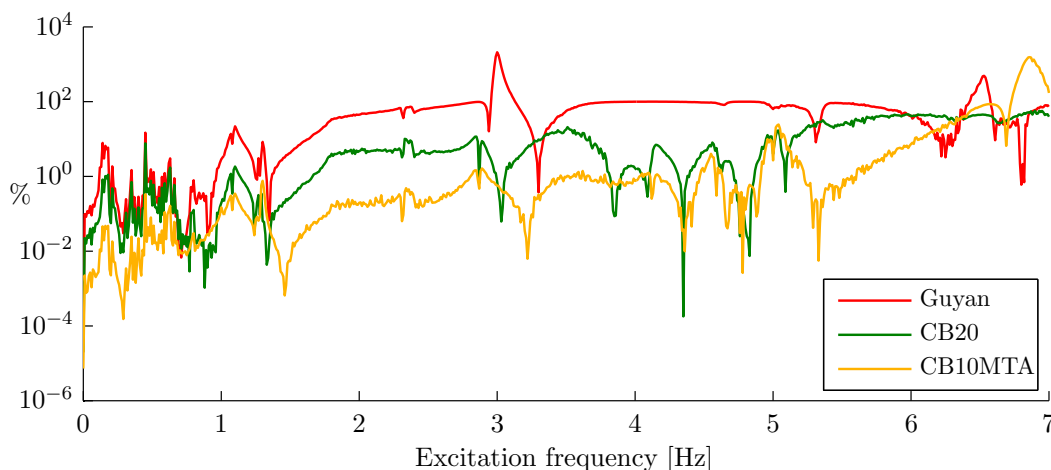
### 7.2.3 Expansion of the response of the reduced foundation models

If a reduced jacket model is used in the complete OWT analysis, the reduced response of the foundation can be expanded to retrieve the response for the detailed jacket model. In order to determine the accuracy of the response after expansion, the elastic energy is computed, this way the complete response of the jacket can be taken into account.

Figure 7.4a shows that expansion of the Guyan reduced response is inaccurate in the frequency range above 2 Hz, as large differences start to appear. However, expansion of the CB20 reduced response provides an accurate result, the relative difference with respect to the reference solution remains small, see Figure 7.4b. Expansion of a CB10MTA reduced response is accurate up to 6 Hz. The relative difference is smaller than for the CB20 reduced jacket, as a result of the improved spatial convergence. As it is less likely that frequencies are excited between 6-7 Hz by the external load, the hypothesis is that expansion of the CB10MTA reduced jacket will provide the most accurate fatigue damage results compared to the other reduced jacket models.



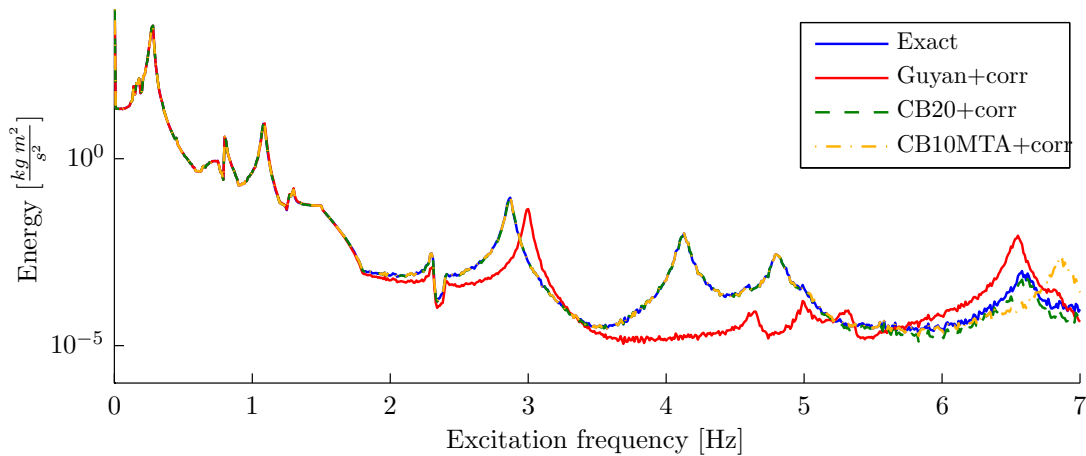
(a) Elastic energy of foundation, computed with the response after expansion of reduced jacket.



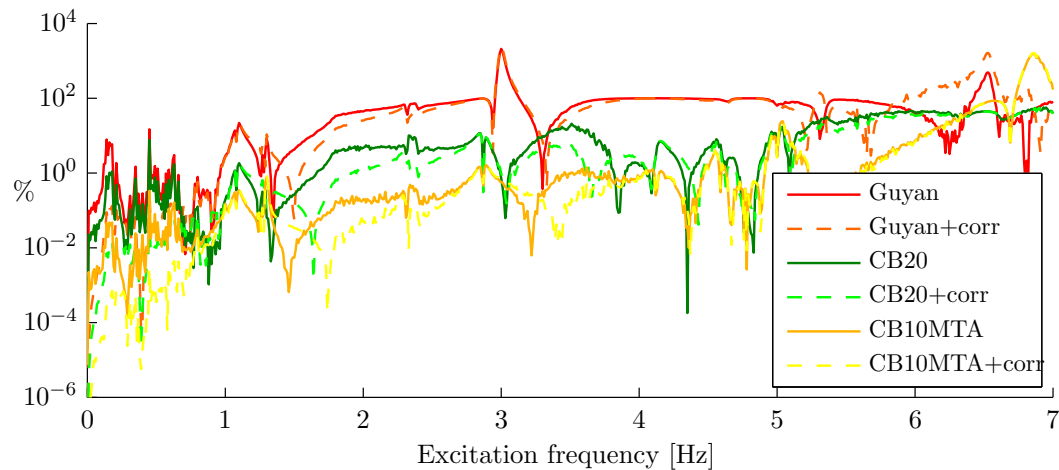
(b) Relative difference of the elastic energy computed with the response after expansion of the reduced jacket with respect to the exact elastic energy. The same observations concerning spectral and spatial convergence are detected as in Figure 7.3b.

**Figure 7.4:** Elastic energy of the jacket after expansion.

Figure 7.5a shows the elastic energy where the quasi-static response due to the residual is taken into account. The difference is not clearly visible, therefore the relative difference with respect to the reference solution is plotted in Figure 7.5b for the response with and without applying the quasi-static residual correction. The relative difference becomes smaller if the quasi-static residual correction is applied, especially at lower excitation frequencies. This result is expected as the structure will behave in a more quasi-static manner at lower frequencies and a quasi-static residual correction will thus have more impact in this frequency range.



(a) Elastic energy of foundation, computed with response after expansion of the reduced jacket with a quasi-static correction due to the residual.



(b) Relative difference of the elastic energy computed with the response after expansion of the reduced jacket (with a quasi-static correction due to residual) with respect to the exact elastic energy. Note that the quasi-static residual correction improves the results especially in the lower frequency range.

**Figure 7.5:** Elastic energy of the jacket after expansion (with a quasi-static correction due the residual).

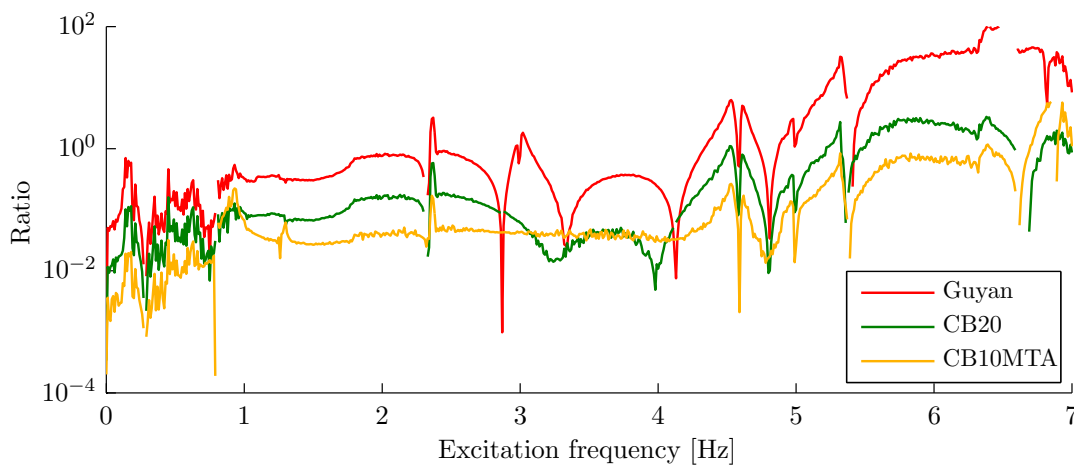
Accurate results are obtained if a model with reduced components is spectrally and spatially converged. In order to check the spatial convergence for the different jacket models, the ratio between the norm of the residual and the norm of the elastic forces is determined, see Figure 7.6.

Up to 2 Hz, the three different ratios have a certain offset towards each other, all the models are spectrally converged within this frequency range. Hence, the difference in the ratios is due to dif-

ference in spatial convergence. It was already expected that the CB10MTA reduced jacket is best spatially converged as this reduction basis includes 10 MTA vectors. At higher frequencies, the difference in spectral convergence appears into the ratios as well, there is no clear offset anymore.

The OWT with a CB10MTA reduced jacket is spatially converged, the residual up to 2 Hz is about 25 times smaller than the elastic forces, with some fluctuations. The OWT with a CB20 reduced jacket is less spatially converged than the CB10MTA reduced jacket up to 2 Hz, the residual is about 10 times smaller than the elastic forces and is increasing at higher frequencies. For higher frequencies the ratio between the residual and the elastic forces becomes more or less the same for the OWT model with a CB20 reduced jacket and the OWT model with a CB10MTA reduced jacket. In the frequency range 2-7 Hz the spatial convergence is better for the OWT model with a CB10MTA reduced jacket, but the spectral convergence is better for the OWT model with a CB20 reduced jacket.

If a Guyan reduced jacket is used in the OWT model, the residual is about 3 times smaller than the elastic forces up to 2 Hz. Therefore it can be concluded that the OWT model with a Guyan reduced jacket is not spatially converged as the residual is quite large, and this will probably have a large impact on the accuracy of the results.



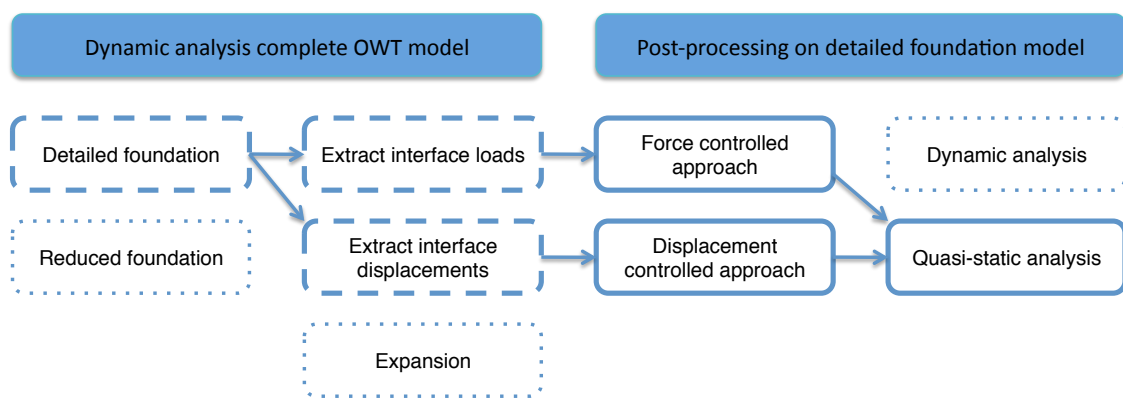
**Figure 7.6: Ratio between the residual and the elastic forces.** Note that the ratio between the residual due to the Guyan reduction and the elastic forces is very large and therefore the Guyan reduced models will be probably not be able to approximate the exact solution well.



## 7.3 Post-processing

In this section, the different calculation procedures in the post-processing phase will be evaluated. The analyses in the post-processing phase are all performed on the detailed jacket model. Differences between the calculation procedures are therefore due to differences in post-processing analyses and due to differences in the input. The input is the interface loads or displacements. When a reduced jacket model is used in the complete OWT model analysis, an error appears in the interface loads/displacements. It will be investigated what the impact is of the error in the interface loads/displacements on accuracy of the response of the detailed jacket after post-processing.

### 7.3.1 OWT with a detailed foundation



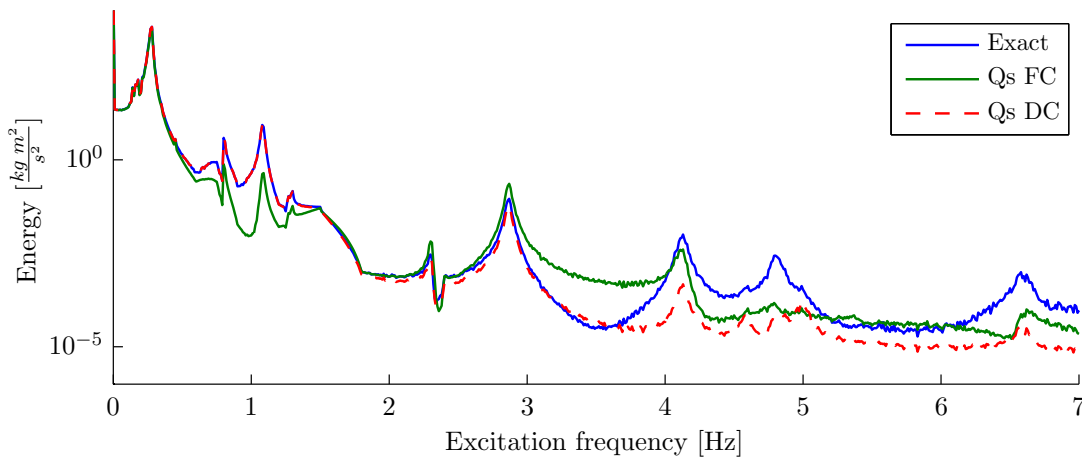
**Figure 7.7:** Schematic overview of post-processing analyses in case of a detailed foundation is integrated in complete OWT model.

If a detailed jacket model is used in the complete OWT analysis, the interface loads/displacements are exact and a dynamic analysis of the detailed jacket model will provide the same response as the reference solution. Therefore, only the accuracy of a quasi-static analysis during post-processing will be investigated. The different calculation procedures that are performed in this subsection are shown in Figure 7.7. In order to compare the different calculation procedures, the elastic energy is computed.

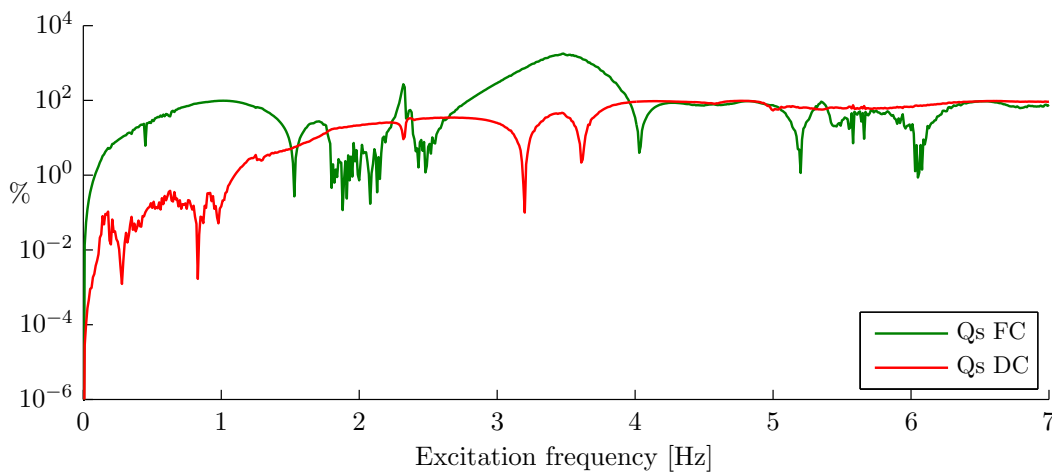
Figure 7.8a shows the elastic energy of the jacket for the different quasi-static analyses. The quasi-static force controlled approach begins to differ from the exact response from around 0.5 Hz and shows an under- and overestimation in the frequency range between 0.5-7 Hz with respect to the reference solution. What the impact is of this under- and overestimation on the accuracy of the fatigue damage results of the structure will be investigated in Section 7.4. Figure 7.8b shows a maximum relative difference around 1 Hz for the quasi-static force controlled approach which is at  $\omega_{free}^{\{1\}}$  of the jacket. Appendix F contains information about the response of one DoF of the jacket structure. The receptance and the flexibility component begin to deviate around 0.5 Hz, see Figure F.4.

The difference between a quasi-static and a dynamic displacement controlled approach starts occurring around  $\omega_{fixed}^{\{1\}}$  of the jacket, in this case at 4.1 Hz. Differences begin to appear around this eigenfrequency and the quasi-static displacement controlled approach underestimates the response

for higher frequencies. The relative difference for the quasi-static displacement controlled approach with respect to the exact solution remains small for frequencies up to 3 Hz, see Figure 7.8b. As it is more likely that frequencies between 0-3 Hz are excited by the external load than frequencies between 3-7 Hz, the hypothesis is that a quasi-static displacement controlled approach will still provide accurate fatigue damage results.



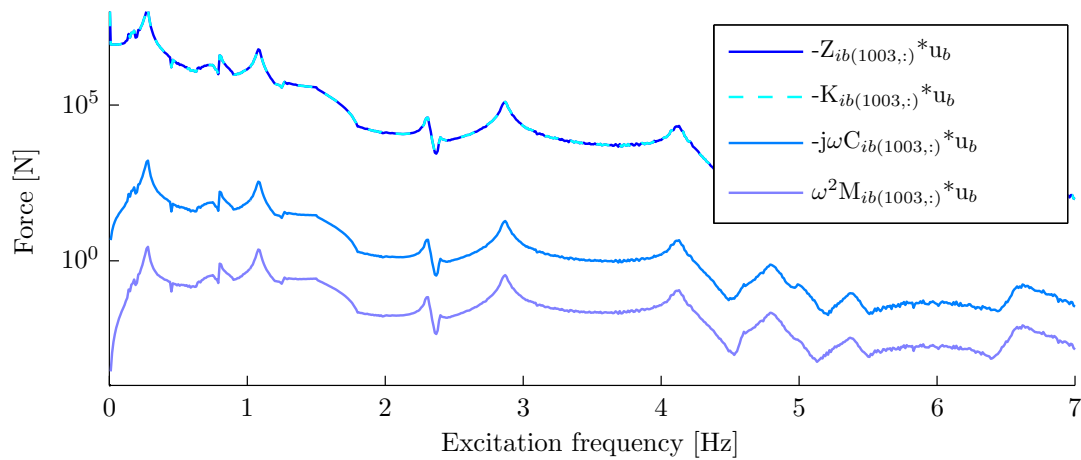
(a) **Elastic energy of foundation.** The response is computed with a quasi-static analysis with interface loads/displacements extracted from OWT model with detailed jacket.



(b) **Relative difference** of the elastic energy computed with the quasi-static post-processing analyses with respect to the exact elastic energy. Note that  $\omega_{free}^{\{1\}}$  of the jacket is around 1 Hz and therefore the relative difference of Qs FC is already large for low frequencies.

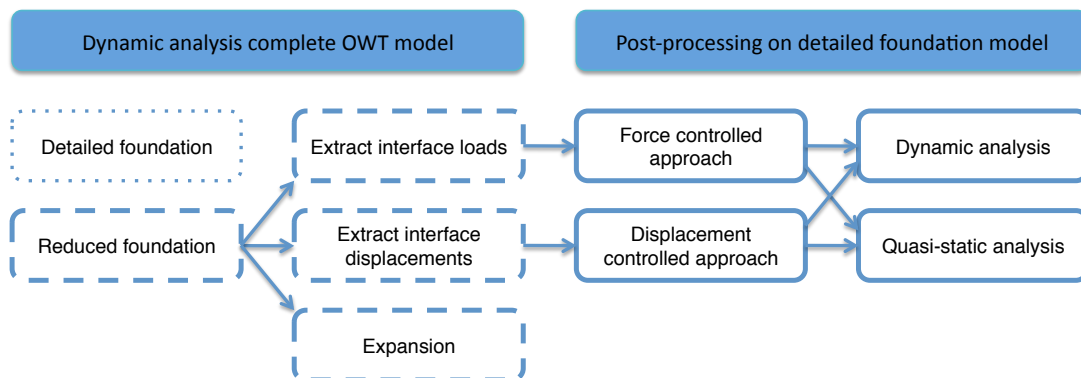
**Figure 7.8:** Elastic energy of different post-processing analyses, using the interface loads/displacements extracted from OWT model with detailed jacket as an input

In order to investigate if the boundary velocities and accelerations can be neglected in the quasi-static displacement controlled approach, the different coupling load terms are computed, see Figure 7.9. The elastic forces are dominant, the damping and inertia forces are much smaller and thus can be neglected in this case.



**Figure 7.9:** Amplitude of coupling load terms,  $-\mathbf{Z}_{ib(1003,:)} \mathbf{u}_b = \omega^2 \mathbf{M}_{ib(1003,:)} \mathbf{u}_b - j\omega \mathbf{C}_{ib(1003,:)} \mathbf{u}_b - \mathbf{K}_{ib(1003,:)} \mathbf{u}_b$ . Note that the elastic coupling forces are dominant.

### 7.3.2 OWT with a Guyan reduced foundation



**Figure 7.10:** Schematic overview of post-processing analyses in case of a Guyan reduced foundation is integrated in complete OWT model.

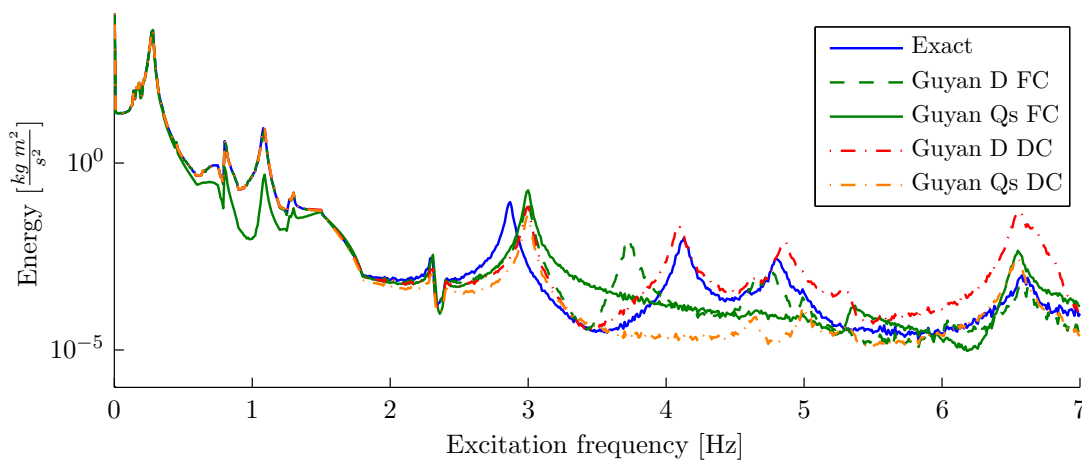
Using a Guyan reduced jacket in the complete OWT model, differences in the eigenfrequencies of the complete OWT model appear. As a result the interface loads/displacements are not accurate. The hypothesis is that these inaccurate interface loads/displacements result in an inaccurate response of the jacket structure after post-processing. Figure 7.10 gives an overview of the different calculation procedures that will be performed in this subsection.

Figure 7.11a shows the elastic energy of the jacket for the different post-processing calculation procedures. The hypothesis is confirmed, all post-processing procedures provide inaccurate results. The eigenfrequencies of the OWT model with a Guyan reduced jacket begin to differ from the exact eigenfrequencies around 3 Hz. The interface loads/displacements are inaccurate and if the input is inaccurate, the output will be inaccurate as well.

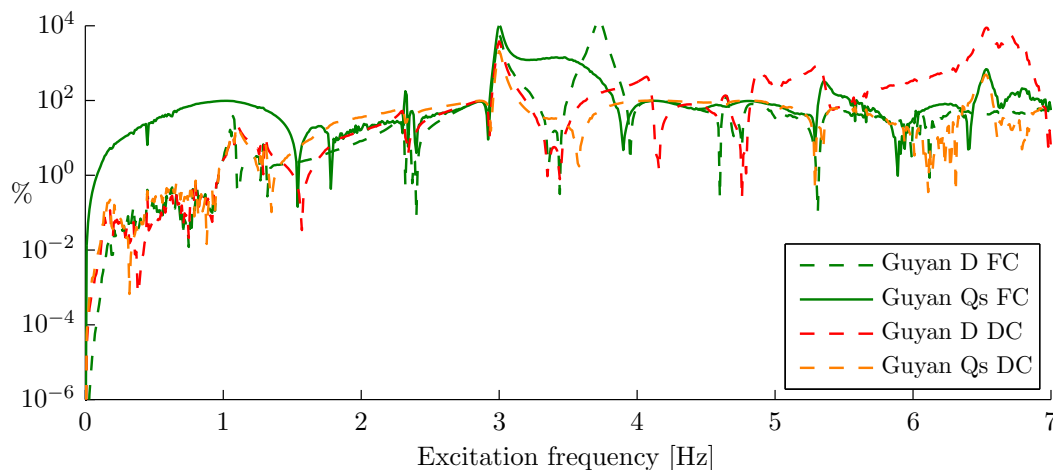
The 25th eigenfrequency of the detailed OWT model is at 4.8 Hz and at 6.5 Hz for the OWT model

with a Guyan reduced jacket. The peaks at 6.5 Hz are clearly visible for the different post-processing analyses. Furthermore, pseudo-resonance peaks occur in the dynamic post-processing analyses due to inaccurate interface loads/displacements. The dynamic force controlled approach shows a peak at 3.7 Hz which is  $\omega_{free}^{\{3\}}$  of the jacket and the dynamic displacement controlled approach shows a peak at 4.1 Hz and at 4.9 Hz which are  $\omega_{fixed}^{\{1\}}$  and  $\omega_{fixed}^{\{6\}}$  of the jacket.

Figure 7.11b shows that the relative difference with respect to the reference solution is large especially for higher excitation frequencies, this is mainly the result of inaccurate interface loads/displacements. The Guyan reduction basis is not spectrally and spatially converged, and is therefore unable to describe the behavior of the structure accurately.



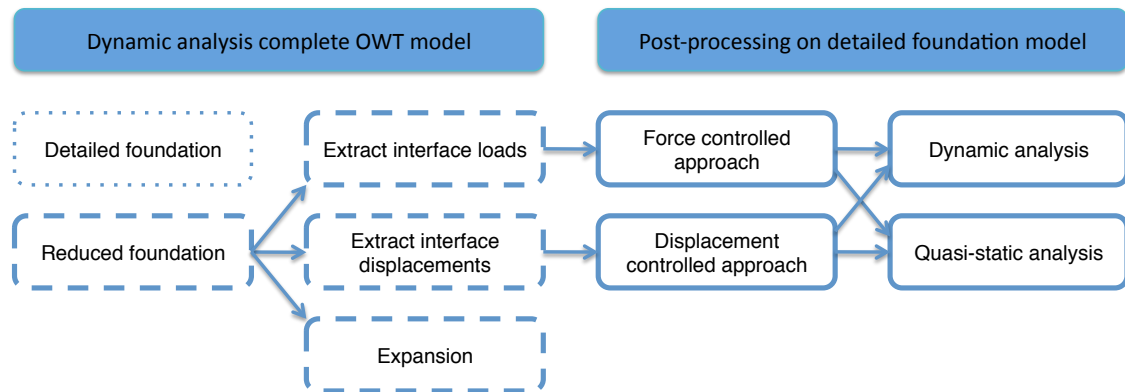
(a) **Elastic energy of foundation.** The response is computed with a dynamic/quasi-static analysis with interface loads/displacements extracted from OWT model with Guyan reduced jacket. Note that pseudo-resonance peaks occur for D FC and D DC due to inaccurate interface loads and displacements.



(b) **Relative difference** of the elastic energy resulting from the different post-processing analyses with respect to the exact elastic energy. As the input is inaccurate above 2 Hz, the relative difference is more or less the same for all post-processing methods between 2-7 Hz.

**Figure 7.11:** Elastic energy of different post-processing analyses, using the interface loads/displacements extracted from OWT model with **Guyan reduced jacket** as an input.

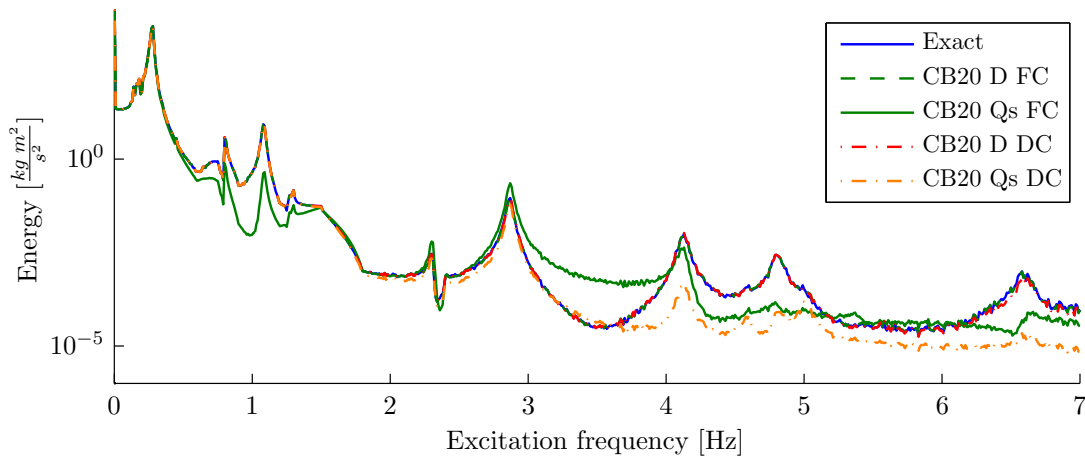
### 7.3.3 OWT with a Craig-Bampton reduced foundation



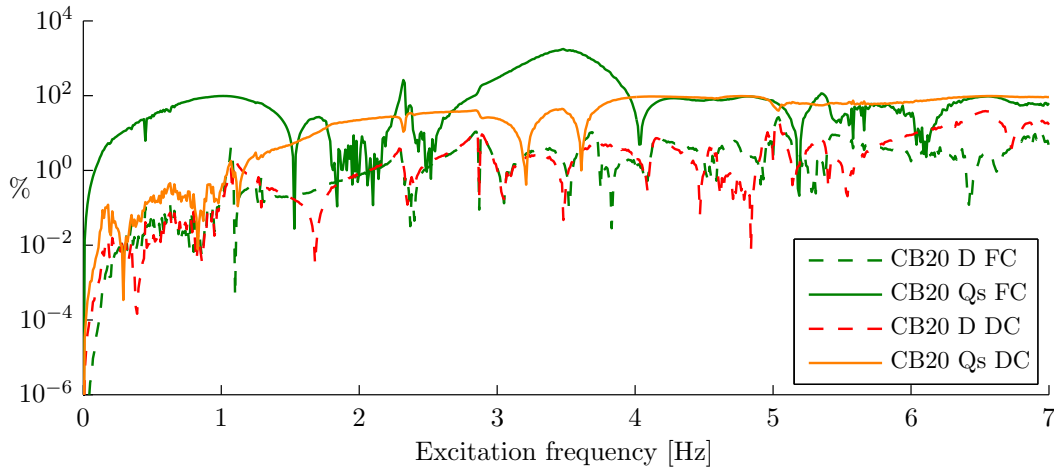
**Figure 7.12:** Schematic overview of post-processing analyses in case of a Craig-Bampton reduced jacket is integrated in complete OWT model.

Using a CB20 reduced jacket model in the complete OWT model, the error in the interface loads/displacements remains very small up to 5 Hz. The hypothesis is that the dynamic post-processing analyses provide accurate results. Figure 7.12 gives an overview of the different calculation procedures that will be performed in this subsection.

Figure 7.13a shows the elastic energy for the different post-processing calculation procedures. The results for the dynamic force and displacement controlled approach follow the exact solution well. As the interface loads/displacements are more accurate, the dynamic post-processing analyses provide accurate results. Next to this, the jacket structure behaves in a dynamic manner in the excitation bandwidth, as a result both quasi-static post-processing analyses do not provide accurate results. The quasi-static force controlled approach is less accurate than the quasi-static displacement controlled approach for frequencies up to 3 Hz, for higher frequencies the relative difference for both quasi-static approaches becomes more or less the same.



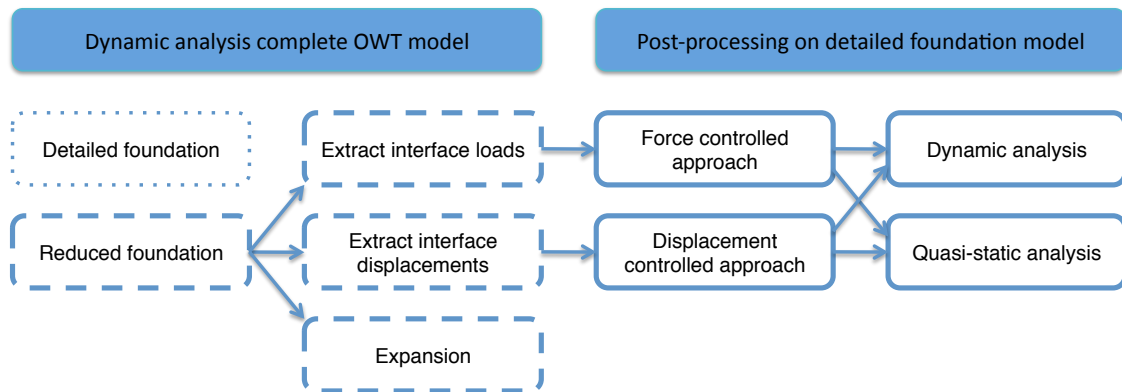
(a) **Elastic energy of foundation.** The response is computed with a dynamic/quasi-static analysis with interface loads/displacements extracted from OWT model with CB20 reduced jacket.



(b) **Relative difference** between the exact elastic energy and the elastic energy resulting from the different post-processing analyses. The interface loads/displacements contain dynamic information due to CB20 reduction, as a result the relative difference is smallest for dynamic post-processing analyses.

**Figure 7.13:** Elastic energy of different post-processing analyses, using the interface loads/displacements extracted from OWT model with **CB20 reduced jacket** as an input.

### 7.3.4 OWT with an Augmented Craig-Bampton reduced foundation



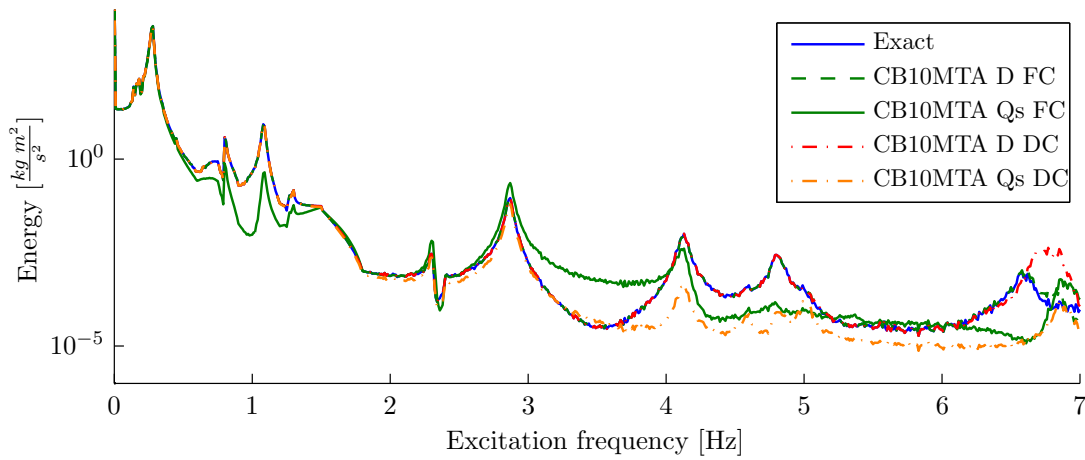
**Figure 7.14:** Schematic overview of post-processing analyses in case of an Augmented Craig-Bampton reduced jacket is integrated in complete OWT model.

Using a CB10MTA reduced jacket model in the complete OWT model, the error in the interface loads/displacements remains very small up to 6 Hz. As the spatial convergence is better than for the OWT model with a CB20 reduced jacket, the hypothesis is that the dynamic post-processing analyses provide even more accurate results. Figure 7.14 gives an overview of the different calculation procedures that will be performed in this subsection.

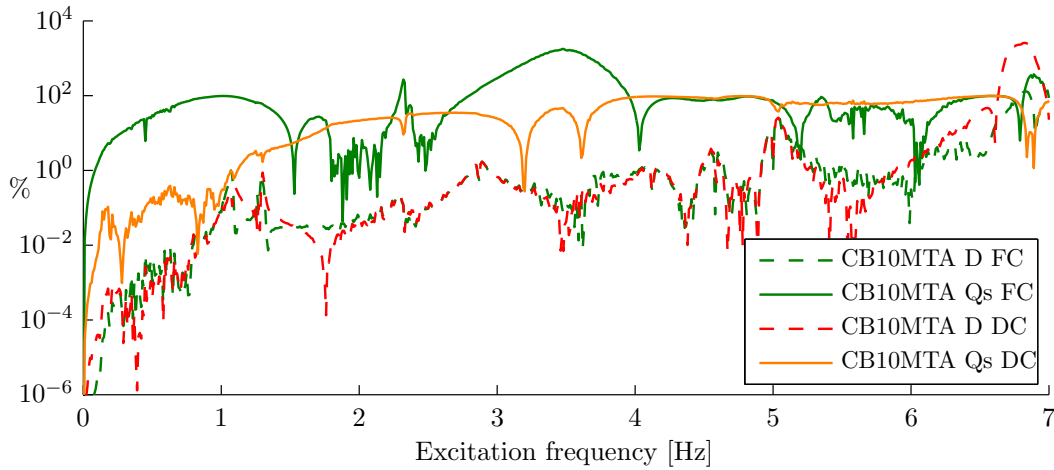
Figure 7.15a shows the elastic energy for the different post-processing calculation procedures. Due to more accurate interface loads/displacements the dynamic post-processing analyses provide accurate results up to 6 Hz and the relative difference remains small, see Figure 7.15b. As the OWT model with a CB10MTA reduced jacket is better spatially converged than the OWT model with a CB20 reduced jacket, the relative differences for the dynamic post-processing analyses are smaller.

Between 6-7 Hz, the results for dynamic post-processing become less accurate. The exact solution shows a resonance peak around 6.6 Hz, this eigenfrequency is shifted to 6.86 Hz for the OWT model with CB10MTA reduced jacket. This effect can be clearly seen in the interface load, Figure 7.3a. Next to this,  $\omega_{fixed}^{\{13\}}$  of the jacket is 6.88 Hz and Figure 7.15a shows that next to the shifting of the eigenfrequency, the fixed interface vibration mode is excited as well in the dynamic displacement controlled approach, as a result the relative difference becomes large.

Likewise the results for quasi-static post-processing analyses in the previous sections, the results of both quasi-static post-processing analyses do not provide accurate results, because  $\omega_{free}^{\{1\}}$  and  $\omega_{fixed}^{\{1\}}$  of the jacket are both within the excitation bandwidth.



(a) **Elastic energy of foundation.** The response is computed with a dynamic/quasi-static analysis with interface loads/displacements extracted from OWT model with CB10MTA reduced jacket.



(b) **Relative difference** of elastic energy resulting from the different post-processing analyses with respect to the exact elastic energy. Note that including MTA vectors provides even more accurate results computed with dynamic post-processing than in Figure 7.13b.

**Figure 7.15:** Elastic energy of different post-processing analyses, using the interface loads/displacements extracted from OWT model with **CB10MTA reduced jacket** as an input.



## 7.4 Fatigue damage calculation



Figure 7.16: Schematic overview of computing damage of a structure.

Often, fatigue is the main design driver for the support structure, so it is interesting to investigate the impact of the error in the responses, due to different calculation procedures, on the fatigue damage and thus the fatigue lifetime of the structure. In order to determine the damage of the structure, the same computations are performed as for the monopile. A schematic overview of these computation steps is given in Figure 7.16. Due to the construction of the jacket, the stress in the elements of the jacket can be the result of the deformations in the local  $y$ -direction or in the local  $z$ -direction. The resulting bending stress in the local- $x$ -direction is computed with the following equation

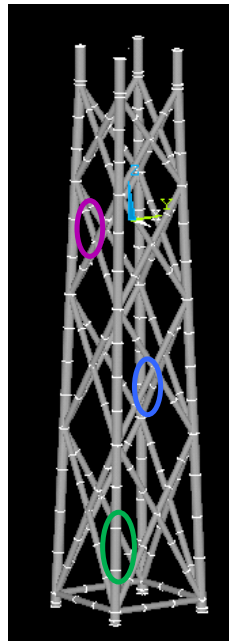
$$\sigma_{xx} = \sqrt{\sigma_{x \text{ due } u_y}^2 + \sigma_{x \text{ due } u_z}^2} \quad (7.1)$$

Torsional stress can occur as well, to take this effect into account, the total stress in the element can be computed following the Von Mises equation. In this case study only the torsional stress and the bending stress  $\sigma_{xx}$  exists, the total stress in an element can be found as follows

$$\sigma_{tot} = \frac{1}{\sqrt{2}} \sqrt{(\sigma_{xx} - \sigma_{yy})^2 + (\sigma_{yy} - \sigma_{zz})^2 + (\sigma_{zz} - \sigma_{xx})^2 + 6\sigma_{xy}^2 + 6\sigma_{yz}^2 + 6\sigma_{zx}^2} \quad (7.2)$$

$$= \frac{1}{\sqrt{2}} \sqrt{2\sigma_{xx}^2 + 6\sigma_{xy}^2} \quad (7.3)$$

The fatigue damage for three different elements in the jacket structure will be computed. Figure 7.17 shows where these elements are located in the structure. High stresses occur in these elements and the elements are well distributed within the jacket structure. The fatigue damage of the jacket model will be computed with and without taking the mean stress into account.



**Figure 7.17:** Elements jacket structure to which damage computations are performed (green= el 174, blue = el 70 and purple=el 121).

Figure 7.18a shows the fatigue damage for the different calculation procedures in element 70. What immediately stands out is that the damage for the quasi-static force controlled approach is significantly underestimated. The quasi-static force controlled approach is highly unconservative, it underestimates the exact fatigue damage about 25%. The relative difference to the reference solution provides more information about the accuracy of the other calculation procedures as well, see Figure 7.18b. The quasi-static displacement controlled approach seems to provide quite accurate damage results. The quasi-static displacement controlled approach provided an accurate response up to 3 Hz, whereas the quasi-static force controlled approach showed already large differences in the response above 0.5 Hz. As it is more likely that frequencies between 0-3 Hz are excited by the external load than the higher frequencies between 3-7 Hz, the large relative difference in the response of the quasi-static displacement controlled approach in the frequency range between 3-7 Hz does not appear in the fatigue damage results. Since the response of the quasi-static force controlled approach begins to differ from the reference solution from 0.5 Hz and this difference in the response results in very inaccurate fatigue damage results.

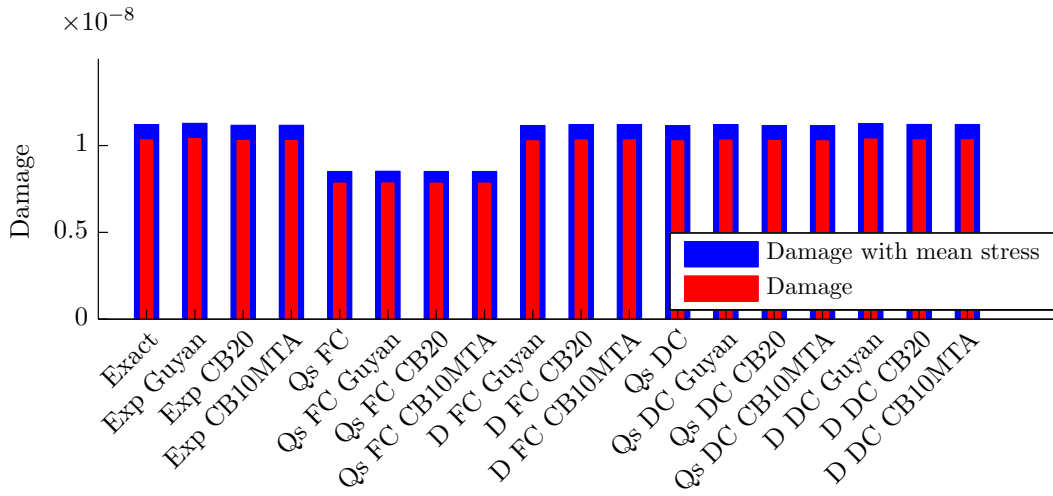
Another interesting aspect is that the fatigue damage of the response after expansion of the reduced CB20 response is underestimated and the fatigue damage of the response after expansion of the reduced Guyan response is overestimated compared to the reference solution. A CB20 reduced jacket and a CB10MTA reduced jacket have a better spectral and spatial convergence than a Guyan reduced jacket. Hence, these models will approximate the exact solution better, but this is on global level. As specific elements are now evaluated, it is possible that a smaller reduction basis overestimates the exact solution in that specific element. The CB10MTA reduced jacket has an improved spatial convergence compared to the other reduced models, but the fatigue damage result is similarly accurate as the result of the CB20 reduced jacket.

The fatigue damage results for a monopile showed that, in general, dynamic post-processing provides more accurate damage results than using the expanded response of the reduced model to

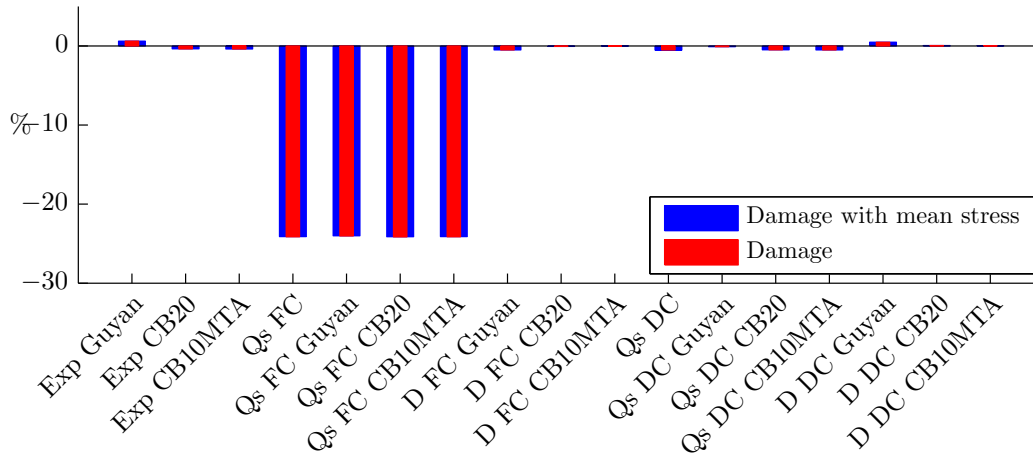
compute the fatigue damage. It is important that the reduction basis can capture the effect of the wave loads on the structure. Since in the post-processing analysis the detailed jacket model is used and the correct wave loads are applied, an error in the interface loads/displacements seems to have less effect on the accuracy of the dynamic post-processing analyses. This conclusion is valid for the jacket structure as well. The relative difference in the fatigue damage results for the dynamic post-processing analyses remain very small. Although large differences appear between 3-7 Hz in the interface loads extracted from the OWT model with a Guyan reduced jacket, the fatigue damage results after dynamic post-processing are quite accurate. Applying the accurate wave loads is of more importance than an error in the interface loads/displacement to retrieve accurate results during dynamic post-processing, as it is less likely that these higher frequencies are excited by the wave and wind loads. Furthermore, Figure 7.18c shows that the fatigue damage results are improved if the response after expansion is corrected with a quasi-static response due to the residual.

Figure 7.19a shows the damage for element 121. More or less the same conclusions can be drawn about the accuracy of the different calculation procedures as for element 70. The quasi-static force controlled is nonconservative and highly inaccurate. Figure 7.19b shows that dynamic post-processing analyses provide in general more accurate fatigue damage results than expansion of the reduced response. The quasi-static displacement controlled approach overestimates the exact fatigue damage and is thus conservative for this element, this overestimation is presumably element dependent as well. Expansion of the Guyan reduced response provides conservative damage results as well in this element. Figure 7.19c shows the fatigue damage results can be improved by the quasi-static residual correction.

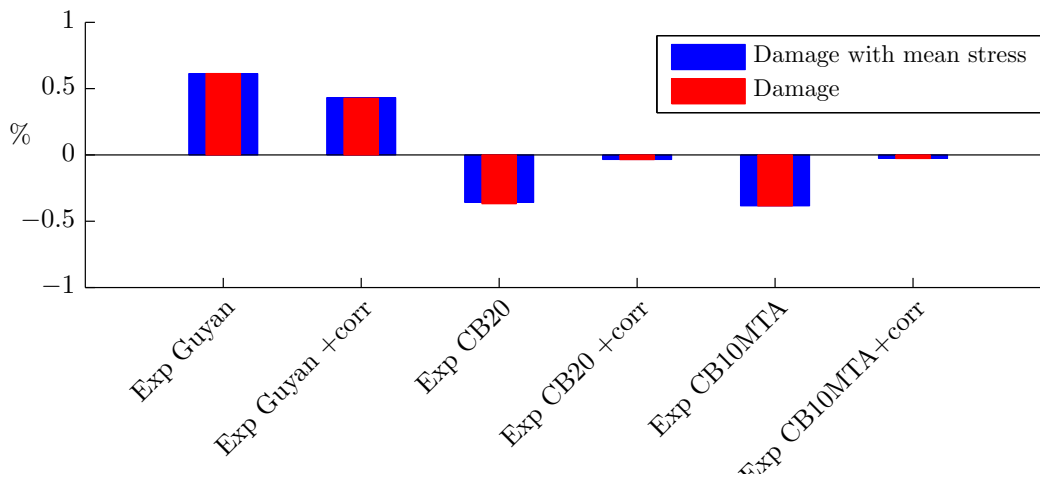
Figure 7.20 shows the damage for element 174. Again more or less the same conclusions can be drawn about the accuracy of the different calculation procedures as for the previous elements. The quasi-static force controlled is nonconservative and highly inaccurate, dynamic post-processing provides accurate results and expansion of reduced responses can provide inaccurate damage results, dependent on the element. In this element expansion of a Guyan reduced response provides a less accurate damage result than expansion of a CB20 reduced response. This proves that a more extensive reduction basis approximates the exact response on global level better, but on local level it can differ. Figure 7.20c shows the damage results can be improved by the quasi-static residual correction.



(a) Fatigue damage in element 70 for the different calculation procedures.

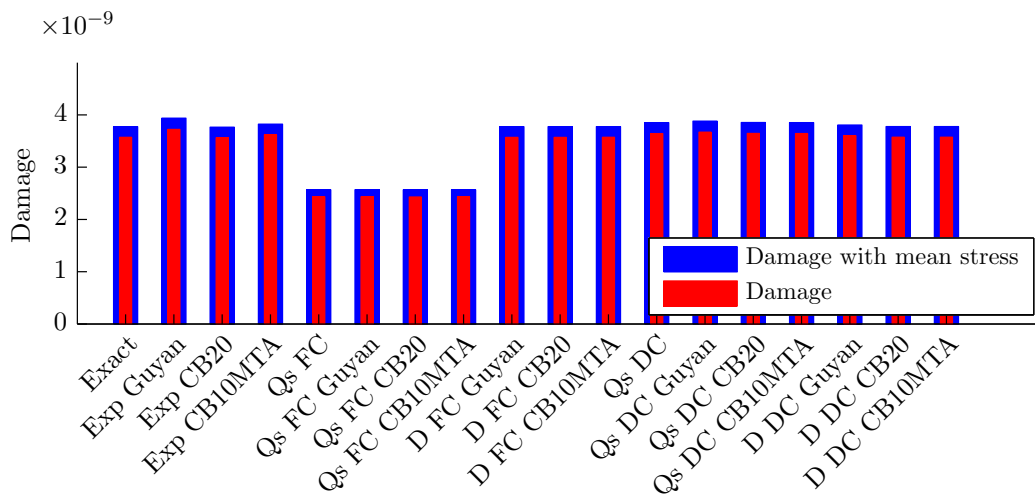


(b) Relative difference between the exact damage and the damage for the different calculation procedures.

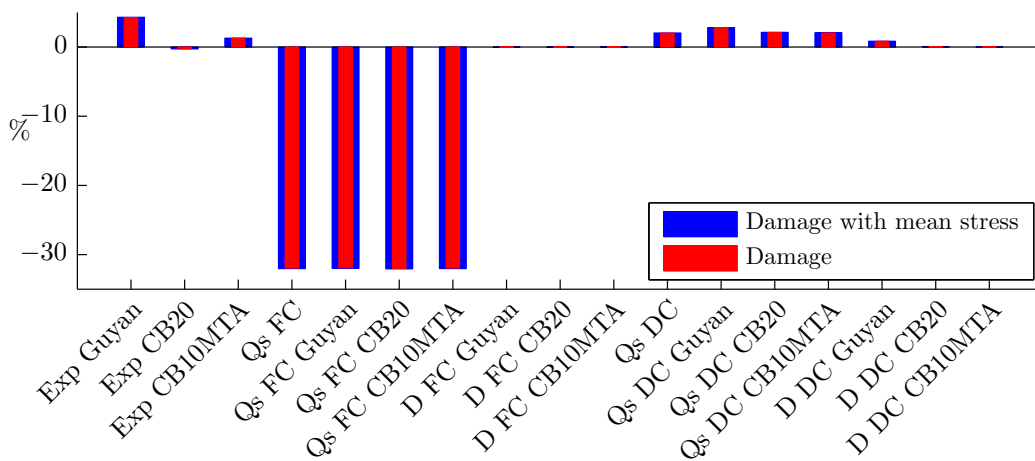


(c) Relative difference between the exact damage and the damage for the different calculation procedures.

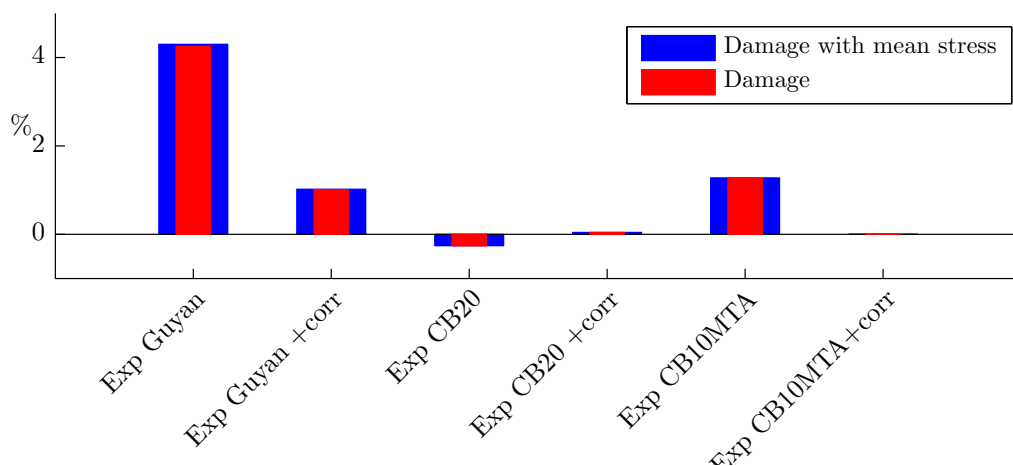
Figure 7.18: Fatigue damage results for the different calculation procedures - Element 70.



(a) Fatigue damage in element 121 for the different calculation procedures.

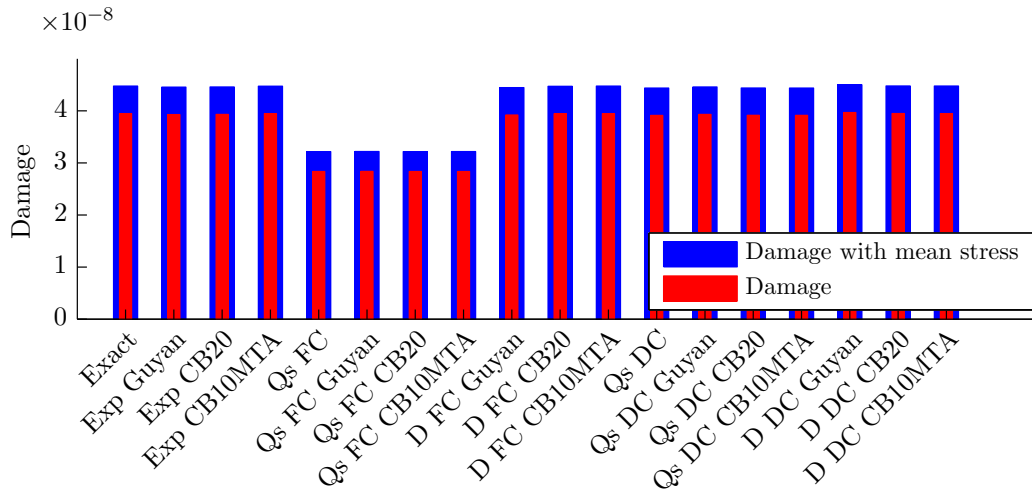


(b) Relative difference between the exact damage and the damage for the different calculation procedures.

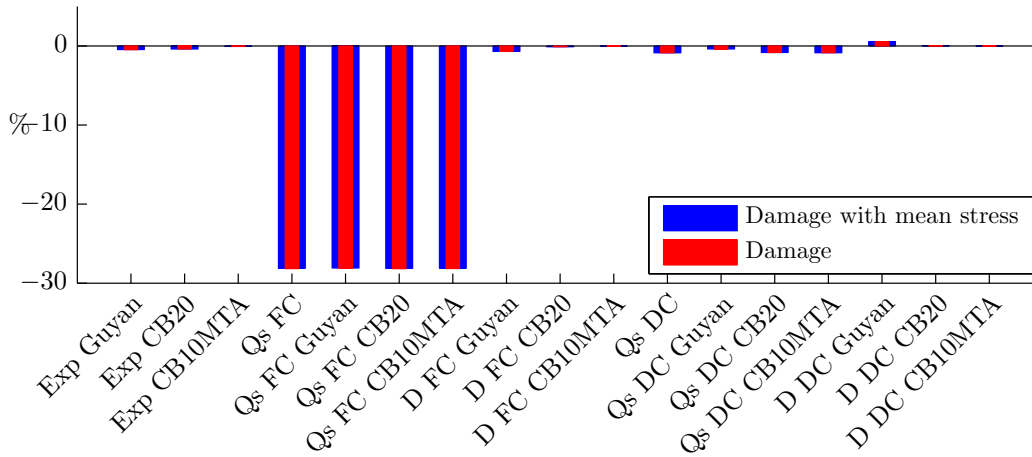


(c) Relative difference between the exact damage and the damage for the different calculation procedures.

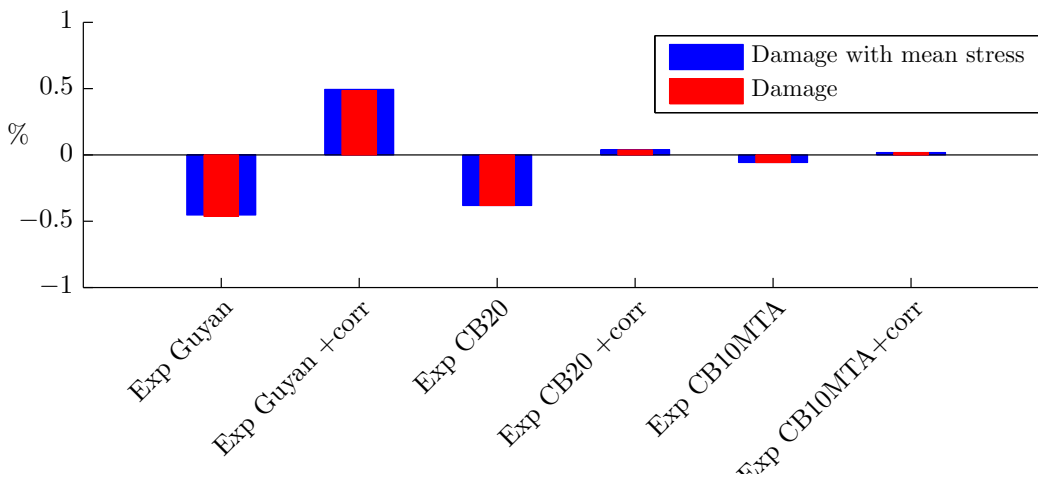
Figure 7.19: Fatigue damage results for the different calculation procedures - Element 121.



(a) Fatigue damage in element 174 for the different calculation procedures.



(b) Relative difference between the exact damage and the damage for the different calculation procedures.



(c) Relative difference between the exact damage and the damage for the different calculation procedures.

Figure 7.20: Fatigue damage results for the different calculation procedures - Element 174.

## 7.5 Summary

In Table 7.2 and 7.3 a summary of the accuracy of the different calculation procedures is given for a OWT model with a jacket model. The upper row describes which jacket model is used in the analysis of the complete OWT model and the left column describes the different calculation procedures.

The accuracy of the different calculation procedures is determined based on the relative difference of the fatigue damage results with respect to the reference solution:

- ✓ - **Accurate** - the relative damage difference is  $<1\%$
- ~ - **Reasonably accurate** - the relative damage difference is between 1-2%
- ✗ - **Inaccurate** - the relative damage difference is  $>2\%$

	Detailed jacket in complete model	Guyan reduced jacket in complete model
<b>Expansion</b>	n/a	✗ <b>Error:</b> OWT model not spectrally and spatially converged
with residual correction	n/a	~ <b>Error:</b> It is improved but still it is not fully accurate
<b>Force controlled</b>		
Dynamic	✓	~ <b>Error:</b> OWT model not spectrally and spatially converged
Quasi-static	✗ <b>Error:</b> Neglecting inertia and damping forces; $\omega_{free}^{\{1\}}$ within excitation bandwidth	✗ <b>Error:</b> Neglecting inertia and damping forces; $\omega_{free}^{\{1\}}$ within excitation bandwidth and OWT model not spatially and spectrally converged
<b>Displacement controlled</b>		
Dynamic	✓	~ <b>Error:</b> Not spatially and spectrally converged
Quasi-static	~ <b>Error:</b> Neglecting inertia and damping forces; $\omega_{fixed}^{\{1\}}$ within excitation bandwidth	~ <b>Error:</b> Neglecting inertia and damping forces; $\omega_{fixed}^{\{1\}}$ within excitation bandwidth and OWT model not spatially and spectrally converged

**Table 7.2:** Accuracy of the different calculation procedures for an OWT with a jacket

	CB20 reduced jacket in complete model	CB10MTA reduced jacket in complete model
<b>Expansion</b>	✓	✓
with residual correction	✓	✓
<b>Force controlled Dynamic</b>	✓	✓
Quasi-static	✗ <b>Error:</b> Neglecting inertia and damping forces; $\omega_{free}^{\{1\}}$ within excitation bandwidth	✗ <b>Error:</b> Neglecting inertia and damping forces; $\omega_{free}^{\{1\}}$ within excitation bandwidth
<b>Displacement controlled Dynamic</b>	✓	✓
Quasi-static	~ <b>Error:</b> Neglecting inertia and damping forces; $\omega_{fixed}^{\{1\}}$ within excitation bandwidth	~ <b>Error:</b> Neglecting inertia and damping forces; $\omega_{fixed}^{\{1\}}$ within excitation bandwidth

**Table 7.3:** Accuracy of the different calculation procedures for an OWT with a jacket



## Chapter 8

# Conclusions and recommendations

The demand for energy will continue to increase in the coming years and offshore wind energy shows great potential to become a key player in Europe's renewable energy future. However, the levelized cost of energy for offshore wind energy should be decreased in order to ensure that the transition to offshore wind energy is economically feasible. One way to realize this cost reduction is by optimizing the structural design of the offshore wind turbine. As the support structure is one of the main cost items of the offshore wind turbine, structural optimization of the support structure should be investigated.

The design of the support structure is driven by the wave and wind loads which excite the structure, and the design is such that it can withstand ultimate loads and has sufficient fatigue lifetime. In order to be able to optimize the structural design of the foundation, one needs to be sure that the calculation procedures to design the support structure provide accurate results. Therefore, the accuracy of the different calculation procedures should be investigated first. Over-dimensioning and applying extra safety factors can be reduced or even eliminated if one knows the results of the calculation procedures are accurate. Section 1.5 presented the thesis objective:

*“Investigate the validity and conservatism of the current calculation procedures for offshore wind turbine support structures and propose improved procedures based on these findings.”*

Throughout this thesis, various studies were performed to determine the validity and conservatism of the different calculation procedures. Firstly, in Chapter 2-4, the qualitative error of the different calculation procedures was determined with information from the literature and supported by equations. Secondly, in Chapter 5-7, the quantitative error of the different calculation procedures was investigated with a case study. Finally, several conclusions and recommendations can be drawn from this research project.

### 8.1 Conclusions

From the theoretical investigation and the case study, it can be concluded that the following aspects tend to influence the accuracy of the results:

- Characteristics of the structure
- Use of a reduced foundation model
- Post-processing method (quasi-static vs. dynamic)

The conclusions regarding these aspects will be discussed below.

### Characteristics of the structure

The accuracy of the different calculation procedures was determined for the monopile and for the jacket. The monopile is a simple tubular structure, whereas the jacket structure is more complex and experiences local dynamics. Therefore, reduction of the jacket structure has more impact on the accuracy of the low frequent interface loads and displacements. Furthermore, the first free interface eigenfrequency,  $\omega_{free}^{\{1\}}$ , of the jacket and of the monopile differ and as this eigenfrequency influences the applicability of a quasi-static analysis, the accuracy of the different calculation procedures is strongly structure dependent.

If  $\omega_{free}^{\{1\}}$  of the foundation structure is within the excitation bandwidth, the response obtained with a quasi-static force controlled approach differs from the exact solution. As  $\omega_{free}^{\{1\}}$  of the jacket model is lower than  $\omega_{free}^{\{1\}}$  of the monopile model, the differences in the response of the jacket with respect to the reference solution are larger. Next to this, it is more likely that frequencies between 0-3 Hz are excited with high amplitudes by the waves and wind than the higher frequencies between 3-7 Hz. Therefore, differences in the response at these higher frequencies do not have large impact on the fatigue damage. As a result the fatigue damage of the monopile computed with a response obtained with a quasi-static force controlled approach only deviates 1% from the reference solution. On the other hand, differences between the exact response of the jacket and the response obtained with a quasi-static force controlled approach already appear in the lower frequency range. Therefore, the error in the response of the jacket obtained with a quasi-static force controlled approach has a large impact on the fatigue damage and is significantly underestimated, the relative difference is around 30%. It is thus important to know if it is likely that the frequencies higher than  $\omega_{free}^{\{1\}}$  of the structure are excited, if so, the error in the response will have a large impact on the fatigue damage results.

Although the foundation models used in this research are simplified, the conclusion can be drawn that the characteristics of the substructure will influence the accuracy of the calculation procedures.

### Use of a reduced foundation model

In order to decrease the computational costs of the analysis of the complete OWT model, a reduced foundation model was integrated. As a result, an error is introduced in the response of the model, since the new set of DoF does not span the full solution space. The error is minimal and thus the OWT model with reduced components provides accurate results if both:

- **OWT model is spectrally converged within the excitation bandwidth**  
The eigenfrequencies of the OWT model with the reduced foundation should be equal to the eigenfrequencies of the detailed OWT model within the frequency range of the external load spectrum.
- **OWT model is spatially converged within the excitation bandwidth**  
To retrieve accurate results, the OWT model with the reduced components should be able to capture the effects of the external loads on the structure.

If the model is not fully spectrally and/or spatially converged, an error is introduced in the response of the model. The response after expansion is an approximation of the exact solution. As a result an error in the equation of motion arises which can be determined by computing the residual. To

improve the accuracy of the response, the quasi-static response of the foundation due to the residual is subtracted from the reduced response after expansion. The accuracy of the fatigue damage results are improved after this quasi-static residual correction. Therefore, in order to decrease the impact of the error in the response on the fatigue damage results, the quasi-static residual correction is a useful method to improve the fatigue damage results if no post-processing on the detailed model is performed.

### Post-processing method (quasi-static vs. dynamic)

The foundation designer could perform a quasi-static analysis to retrieve the response of the detailed foundation. Differences between a quasi-static and a dynamic analysis start to appear around  $\omega_{free}^{\{1\}}$  or  $\omega_{fixed}^{\{1\}}$ , the first fixed interface eigenfrequency, of the foundation for, respectively, the force or the displacement controlled approach. A quasi-static analysis of the foundation provides an accurate result if:

- Force controlled approach:**  $\omega_{free}^{\{1\}} > \max(\omega_{ext})$   
 The force controlled approach applies the interface loads on the foundation to retrieve the response of the detailed foundation. The response for all the DoF of the foundation is computed, therefore a difference between a quasi-static and a dynamic analysis starts to appear around  $\omega_{free}^{\{1\}}$ . If  $\omega_{free}^{\{1\}}$  is higher than the highest excitation frequency, the structure will behave in a quasi-static manner within the excitation bandwidth.
- Displacement controlled approach:**  $\omega_{fixed}^{\{1\}} > \max(\omega_{ext})$   
 The displacement controlled approach applies the interface displacements on the foundation and the response for the internal DoF of the foundation is computed. The difference between a quasi-static and a dynamic analysis for a displacement controlled approach starts to appear around  $\omega_{fixed}^{\{1\}}$ . If  $\omega_{fixed}^{\{1\}}$  is higher than the highest excitation frequency, the structure with fixed interface(s) will behave in a quasi-static manner within the excitation bandwidth.

In order to post-process on the detailed foundation model to retrieve the response of the foundation, the interface loads or displacements are necessary as an input for, respectively, the force or displacement controlled approach. These interface loads and displacements can be inaccurate if a reduced foundation model is used in the dynamic analysis of the complete OWT model. Despite errors in the interface loads/displacements, dynamic post-processing on the detailed foundation model provides accurate fatigue damage results, for both test cases.

## 8.2 Recommendations

### 8.2.1 Recommendations for calculation procedure of support structure

In order to choose the most accurate calculation procedure, the decision tree as given in Figure 8.1 can be used. Dynamic post-processing on the detailed foundation model is expensive, therefore expansion of the reduced response or quasi-static post-processing on the detailed foundation model is preferred over dynamic post-processing. To choose the most accurate calculation procedure, three aspects need to be evaluated:

1. Determine if reduced components are used in the complete OWT model, if not the 'exact' response of the model can directly be extracted from a dynamic analysis of the complete model.

2. If reduced components are integrated in the complete OWT model, determine if the model is spectrally and spatially converged. If so, an accurate response of the model can be obtained after expansion of the reduced response. If not, it is preferable to update the reduced models to ensure the OWT model is spectrally and spatially converged. If this is not possible, the response after expansion can be improved by applying the quasi-static correction due to the residual force. One can also choose to perform a post-processing analysis on the detailed foundation model to retrieve the response of the detailed foundation model.
3. If one wants to perform a post-processing analysis on the detailed foundation model, it should be determined if a quasi-static analysis is sufficiently accurate. If  $\omega_{fixed}^{\{1\}}$  of the foundation is higher than  $\max(\omega_{ext})$ , one can perform a quasi-static displacement controlled approach. If  $\omega_{free}^{\{1\}}$  of the foundation is higher than  $\max(\omega_{ext})$  as well, one can choose between a quasi-static force or displacement controlled approach, as both calculation procedures will provide accurate results.

### 8.2.2 Recommendations for future research

With the knowledge obtained in this project, some recommendations for future research can be formulated.

- **Apply the different calculation procedures in BHawC with different load cases**

As the accuracy of the different calculation procedures is determined with simple models based on one load case, it will be interesting to investigate whether the same conclusions can be drawn when the OWT model with the monopile and the jacket model is integrated in BHawC and the different calculation procedures are evaluated for various realistic load cases. The external load spectrum has influence on the accuracy of the different results, especially when reduced foundation models are used. If the wave loads are dominant, reduction of the wave loads will have a larger effect on the accuracy of the response for the different calculation procedures. Furthermore, applicability of a quasi-static analysis depends on the excitation bandwidth. Therefore, the accuracy of the different calculation procedures should be determined for different realistic load cases.

- **Set up clear guidelines for spatial convergence**

The spectral convergence of a model can be checked by comparing the eigenfrequencies of the detailed model with the eigenfrequencies of the model in which reduced components are integrated. If the model is spectrally converged, the spatial convergence can be checked with the residual. If the residual is small compared to the elastic forces, the model is spatially converged. If, on the other hand, the ratio between the residual and the elastic forces is large, the magnitude of the error on the response is not clear. Therefore, the spatial convergence should be determined using error estimation methods. The work on error estimation conducted in the PhD thesis of Sven Voormeeren can be used to determine the (lack of) spatial convergence and an acceptable error should be defined [37].

- **Determine an efficient and accurate calculation procedure for more complex models**

As the models used in this research are relatively simple models with a maximum of 1155 DoF, the different calculation procedures should be investigated for more complex models. If a more detailed and complex model is used, the obtained results will be more accurate and stress concentrations can be determined better. Roel Engels created a detailed model of the monopile with 86747 DoF [11]. This model was reduced and integrated in the aero-elastic model. Using more complex models, the computation costs become significant and reduction

will be necessary. Moreover, quasi-static or dynamic post-processing on the detailed model will even not be feasible due to high computation costs. An efficient and accurate method has to be determined to retrieve the most important information, such as stress concentrations and maximum loads from the complex model. This may include performing a post-processing analysis on a reduced model. However, the reduced foundation model used to perform the post-processing analysis will be more extensive than the reduced foundation model integrated in the aero-elastic model.

- **Validate results with real OWTs and loads**

Real OWTs have an infinite amount of DoF. Modeling the different procedures always represent a simplification of reality. In order to investigate whether the computed results are accurate, a validation with the real loads and the response of an OWT should be performed. With strain gauges and acceleration sensors, the different loads and responses can be measured during the lifetime of the OWT.

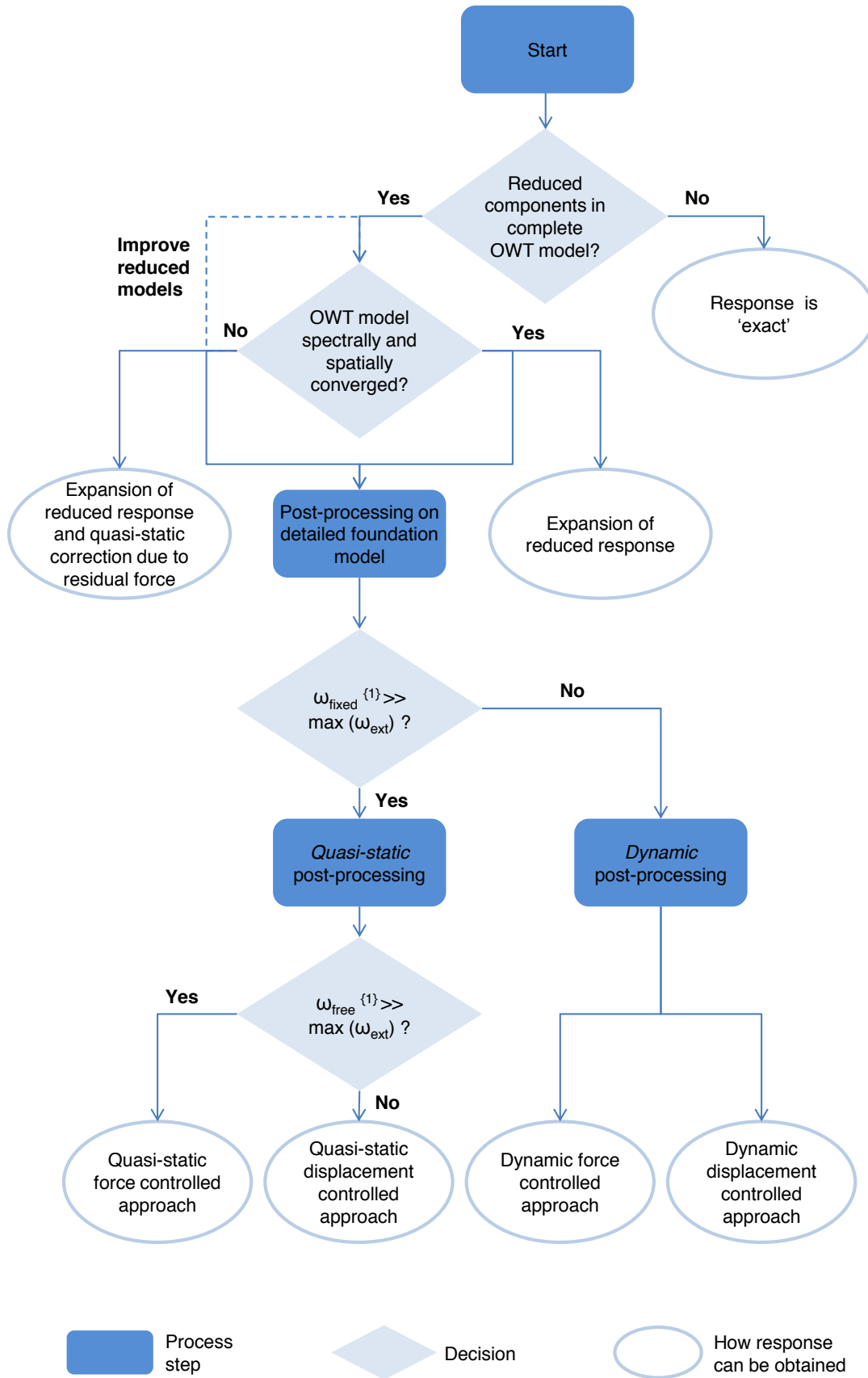


Figure 8.1: Decision tree to choose accurate calculation procedure

## Appendix A

# Proper Orthogonal Decomposition Method

The *proper orthogonal decomposition* (POD) method is a mathematical data analysis method to efficiently calculate the principle components in a large set of data. The principle components are often referred to as *proper orthogonal modes* (POMs). The method is well suited to extract the spatial force vectors of the wave load time series.

The POD method is mathematically defined as orthogonal linear transformation, transforming data dependent on  $n$  possibly correlated variables into a reduced or equal set of uncorrelated variables, called principal components.

A number of snapshots  $m$  are obtained from some time varying signal. Each snapshot is a vector  $\mathbf{z}_i$  containing the values of  $n$  output variables. These vectors can for instance represent the external loading at a specific time. The snapshots  $m$  are collected in a matrix  $\mathbf{Z}$ , having the dimensions  $(n \times m)$ .

One can now construct the sample covariance matrix:

$$\mathbf{C} = \sum_{i=1}^m [E(\mathbf{z}_i - \boldsymbol{\mu})(\mathbf{z}_i - \boldsymbol{\mu})^T] \quad (\text{A.1})$$

where  $\boldsymbol{\mu}$  is the average of the snapshots. Now the snapshots are chosen such that they have zero mean.

$$\mathbf{C} = \frac{1}{m} \sum_{i=1}^m \mathbf{x}_i \mathbf{x}_i^T = \frac{1}{m} \mathbf{X} \mathbf{X}^T \quad (\text{A.2})$$

The eigenvalue problem for matrix  $\mathbf{C}$  is given by:

$$\mathbf{C} \phi_j = \lambda_j \phi_j \quad (\text{A.3})$$

The eigenvectors  $\phi_j$  represent the proper orthogonal modes (POMs), the corresponding eigenvalues  $\lambda_j$  are defined as the proper orthogonal values (POVs). Note that the POMs represent the spatial force vectors and the POVs the amount of energy captured by these modes.

Computing the eigensolutions of  $\mathbf{C}$  is one approach to obtain the POMs and POVs. Another approach is *singular value decomposition* (SVD), this method will provide some additional information in the decomposition. The SVD of  $\mathbf{X}$  is:

$$\mathbf{X} = \mathbf{U} \boldsymbol{\Sigma} \mathbf{V}^T \quad (\text{A.4})$$

The matrix  $\mathbf{U}$  is of dimensions  $(n \times n)$  and contains the left singular vectors, the matrix  $\mathbf{V}$  is of dimensions  $(m \times m)$  and contains the right singular vectors. The matrix  $\mathbf{\Sigma}$  has the dimensions  $(n \times m)$  and contains the singular values. Since  $\mathbf{U}$  and  $\mathbf{V}$  are unitary matrices the following holds:

$$\mathbf{X}\mathbf{X}^T = \mathbf{U}\mathbf{\Sigma}\mathbf{V}^T\mathbf{V}\mathbf{\Sigma}\mathbf{U}^T = \mathbf{U}(\mathbf{\Sigma}\mathbf{\Sigma}^T)\mathbf{U}^T \quad (\text{A.5})$$

$$\mathbf{X}^T\mathbf{X} = \mathbf{V}\mathbf{\Sigma}\mathbf{U}^T\mathbf{U}\mathbf{\Sigma}\mathbf{V}^T = \mathbf{V}(\mathbf{\Sigma}\mathbf{\Sigma}^T)\mathbf{V}^T \quad (\text{A.6})$$

The right hand side of equation (A.5) and (A.6) describe the eigenvalue decomposition of  $\mathbf{X}\mathbf{X}^T$  and  $\mathbf{X}^T\mathbf{X}$ . The singular values of  $\mathbf{X}$  are found by taking the square roots of the eigenvalues of  $\mathbf{X}\mathbf{X}^T$ , these eigenvalues correspond to the proper orthogonal values multiplied by the number of samples  $m$ . The left singular vectors in matrix  $\mathbf{U}$  correspond to the POMs. The right singular vectors in matrix  $\mathbf{V}$  contain the time modulation of the corresponding POM, normalized by the singular value [11, 24, 37].



## Appendix B

# Newmark time integration method

An efficient and commonly used single-step integration formula was published in 1959 by N.M. Newmark. The state vector of the system at a time  $t_{n+1} = t_n + h$  is deduced from the already known state vector at time  $t_n$ , through a Taylor series expansion of the displacements and velocities. This allows us to compute the velocities and displacements of a system at time  $t_{n+1}$ :

$$\begin{aligned}\dot{\mathbf{q}}_{n+1} &= \dot{\mathbf{q}}_n + \int_{t_n}^{t_{n+1}} \ddot{\mathbf{q}}(\tau) d\tau \\ \mathbf{q}_{n+1} &= \mathbf{q}_n + h\dot{\mathbf{q}}_n + \int_{t_n}^{t_{n+1}} (t_{n+1} - \tau)\ddot{\mathbf{q}}(\tau) d\tau\end{aligned}\quad (\text{B.1})$$

The approximation then consists of evaluating the integral terms of the acceleration by numerical quadrature. Therefore, let us express  $\ddot{\mathbf{q}}(\tau)$  in the time interval  $[t_n, t_{n+1}]$  as a function of  $\ddot{\mathbf{q}}_n$  and  $\ddot{\mathbf{q}}_{n+1}$  at the interval limits:

$$\begin{aligned}\int_{t_n}^{t_{n+1}} \ddot{\mathbf{q}}(\tau) d\tau &= (1 - \gamma)h\ddot{\mathbf{q}}_n + \gamma h\ddot{\mathbf{q}}_{n+1} + \mathbf{r}_n \\ \int_{t_n}^{t_{n+1}} (t_{n+1} - \tau)\ddot{\mathbf{q}}(\tau) d\tau &= \left(\frac{1}{2} - \beta\right)h^2\ddot{\mathbf{q}}_n + \beta h^2\ddot{\mathbf{q}}_{n+1} + \mathbf{r}'_n\end{aligned}\quad (\text{B.2})$$

$\mathbf{r}_n$  and  $\mathbf{r}'_n$  are the corresponding error measure. The constants  $\gamma$  and  $\beta$  are parameters associated with the quadrature scheme. By substituting equation (B.2) into equation (B.1) the following approximation formulas for the Newmark method is obtained:

$$\begin{aligned}\dot{\mathbf{q}}_{n+1} &= \dot{\mathbf{q}}_n + (1 - \gamma)h\ddot{\mathbf{q}}_n + \gamma h\ddot{\mathbf{q}}_{n+1} \\ \mathbf{q}_{n+1} &= \mathbf{q}_n + h\dot{\mathbf{q}}_n + \left(\frac{1}{2} - \beta\right)h^2\ddot{\mathbf{q}}_n + \beta h^2\ddot{\mathbf{q}}_{n+1}\end{aligned}\quad (\text{B.3})$$

There is assumed that the equations of dynamics are linear, that the matrices  $\mathbf{M}$ ,  $\mathbf{C}$  and  $\mathbf{K}$  are independent of  $\mathbf{q}$ .  $\ddot{\mathbf{q}}_{n+1}$  can be computed as follows

$$[\mathbf{M} + \gamma h\mathbf{C} + \beta h^2\mathbf{K}]\ddot{\mathbf{q}}_{n+1} = \mathbf{p}_{n+1} - \mathbf{C}[\dot{\mathbf{q}}_n + (1 - \gamma)h\ddot{\mathbf{q}}_n] - \mathbf{K}[\mathbf{q}_n + h\dot{\mathbf{q}}_n + \left(\frac{1}{2} - \beta\right)h^2\ddot{\mathbf{q}}_n]\quad (\text{B.4})$$

Solving this equation implies inverting a linear system of equations associated with the time stepping matrix

$$\mathbf{S} = [\mathbf{M} + \gamma h\mathbf{C} + \beta h^2\mathbf{K}]\quad (\text{B.5})$$

Matrix  $\mathbf{S}$  is symmetric and positive definite. This matrix relates the accelerations at  $t_{n+1}$  to a pseudo-force and can be interpreted as an inertia matrix. Note that this matrix converges towards the mass

matrix when the time-step decreases [28].

$S$  is not changing unless the time step is changed. For a constant time step, the iteration matrix should only be factorized once. Once the accelerations are computed, the velocities and displacements  $\dot{\mathbf{q}}_{n+1}$  and  $\mathbf{q}_{n+1}$  are obtained according to equation (B.3). Let us note that the accuracy of the numerical response can be estimated by evaluating the variation of the energies.

### B.1 Implicit Newmark scheme

Implicit scheme means that  $\beta \neq 0$ , the state vector at time  $t_{n+1}$  is a function of its own time derivative as well. One has to solve a linear step of equations to find  $\ddot{\mathbf{q}}_{n+1}$ , and then  $\dot{\mathbf{q}}_{n+1}$  and  $\mathbf{q}_{n+1}$  can be computed. To ensure the system is stable  $\gamma$  should be larger than  $\frac{1}{2}$  and  $\beta \geq \frac{1}{4}(\gamma + \frac{1}{2})^2$ , so when  $\gamma = \frac{1}{2}$ ,  $\beta = \frac{1}{4}$ .

### B.2 Explicit Newmark scheme

For the explicit Newmark scheme,  $\beta = 0$ , this means that the state vector at time  $t_{n+1}$  can be deduced directly from the results at the previous time step. Therefore no system of equations has to be solved.  $\gamma$  should be at least  $\frac{1}{2}$  and the time step  $h$  should be smaller than  $\frac{2}{\omega}$ , where  $\omega$  is the highest possible eigenfrequency in the system. Otherwise the solution will become unstable.

# Appendix C

## 3D Euler beam element

### C.1 Shape functions

A 3D beam element with two nodes has six degrees of freedom per node, three translations and three rotations, see Figure C.1.

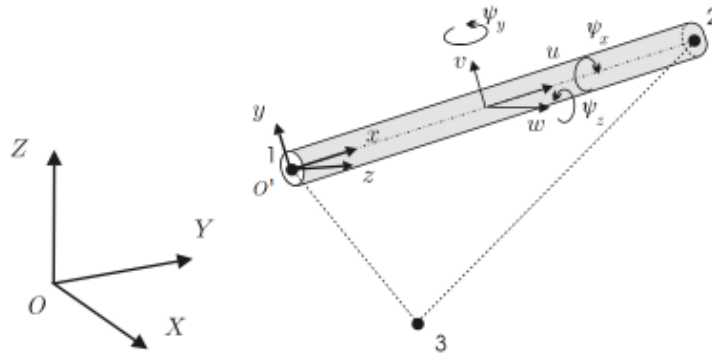


Figure C.1: 3D beam element.

The displacements in the axial direction and can be approximated with the following function [28]

$$u(x, t) = \mathbf{F}_e(x) \mathbf{q}_e(t) \quad (\text{C.1})$$

$\mathbf{F}_e(x) = [\phi_1(x) \ \phi_2(x)]$  is the shape function matrix of element  $e$ ,  $\mathbf{q}_e(t) = [u_1(t) \ u_2(t)]$  is the set of degrees of freedom of element  $e$  and  $u$  is the displacement in the local  $x$ -direction.

$$\mathbf{F}_e(x) = \left[ 1 - \frac{x}{\ell} \quad \frac{x}{\ell} \right] \quad (\text{C.2})$$

An Euler beam element estimates lateral deflection, the displacement  $v$  in the local  $y$ -direction can





## Appendix D

# Verification in Ansys for stress computations 3D structures

Subsection 5.3.1 and 5.3.2 explain in which way strains and stresses can be computed per element. The displacements per element are converted into strains and with the Hooke's law stresses can be found.

The displacement per element should be defined in the local axes of the element. Hence, the global displacements should be transferred to local displacement following the rotation matrix. Firstly, the transformation from local to global displacements will be explained and secondly the stress computations in Matlab will be verified in Ansys.

### D.1 Transformation from global to local axes

Figure C.1 shows a 3D beam element in arbitrary axes. To convert the local displacements to the global displacements a transformation matrix should be constructed.

The direction  $\vec{e}_x$  of the elements neutral axis is defined in the structural frame by the components

$$\vec{e}_x = \left[ \frac{X_2 - X_1}{\ell} \quad \frac{Y_2 - Y_1}{\ell} \quad \frac{Z_2 - Z_1}{\ell} \right] \quad (D.1)$$

The direction  $\vec{e}_y$  and  $\vec{e}_z$  corresponding to the principal axes are constructed with help of a third point  $P_3 = (X_3, Y_3, Z_3)$  in plane  $Oxz$ .

$$\vec{d}_i = [X_i - X_1 \quad Y_i - Y_1 \quad Z_i - Z_1] \quad (D.2)$$

where  $\vec{e}_y$  is obtained from the following vector operation.

$$\vec{e}_y = \frac{\vec{d}_3 \times \vec{d}_2}{\|\vec{d}_3 \times \vec{d}_2\|} \quad (D.3)$$

The direction  $\vec{e}_z$  is obtained by taking the cross product of the other principal directions.

$$\vec{e}_z = \vec{e}_x \times \vec{e}_y \quad (D.4)$$

The rotation operation  $\mathbf{R}$  describes the frame transformation.

$$\begin{bmatrix} x \\ y \\ z \end{bmatrix} = \mathbf{R} \begin{bmatrix} X \\ Y \\ Z \end{bmatrix} \quad (\text{D.5})$$

$$\mathbf{R} = \begin{bmatrix} \vec{e}_X \cdot \vec{e}_x & \vec{e}_Y \cdot \vec{e}_x & \vec{e}_Z \cdot \vec{e}_x \\ \vec{e}_X \cdot \vec{e}_y & \vec{e}_Y \cdot \vec{e}_y & \vec{e}_Z \cdot \vec{e}_y \\ \vec{e}_X \cdot \vec{e}_z & \vec{e}_Y \cdot \vec{e}_z & \vec{e}_Z \cdot \vec{e}_z \end{bmatrix} \quad (\text{D.6})$$

Displacements and rotations in local and global axes are linked as follows.

$$\begin{bmatrix} u \\ v \\ w \end{bmatrix} = \mathbf{R} \begin{bmatrix} U \\ V \\ W \end{bmatrix} \quad \begin{bmatrix} \psi_x \\ \psi_y \\ \psi_z \end{bmatrix} = \mathbf{R} \begin{bmatrix} \psi_X \\ \psi_Y \\ \psi_Z \end{bmatrix} \quad (\text{D.7})$$

The transformation from local to global degrees of freedom per element will be

$$\mathbf{q}_{el} = \mathbf{T} \mathbf{q}_{eS} \quad (\text{D.8})$$

$$\mathbf{T} = \begin{bmatrix} \mathbf{R} & \mathbf{0} & \mathbf{0} & \mathbf{0} \\ \mathbf{0} & \mathbf{R} & \mathbf{0} & \mathbf{0} \\ \mathbf{0} & \mathbf{0} & \mathbf{R} & \mathbf{0} \\ \mathbf{0} & \mathbf{0} & \mathbf{0} & \mathbf{R} \end{bmatrix} \quad (\text{D.9})$$

## D.2 Ansys verification stress computations

### D.2.1 Monopile structure

The monopile structure used in the OWT model is constructed in ANSYS to verify if the stresses computed in Matlab are accurate. The monopile is constructed in the same manner as in Matlab. The monopile is divided into 10 elements. The monopile has a length of 30 meters, a diameter of 6 meters and a wall thickness of 0.08 meters. The node numbers and its position are summarized in Table D.1. Figure D.1 shows the monopile model in Ansys, the monopile is constrained at the bottom in all directions. A random load is applied on the top of the monopile and the stresses in the structure are computed, Table D.2. The global displacements in every node are converted to the local displacements with the transformations matrix and stresses are computed following Subsection 5.3.2.

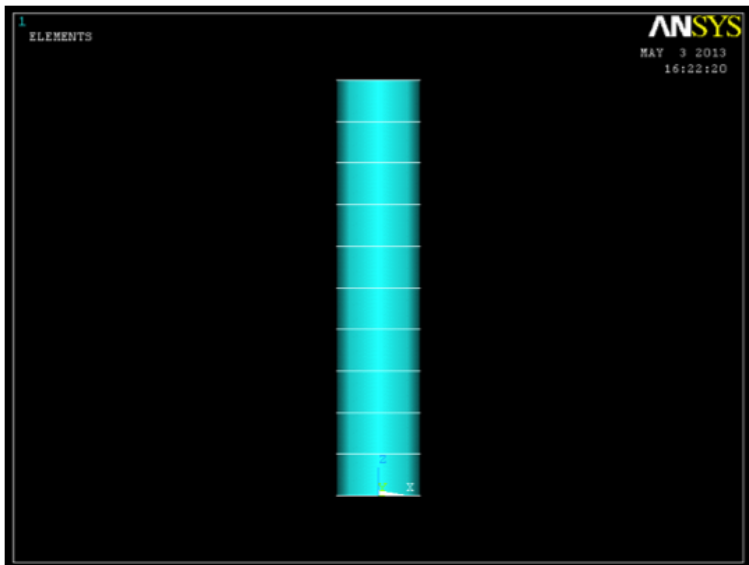


Figure D.1: Monopile in ANSYS.

Node	x	y	z
1	0	0	0
2	0	0	3
3	0	0	6
4	0	0	9
5	0	0	12
6	0	0	15
7	0	0	18
8	0	0	21
9	0	0	24
10	0	0	27
11	0	0	30

Table D.1: Position of nodes of the structure.

Force	Magnitude [N]
$F_x$	100
$F_y$	-50
$F_z$	-25
$M_x$	25
$M_y$	100
$M_z$	-50

Table D.2: External load at the top of the structure.

Table D.3 shows that the stresses computed in Matlab are identical to stresses computed in ANSYS. The transformation from global to local displacements is correct.

Node	Bending stress [Pa]		Axial stress [Pa]		Torsional stress [Pa]	
	ANSYS	Matlab	ANSYS	Matlab	ANSYS	Matlab
1	1589.8	1589.8	-16.803	-16.8027	-11.504	-11.5045
2	1435.5	1435.5	-16.803	-16.8027	-11.504	-11.5045
3	1281.1	1281.1	-16.803	-16.8027	-11.504	-11.5045
4	1126.8	1126.8	-16.803	-16.8027	-11.504	-11.5045
5	972.45	972.4518	-16.803	-16.8027	-11.504	-11.5045
6	818.11	818.1133	-16.803	-16.8027	-11.504	-11.5045
7	663.78	663.7795	-16.803	-16.8027	-11.504	-11.5045
8	509.45	509.4549	-16.803	-16.8027	-11.504	-11.5045
9	355.15	355.1513	-16.803	-16.8027	-11.504	-11.5045
10	200.92	200.9171	-16.803	-16.8027	-11.504	-11.5045
11	47.434	47.4342	-16.803	-16.8027	-11.504	-11.5045

Table D.3: Stress in element, comparison Matlab and ANSYS results.



### D.2.2 More complex 3D structure

The monopile is a simple structure and the transformation from the global to the local axis is simple. The x-axis in the local frame is in the direction of the element's neutral axis, whereas the element's neutral axis is equal to the z-axis in the global frame. In order to verify if the transformation from global to local displacements is valid for elements which neutral axis does not coincide with one of the global axes, a more complex structure is constructed in ANSYS, see Figure D.2. Such a structure is more comparable to a jacket structure where the neutral axis of different elements neither coincide with one of the global axes.

The structure is constructed of PIPE16 elements with a diameter of 0.8 meters and a wall thickness of 5 centimeters. The coordinates of the different nodes are summarized in Table D.4 and the random load applied on the top of the structure is given in Table D.5.



Figure D.2: More complex structure model in ANSYS.

Node	x	y	z
1	0	0	0
2	5	0	10
3	5	5	20
4	2	2	30

Table D.4: Position of nodes of the structure.

Force	Magnitude [N]
$F_x$	1
$F_y$	-2
$F_z$	-3
$M_x$	2
$M_y$	-3
$M_z$	-1

Table D.5: External load at the top of the structure.

Table D.6 shows the stresses computed in ANSYS and Matlab. Again, the stresses computed in Matlab are similar to the stresses in ANSYS. It can be concluded that the method used in Matlab provides accurate stress values.

Node	Bending stress [Pa]		Axial stress [Pa]		Torsional stress [Pa]	
	ANSYS	Matlab	ANSYS	Matlab	ANSYS	Matlab
1 - el 1	3260.0	3236.0	26.572	26.5725	580.50	580.4959
2 - el 1	2358.0	2358.0	26.572	26.5725	580.50	580.4959
2 - el 2	2536.7	2536.7	15.184	15.1843	344.00	343.9976
3 - el 2	810.46	810.5	15.184	15.1843	344.00	343.9976
3 - el 3	1062.7	1062.7	25.786	25.7865	-15.490	-15.4899
4 - el 3	177.19	177.2	25.786	25.7865	-15.490	-15.4899

Table D.6: Stress in element, comparison Matlab and ANSYS results.

## Appendix E

# OWT models - eigenfrequencies and eigenmodes

### E.1 OWT model with a monopile

Eigenfrequency	OWT with detailed monopile [Hz]	OWT with Guyan reduced monopile Hz]	OWT with CB10 reduced monopile [Hz]
1st	0.2961	0.2961	0.2961
2nd	0.2984	0.2984	0.2984
3rd	0.7627	0.7627	0.7627
4th	0.7848	0.7848	0.7848
5th	0.8046	0.8046	0.8046
6th	1.1666	1.1666	1.1666
7th	1.2589	1.2589	1.2589
8th	1.2672	1.2672	1.2672
9th	1.9117	1.9117	1.9117
10th	2.0489	2.0489	2.0489
11th	2.1595	2.1595	2.1595
12th	2.3805	2.3805	2.3805
13th	2.4269	2.4269	2.4269
14th	3.7332	3.7332	3.7332
15th	4.4264	4.4265	4.4266
16th	4.6729	4.6729	4.6729
17th	4.7970	4.7970	4.7970
18th	5.0688	5.0688	5.0697
19th	5.4423	5.4423	5.4424
20th	5.6890	5.6891	5.6904
21th	5.7764	5.7787	5.7765
22th	5.9048	5.9052	5.9048
23th	8.5821	8.5825	8.5821
24th	9.2649	9.2706	9.2650
25th	9.5888	9.5901	9.5888

Table E.1: Eigenfrequencies of OWT model with different monopile models.

## E.1.1 Eigenmodes monopile

Mode number	Frequency [Hz]	Mode shape description
1	6.7316	1st bending mode
2	6.7316	1st bending mode
3	26.758	1st torsional mode
4	42.188	2nd bending mode
5	42.188	2nd bending mode
6	43.146	1st longitudinal mode
7	80.935	2nd torsional mode
8	118.15	3rd bending mode
9	118.15	3rd bending mode
10	130.50	2nd longitudinal mode

Table E.2: Mode shape description of the monopile model.

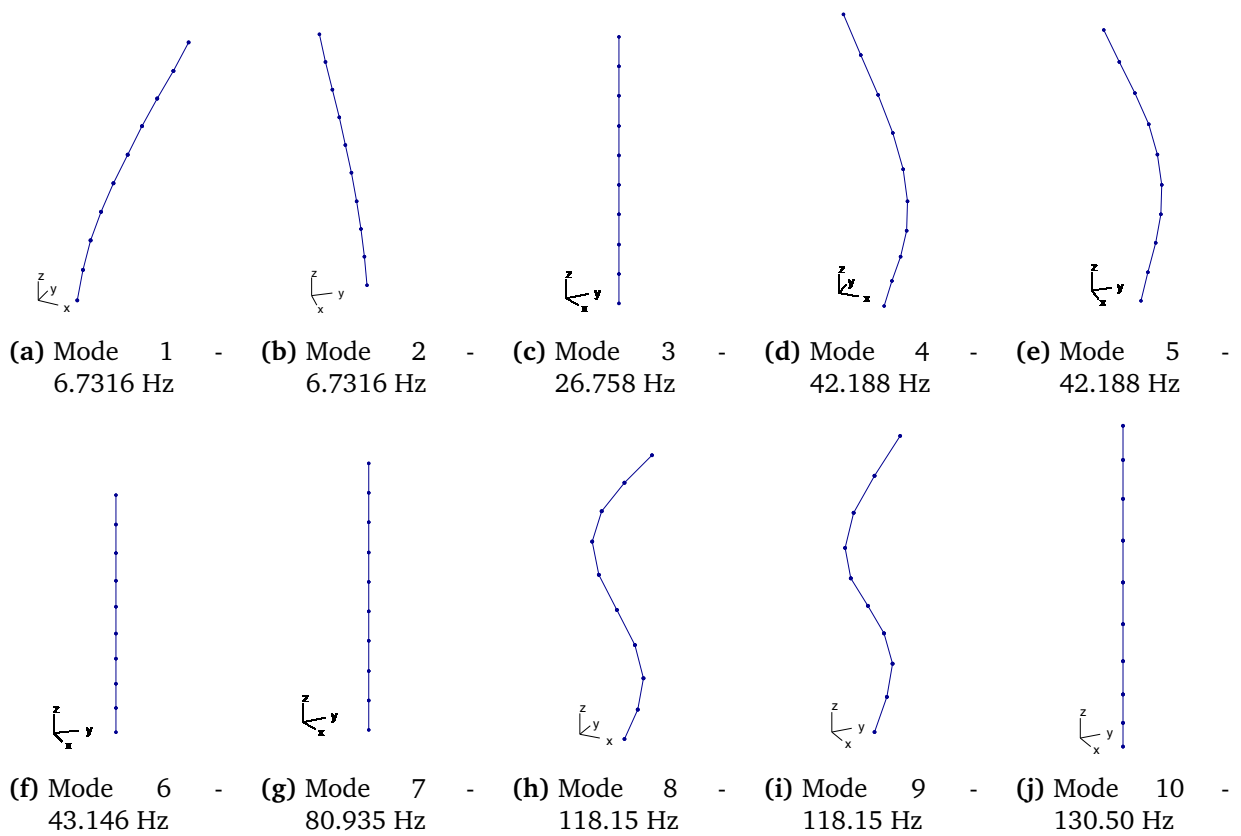


Figure E.1: First 10 eigenmodes of the monopile.

## E.1.2 Eigenmodes OWT with a monopile

Mode number	Frequency [Hz]	Mode shape description
1	0.2961	1st global bending, side-side
2	0.2984	1st global bending, fore-aft
3	0.7627	1st asymmetric flapwise yaw
4	0.7848	1st asymmetric flapwise pitch
5	0.8046	1st flapwise collective
6	1.1666	1st edgewise collective
7	1.2589	1st asymmetric edgewise yaw
8	1.2672	1st asymmetric edgewise pitch
9	1.9117	2nd global bending, fore-aft
10	2.0489	2nd global bending, side-side

Table E.3: Mode shape description of OWT model with a monopile.

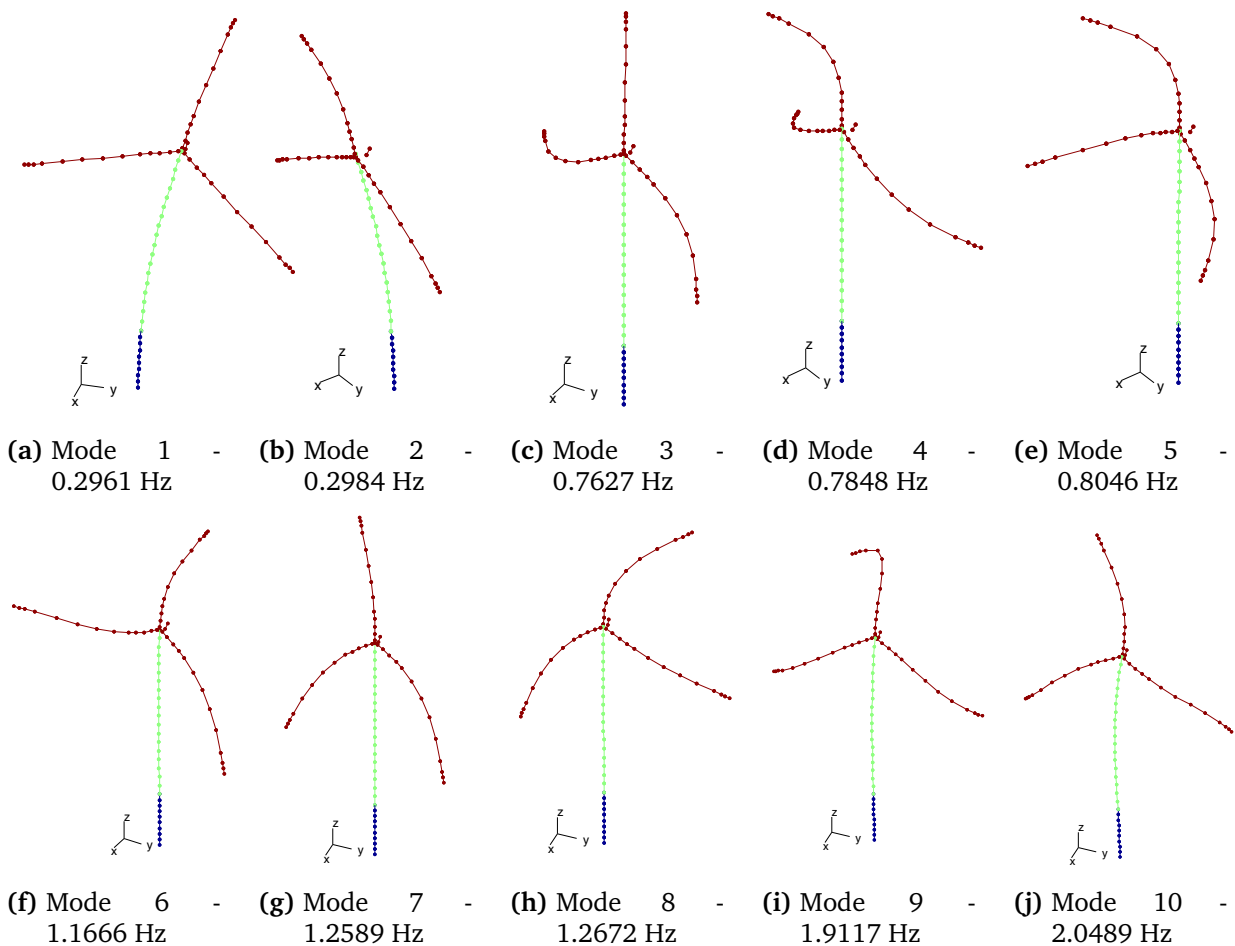


Figure E.2: First 10 eigenmodes of OWT with a monopile.

## E.2 OWT model with a jacket

Eigenfrequency	OWT with detailed jacket [Hz]	OWT with Guyan reduced jacket Hz]	OWT with CB20 reduced jacket [Hz]	OWT with CB10+MTA reduced jacket [Hz]
1st	0.2745	0.2745	0.2745	0.2745
2nd	0.2764	0.2764	0.2764	0.2764
3rd	0.7523	0.7523	0.7523	0.7523
4th	0.7801	0.7801	0.7801	0.7801
5th	0.8014	0.8014	0.8014	0.8014
6th	1.0075	1.0087	1.0075	1.0076
7th	1.0834	1.0858	1.0836	1.0835
8th	1.2464	1.2468	1.2464	1.2465
9th	1.2620	1.2621	1.2620	1.2620
10th	1.2967	1.2980	1.2968	1.2968
11th	2.0006	2.0071	2.0008	2.0009
12th	2.3062	2.3108	2.3064	2.3063
13th	2.3949	2.3953	2.3949	2.3949
14th	2.7922	2.8732	2.7946	2.7959
15th	2.8637	2.9974	2.8660	2.8674
16th	2.8671	3.0003	2.8698	2.8683
17th	4.0632	4.4398	4.0638	4.0643
18th	4.1241	4.6202	4.1253	4.1245
19th	4.2036	4.6493	4.2059	4.2074
20th	4.4353	4.8582	4.4353	4.4353
21th	4.5818	4.9911	4.5863	4.5860
22th	4.6535	5.3350	4.6553	4.6568
23th	4.6989	5.4589	4.6991	4.6990
24th	4.7355	6.0333	4.7355	4.7355
25th	4.8056	6.5433	4.8058	4.8059
26th	4.8136	6.8199	4.8136	4.8137
27th	4.9086	9.3293	4.9093	4.9105
28th	4.9937	9.5999	5.0092	5.0098
29th	5.3942	9.8043	5.3957	5.3944
30th	5.4668	10.3002	5.4671	5.4671
31th	5.5992	10.3937	5.5992	5.5992
32th	5.8717	11.1509	5.8735	5.8750
33th	6.3396	11.1880	6.3417	6.3447
34th	6.5909	11.9042	6.6016	6.8636
35th	6.6084	12.7473	6.8817	7.1181
36th	6.8276	14.5440	6.8920	7.6774
37th	6.8821	14.6783	6.9995	8.0276
38th	6.8831	15.1032	7.2468	8.4426
39th	6.9974	15.3861	7.2775	8.5748
40th	7.2468	15.5581	7.4813	8.7920

Table E.4: Eigenfrequencies of model with different jacket models.

## E.2.1 Eigenmodes jacket

Mode number	Frequency [Hz]	Mode shape description
1	1.0597	1st bending mode
2	1.0597	1st bending mode
3	2.9590	1st torsional mode
4	3.7267	2nd bending mode
5	3.7267	2nd bending mode
6	4.4353	1st breathing mode
7	4.6806	2nd breathing mode
8	4.7355	2nd torsional mode
9	4.7581	3rd bending mode
10	4.7581	3rd bending mode

Table E.5: Mode shape description of the jacket model.

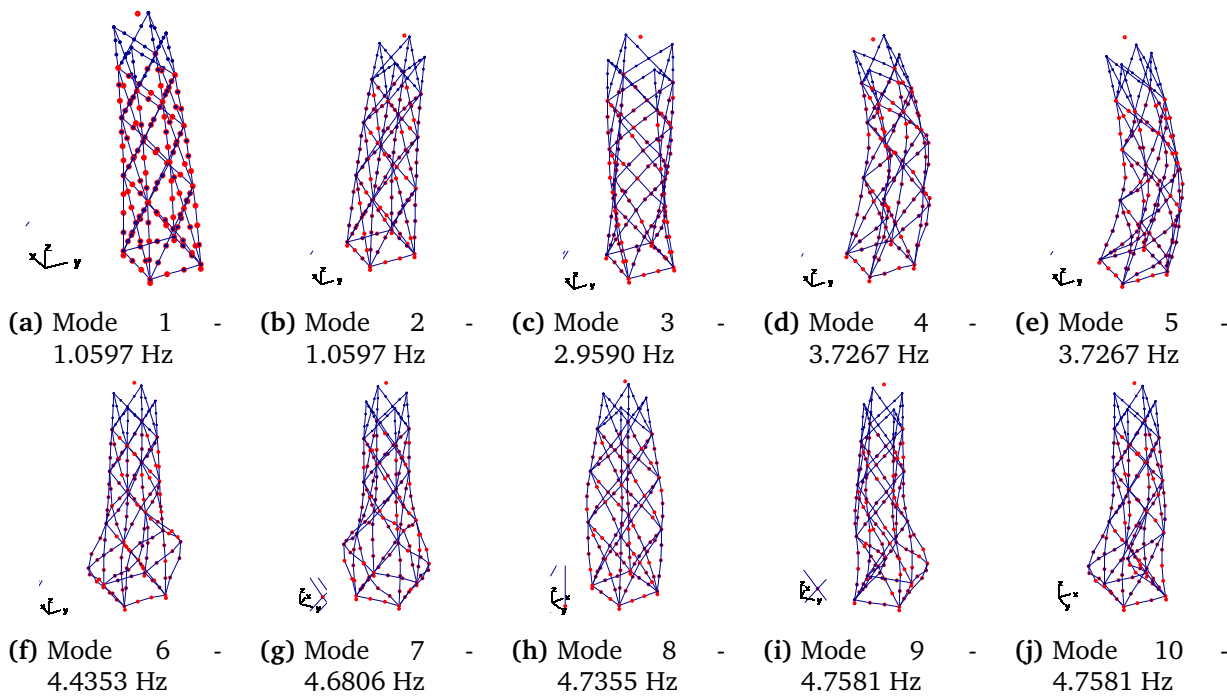


Figure E.3: First 10 eigenmodes of the jacket.

## E.2.2 Eigenmodes OWT with a jacket

Mode number	Frequency [Hz]	Mode shape description
1	0.2745	1st global bending, side-side
2	0.2764	1st global bending, fore-aft
3	0.7523	1st asymmetric flapwise yaw
4	0.7801	1st asymmetric flapwise pitch
5	0.8014	1st flapwise collective
6	1.0075	1st edgewise collective
7	1.0834	1st asymmetric edgewise yaw
8	1.2464	1st asymmetric edgewise pitch
9	1.2620	2nd global bending, fore-aft
10	1.2967	2nd global bending, side-side

Table E.6: Mode shape description of OWT model with a jacket.

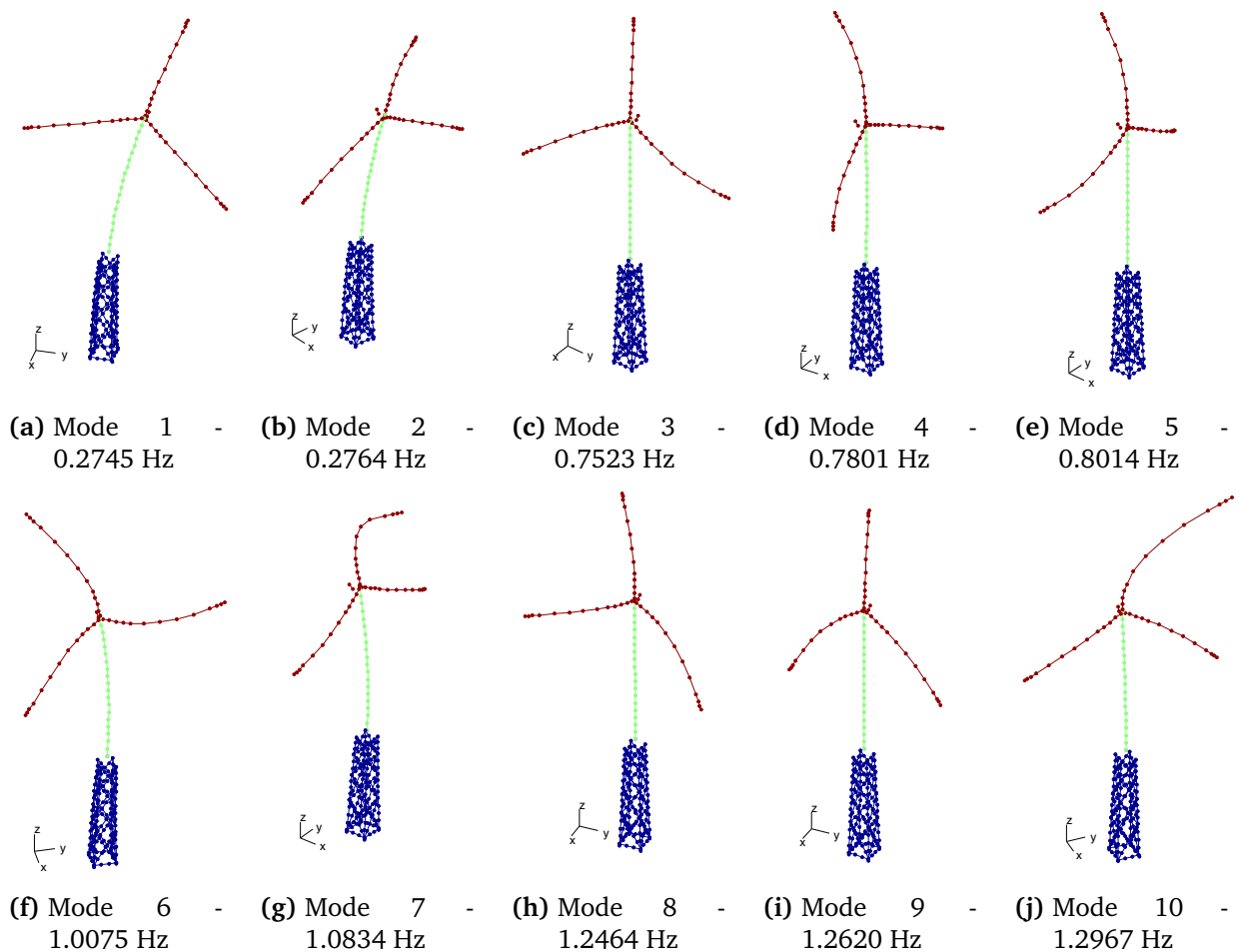
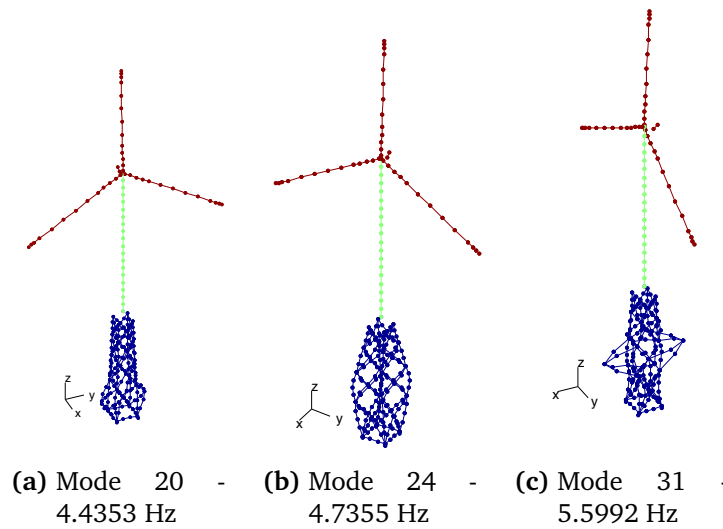


Figure E.4: First 10 eigenmodes of OWT with a jacket.

Figure E.5 show some extra mode shapes, as these mode shapes are interesting because only the jacket structure is deforming and that the rest of the turbine model does not participate in this mode shape. The shape of the deformation of the jacket structure and the frequencies related to those free interface modes of the jacket model, corresponding to the 6th, 8th and 11th eigenmode, respectively. If the jacket structure is reduced and one wants to describe the behavior of the structure accurately, these modes need to be included in the reduction basis.



**Figure E.5:** Eigenmodes OWT with a jacket.



## Appendix F

# Response of one DoF - Monopile and Jacket

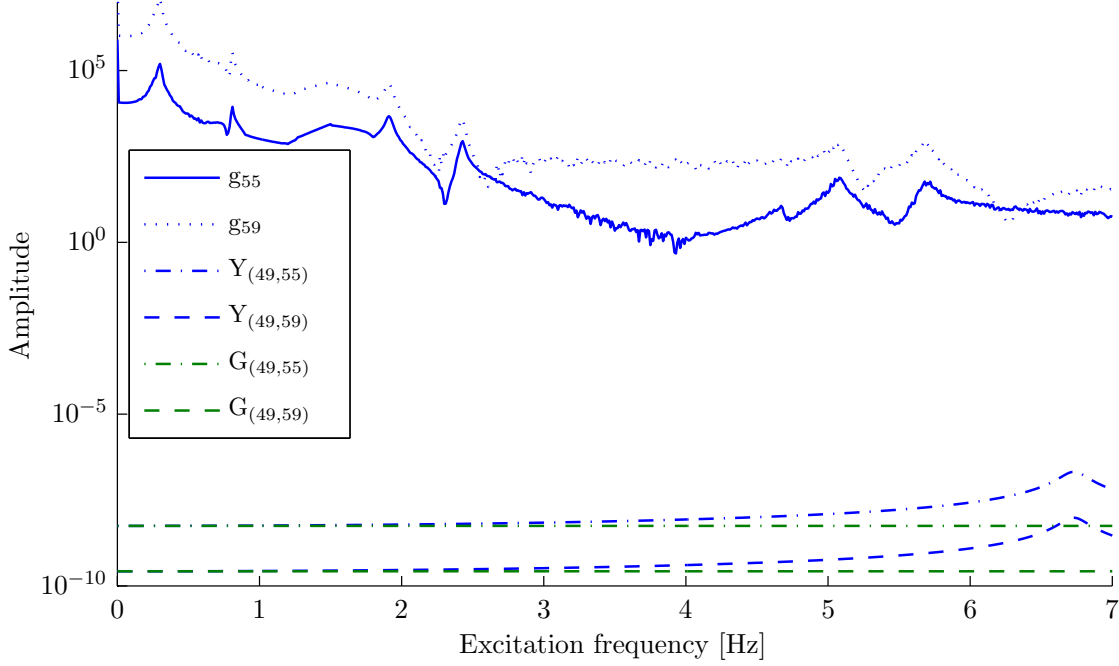
In order to determine the differences in the response of foundation due to a dynamic and a quasi-static analysis, one degree of freedom of the response  $\mathbf{u}^{(f)}$  is chosen to evaluate for both foundation models. The response of node 10 in the x-direction,  $\mathbf{u}_{49}$ , is evaluated for the monopile and node 49 in the x-direction,  $\mathbf{u}_{1003}$ , for the jacket.

### F.1 Monopile

The equations to compute the response of the monopile in node 10 in the x-direction with the different post-processing analyses will be presented. As the structure is excited only in the x-direction, the interface load has only two terms, a force in the x-direction and a moment around the y-axis. The equation to compute the response of the foundation with a force controlled approach is given below. Figure F.1 is a visualization of these equations, the difference between the dynamic and the quasi-static analysis begins to appear near  $\omega_{free}^{\{1\}}$  of the monopile. The receptance component shows a resonance peak at this first eigenfrequency, whereas the flexibility component is constant for all excitation frequencies.

$$\mathbf{u}_{49} = \mathbf{Y}_{(49,55)}\mathbf{g}_{55} + \mathbf{Y}_{(49,59)}\mathbf{g}_{59} = \mathbf{u}_{(49,55)} + \mathbf{u}_{(49,59)} \quad (\text{F.1})$$

$$\mathbf{u}_{49,QsFC} = \mathbf{G}_{(49,55)}\mathbf{g}_{55} + \mathbf{G}_{(49,59)}\mathbf{g}_{59} = \mathbf{u}_{(49,55)QsFC} + \mathbf{u}_{(49,59)QsFC} \quad (\text{F.2})$$



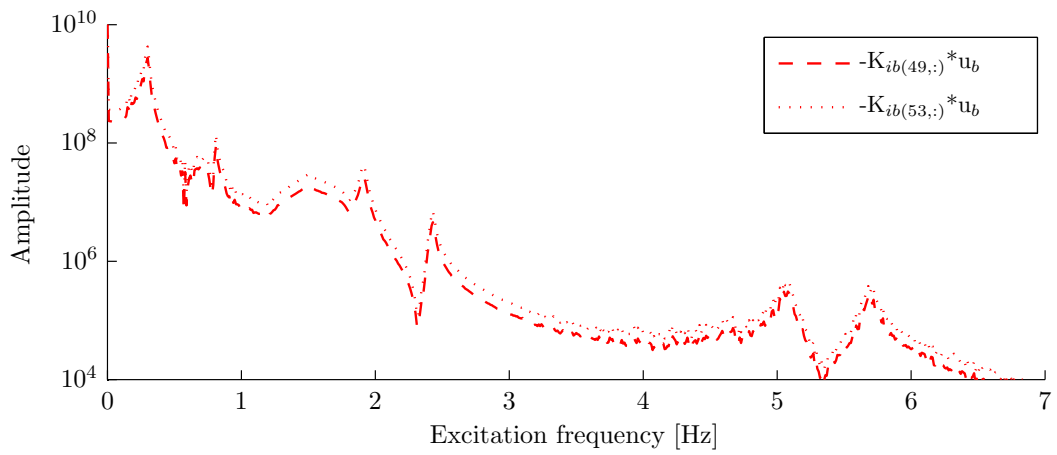
**Figure F.1:** Force controlled approach: Visualization of equations (F.1) and (F.2).

The displacement controlled approach uses the interface deformations as an input. The interface deformation in this case has only two terms, a displacement in the x-direction and a rotation around the y-axis. The equations to compute the response of the foundation with a displacement controlled approach are given below. Figure F.2 is a visualization of these equations, the difference between the dynamic and the quasi-static analysis begins to appear near  $\omega_{fixed}^{\{1\}}$  of the monopile, which is outside the excitation bandwidth. No difference seems to appear between the receptance and the flexibility component for the displacement controlled approach. Therefore, the quasi-static displacement controlled approach will provide an accurate response.

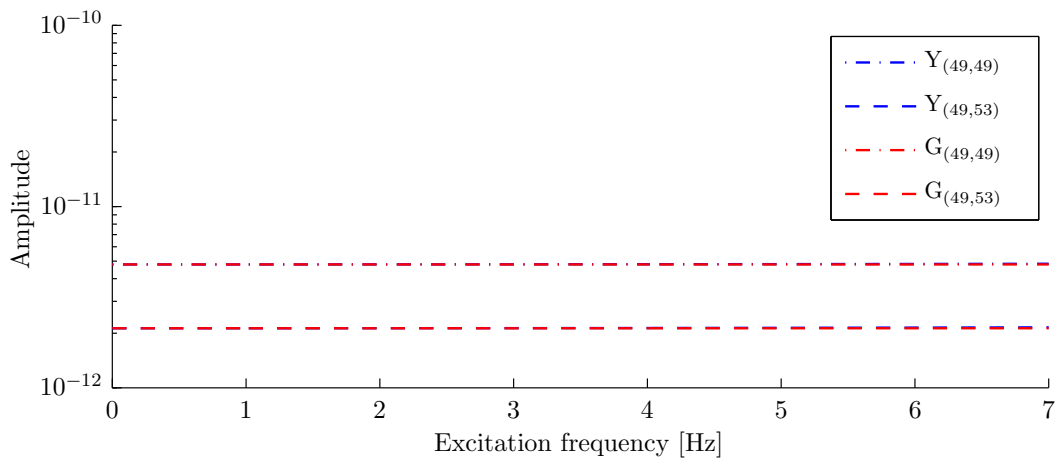
$$\mathbf{u}_{49} = \mathbf{Y}_{ii(49,49)}(-\mathbf{Z}_{ib(49,:)}\mathbf{u}_b) + \mathbf{Y}_{ii(49,53)}(-\mathbf{Z}_{ib(53,:)}\mathbf{u}_b) \quad (\text{F.3})$$

$$\mathbf{u}_{49,QsDC} = \mathbf{G}_{ii(49,49)}(-\mathbf{K}_{ib(49,:)}\mathbf{u}_b) + \mathbf{G}_{ii(49,53)}(-\mathbf{K}_{ib(53,:)}\mathbf{u}_b) \quad (\text{F.4})$$

Figure F.3 shows the response of node 10 in the x-direction. No difference seems to appear between the response obtained with quasi-static displacement controlled approach and the exact response. Figure F.1 shows that the difference between the receptance and the flexibility matrix for the force controlled approach increases from around 3 Hz. In Figure F.3 the response computed with a quasi-static force controlled approach begins to deviate from the exact response from around 3 Hz and is at a maximum at  $\omega_{free}^{\{1\}}$  of the monopile.



(a) Visualization of load terms of equations (F.3) and (F.4).



(b) Visualization of receptance/flexibility terms of equations (F.3) and (F.4).

Figure F.2: Displacement controlled: Visualization of equations (F.3) and (F.4).

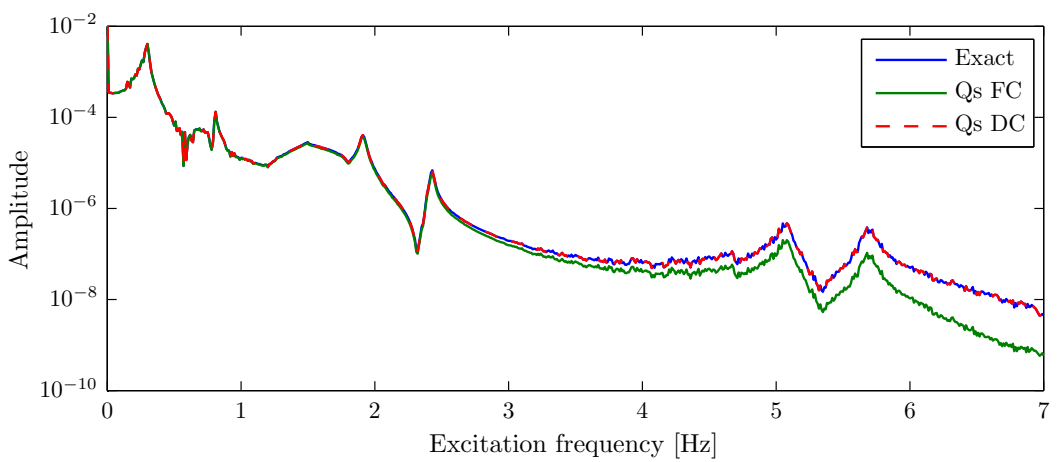


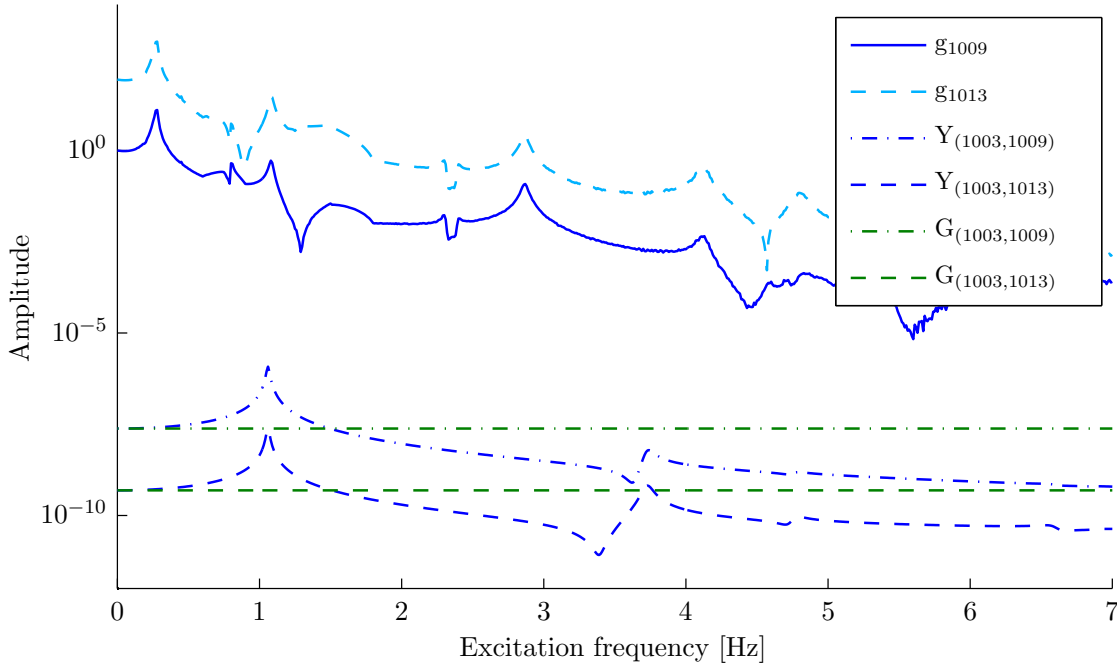
Figure F.3: Response of node 10 in the x-direction for different calculation procedures.

## F.2 Jacket

The equations to compute the response of the jacket in node 49 in the x-direction with the different post-processing analyses will be presented. As the structure is excited only in the x-direction, the interface load has only two terms, a force in the x-direction and a moment around the y-axis. The equation to compute the response of the foundation with a force controlled approach is given below. Figure F.4 is a visualization of these equations, the difference between the dynamic and the quasi-static analysis begins to appear near  $\omega_{free}^{\{1\}}$  of the monopile. The receptance component shows a resonance peak at this first eigenfrequency, whereas the flexibility component is constant for all excitation frequencies.

$$\mathbf{u}_{1003} = \mathbf{Y}_{(1003,1009)}\mathbf{g}_{1009} + \mathbf{Y}_{(1003,1013)}\mathbf{g}_{1013} = \mathbf{u}_{(1003,1009)} + \mathbf{u}_{(1003,1013)} \quad (\text{F.5})$$

$$\mathbf{u}_{1003,QsFC} = \mathbf{G}_{(1003,1009)}\mathbf{g}_{1009} + \mathbf{G}_{(1003,1013)}\mathbf{g}_{1013} = \mathbf{u}_{(1003,1009)QsFC} + \mathbf{u}_{(1003,1013)QsFC} \quad (\text{F.6})$$



**Figure F.4:** Force controlled approach: Visualization of equations (F.5) and (F.6).

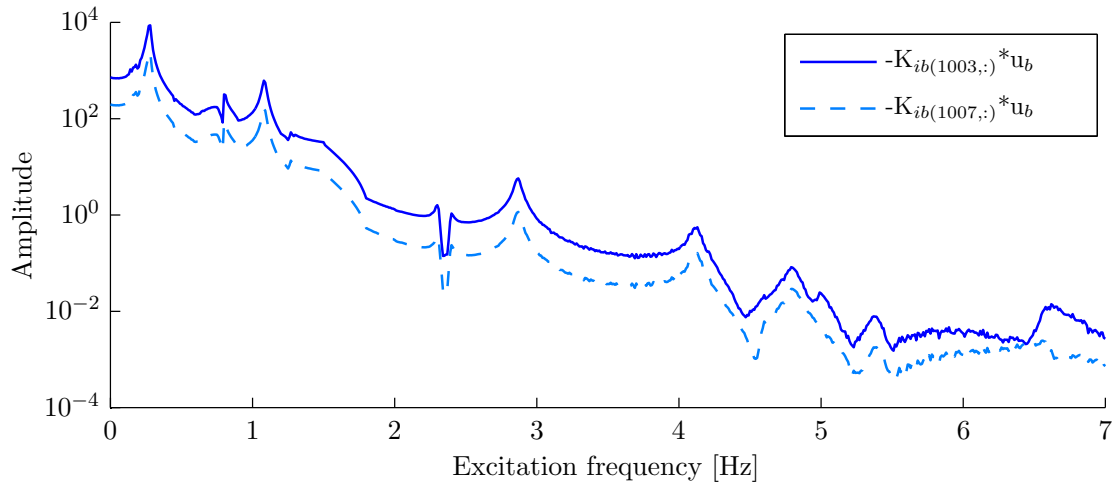
The displacement controlled approach uses the interface deformations as an input. The interface deformation in this case has only two terms, a displacement in the x-direction and a rotation around the y-axis. The equations to compute the response of the foundation with a displacement controlled approach are given below. Figure F.5 is a visualization of these equations, the difference between the dynamic and the quasi-static analysis begins to appear near  $\omega_{fixed}^{\{1\}}$  of the jacket, small resonance peaks are visible for the receptance component. As a result, the response obtained with the quasi-static displacement controlled approach will differ from the exact response.

$$\mathbf{u}_{1003} = \mathbf{Y}_{ii(1003,1003)}(-\mathbf{Z}_{ib(1003,:)}\mathbf{u}_b) + \mathbf{Y}_{ii(1003,1007)}(-\mathbf{Z}_{ib(1007,:)}\mathbf{u}_b) \quad (\text{F.7})$$

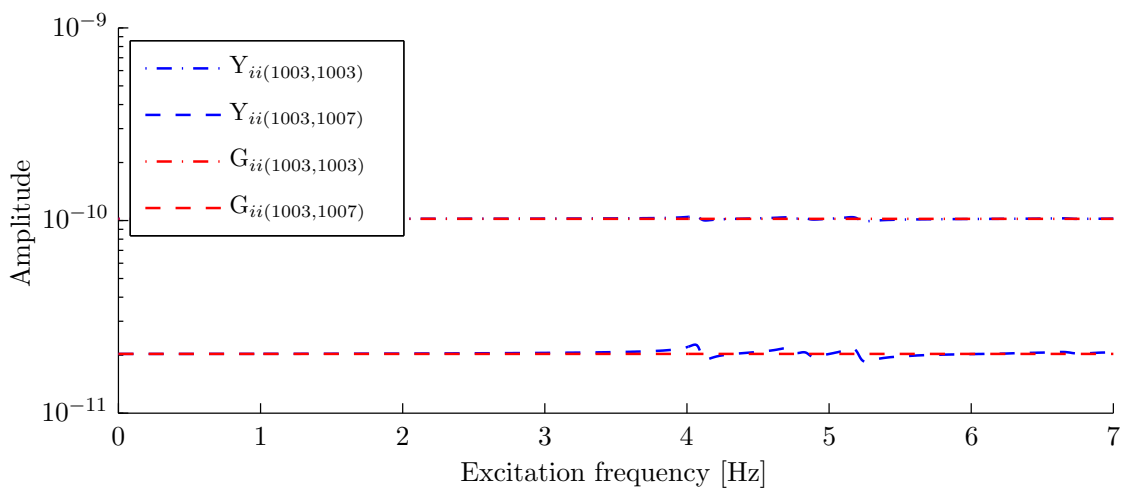
$$\mathbf{u}_{1003,QsDC} = \mathbf{G}_{ii(1003,1003)}(-\mathbf{K}_{ib(1003,:)}\mathbf{u}_b) + \mathbf{G}_{ii(1003,1007)}(-\mathbf{K}_{ib(1007,:)}\mathbf{u}_b) \quad (\text{F.8})$$

Figure F.6 shows the response of node 49 in the x-direction. Small differences appear between the response computed with quasi-static displacement controlled approach and the exact response. At

the higher frequencies the response obtained with quasi-static displacement controlled approach underestimates the exact response. Figure F.4 shows that the difference between the receptance and the flexibility component for the force controlled approach appear near 0.5 Hz. In Figure F.6 the response computed with a quasi-static force controlled approach starts to differ from the exact response from around 0.5 Hz.

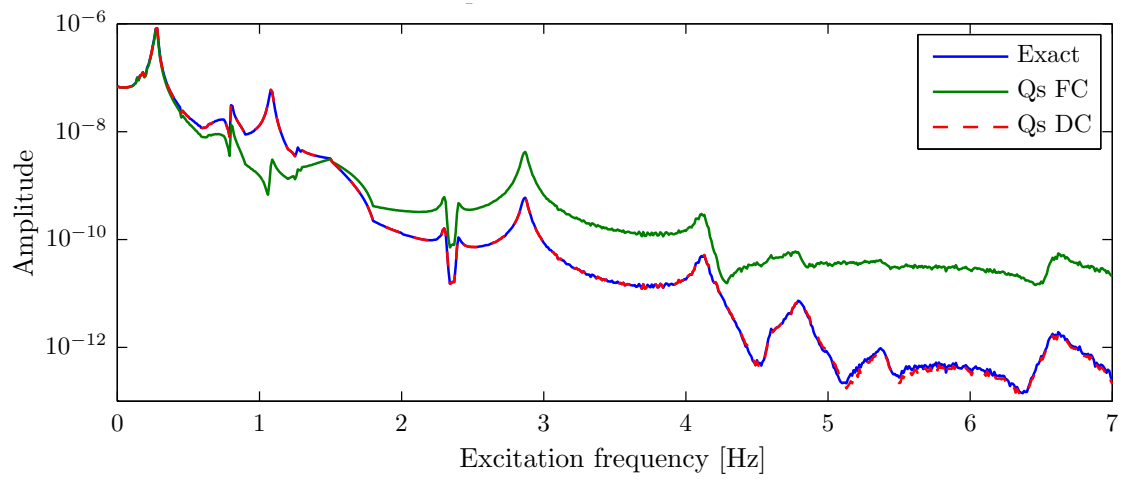


(a) Visualization of load terms of equations (F.7) and (F.8).



(b) Visualization of receptance/flexibility terms of equations (F.7) and (F.8).

**Figure F.5:** Displacement controlled: Visualization of equations (F.7) and (F.8).



**Figure F.6:** Response of node 49 in the x-direction for different calculation procedures.

# Bibliography

- [1] Foundation structures. <http://www.theengineer.co.uk/in-depth/the-big-story/wind-energy-gets-serial/1012449.article>.
- [2] Website stress-strain relation. <http://physics.stackexchange.com/questions/16698/yield-strength-versus-ultimate-strength>.
- [3] *Eurocode 3: Design of steel structures Part 1-9: Fatigue*. 2007.
- [4] G.B. Airy. Tides and waves. 1841.
- [5] Seçil Ariduru. Fatigue life calculation by rainflow cycle counting method. Master's thesis, Middle East Technical University, Ankara, Turkey, 2004.
- [6] C. Arnan Ribas. Finite elements analysis of stresses in beam structures. Master's thesis, Universitat Politècnica de Catalunya, Spain, 2012.
- [7] C. Böker. *Load simulation and local dynamics of support structures for offshore wind turbines*. Shaker, 2009.
- [8] BP. Bp energy outlook 2030. 2012.
- [9] R.R. Craig and M.C.C. Bampton. Coupling of substructures for dynamic analysis. *AIAA Journal*, 6(7):1313–1319, 1968.
- [10] N.E. Dowling. Mean stress effects in stress-life and strain-life fatigue. In *2nd SAE Brasil International Conference on Fatigue, São Paulo*, 2004.
- [11] R. Engels. Superelement modeling of offshore wind turbine support structures. Master's thesis, University of Twente, the Netherlands, 2013.
- [12] European Wind Energy Association (EWEA). *The European offshore wind industry: key trends and statistics 2012*. 2013.
- [13] European Wind Energy Association (EWEA). *Wind Energy Factsheets*. 2013.
- [14] O. Faltinsen. *Sea loads on ships and offshore structures*. Cambridge University Press, 1993.
- [15] J.D. Fenton. Numerical methods for nonlinear waves. *Advances in coastal and ocean engineering*, 5:241–324, 1999.
- [16] R. Guyan. Reduction of mass and stiffness matrices. *AIAA Journal*, 3(2):380, 1965.
- [17] R. Haghi. Integrated design and optimization of an offshore wind turbine monopile support structure. Master's thesis, Delft University of Technology, the Netherlands, 2011.

- [18] International Energy Agency (IEA). World energy outlook. 2011.
- [19] D. de Klerk, D.J. Rixen, and S.N. Voormeeren. General framework for dynamic substructuring: History, review, and classification of techniques. *AIAA journal*, 46(5):1169, 2008.
- [20] M.J. Kühn. *Dynamics and design optimisation of offshore wind energy conversion systems*. 2001.
- [21] T. Kuin. Analysis of load transfer in grouted connections of owec foundations. Master's thesis, Delft University of Technology, the Netherlands, 2012.
- [22] M. Matsuishi and T. Endo. Fatigue of metals subjected to varying stress. *Japan Society of Mechanical Engineers, Fukuoka, Japan*, pages 37–40, 1968.
- [23] M.B. van der Meulen. Influence of nonlinear irregular wave modeling on the dynamic response of an offshore wind turbine. Master's thesis, Delft University of Technology, the Netherlands, 2012.
- [24] B. Nortier. Residual vectors & error estimation in substructure based model reduction. Master's thesis, Delft University of Technology, the Netherlands, 2011.
- [25] Hewlett Packard. The fundamentals of modal testing. Technical report, application note 243-3, 1997.
- [26] P. Passon. Design of offshore wind turbine foundations in deeper water. In *TORQUE 2010: The Science of Making Torque from Wind, June 28-30, Crete, Greece*, 2010.
- [27] D. Rixen. Mechanical analysis for engineering - lecture notes. Technical report, 2011.
- [28] D. Rixen. Numerical methods in engineering dynamics - lecture notes. Technical report, 2011.
- [29] T. Sarpkaya. *Wave force on offshore structures*. Cambridge University Press, 2010.
- [30] M. Seidel, M. von Mutius, P. Rix, and D. Steudel. Integrated analysis of wind and wave loading for complex support structures of offshore wind turbines. In *Proceedings of the Offshore Wind Conference. Copenhagen*, 2005.
- [31] M. Seidel, M. von Mutius, and D. Steudel. Design and load calculations for offshore foundations of a 5 mw turbine. In *Conference proceedings DEWEK*, 2004.
- [32] H. Subroto and P. Godfroy. Optimization of the integrated tower and monopile support structure – A first step in the elaborate path to integrated design optimization of an OWT support structure. In *Proceedings of TORQUE 2010, the science of making torque from wind*, 2010.
- [33] B. Torstenfelt. Finite elements - an introduction to elasticity and heat transfer applications. Technical report.
- [34] P. van der Valk. Model reduction & interface modeling in dynamic substructuring. Master's thesis, Delft University of Technology, the Netherlands, 2010.
- [35] J. van der Tempel. *Design of support structures for offshore wind turbines*. Duwind, 2006.
- [36] W.G. Versteijlen, A. Metrikine, J.S. Hoving, E.H. Smidt, and W.E. de Vries. Estimation of the vibration decrement of an offshore wind turbine support structure caused by its interaction with soil. Master's thesis, Delft University of Technology, the Netherlands, 2011.



- 
- [37] S.N. Voormeeren. *Dynamic Substructuring Methodologies for Integrated Dynamic Analysis of Wind Turbines*. PhD thesis, Delft University of Technology, the Netherlands.
- [38] S.N. Voormeeren, P.L.C. Valk, B.P. Nortier, D.P. Molenaar, and D.J. Rixen. Accurate and efficient modeling of complex offshore wind turbine support structures using augmented superelements. *Wind Energy*, 2013.
- [39] F. Vorpahl, W. Popko, and D. Kaufer. Description of a basic model of the “upwind reference jacket” for code comparison in the oc4 project under iea wind annex xxx. *Fraunhofer Institute for Wind Energy and Energy System Technology (IWES)*, 4, 2011.
- [40] P. Wegener. A critical evaluation of the current design standard for offshore wind turbine monopile foundations – a comparison between the winkler and the elastic foundation model for large diameter piles. Master’s thesis, Delft University of Technology, the Netherlands, 2010.
- [41] C. Willow and B. Valpy. Offshore wind, forecasts of future costs and benefits. Technical report, June 2011.



